High Performance Engineering Polymers: Design, Properties, and Performance

Joseph Michael Dennis

Dissertation submitted to the faculty of the Virginia Polytechnic Institute and State University in partial fulfillment of the requirements for the degree of

Doctor of Philosophy

In

Macromolecular Science and Engineering

Timothy E. Long

S. Richard Turner

John B. Matson

Robert B. Moore

Michael J. Bortner

April 18th, 2017

Blacksburg, VA

Keywords: Polysulfone, Polyester, Polyurea, Segmented Copolymers, Isocyanate-free, Decahydronaphthalate, BPA-replacement, Free volume

High Performance Engineering Polymers: Design, Properties, and Performance

Joseph Michael Dennis

ABSTRACT

The facile synthesis of engineering thermoplastics enabled the development of structure-morphology-property relationships for a wide range of applications. Utilizing step-growth polymerization techniques, a myriad of reaction conditions probed various polymer families including polysulfones, polyesters, polyimides and polyureas. Copolymers ranging from random to segmented sequences provided insight into the influence of segment length on physical properties. Melting temperatures, glass transition temperatures, and mechanical properties responded systematically to segment length and morphology. Leveraging several complementary analytical techniques identified critical segment lengths required for phase separation and crystallization within these copolymers. Introduction of hydrogen bonding further complicated the interrelationships between thermal and mechanical properties, and possible co-crystallization between dissimilar segments occurred. Finally, branching out from linear copolymers to other topologies determined the influence of branch length on rheological and mechanical properties. The commercially-viable synthesis of these various thermoplastics further highlights the immediate impact on state-of-the-art materials, and the fundamental development described herein provides a road map for future development in this field.

EXTENDED ABSTRACT

The facile synthesis of engineering thermoplastics enabled the development of structure-morphology-property relationships for a wide range of applications. Utilizing step-growth polymerization techniques, a myriad of reaction conditions probed various polymer families including polysulfones, polyesters, polyimides and polyureas. Copolymers ranging from random to segmented sequences provided insight into the influence of segment length on physical properties. Random sequences of comonomers within cycloaliphatic copolyesters provided systematic and predictable changes in the glass transition temperatures (T_gs). Introducing more rigid monomers, such as 1,1,3,3-tetramethylcyclobutane-2,4-diol, increased the T_g well above 110 °C and approached 145 °C. These important milestones highlight the temperature range as dishwasher-safe materials and potential BPA-polycarbonate replacements.

Increasing the length-scale from monomers to segmented block copolymers, the behavior of melting temperatures (T_ms), T_gs, and mechanical properties changed dramatically. Importantly, the added complexity of blocks within the copolymers revealed an interrelationship of properties with morphology. Leveraging several complementary analytical techniques identified critical segment lengths required for phase separation and crystallization within these copolymers. Below the critical segment length for phase separation, the segmented block copolymers behaved similarly to random copolymers as a result of block miscibility. However, above a critical segment length, the copolymers phase separated and enabled physical properties otherwise not realized in a random copolymer. Specifically, crystallization behavior dramatically changed with morphology development. Miscible segments suppressed crystallization at relatively low incorporations of the co-segment, but phase separation enabled crystallization by restricting the co-segment impurity to another phase. The realization of the

complicated morphological development unveils a family of high performance materials for automotive and structural applications.

Introduction of hydrogen bonding further complicated the interrelationships between thermal and mechanical properties. The directional organization and strength of hydrogen bonding provided a platform for novel thermoplastics. Copolyureas, containing similar structured monomers, highlighted the complex influence of hydrogen bonding on T_ms and T_gs. Copolymerizing 1,8-diaminooctane and 2,2-(ethylenedioxy)bis(ethylamine) with urea generated semicrystalline copolyureas without a suppression of T_ms with comonomer incorporation. This behavior is in stark contrast to equivalent copolyesters, which lack hydrogen bonding. With tailorable (thermo)mechanical properties and biodegradability, these copolymers offer potential solutions in agricultural and food packaging applications.

Finally, branching out from linear copolymers to other topologies determined the influence of branch length on rheological and mechanical properties. Maintaining low incoporations of a trifunctional monomer accessed long-chain branched poly(ether imide)s without gelation. The combinatorial effects of increasing polydispersity and decreasing branch length dramatically changed the influence of shear rate on melt viscosities. Even though weight-average molecular weights remained relatively constant, the increase in the high and low molecular weight fractions provided improved physical properties over the linear analogue. In particular, the higher concentration of low molecular weight species reduced melt viscosities, potentially improving extruder throughput.

ACKNOWLEDGEMENTS

"The Lord is my shepherd, I shall not want. He makes me lie down in green pastures; He leads me beside quiet waters. He restores my soul; He guides me in the paths of righteousness. For His name's sake. Even though I walk through the valley of the shadow of death, I fear no evil, for You are with me; Your rod and Your staff, they comfort me. You prepare a table before me in the presence of my enemies; You have anointed my head with oil; My cup overflows. Surely goodness and lovingkindness will follow me all the days of my life, and I will dwell in the house of the Lord forever."

Psalm 23:1-6

These verses provide strength and patience all throughout my life. Graduate school pushed these to the limit, but the Lord and others, whom I love, kept me sane. I am thankful to them all for their support, love and kindness throughout these several years of trials and tribulations. Lindsay Johnson constantly kept me grounded, and her unwavering love provided a rock for which I could stand. Loki Dog's (a.k.a Princess Loki) constant ridiculousness was a welcomed comic relief and surprise every day I came home. My brothers', Jake and Dave, continued reminders of the splendors of brotherly love broke many of the monotonous days into digestible pieces. Thank you to my parents for their sacrifices that enabled me to achieve this recognition, and my sister Sandy for her unconditional love for me and my successes. Thank you to Lindsay's parents for their support and the opportunities they provided me. The relaxing visits and plethora of fun activities provided a wonderful release from the rigors of school.

To all of my colleagues, professors and committee members, thank you. Much of my academic success resides in the many hours of collective discussions and collaborations across

the departments. This includes discussions at work, and those outside. A good friend holds that "good science is discovered over good beer", and to this I find no fault. Many discussions around the bar stool have brought forth many "Eureka!" moments, and born successful collaborations. Another instrumental person in my academic career at Virginia Tech is Brent Bowden. His relaxed attitude, kindness and constant positive outlook for students brightened even the toughest of days. I am sure that behind the scenes, well beyond my knowledge, he has underpinned many of the amazing opportunities I enjoyed as a graduate student.

Last, but not least, I would like to thank Tim for all his support. Under his guidance, I have grown substantially personally, and professionally. The list of roles he has shared in my life is long, but importantly he is a friend and mentor.

Chapter 1: Introduction

1.1 Dissertation Overview

Amide-containing segmented block copolymers offer a wide variety of physical properties and provide a critical solution for many applications. The hydrogen-bonding segments in these copolymers provide physical crosslinks and develop hard domains for mechanical integrity. Copolymerizing these "hard segments" with low-T_g oligomers results in materials with high extensibility and low hysteresis. Furthermore, the thermally labile hydrogen bonds and crystal structures provide a potential avenue for recyclable, rubber-like materials. Generally, amide groups are used extensively to provide the hard segment in these copolymers. The synthetic accessibility and beneficial molecular characteristics (e.g. hydrogen bonding, and polarity) provide a myriad of materials with tunable physical properties.

The extensive understanding of the structure-morphology-property relationships developed for these thermoplastic elastomers provide an important foundation for the investigation into segmented block copolymers of engineering thermoplastics. In particular, copolymers where one block crystallizes and the other remains amorphous illustrates an analogous morphology as the amide-containing elastomers. However, in this case, both segments are below the glass transition temperature at room temperature. Through a systematic study of varying both segment lengths, we developed critical structure-morphology-property relationships that provide a fundamental understanding to enable applications beyond the scope of the parent homopolymers.

To supplement the influence of segment length in engineering thermoplastics, we investigated the influence of monomer-length sequences in copolyesters. Reducing the segment

lengths from the oligomer length scale to monomer length scale provided insight into "ideal" copolymer mixing and resulting properties. Furthermore, utilizing isomeric monomer mixtures eliminated the polymers propensity to crystallize, generating relatively simple copolymers for in-depth structure-property characterization. Leveraging complementary analytical techniques generated an understanding of monomer rigidity on segmental motions, and demonstrated a correlation between segment mobility and thermal properties.

Thus far, the influence of *linear* copolymer segments on physical and thermal properties provided a foundation for exploration into *non-linear* engineering thermoplastics. Branching along the polymer backbone introduces another variable for tuning of physical properties, particularly the rheological response of the molten material. These melt flow properties are a critical aspect to engineering thermoplastics because post-polymerization processing is generally a variation of melt extrusion. Long-chain branches, where the length is sufficiently long enough for entanglements, dramatically influence the rheological performance. Through controlled monomer ratios, the systematic series of long-chain branched polymers helped develop structure-property relationships and isolate the influence of branch length on rheological properties.

Returning to hydrogen bonding copolymers and beginning with random copolymers positions us to provide a perspective on the influence of hydrogen bonding in engineering thermoplastics. Building on the foundations outlined above, urea-containing random copolymers begin to elucidate the specific advantages hydrogen bonding provides without the added complication of a soft segment. Utilizing melt polymerization methodology enabled the direct synthesis of random polyurea copolymers with high melting points (*circa* 270 °C) and good mechanical properties. Introduction of heteroatoms along the polymer chain dramatically influenced the thermal and mechanical properties, but the copolymers maintained crystallinity

across the compositional range. Presumably, the strong hydrogen bonding provided by the urea group enabled co-crystallization of the two distinct repeat units. Although currently a preliminary example, the synthetic ease of polyureas via melt polycondensation highlights a novel platform to generate a variety of structure-property-morphology relationships focused around the influence of hydrogen bonding in engineering thermoplastics.

Leveraging systematic structural changes highlights specific contributions to the physical properties of the resulting polymers. Length scales ranging from monomer to oligomeric segments, elucidating the role of segment length on mechanical, thermal and morphological properties provides a comprehensive understanding to enable tunable performance in engineering thermoplastics. From the relationships established here, a plethora of exciting research pathways are envisioned to further probe fundamental understanding of the nexus of structure, morphology and properties. Each prospect provides another perspective to enable sustainable, smarter, or multifunctional materials for emerging technologies, and *Invent the Future*®.

Chapter 2: Amide-Containing Segmented Copolymers

(Published in *Progress in Polymer Science* **2015,** 45, 1-22.)

Daniel J. Buckwalter, Joseph M. Dennis, Timothy E. Long

Department of Chemistry, Macromolecules and Interfaces Institute

Virginia Tech, Blacksburg, VA 24061, United States

2.1 Abstract

This review highlights the synthesis, physical properties, and emerging technologies of state-of-the-art segmented copolymers containing amide hydrogen bonding sites. Amide hydrogen bonding plays a crucial role in the physical properties associated with amide-containing segmented copolymers. Amide hard segments are accessible in many different forms from amorphous alkyl amides to crystalline aramids and greatly influence copolymer morphology and mechanical properties. Variations in copolymer structure allow for the fine-tuning of physical properties and the ability to predict mechanical performance based upon structural modifications. This review includes various synthetic methods for producing well-defined amide-containing segmented copolymers as well as common applications. Also, the morphological and mechanical properties associated with modifications in copolymer structure are discussed.

2.2 List of Abbreviations Used

ABS, poly(acrylonitrile butadiene styrene); CLA, ε-caprolactam; CLO, ε-caprolactone; HMDA, hexamethylenediamide; HMDI, 4,4'-methylenebis(cyclohexyl isocyanate); HS, hard segment; PA, poly(amide); PAEI, poly(amide ester imide); PAIU, poly(amide imide urethane);

PAU,poly(amide urethane); PBA, poly(butylene adipate); PDMS, poly(dimethyl siloxane); PDMS-PA, poly(dimethyl siloxane) poly(amide); PDMS-PAr,poly(dimethyl siloxane) poly(aramid); PEA, poly(ester amide); PEBA, poly(ether-b-amide); PEEA, poly(ether ester amide); PEG, poly(ethylene glycol);PEO, poly(ethylene oxide); PEUA, poly(ester urethane amide); PLLA, poly(l,l-lactide); PPE, poly(2,6-dimethyl-1,4-phenylene ether); PPG, poly(propyleneglycol); PTMO, poly(tetramethylene oxide); PUUA, poly(urethane urea amide); ROP, ring opening polymerization; SS, soft segment; Ti(*i*-OCH_3)$_4$, titanium(IV) methoxide; T*i*(OBu)$_4$, titanium (IV) isopropoxide; TPE, thermoplastic elastomer.

2.3 Introduction

Segmented copolymers typically consist of two covalently linked oligomeric segments with very different physical characteristics termed the hard segment (HS) and soft segment (SS). Generally, the HS and SS are molecularly incompatible with each other due to differences in the hydrophobic/hydrophilic nature of each segment. Also, strong intermolecular interactions between the HS structures, such as hydrogen bonding, lead to physical crosslinking between polymer chains.[1-3] The inherent incompatibility of the two copolymer segments in concert with physical crosslinking intermolecular interactions results in the formation of a microphase-separated morphology.[4] Factors necessary to generate a microphase-separated system include the overall degree of polymerization (N), volume fraction of the segment (f), and Flory-Huggins interaction parameter (χ).[5] Microphase-separated morphologies consist of amorphous, semi-crystalline, or combination of both HS microdomains dispersed throughout the soft polymer matrix (Figure 1). The extent and nature of the microphase-separated morphology, controlled

through copolymer composition, significantly affects the mechanical properties of a copolymer.[6]

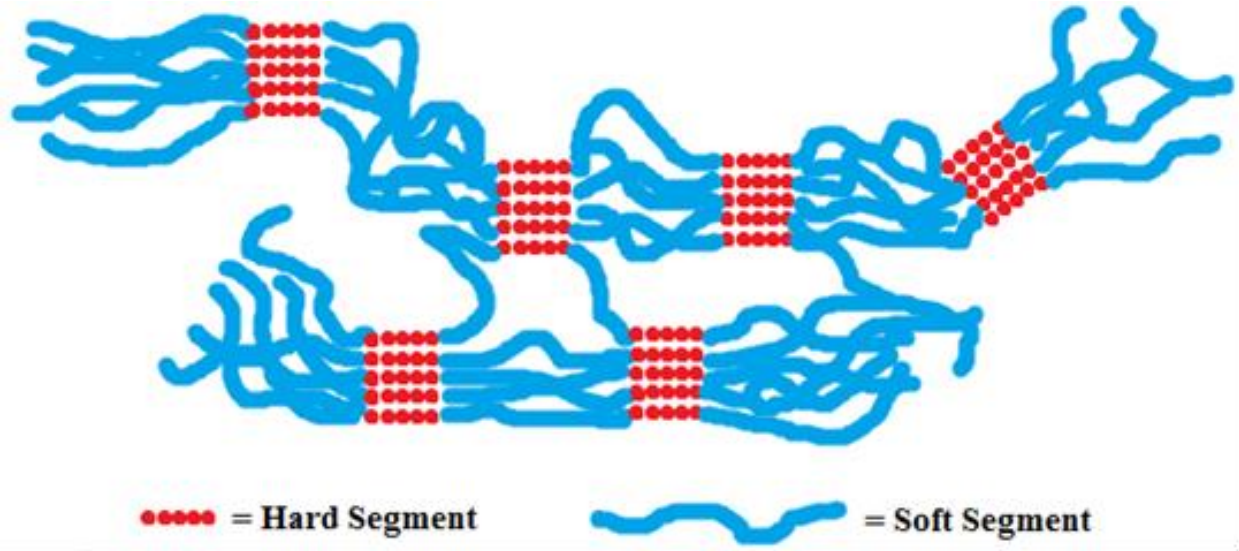

Figure 1. Illustration of a microphase-separated segmented copolymer morphology.

Soft segment compositions typically include a low T_g oligomeric sequence such as poly(tetramethylene oxide) (PTMO), poly(ethylene glycol) (PEG), poly(propylene glycol) (PPG), poly(dimethyl siloxane) (PDMS), or a polyester, which impart flexibility and incompatibility with the HS.[7-10] Incorporation of polyethers into segmented copolymers serve as the soft, flexible, low T_g segment, which promotes microphase separation. Polyether SS oligomers are commercially available with varied functionality, composition, and molecular weight. These SS provide alkali and solvent resistance, varying hydrophilicity, and hydrolytic stability. However, limitations exist for polyether SS in some applications due to UV radiation sensitivity.[11] PDMS is often employed in polyamide (PA) segmented copolymers, and offers UV, thermal, and oxidative stability as well as high gas permeability, hydrophobicity, and physiological inertness.[12] PDMS is one of the most flexible polymer chains, and combined with unique physical properties, provide an excellent SS for segmented copolymers.[13] Most HS include highly polar groups, which form physical crosslinks necessary to impart microphase-

separated morphologies and subsequent copolymer physical properties through intermolecular interactions such as hydrogen bonding.[14] Examples of common polar HS structures include amides,[15] urethanes,[16, 17] ureas,[18, 19] imides,[20, 21] esters,[22, 23] or a combination of two or more of these functionalities.[24-26] HS structure (aromaticity, symmetry, and number of hydrogen bonding groups) and size (molecular weight, number of repeat units) play an important role in determining the physical properties of a copolymer.[27, 28] Through variations in the HS architecture and subsequent intermolecular interactions, researchers effectively tuned the physical properties of many different amide-containing segmented copolymers (Figure 2).

Poly(ether-*block*-amide), PEBA

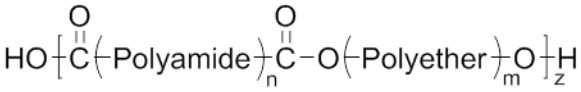

Poly(ether ester amide), PEEA

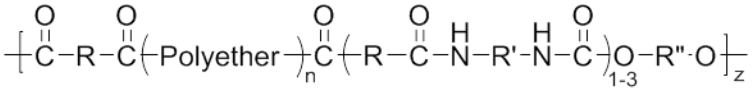

Poly(ester amide), PEA

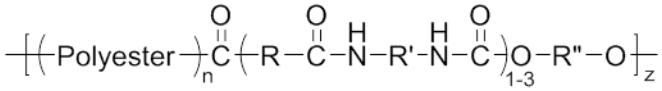

Poly(oxamide) segmented copolymers

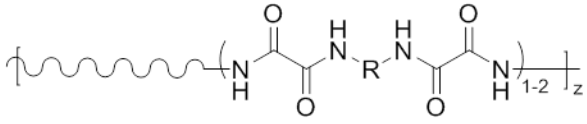

= PTMO or PDMS

Poly(dimethyl siloxane)-poly(amide) segmented copolymer, PDMS-PA

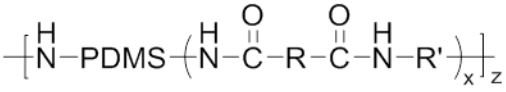

Figure 2. Structures of amide-containing segmented copolymers discussed.

The amide functionality possess strong hydrogen bonding characteristics that are well-suited for the formation of strong physical crosslinks necessary for enhanced physical properties of a segmented copolymer. When compared to other hydrogen bonding groups commonly found in segmented copolymers, amide groups impart one of the strongest intermolecular interactions. Using group contribution method calculations, the cohesive energy density of hydrogen bonding for urea, amide, urethane, and imide was 2079, 1862, 1385, and 980 J/cm^3, respectively, and the hydrogen bonding energy of amide groups was 32.5 kJ/mol.[29] Primarily a result of hydrogen bond donor-acceptor sequencing within the functional group, this structural aspect becomes an important consideration when designing amide-containing segmented copolymers, and to ascertain the morphology and physical properties required for thermoplastic elastomers. Formation of PA segmented copolymers involves many different synthetic methods. Polymerization between amines and acid chlorides or carboxylic acids are efficient, often utilizing a catalyst in the case of low temperature carboxylic acid/amine polymerization.[30-32] The use of diesters and diamines are also useful for PA synthesis, but the polymerization is often inefficient due to the ester reactivity and required use of a catalyst such as an enzyme.[33] Other PA polymerization strategies include ring opening polymerization of caprolactam or polymerization between a dicarboxylic acid and diisocyanate.[34] Researchers continue to actively probe HS symmetry and SS composition effects on microphase-separation. As the field of amide-containing segmented copolymers grows rapidly with current research thrusts, this review discusses the various types of amide-containing segmented copolymers with emphasis on their associated synthesis, applications, and properties.

2.4 Poly(ether-block-amide) Segmented Copolymers

Poly(ether-*block*-amide) (PEBA) segmented copolymers are high performance block copolymers consisting of soft polyether blocks and hard PA blocks commercialized under the trademark Pebax®. Arkema Inc. first commercialized Pebax® thermoplastic elastomers in 1981 as part of an initiative to develop "soft" nylon materials. Development of Pebax® copolymers provided high performance materials with tunable mechanical properties. Altering the composition and length of the soft and hard blocks provides a high level of variability in copolymer physical properties.[35]

Commercial applications for PEBA segmented copolymers, in particular Pebax®, include advanced gas separation membranes, biomedical devices (e.g., angioplasty balloons), food packaging, various textile modifiers (e.g., melt spun fibers), mechanical parts, construction materials, electronic equipment (e.g., wire coatings), aviation industry, and automotive applications requiring tough, elastic materials.[36-40] Pebax® possesses the ability to act as efficient gas separation membranes and the ability to alter the selectivity for a particular gas, leading to a recent increased interest in PEBA copolymers for gas separation membranes. For example, the separation of polar and nonpolar gas mixtures relied on altering the copolymers chemical composition to obtain optimal separation for a given mixture.[41] PEBA block copolymers with a low PA content exhibited the highest levels of gas permeation. Armstrong et al. also demonstrated the dramatic effect of polyether mechanical orientation on gas diffusion through PEBA membranes. Uniaxial orientation of the SS occurred after applying 400% strain to a PEBA composed of PTMO/nylon-12, and an observed decrease in the gas diffusion up to 3.5x resulted. Strain-induced crystallization of PTMO severely restricts diffusion of gas through the SS leading to a decrease in gas permeation.[42] Another application for PEBA block copolymers

receiving attention recently is use as antistatic agents. Wang et al. recently published a report on the blending of acrylonitrile-butadiene-styrene (ABS) resin with a PEBA composed of PTMO/nylon-6 to impart antistatic properties to the blended material. Through variations in the ratio of PEBA and ABS in the blends, they were able to reduce the surface resistivity 4 orders of magnitude and retain persistent antistatic abilities.[43]

Synthesis of PEBA segmented copolymers relies on the covalent attachment of two oligomeric sequences to form block copolymers. The most common PEBA precursors include nylon-6 and nylon-12 as the hard amide block and PEG or PTMO as the soft flexible segment. One method for preparation of PEBA block copolymers required the melt polycondensation of carboxylic acid terminated nylon oligomers with alcohol terminated PEs at high temperatures (~250 ˚C). A catalysis, such as $Ti(OR)_4$, are often necessary to drive the formation of ester linkages between the two different blocks.[37] The polyether selection for copolymerization with PA oligomers affects the rate of esterification, primarily due to the moisture content in polyether oligomers with the reported observed reactivity as follows: PEG < PPG < PTMO.[44] Peyravi et al. described a slightly different synthetic strategy for producing PEBA copolymers through a three step route (Scheme 1). First, end-capping of nylon-6 with an excess of adipic acid at high temperature yielded a carboxylic acid terminated oligomer. Chain extension with hexamethylenediamine and copolymerization with PEG, $Ti(OBu)_4$, and Irganox 1010 in the melt provided the desired PEG/nylon-6 segmented block copolymer.[45] The stepwise method established an easy route for varying copolymer composition and reliable thermoplastic elastomers (TPE) with crystalline micro-domains. Preparation of PEBA films relies on melt pressing or a solution casting procedure. Both methods proved useful for film formation, but the

thickness of films had a significant effect on the morphology displayed, particularly with solution casting methods.[46]

Scheme 1. Synthesis of PEO-nylon-6 poly(ether-*block*-amide) segmented copolymer through a three-step melt polycondensation method. Reprinted with permission[45] Copyright 2010, John Wiley and Sons.

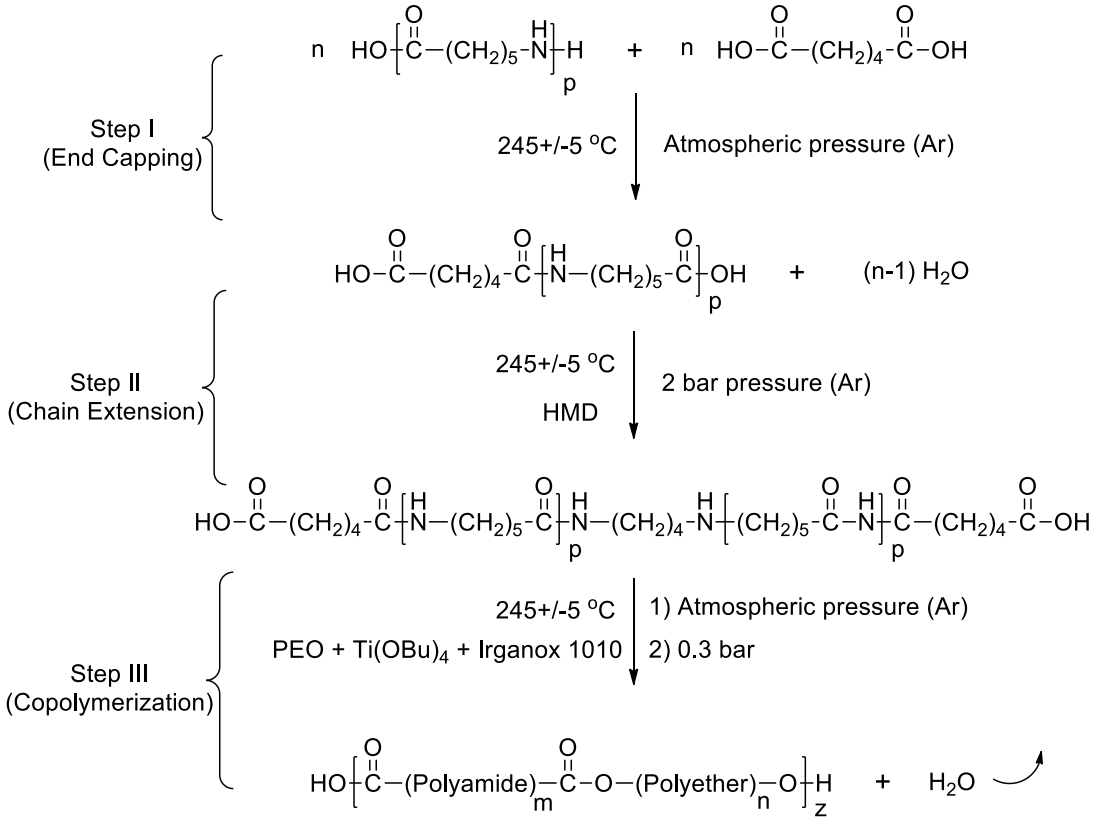

PEBA segmented copolymers exhibit a complex morphology induced by microphase separation, and a high degree of crystallization of hard segments. X-ray diffraction (XRD), differential scanning calorimetry (DSC), and nuclear magnetic resonance (NMR) spectroscopy have elucidated the finely microphase-separated morphology, which revealed well defined PA crystals spread throughout amorphous and semi-crystalline PE/PA phases in PEG/nylon-12 containing PEBA block copolymers.[47] The crystallization behavior of Pebax® suggested the

block copolymer microphase separation occurred through HS crystallization into amorphous and crystalline regions instead of the formation of hard and soft domains commonly observed in segmented copolymers.[48] The long ribbon-like PA crystalline regions provide copolymer strength upon mechanical deformation. Atomic force microscopy (AFM) and small angle X-ray scattering (SAXS) analysis revealed the formation of nanofibrils oriented in the direction of an applied strain, which acted as the load-bearing nanostructures that dominated the mechanical properties (Figure 3).[49] Strain induced fibrillation occurs in a three stage molecular orientation that started with alignment of the PTMO soft block. Further strain caused a rotation of the PA lamellae and eventual plastic deformation, which ultimately led to fibril formation.[50] Uniaxial deformation of PEBA copolymers also affected the T_m of the polyether soft segment. DSC studies showed the appearance of a higher polyether T_m, which increased in intensity with the increase in strain without changes in the PA T_m.[51]

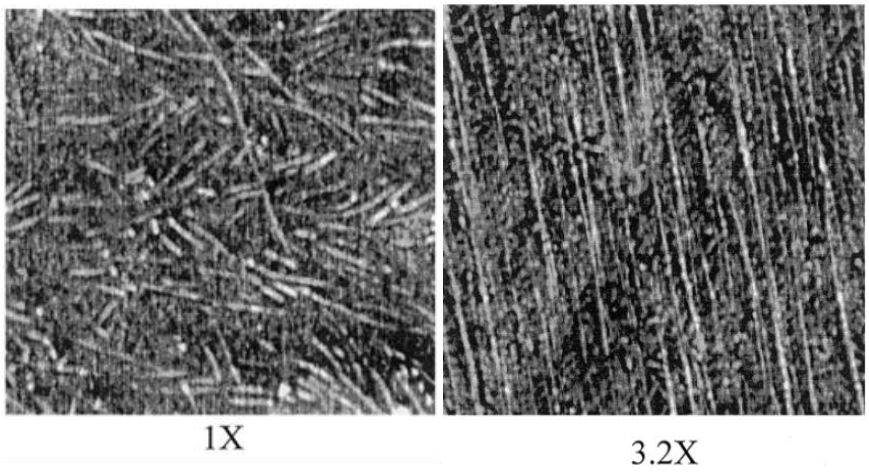

Figure 3. AFM phase images of Pebax® 3533 film under a 1x and 3.2x elongation with the stress direction close to vertical and images are 1µm x 1 µm. Reprinted with permission[49] Copyright 2002, John Wiley and Sons.

The stability and nature of PA hard segments greatly determine the effects of thermal energy on PEBA block copolymers. Loss of PA hydrogen bonding at high temperatures coincides with melting of the crystalline PA domains and leads to flow of PEBA block copolymers. Linear viscoelasticity studies revealed that as the temperature of the melt increases, the well-defined microphase-separated structure transitioned from a weak to a stiff structure after a large-amplitude oscillation shear. AFM also indicated a change in the microphase-separated morphology of the PEBA melt with increased temperature.[52]

PEBA segmented block copolymers demonstrated thermal degradation temperatures under non-oxidative conditions from 380 – 415 ˚C ($T_{d,\ 10\%}$), similar to the nylon-12 oligomers. Besides the polyether T_g, DSC revealed a nylon-12 T_m between 161 – 165 ˚C.[44] Dynamic mechanical analysis often showed a large rubbery plateau, indicative of microphase-separated morphologies with a drop in storage modulus that corresponded to a PA T_g.[44] Figure 4 depicts the DMA storage modulus and tan δ curves for a PTMO/nylon-12 containing PEBA and reveals the evidence of multiple transitions. Transition 1 included transitions that occurred in the amorphous polyether and PA regions. Transition 2 corresponded to the T_g of the PTMO soft segment, and transition 3 to the crystallization and melting of PTMO. The region labeled as transition 4 arose from the PA T_g and increased with increased PA content, which overlapped to some degree with polyether melting. The sudden increase in tan δ in the transition 5 region corresponded to melting of the PEBA copolymer.[53] The DMA polyether T_g often resided at slightly higher temperatures than those observed with DSC due to some degree of phase mixing with the amorphous HS domains.[54, 55] The storage modulus of the rubbery plateau scaled with the PA HS mol%, similar to poly(urea) and poly(urethane) segmented copolymers.[56]

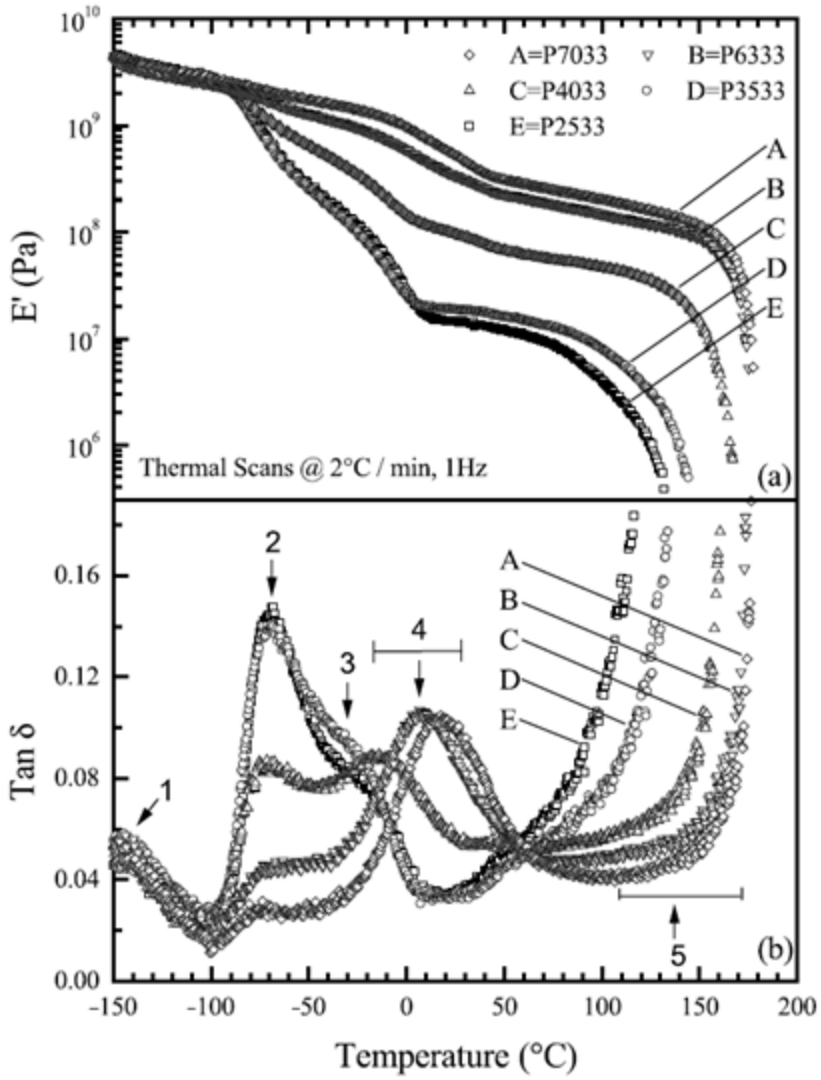

Figure 4. DMA traces of the (a) storage modulus and (b) tan δ of Pebax® films composed of nylon-12 and PTMO with transitions 4 and 5 indicating a general temperature range. Reprinted with permission[53] Copyright 2003, Elsevier.

Tensile properties of PEBA segmented block copolymers demonstrated a dependence on copolymer composition and often exhibited high elongation values (Figure 5). An increased mol% PA in Pebax® films from 12 to 73% revealed an increase in the stress at break and Young's modulus. Furthermore, a decrease in strain at break occurred with each increase in the

mol% PA.[53] The decrease in strain at break with an increased HS wt% content was common for many segmented copolymers such as poly(urea)s and poly(urethane)s.[57-59]

Overall, PEBA segmented block copolymers provide high performance TPE materials with tunable thermomechanical and tensile properties for a wide range of applications. Earlier literature has probed the complex morphology of these segmented block copolymers using a compilation of analytical techniques. These studies have identified that the complex, crystalline, phase separated morphology imparts the impressive mechanical properties of PEBA segmented block copolymers, and can be influenced by copolymer composition. However, the comparative studies for Pebax® copolymers are restricted due to the ill-defined structure of each commercial product. Some literature has investigated analogous copolymers to isolate individual effects within this complex copolymer,[56-58] but further development of the molecular weight, hydrogen bonding, polydispersity, and sequence effects on physical properties is needed. As a result, potential improvements over commercial analogues are envisioned for the tensile or barrier properties by targeting these structure-property relationships. Also, blending of these copolymers with other commercial products would broaden the utility of the PEBA materials beyond the scope discussed currently. Perhaps synergistic effects are envisioned through mechanical or chemical compatibilization of PEBA copolymers and improve upon elastic hysteresis. Most issues are resolved, but understanding more of the structure dependence on the physical properties of PEBA copolymers by strict composition control is needed.

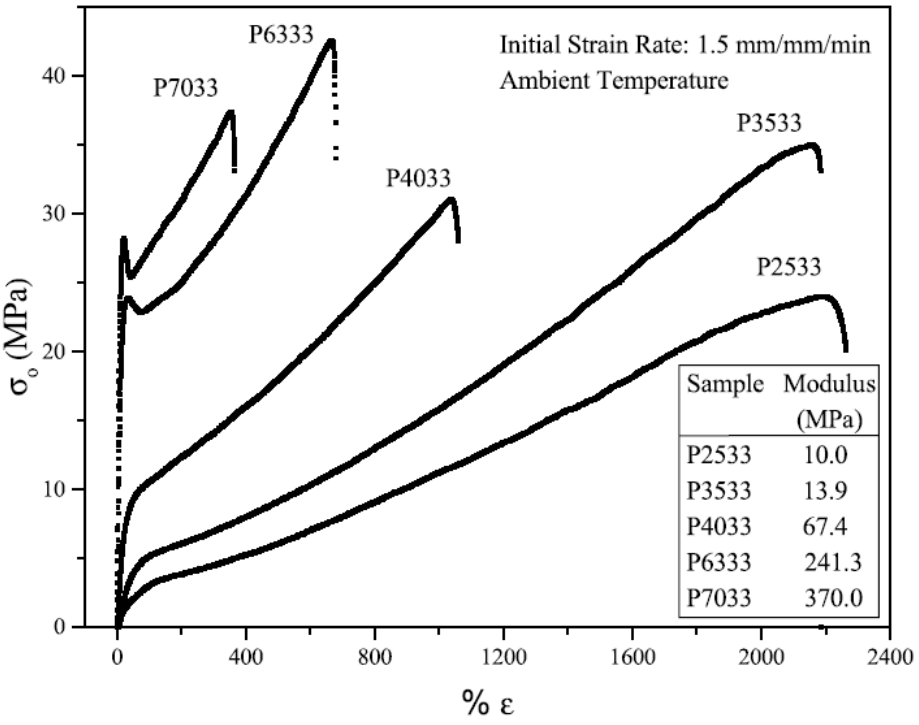

Figure 5. Stress vs. strain curve for Pebax® films increasing in mol% PA content with P2533 containing 12 mol% and P7033 containing 73 mol%. Reprinted with permission[53] Copyright 2003, Elsevier.

2.5 Poly(ether ester amide) Segmented Copolymers

Poly(ether ester amide) (PEEA) segmented copolymers are typically composed of a polyether oligomeric soft segment covalently linked to a short amide-containing HS through an ester linkage, which yields a flexible, elastic copolymer. The HS is responsible for forming the often semi-crystalline physical crosslinks in PEEA copolymers, and thereby improving the mechanical properties of low T_g polyethers. PEEA copolymers exhibit good mechanical properties, high T_m's, and fast HS crystallization from incorporating monodisperse amide segments. Applications for PEEA segmented copolymers include engineered plastics, thermoplastic elastomers, and elastic textile fibers.[60, 61] Furthermore, bioengineered PEEA

segmented copolymers have demonstrated biocompatibility and enzymatically degradable properties for controlled drug delivery.[62] Hydrophilic PEEA copolymers contained poly(L,L-lactide) (PLLA), PLLA-PEG-PLLA macromonomers,[63] or poly(ϵ-caprolactone) and sebacoyl chloride,[62] for example, with various hydrophilic diamines. As a result, these biocompatible, microphase-separated PEEA copolymers are identified as promising candidates for oral drug delivery applications.[63] Other similar copolymers, containing PEG and a diamide-containing HS, also demonstrated good properties for use in biomedical devices.[64]

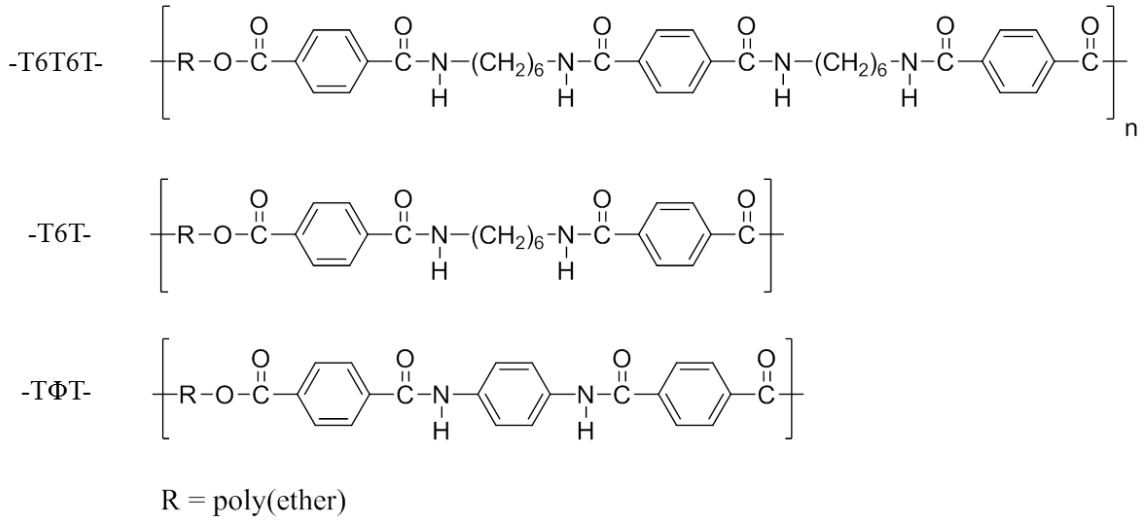

Figure 6. Aramid hard segment structures commonly found in PEEA segmented copolymers.

PEEA segmented copolymers are commonly synthesized through melt polycondensation of a soft hydroxy terminated polyether oligomer, such as PTMO, with a monodisperse methyl ester terminated oligoamide monomer and diol chain extender. Other commonly utilized PEs include PEG and the high T_g polyester, poly(2,6-dimethyl-1,4-phenylene ether) (PPE).[65, 66] Along with a high T_g of 200 °C, PPE also possess good flame retardation, low moisture uptake, and high toughness, but exhibits poor processability and low solvent resistance.[15] The amide ester

monomers used are usually comprised of aramids, containing multiple terephthalamide groups, or oligolactam containing monomers.[67, 68] Furthermore, the aramid monomers are typically composed of 2 or 3 terephthalamide units separated with a short alkyl or aromatic spacer (Figure 6). The rapid crystallization of the aramid segments imparts an increase in the dimensional stability, mechanical properties, and solvent resistance of PEEA copolymers.[69] Melt polymerization conducted under inert atmosphere at high temperature and low pressure proved successful. For example, a one-pot polymerization strategy began with a reaction vessel with the polyether oligomer, diol chain extender, oligoamide-dimethyl, and catalyst solution. The polymerization proceeds through slowly increasing the temperature in a stepwise fashion up to 250 – 280 ˚C with the application of reduced pressure to achieve high conversion through removal of the condensate (Scheme 2).[70, 71] Utilizing an aramid with a high melting point, such as TΦT-dimethyl (371 ˚C m.p.) required the use of solvent, such as NMP, for polymerization in some cases.[72] A similar synthetic method for producing PEEA tri-block copolymers utilized a uniform monomethyl aramid to end-cap a PTMO middle block, with variations of PTMO molecular weight occurred through extension with terephthalate. This synthetic method yielded ductile PEEA tri-block copolymers that exhibited elastic behavior, even at low molecular weights (>6000 g/mol).[73]

Scheme 2. Melt polymerization of a PPE-2T/C12/T6T6T PEEA segmented copolymer. Reprinted with permission[71] Copyright 2004, Elsevier.

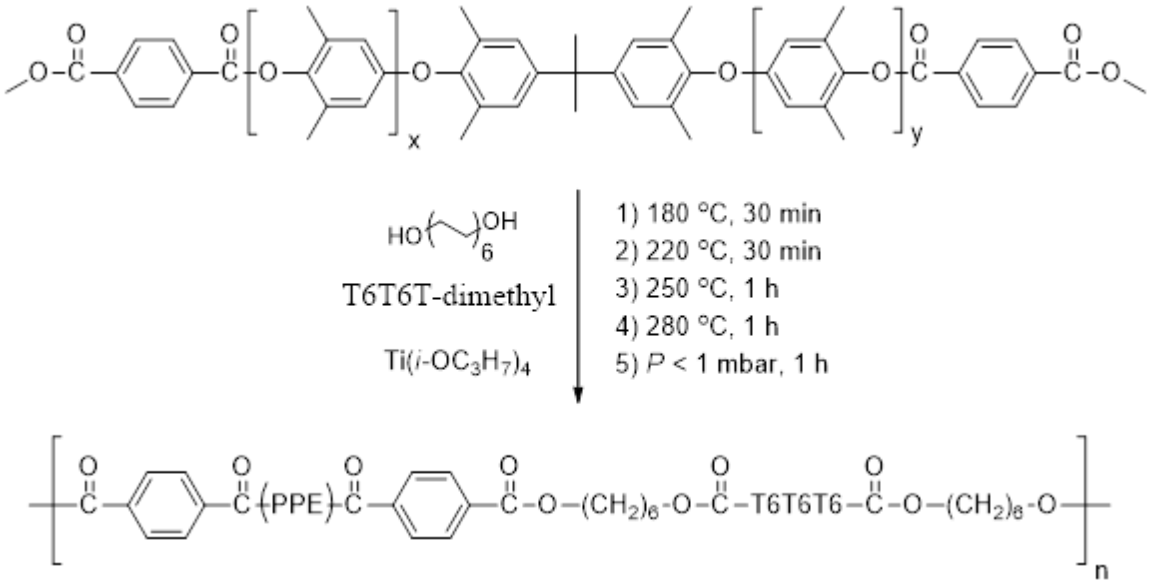

The role of hydrogen bonding plays an important role in determining copolymer bulk morphologies and physical properties as in other segmented copolymers. PEEA segmented copolymers demonstrated high levels of microphase separation and crystallinity, which depended on the amide-containing HS structure.[74, 75] Comparisons of hydrogen bonding PTMO-T6T6T and non-hydrogen bonding PTMO-TPTPT (tetra amidepiperazine terephthalamide) segmented copolymers revealed the important role of hydrogen bonding in poly(ether ester amide) segmented copolymers. Tensile analysis of PTMO-TPTPT demonstrated lower storage moduli and lower yield stress due to the lack of hydrogen bonding (Figure 7). The reduced reinforcing effect of HS crystallites and poor crystalline packing caused significant reduction in mechanical properties.[70] Van der Schuur et al. showed that increasing the number of amide hydrogen bonding groups in the HS from 2 (T6T) to 6 (T6T6T6T) led to an increase in storage modulus, T_m, and onset of flow for the PEEA segmented copolymers.[76] The increased amide length also resulted in improved elastic properties partly due to increased thickness of the crystallites. The presence of a uniform, monodisperse crystallizable HS yielded more complete crystallization within the copolymer and improved mechanical properties when compared to PEEA copolymers

containing polydisperse HSs (Figure 8).[79] Polydisperse HSs produced lower moduli, yield strength, DMA onset of flow, and elastic properties as well as an increased temperature dependence on the DMA rubbery plateau. The reduced mechanical properties of PEEAs with non-uniform HS occurred due to the presence of liquid-liquid, demixed phase content and reduced crystallinity.[77, 78] Husken et al. investigated how changes in the T6T6T semi-crystalline HS composition in PEG-T6T6T segmented copolymers altered the hydrophobicity of the PEEAs surface. The contact angle decreased as the concentration of T6T6T HS decreased, which indicated an increase in the hydrophilicity of the PEEA surface.[79] HS content not only affected copolymer bulk morphologies and mechanical properties, but also the surface properties of PEEA segmented copolymers.

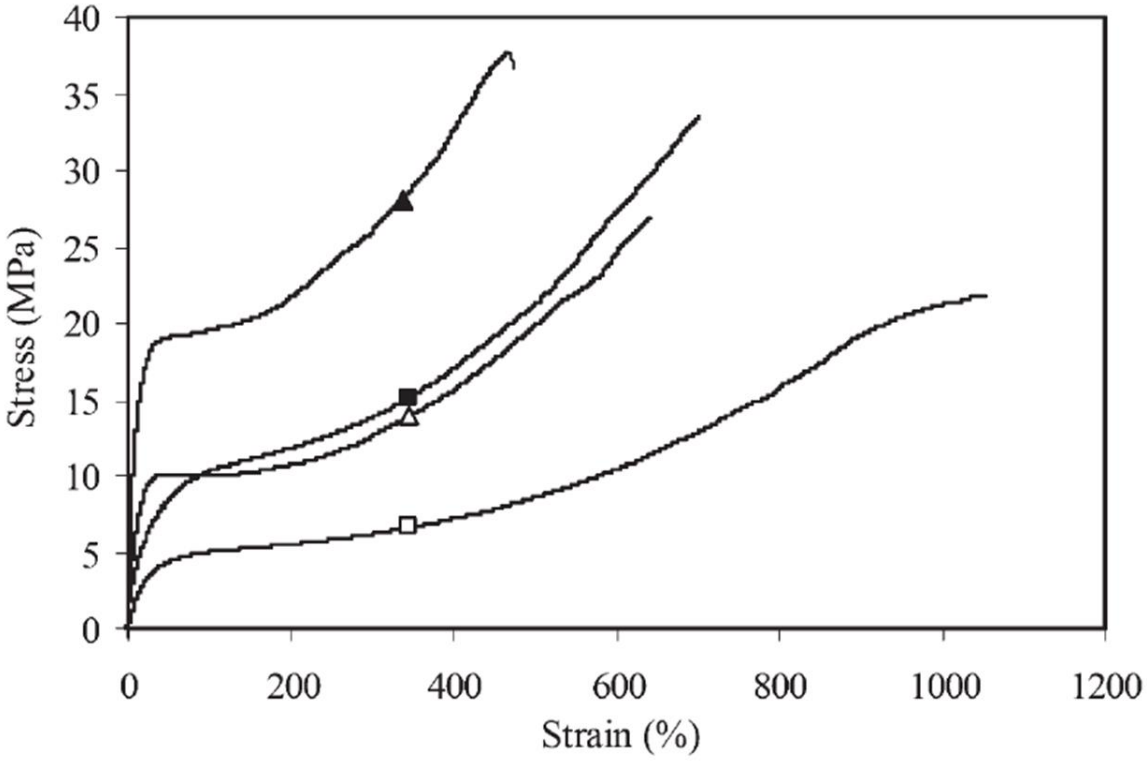

Figure 7. Stress-strain curves for hydrogen bonding $PTMO_{1000}$-T6T6T (▲), $PTMO_{2000}$-T6T6T (■) copolymers and non-hydrogen bonding $PTMO_{1000}$-TPTPT (Δ), $PTMO_{2000}$-

TPTPT (□) segmented copolymers. Reprinted with permission[70] Copyright 2009, John Wiley and Sons.

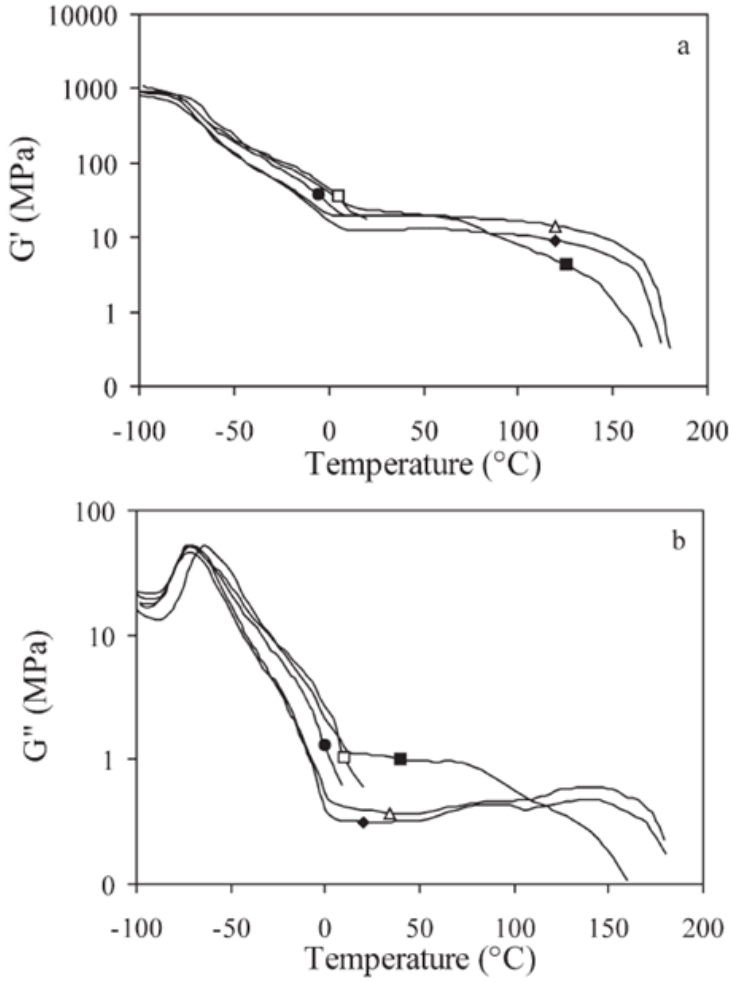

Figure 8. Storage (a) and loss modulus (b) as a function of temperature for $PTMO_{2000}$-T6A6T segmented copolymers with increasing HS PDI: monodisperse (Δ), 1.03 (♦), 1.07 (●), 1.09 (□), and 1.20 (■). Reprinted with permission[77] Copyright 2008, John Wiley and Sons.

The propensity of the HS to crystallize also had a dramatic effect on morphology and the subsequent physical properties of PEEA segmented copolymers. DSC and WAXD techniques revealed that the amide-containing HS of PEEA copolymers rapidly crystallize due to the nature and uniformity of the oligoamides used for polymerization.[80] Copolymers composed of a

crystalline HS showed lower polyether T_g values than amorphous HSs, which indicated an increased phase-separated morphology with the presence of crystalline HS. HS crystallinity also imparted increased moduli and elasticity in PEEA copolymers.[4] The temperature where the polyether T_g appeared in PEEA copolymers, with changes in copolymer composition, provided insight into the level of crystallinity that a particular oligoamide HS possessed.[81] For example, PEEA copolymers containing the same PTMO molecular weight demonstrated SS T_gs of -70 and -55 ˚C, the copolymer with a T_g of -70 ˚C would have a higher degree of HS crystallinity resulting in greater crystallinity-induced, microphase separation. The copolymer that exhibited a T_g of -55 ˚C would inherently include amorphous hard domains mixed with the soft matrix, thereby increasing the PTMO T_g. Despite the highly crystalline oligoamide segments of many PEEA HSs, the elastomers often appear transparent due to the inability of the small amide nanoribbons to scatter light, as in the case of PTMO-TΦT PEEA copolymers.[74] PEEA segmented copolymers composed of non-crystallizable oligoamide HS, such as *m*-xylene isophthalamide, showed liquid-liquid demixing leading to phase separation. The bulk morphology of non-crystalline PEEA copolymers exhibited spherical HS domains of varied size spread throughout the polyether matrix (Figure 9). PEEA copolymers containing 2 *m*-xylene isophthalamide units revealed minimal phase separation, resulting in reduced elastic properties than the semi-crystalline analogue.[82] Incorporation of chemical crosslinks through trifunctional polyether oligomers into to the non-crystalline PEEA copolymers did not demonstrate an effect on the polyether T_g or storage modulus. However, a large decrease in tensile properties and compression set, over the comparable semi-crystalline material, resulted due to the decrease in physical crosslinks.[83]

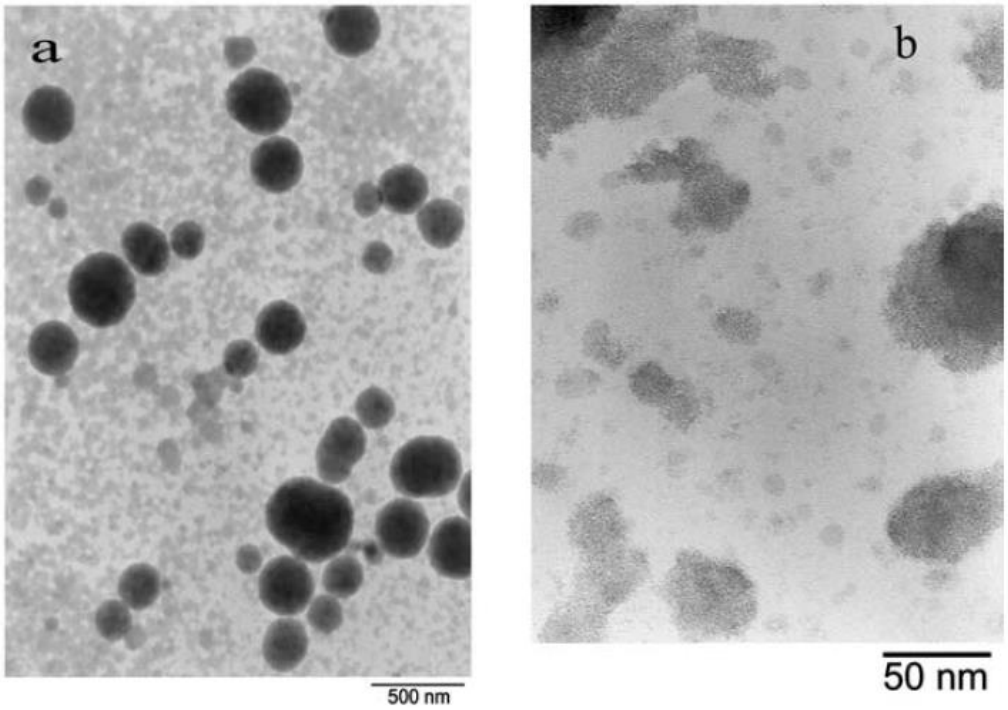

Figure 9. TEM images of PEEA copolymers comprised of uniform *m*-xylylene isophthalamide non-crystallisable HS and poly(propylene oxide) SS: 52,000x (a) and 120,000x (b). Reprinted with permission[82] Copyright 2005, Elsevier.

Dynamic mechanical behavior of PEEA segmented copolymers revealed large temperature-insensitive rubbery plateaus typical of highly microphase-separated segmented copolymers. The range of the plateau region and storage moduli are highly dependent on copolymer composition, allowing for the tailoring of mechanical properties through structural alterations.[24,26,29] Increasing polyether SS length resulted in a systematic decrease in the observed flow temperature and storage moduli of PEEA copolymers due to a decreased wt% HS composition.[25, 81, 84] Husken et al. studied the effect of alkyl spacing between terephthalamide groups in a crystalline tetra-amide HS (TxTxT, x = alkyl spacer) on the dynamic mechanical behavior of PEEA segmented copolymers (Figure 10). The temperature for the onset of flow

decreased linearly with insignificant change in the rubbery plateau storage moduli as the alkyl spacing between terephthalamide groups increased from 2 to 8 methylene groups. Presence of an odd spacer revealed an odd-even effect that resulted in lower values for the onset of flow and storage moduli primarily due to lower crystallinity.[85]

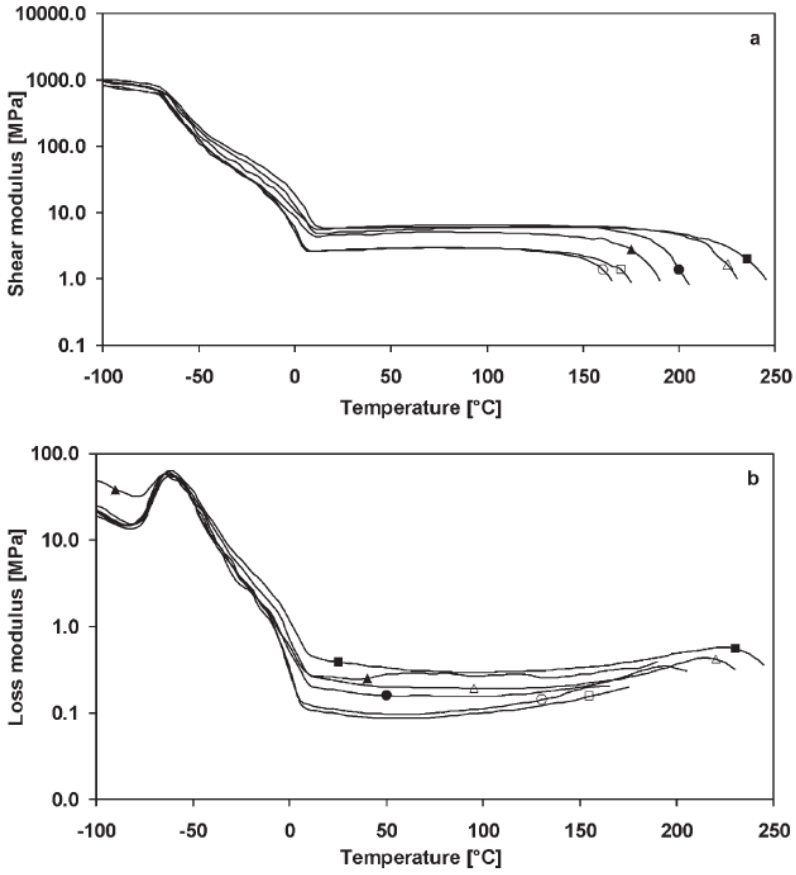

Figure 10. Effect of alkyl spacing between terephthalamide groups in the HS on the shear modulus (a) and loss modulus (b) of $(PTMO_{1000}\text{-}T)_{6000}$-TxTxT segmented copolymers with increasing even and odd spacing: T2T2T (■), T4T4T (Δ), T6T6T (●), T8T8T (▲), T3T3T (□), T7T7T (○). Reprinted with permission[85] Copyright 2004, Elsevier.

Niesten et al. investigated the tensile and elastic properties of a series of PEEA segmented copolymers, and the investigators found that varying the aramid (TΦT) content in

PTMO based PEEA segmented copolymers yielded a linear increase in Young's modulus typical of segmented copolymers. However, strain at break proved independent of TΦT content and there was also minimal effect on the stress at break. Elasticity of the copolymers appeared to increase with the decrease in TΦT content, but poor mechanical properties occurred at very low concentrations.[86] Biemond et al. investigated the effect of temperature on the tensile properties for a PTMO-T6A6T PEEA segmented copolymer. Insignificant change in the modulus was observed as the temperature increased from 20 to 110 ˚C, which indicated no changes in the polyether matrix. However, yield stress and yield strain systematically decreased with increasing temperature and the strain at break also showed a decrease over this temperature range (Figure 11).[87] Krijgsman et al. demonstrated the tensile properties of PTMO-T6T6T extruded fibers containing various PTMO SS lengths. All the tested fibers exhibited a strain at break >1000% with minimal strain hardening and the modulus and stress at break increased with the increase in T6T6T wt% content.[88] Niesten et al. also proposed that during mechanical deformation, disruption of the crystalline network occurred when large lamellae were deformed into smaller lamellae structures and became oriented perpendicular to the polymer chains. The oriented lamellae then broke down further into square crystallites, which orient parallel to the chain direction and lead to eventual film fracture (Figure 12).[89]

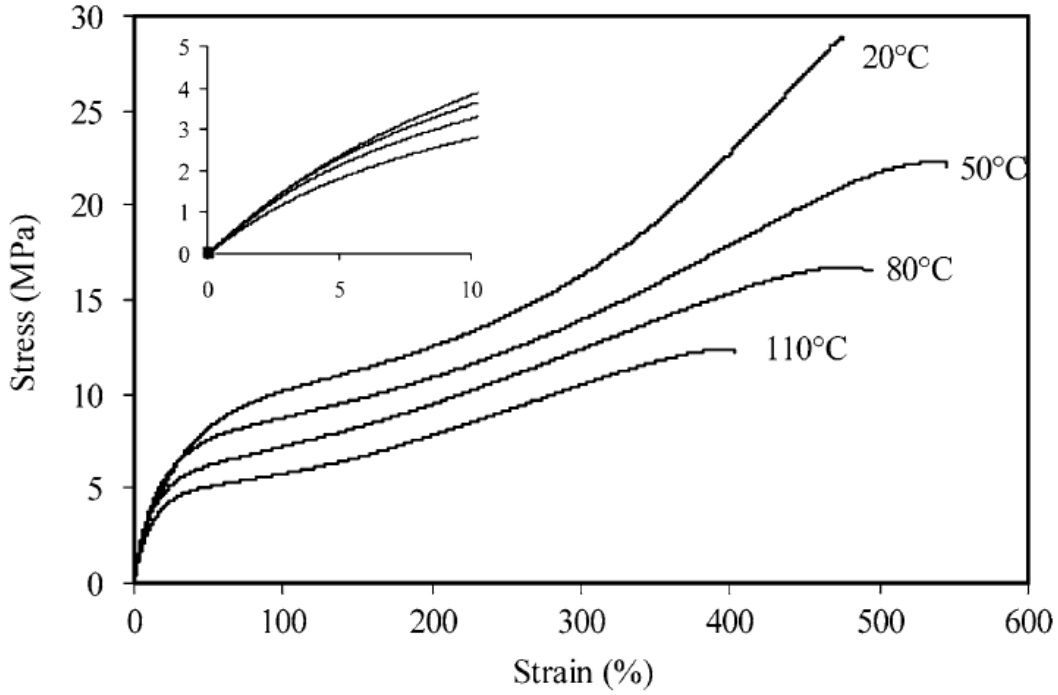

Figure 11. Effect of temperature on the stress-strain curves of PTMO2000-T6A6T segmented copolymers. Reprinted with permission[87] Copyright 2008, Springer.

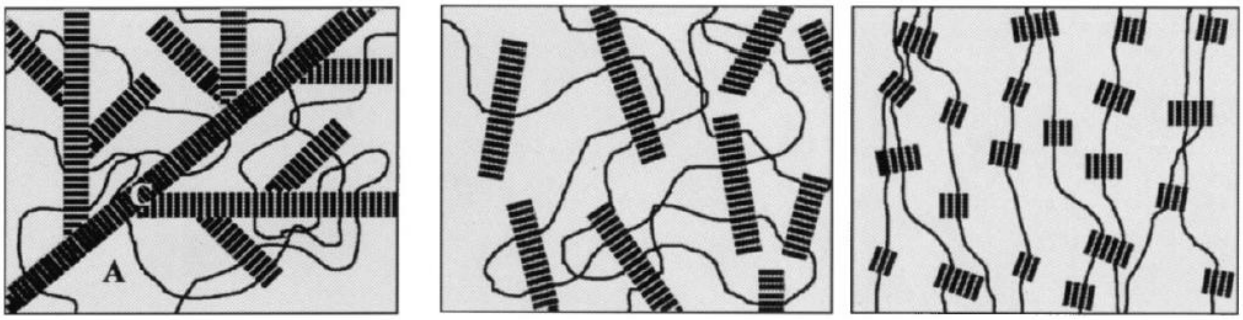

Figure 12. Schematic representation of the microstructural changes upon mechanical deformation for PTMO-TΦT segmented copolymers. Reprinted with permission[89] Copyright 2001, Elsevier.

The studies described here have been comprehensive on the incorporation of low amounts of monodisperse crystallizable hard segments into a polyether soft matrix. Highly elastic materials were formed and the structure-property relationships were derived for these copolymers. Although the elastic behavior of these materials was studied in great detail, the full material spectrum of these copolymers has been glanced over due to the limited incorporation of hard segment (typically >20%). Currently, the literature is lacking in the higher incorporation percentages of hard segments and investigation into an inverted morphology. Quite possibly this would result in a rubber-toughened engineering thermoplastic, and thereby increasing the utility of the PEEA copolymers. Furthermore, the literature touts the chemical resistance of these elastomeric materials, but does not provide sufficient evidence for this claim. It is expected that the solvent resistance would be increased due to the introduction of crystallinity into amorphous polyethers, however, further investigation into the solvent resistance of these copolymers should be considered. With plausible applications such as elastic fibers, the hydrolytic stability of these amide-containing copolymers is of concern. Although the amide segments are, for the majority, in a crystalline state, the increased hydrophilicity observed could indicate issues with high temperature applications. Finally, blending of polyamides with polyethers using these copolymers could elucidate compatibilization of the PEEA's. Perhaps the crystalline phase will act as a physical anchor into the polyamide homopolymer and reduce interfacial failure between polyamide and polyether.

2.6 Poly(ester amide) Segmented Copolymers

Poly(ester amide) (PEA) segmented copolymers are another class of segmented copolymers containing ester groups, except that PEAs utilize long polyester segments that function as the copolymer SS. Aliphatic polyesters typically demonstrate poor physical and

mechanical properties, but incorporation of amide segments into the polyester backbone, as with PEA copolymers, provides a useful segmented copolymer. PEA copolymers exhibit TPE behavior and tunable properties through changes in copolymer composition.[90] PEAs also demonstrate favorable properties of both polyesters and PA including degradability, excellent toughness, and good processing properties. The biodegradation of PEA segmented copolymers serves as a driving force for the development and understanding of more environmentally friendly plastics as a result of the growing issue of plastic waste in the environment.[91] Besides PEA TPE applications, copolymers also showed promise for biomedical applications because of biocompatiblility, and tunable biodegradation rates.[92] Lips et al. reported the *in vivo* use of aliphatic PEA copolymers as biodegradable implants, which slowly degraded over time through ester bond cleavage illustrating the suitability of PEAs as biomedical implants.[93] Pang et al. developed functionalized, water soluble PEA copolymers based on L-arginine, DL-2-allylglycine, oligoethylene glycol, and an aliphatic diacid. *In vitro* toxicity studies revealed no cytotoxicity after exposure to the PEA segmented copolymers, again supporting the potential biomedical applications of the copolymers and their derivatives.[94]

Synthesis of poly(ester amide) segmented copolymers included melt polymerization of a small diester, aliphatic diol, and oligoamide monomers such as dimethyl terephthalate, hexanediol, and T6T6T-dimethyl for example (Scheme 3). Melt polymerization proceeded with all monomers in the reaction flask under inert atmosphere with a catalyst, such as $Ti(i\text{-}OCH_3)_4$, and heated to ~180 ˚C. Increasing the polymerization temperature to ~ 250 ˚C and applying a low vacuum removed the excess hexane diol to achieve high molecular weight macromolecules. Lastly, increasing the temperature again 10 to 20 ˚C and placing the polymerization under a high vacuum further drove the polymerization to completion.[95] The use of diisocyanates was also

useful for synthesis of PEA segmented copolymers. Jeong et al. demonstrated the polycondensation of 4,4'-methylenediphenyl diisocyanate, diacid poly(ester) oligomers, and aliphatic dicarboxylic acids in solution at 200 ˚C, which yielded elastomeric films with good tensile properties.[96] Another route for polycondensation of PEA segmented copolymers included the use of biocatalytic methods for polymerization. Synthesizing poly(dimethyl siloxane) based PEAs through a bulk polymerization strategy with an immobilized *Candida antartica* Lipase B (Novozym 435), which catalyzes the polymerization of a diester, diamine, and aliphatic diol afforded a useful PEA segmented copolymer. However, amide formation occurred faster with this polymerization strategy and led to a block-like sequence distribution within the copolymers.[97, 98]

Scheme 3. Melt polymerization of PEA segmented copolymer composed of poly(hexamethylene terephthalate) and T6T6T. Reprinted with permission[95] Copyright 2010, John Wiley and Sons.

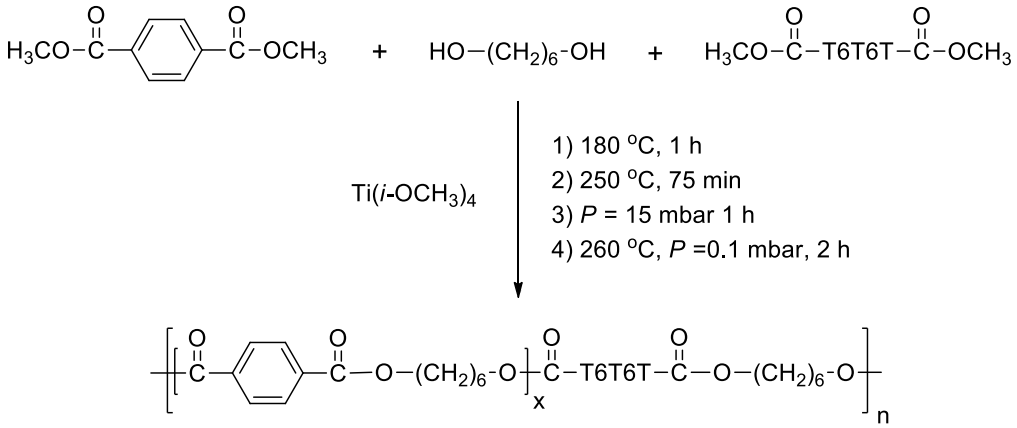

Anionic ring-opening polymerization (ROP) strategies utilizing ϵ-caprolactone (CLO) and ϵ-caprolactam (CLA) also provided excellent PEA segmented copolymers. Chromcová et al. reported the anionic ROP of CLO and CLA using a polymerization casting technique at 150 ˚C with 1 mol% CLA-MgBr initiator that provided tough PEA copolymers.[99] Similarly, Bernášková

et al. demonstrated the preparation of PEA copolymers through anionic ring-opening polymerization of CLA in the presence of poly(ϵ-caprolactone) (PCLO) at temperatures ranging from 90 to 180 ˚C. Anionic ring-opening polymerization of CLA and PCLO initiated with solid CLA-MgBr yielded ductile films with reduced tensile properties compared to PEA copolymers produced from CLA and CLO alone.[100]

Others have reported PEA segmented copolymers possessing a poly(ester) T_g, as well as T_m's of the crystalline polyester and amide-containing HS, suggesting a complex three phase morphology. [95] However, some PEA copolymers that contain non-uniform HS lengths displayed two melting transitions attributed to crystals containing a single ester amide group and those containing 2 or more ester amide groups.[90] The T_g of the poly(ester) SS in PEA copolymers often depended on the copolymer wt% HS content. For example, a PEA segmented copolymer composed of a poly(butylene adipate) (PBA) SS and bisamide HS exhibited an increase in the PBA T_g from -52 ˚C for the homopolymer to -5 ˚C for the PEA containing 85 mol% HS (Figure 13). This change in T_g indicated an increase in phase mixing of the soft polyester segments with the amide HS at higher mol% HS content. The increase in mol% HS also revealed an increase in the HS T_m and DMA onset of flow. [90] The trend of increased T_g and T_m of PEA copolymers with the increase in mol% HS was typically observed for PEA segmented copolymers.[90, 101, 102]

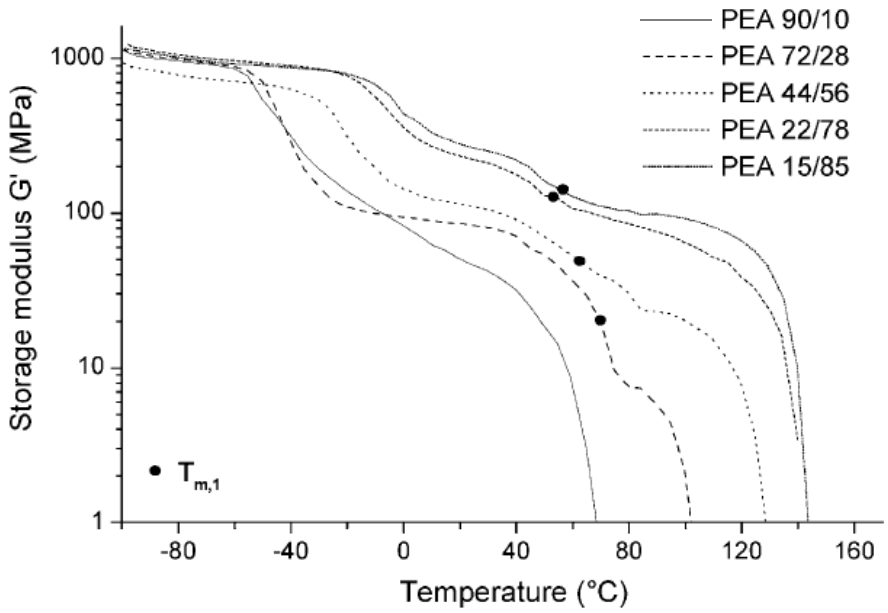

Figure 13. Dynamic mechanical behavior of PEA segmented copolymers with increasing mol% HS (10 – 85%). Reprinted with permission[90] Copyright 2005, Elsevier.

PEA segmented copolymers demonstrate tensile properties typically observed for TPEs with high stress and strain at break. Varying the amide HS content of PEA copolymers allowed for the fine tuning of the tensile properties that a PEA copolymer containing a crystallizable bisamide HS exhibited. For example, varying the molar ratios of bisamide-diol, 1,4-butanediol, and dimethyl adipate resulted in a systematic increase in tensile properties when the HS increased from 10 to 85 mol% (Figure 14). The PBA-bisamide copolymer showed an increase in modulus from 70 to 524 MPa and stress at break from 8 to 28 MPa with a corresponding decrease in the strain at break.[90]

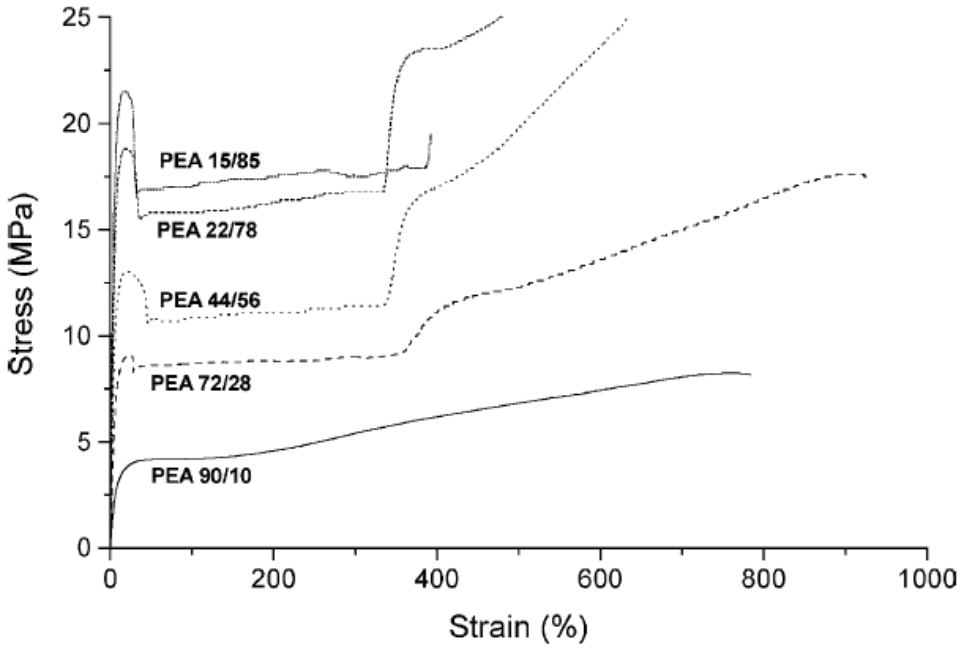

Figure 14. Effect of HS mol% (10 – 85%) on the tensile properties of PBA-bisamide PEA segmented copolymers. Reprinted with permission[90] Copyright 2005, Elsevier.

PEA segmented copolymers with various ratios of CLA and CLO exhibited systematically decreased T_g values with the decrease in lactam units from 48 ˚C for PCLA to -57 ˚C for PCLO. A decrease in the onset of flow occurred with increasing molar ratios of the SS lactone units and copolymers containing 30 to 90% lactone units yielded tough materials.[99] Hydrolytic degradation studies of PEA copolymers comprised of CLA and CLO units showed degradation in phosphate buffer occurred through ester bond cleavage. When compared to CLO homopolymers, PEA copolymers composed of CLA and CLO demonstrated increased degradation rates of hydrolysis due to the presence of hydrophilic CLA units.[103]

Overall, the structure-property relationships of PEA copolymers were similar to other segmented copolymers with respect to variations in the copolymer HS wt%, and possessed tunable mechanical properties for a wide range of applications. PEAs offer an avenue for a

combination of ester and amide physical characteristics and the literature has provided several good examples of the advantages of this synergy. However, further opportunities exist for exploration. The morphology of these copolymers is substantially lacking as compared to the fields previously discussed in this review. In contrast to the PEEA and PEBA copolymers, a single, composition-dependent T_g seems to be more prevalent, indicating less propensity for phase separation. Exploration into the cause of such a discrepancy would reveal a better understanding of the physical constraints offered by these PEA copolymers.

Several different, and creative synthetic methods have been shown as plausible paths to afford the segmented PEA's, but only a few examples of the possible library of polymer structures has been explored. Utilizing other commercially available monomers could provide better phase separation or lower water sorption properties. Also, adjusting the topology from linear to branched, crosslinked or dendritic structures invites entirely new fields of materials. The current field is in its infancy and would benefit from adopting studies developed for other amide-containing segmented block copolymers.

2.7 Poly(oxamide) Segmented Copolymers

Oxamide groups are a specific type of hydrogen bonding moiety that contain two adjacent amide groups covalently bonded. Studies have shown that oxamide groups exhibit strong hydrogen bonding interactions and form semi-crystalline nanostructures in some cases.[104, 105] The oxalate precursors provide increased reactivity toward amines compared to traditional esters and the oxamide functionality allows for development of unique hydrogen bonding structures for segmented copolymers (Figure 15). Few examples currently exist in literature that describes the synthesis and properties of oxamide-containing segmented copolymers. Schulze first reported the synthesis of poly(oxamide) segmented copolymers in a 1978 patent that

described the methods for synthesis of PPG poly(oxamide) segmented copolymers.[106] Leir et al. published patents in 2007 that detailed the synthesis and processing methods for PDMS poly(oxamide) segmented copolymers, which yielded optically clear TPEs with shore A hardness values from 14 to 88 depending on copolymer composition.[107-110] More recently, Sajbrandi et al. published a report for the synthesis and characterization of PTMO poly(oxamide) segmented copolymers, which provided insight into the structure-property relationships of poly(oxamide) segmented copolymers containing monodisperse oxamide segments.[111, 112] Furthermore, our recent research has focused on the development and understanding of poly(oxamide) segmented copolymers through detailed structure-property relationship studies, and synthesis of novel oxamide-containing segmented copolymers.[113-115]

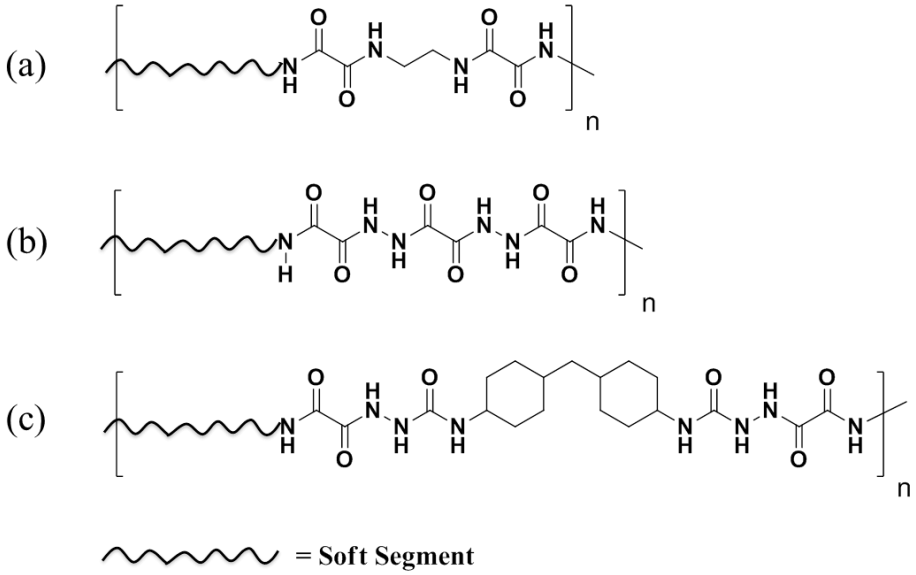

Figure 15. Hard segment structures of (a) poly(oxamide), (b) poly(trioxamide), and (c) poly(urea oxamide) segmented copolymers.

The most common source of oxamide groups for the synthesis of poly(oxamide) segmented copolymers is diethyl oxalate. All published poly(oxamide) copolymers are

comprised of an oligomeric SS and oxamide-containing HS of uniform length. Preparation of poly(oxamide) copolymers began with the end-capping of amine-terminated polyethers or PDMS oligomers with an excess of diethyl oxalate in the bulk from 0 to 23 ˚C or solution at 23 ˚C, which yielded difunctional ethyl oxalate terminated oligomers. After removal of excess diethyl oxalate, step-growth polymerization with a 1:1 stoichiometric amount of diamine provided the desired poly(oxamide) segmented copolymer (Scheme 4).[111, 113] Depending on the nature of the reactants, polymerization of ethyl oxalate terminated oligomers with diamines required various polymerization temperatures. Ethyl oxalate terminated PDMS oligomers efficiently polymerized with diamines from 23 to 120 ˚C without catalyst and afforded optically clear, elastic films.[114] PTMO based poly(oxamide) copolymers were melt polymerized at 190 to 250 ˚C with a $Ti(OBu)_4$ catalyst and resulted in yellow, transparent films.[111] Other oxamide-containing segmented copolymers recently developed included PDMS poly(urea oxamide) and PPG poly(trioxamide). These novel copolymers were obtained through solution polymerization of oxamic hydrazide terminated oligomers with 4,4′-methylenebis(cyclohexyl isocyanate) (HMDI) or oxalyl chloride (Scheme 5).[113, 115]

Scheme 4. Synthesis of PTMO polyoxamide segmented copolymers. Reprinted with permission[111] Copyright 2012, Elsevier.

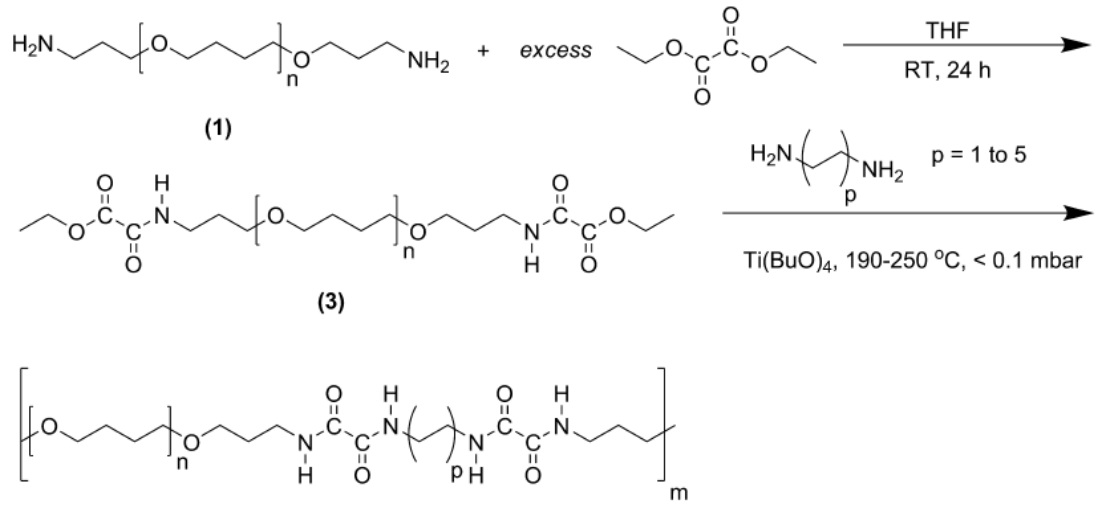

Scheme 5. Synthesis of PDMS polyoxamide segmented copolymers.

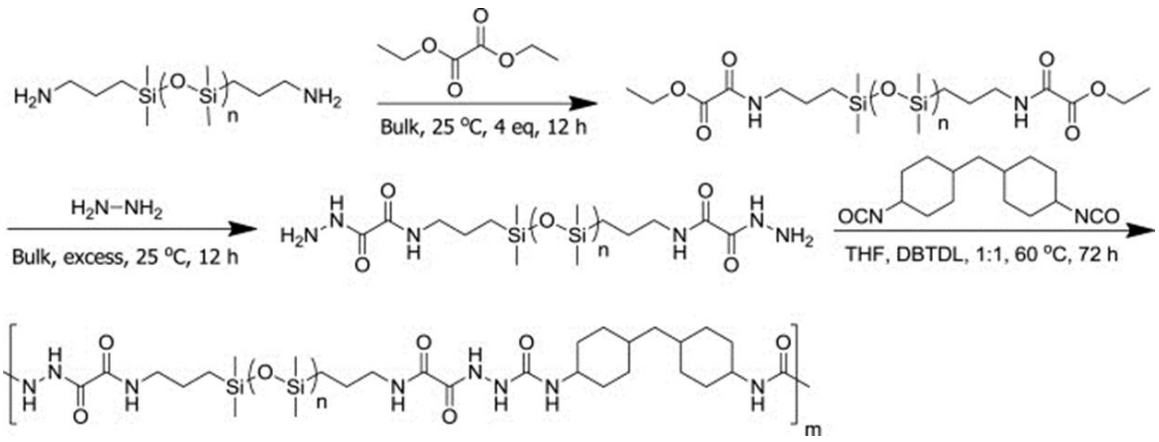

Poly(oxamide) segmented copolymers exhibited microphase-separated bulk morphologies. The bisoxamide HS formed hydrogen bonding physical crosslinks and possessed a semi-crystalline nanostructure observed with DSC, WAXD, and AFM (Figure 16). Melting of the crystalline bisoxamide HS domains resulted in the onset of flow for each copolymer. PTMO based poly(oxamide)s also showed a high moduli >120 MPa with stress and strain at break up to 27 MPa and 900%, respectively.[111] Poly(oxamide) copolymers based on PDMS demonstrated a Young's modulus, stress at break, and strain at break of 96 MPa, 8 MPa, and 940%, respectively. However, copolymer composition and level of crystallinity greatly affected the mechanical properties.[114] DMA revealed long, temperature-insensitive, service windows up to 180 ˚C for

PDMS poly(oxamide) copolymers, and the rubbery plateau length and storage moduli varied with copolymer composition (Figure 17).[111, 113, 114]

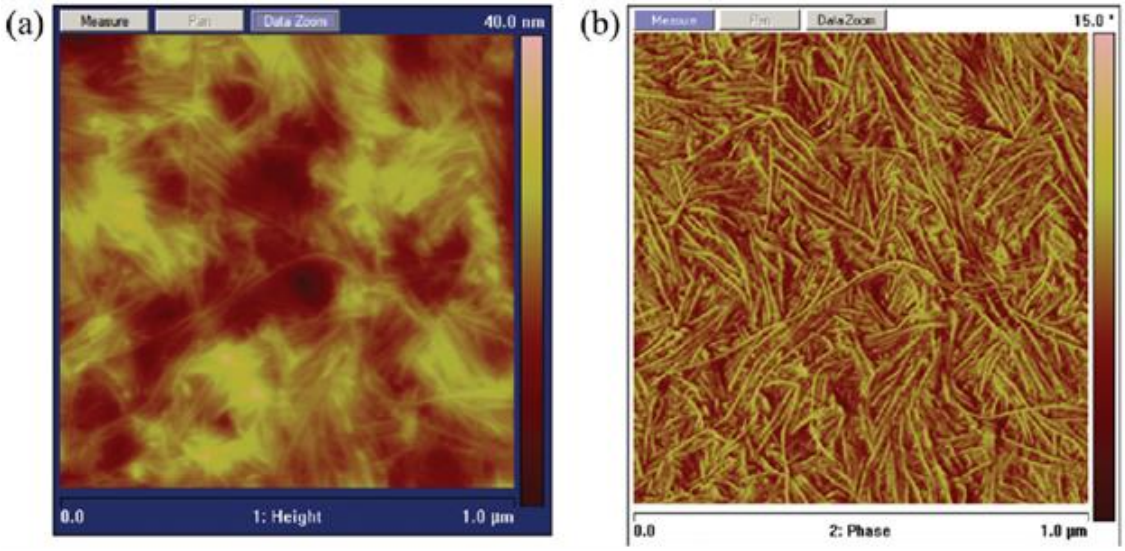

Figure 16. AFM (a) height and (b) phase image of PTMO poly(oxamide) segmented copolymer containing two oxamide groups in the HS. Reprinted with permission111 Copyright 2012, Elsevier.

Recent reports include the structure-property relationships of poly(oxamide) copolymers for both PTMO and PDMS based copolymers. The distance between oxamide groups and number of oxamides in the HS resulted in large differences in the mechanical properties of the copolymers. Sijbrandi et al. demonstrated that two oxamide groups in the HS provided sufficient physical crosslinking to impart microphase separation and copolymers that contain a single oxamide group exhibited poor mechanical properties due to insufficient physical crosslinking. Increasing from two to three oxamide groups in the HS caused an increase in the onset of flow temperature and storage modulus, but resulted in negligible gains in tensile properties over the two oxamide-containing copolymers.[111] Spacing between oxamide groups also proved

important, and the most significant effects were observed in PDMS-based copolymers. As oxamide spacing increased, the T_m and onset of flow decreased due to a reduction in the cooperative effects of neighboring hydrogen bonds.[111, 114] This effect was clearly illustrated by variable temperature FTIR spectroscopy, which revealed the order-to-disorder transition for hydrogen bonding occurred at lower temperatures as the oxamide spacing increased (Figure 18). A reduction in the tensile properties, and increased hysteresis also occurred as a result of the increase in distance between oxamide groups.[114] The structure-property relationship studies of poly(oxamide) segmented copolymers suggested that short, even spaced oxamide linkers provide optimal physical properties.

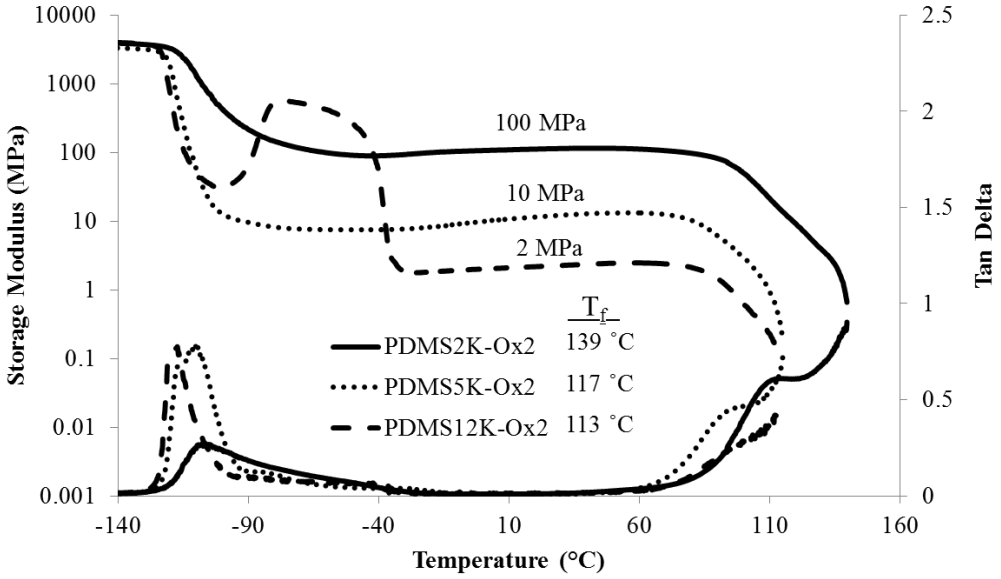

Figure 17. DMA traces of PDMS poly(oxamide) copolymers with PDMS2000, PDMS5000, and PDMS12000 SS. Reprinted with permission114 Copyright 2013, Elsevier

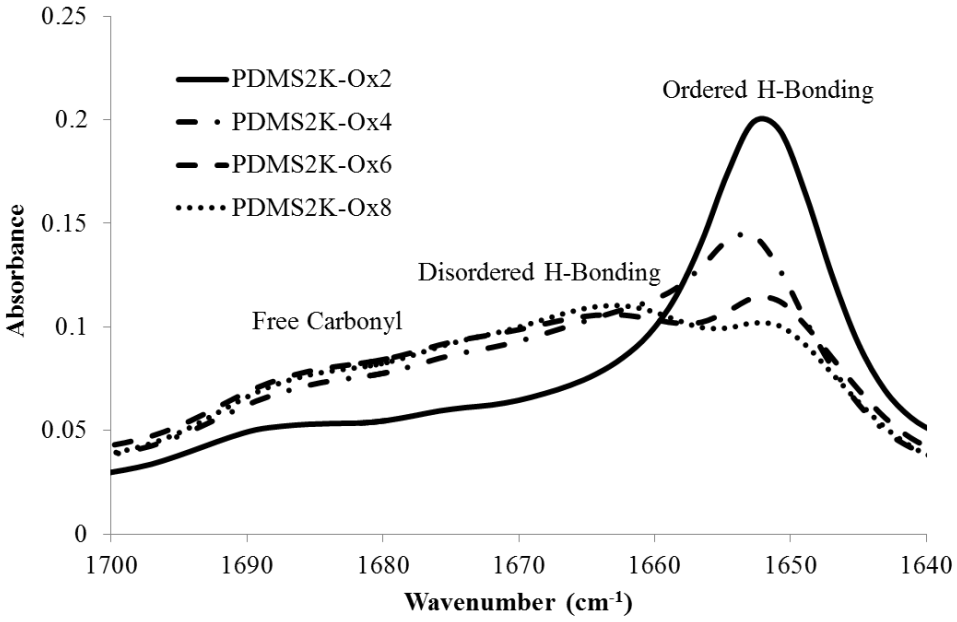

Figure 18. FTIR spectra at 100 ˚C of PDMS2000 poly(oxamide) segmented copolymers with 2, 4, 6, and 8 methylene groups between oxamides in the HS. Reprinted with permission114 Copyright 2013, Wiley

The recent development of poly(urea oxamide) copolymers represents a new family of segmented copolymers. These copolymers comprised of a HS of oxamide and urea hydrogen bonding groups which are covalently bonded together. Poly(urea oxamide) segmented copolymers yielded tough, elastic films with superior tensile properties compared to traditional poly(urea) analogs. The enhanced hydrogen bonding of the urea oxamide HS led to increased microphase-separated morphologies, and improved service windows compared to polyurea analogs. Poly(urea oxamide) copolymers also demonstrated a higher Young's moduli and stress at break, but a decrease in the strain at break resulted.[113, 115]

Oxamide-containing segmented copolymers are an important class of TPEs, which possess unique hydrogen bonding motifs leading to tunable thermomechanical, and tensile

properties under mild polymerization conditions. With these materials emerging as a strong competitor for current TPE applications, there is a new scientific frontier to be explored. The unique, hydrogen bonding oxamide segment proves to be advantageous in the design of TPE's with its compatibility under several reaction conditions. Currently only a few hard and soft segments have been utilized. More intricate hard segments that incorporate the oxamide linkage would help to identify the robustness of this commercially available starting material. The ease of reaction on the activated carbonyls, small molecule solubility, and thermal stability provides a platform for developing high performance materials. Future comparative studies of oxamide containing copolymers to the Pebax® and PEEA TPE's would help to categorize the oxamide containing materials, and encourage further structure-property relationships. Reproducing the extensive studies developed for the Pebax® and PEEA copolymers on the oxamide copolymers would promote a fundamental understanding, and expand current applications. For instance, more exploration into the phase behavior of these materials with an emphasis on the SS structure will identify preferable SSs. Furthermore, studies into topological effects on the hydrogen bonding capabilities of the oxamide structure would bring this field into new and exciting avenues.

2.8 Poly(dimethyl siloxane) Poly(amide) Segmented Copolymers

Segmented copolymers comprised of a PDMS SS and amide-containing HS represent a special class when compared to other amide-containing segmented copolymers due to the nature of the PDMS SS. A high degree of incompatibility between PDMS and polar amide-containing HSs exist, and lead to extensive, microphase-separated morphologies with a wide range of physical properties. Applications of PDMS poly(amide) (PDMS-PA) segmented copolymers include adhesives, cosmetics, fabric-finishing agents, anti-cloud coatings, and production of

organic-inorganic hybrid composites.[110, 116-118] PDMS-PA copolymers also provide efficient gas permeable membranes for applications with a membrane-liquid interface due to the high tensile strength and low interface resistance that yields highly oxygen permeable membranes.[119] Studies into the biomedical applicability of PDMS-PA copolymers demonstrated the effects of copolymer composition on surface interactions of various biomolecules as well as compatibility with blood, and PDMS-PA copolymers are inert *in vivo*.[120, 121] A number of PDMS-PA segmented copolymers were reported that included organometallic structural features. For example, two PDMS-PA copolymers containing pendent trichlorogermyl or ferrocene groups both exhibited good thermal and mechanical properties for use as protective coatings.[122, 123] However, a majority of the research conducted on PDMS-PA copolymers included PDMS poly(aramid) (PDMS-PAr) segmented copolymers that Imai et al. introduced in 1989.[124]

McGrath et al. first introduced the synthesis of PDMS-PA segmented copolymers that typically required step-growth polymerization of an amino-alkyl terminated PDMS oligomer with a di-functional monomer.[125] Policastro et al. reported the step-growth polymerization of aminopropyl terminated PDMS with 2,2'-*p*-phenylenebis(4,4-dimethyl-5-oxazolone) in $CHCl_3$, which yielded transparent, elastic films.[126] Another synthetic route to PDMS-PA copolymers involved polycondensation of diester monomers with diamino PDMS oligomers. The polarity differences of PDMS and the polar diester monomer resulted in heterogeneous reactions, often leading to poor polymerization. The most common synthetic route for polymerization included polar diacid chloride monomers with diamino PDMS oligomers.[116, 124] For example, aminophenyl aniline, isophthaloyl chloride, triethylamine, and aminopropyl terminated PDMS successfully polymerized at 0 ˚C in $CHCl_3$ for 1 h and then at 23 ˚C for 5 h under nitrogen atmosphere (Scheme 6). A one or two-step solution polymerization strategy provided the desired

PDMS-PAr copolymers, but the two-step strategy yielded copolymers with more defined microphase-separated morphologies and tensile properties.[124] A similar polymerization strategy utilized 1,3-bis(3-aminopropyl)-l,l,3,3-tetramethyldisiloxane (BATS) for the polymerization of PDMS-PAr, which provided transparent plastic films useful for surface coatings and biomaterial applications.[127] Copolymers containing random sequences of diamino disiloxane and aramid segments yielded tough, single phase materials with reduced tensile properties over the phase separated copolymers.[128]

Scheme 6. Synthesis of PDMS-PAr segmented copolymers through a one or two-step polymerization scheme. Reprinted with permission[124] Copyright 1989, American Chemical Society.

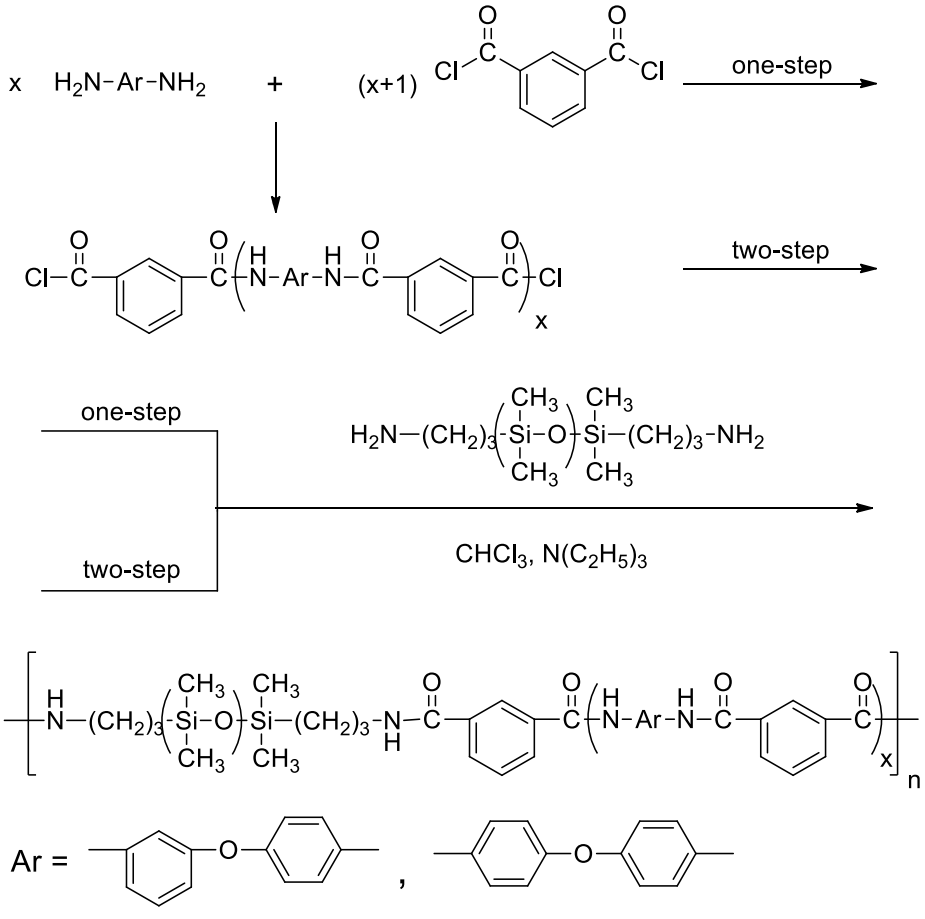

The microphase-separated bulk morphologies of PDMS-PA segmented copolymers change with variations in copolymer composition.[129, 130] The surface of PDMS-PA segmented copolymers contained primarily only PDMS SS, even at lower PDMS wt% composition due to the low PDMS surface energy. The phase-separated bulk morphology resided deeper in the films, which resulted in the observed mechanical properties.[131] Randomly sequenced aramid HS of PDMS-PAr copolymers exhibited high T_g values ranging from 150 to 240 ˚C, but depended on wt% HS content and length of aramid HS. Copolymers with alternating hard and soft segments showed only a PDMS T_g (-123 ˚C) and the lack of aramid T_g is attributed to the semi-crystalline nature of the uniform aramid HS.[132] The dynamic mechanical behavior of PDMS-PAr revealed a relatively temperature-insensitive rubbery plateau with storage moduli that decreased with an increase in the PDMS wt% content (Figure 19). Molecular weight of the aramid HS sequence, or PDMS wt%, ultimately determined the temperature for the onset of flow of each PDMS-PAr copolymer. The highest temperature for the onset of flow results with the lowest PDMS wt% copolymer composition and gradually decreases as the PDMS content increases.[133]

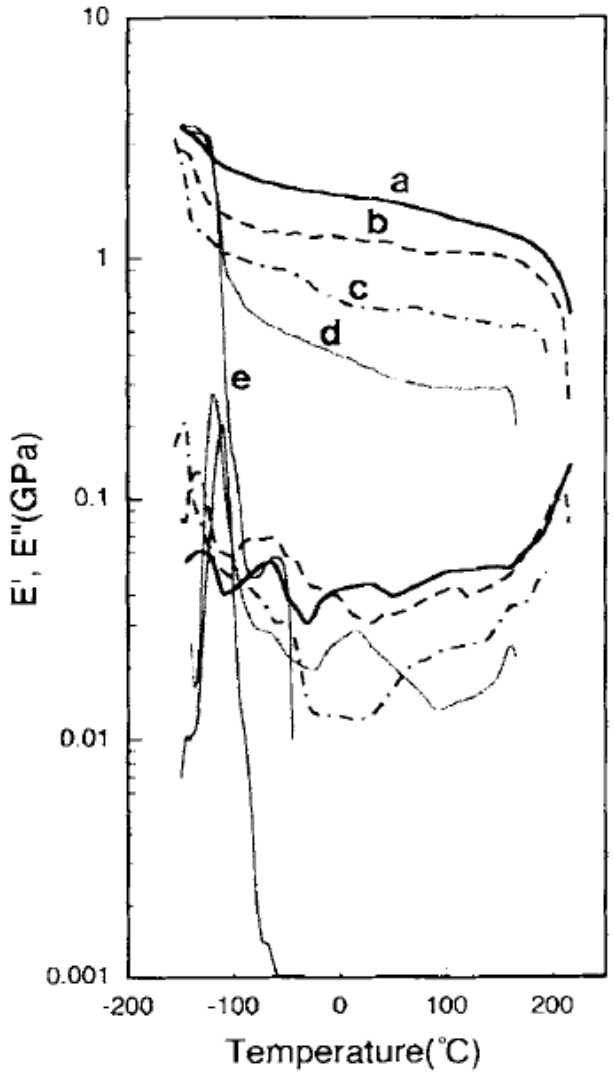

Figure 19. DMA of PDMS-PAr segmented copolymers at a PDMS wt% content of (a) 26 wt%, (b) 35 wt%, (c) 46 wt%, (d) 53 wt%, and (e) 75 wt%. reprinted with permission[133] Copyright 1998, John Wiley and Sons.

Regularity of aramid HSs in PDMS-PAr copolymers also had a significant impact on tensile properties. Copolymers composed of random HS sequences demonstrated an increase in stress at break with the decrease in copolymer PDMS content with values ranging from 54 to 6 MPa for PDMS-PAr copolymers containing 20 to 73 wt% PDMS (1680 g/mol), respectively.

Copolymer moduli increased and strain at break decreased with the decrease in copolymer PDMS content. Copolymers that possessed a uniform aramid HS exhibited lower moduli and stress at break than the randomly sequenced HS counterparts, but show a large increase in the strain at break.[132] An aramid homopolymer, composed of 3,4'-diaminodiphenyl ether and isophthaloyl chloride, demonstrated a very high stress at break of ~100 MPa and an elongation similar to a PDMS-PAr containing 55 wt% SS.[119] Generally for PDMS-PA segmented copolymers, lower PDMS wt% content leads to increased stress at break and moduli. The PDMS-PA copolymers prove to be an advantageous material to pursue, however more exploration into hard segments is needed to establish similar structure-property relationships observed in analogous amide-containing segmented copolymers. Also, adaptation of the extensive studies provided in the other amide-containing segmented copolymers would broaden the collective understanding of these copolymers and drive the development of application-specific PDMS-PA materials.

2.9 Poly(amide) Segmented Copolymers Containing Urethane, Urea, and Imide Groups

Many examples of segmented PA copolymers containing other hydrogen bonding groups exist in literature such as poly(amide ester imide) (PAEI)[134], poly(amide imide urethane) (PAIU)[135], poly(amide urethane) (PAU), poly(ester urethane amide) (PEUA)[136] and poly(urethane urea amide) (PUUA)[137] segmented copolymers. Applications for these types of PA segmented copolymers include electrical insulating materials, circuit board materials, chiral phases for enantiomeric separations, protective coatings, and slowly biodegrading materials.[136, 138-140] Some of these segmented copolymers also find applications as biomedical devices. For example, PUUA segmented copolymers composed of a polyether SS showed promising

properties for antithrombogenic applications due to favorable surface properties of the copolymer and the ability to tune the surface properties through structural variation.[141]

A wide range of synthetic strategies enabled the production of these segmented copolymers. Synthesis of PEG-containing PAEI segmented copolymers with a carboxylic acid terminated imide-PEG-imide oligomer and various aromatic diamines occurred through solution polymerization in a mixture of pyridine, NMP, TPP, and $CaCl_2$ as a condensing agent.[134] Mallakpour et al. reported the two-step synthesis of PAIU segmented copolymers that contained a PEG SS through a pre-polymerization method in NMP with no catalyst.[135] Novel amide imide diacid monomers containing various chiral amino acids and excess MDI afforded a pre-polymer that were subsequently polymerized with a PEG diol to yield a ductile, free-standing film.[142] Baez et al. formed a prepolymer with PCL diol and 1,6-hexanediisocyanate in DMAc at 80 ˚C to synthesize PEUA copolymers. Chain extension in DMAc with a diamide-diol monomer provided the final PEUA copolymer and a ductile film is obtained after solution casting.[140] Using a amide-diamine chain extender instead of amide-diol, and the same prepolymer method for the preparation of PUUA segmented copolymers resulted in an excellent TPE with a service window exceeding 250 ˚C.[137]

PAEI segmented copolymers containing a PEG SS were highly soluble copolymers with good thermal stability. DSC and XRD of the PAEI copolymers revealed a single T_g and semi-crystalline HS domains.[134] Optically active PAIU segmented copolymers containing a polyether SS demonstrated higher thermal stability compared to poly(ether urethane) copolymers with 10% weight loss observed at ~300 ˚C. PAIU copolymers also revealed two T_gs, one for both the SS and HS, as well as evidence of a phase-mixed morphology despite the semi-crystalline nature of the HS.[139] The amide-imide diacid structure greatly affected the thermal stability of PAIU

copolymers and copolymers that contained 4,4'-(hexafluoroisopropylidene)-*N*,*N*-bis(phthaloyl-leucine-*p*-amidobenzoic acid) HS content showed the poorest thermal stability.[143] Even though polyether based PAIU segmented copolymers exhibited microphase-separated morphologies, the films lacked a temperature-insensitive rubbery plateau region in the DMA. The thermomechanical behavior and flow temperature of PAIU copolymers are highly dependent on the type of polyether SS used as well as the HS wt% content.[139]

PEUA segmented copolymers based on PCL were elastic, microphase-separated copolymers with biodegradable amide linkages. Copolymers exhibited a T_m for both segments and the HS T_m increases with the increase in HS wt%. The PCL based PEUA copolymers showed good tensile properties with elongation values at lower wt% HS content to 1500%. Stress at break did not significantly change with HS wt% unlike the moduli, which increased with higher HS wt% from 37 to 210 MPa.[140] Van der Schuur et al. investigated the structure-property relationships of PUUA segmented copolymers that particularly focused on the length of the amide HS (hexamethylenediamine, 6T6, and 6T6T6). PUUA copolymers containing 6T6 HS exhibited microphase separation through crystallization, similar to the PEEA segmented copolymers previously discussed. DMA showed an increase in the onset of flow and service window storage moduli for PUUA copolymers with increased HS length (Figure 20). Copolymers that contained 6T6 HS exhibited enhanced tensile properties over the hexamethylenediamine HS and superior thermomechanical behaviors compared to a commercial thermoplastic urethane.[137] The presence of amide groups in the hard segment of PUUA copolymers imparted improved mechanical strength and energy dissipation due to higher amounts of HS interconnectivity when compared to poly(urethane urea) analogs.[144]

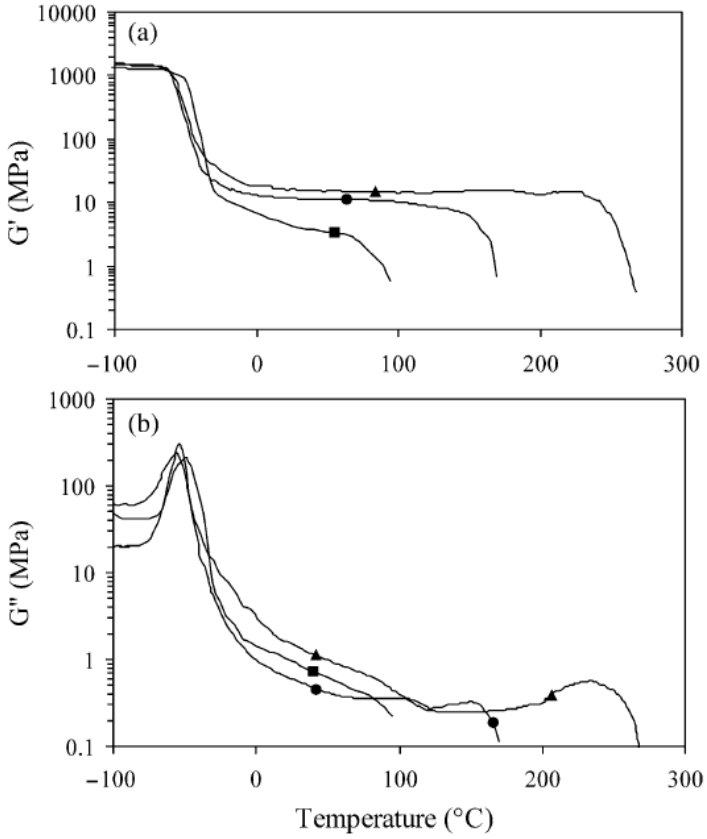

Figure 20. Effect of amide HS length on the (a) storage modulus and (b) loss modulus of PUUA segmented copolymers: HMDA (■), 6T6 (●), 6T6T6 (▲). Reprinted with permission[137] Copyright 2006, Elsevier.

As evidenced by the wide range of structures obtained in previous reports, amide-containing segmented copolymers have the ability to enhance tensile, chemical resistance, thermomechanical, and biocompatibility over the current commercial materials. A wide range of structures have been illustrated, and more can be envisioned beyond the current literature. Only a few soft segments have been utilized in each of the above cases, and further studies on soft segment effects on these amide-containing copolymers would help in the translation of the complex structures into current applications. Also, the field would benefit from a comparative study on the effect each hydrogen bonding moiety has on the resulting physical properties. The

above materials are very complex in structure, and the competitive or cooperative hydrogen bonding between urethanes, amides, imides and ureas is suspected. Understanding the chemical interaction of these linkages may enlighten the drastic changes in physical properties observed between each of these materials.

2.10 Conclusions and Outlook

Amide hydrogen bonding groups in segmented copolymers play an important role in determining the thermal and mechanical properties of PA segmented copolymers. The strong hydrogen bonding intermolecular interactions of amide groups provide the physical crosslinks necessary for imparting microphase-separated morphologies. The ability and strength of amide HS hydrogen bonding relies primarily on the structure of the HS and number of amide groups present. The extent of crystallinity that an amide HS possesses also significantly affects the microphase separation, mechanical properties, thermal stability, and appearance of the segmented copolymer. Multiple researchers demonstrated a wide range of copolymer physical properties and potential applications through changes in copolymer composition. Variations in the soft segment structure (PEG, PPG, PTMO, PDMS, polyester, PPE) as well as the molecular weight greatly influenced copolymer performance. The literature contains reports of a wide variety of segmented copolymers with various amide HS architectures, ranging from aramids to oxamides and exemplifies the potential for tuning segmented copolymers through structural modifications.

Poly(ether-*block*-amide) (PEBA) segmented copolymers are high performance thermoplastic elastomers with excellent physical properties such as high tensile strength, large workable temperature windows, chemical resistance, and good processability. Synthesis of PEBA segmented copolymer is well developed and provides a method for synthesis of a wide

variety of PEBA structures. A large and diverse number of applications for PEBA copolymers will exist as new structures and physical properties are realized. New copolymer architectures and the use of organic and inorganic modifying agents will open new horizons for PEBA segmented copolymers. Poly(ether ester amide) (PEEA) copolymers possess many options for new structural copolymers based upon current understanding of the structure-property relationships of PEEA segmented copolymers. PEEA copolymers have excellent elastomeric, tunable physical properties aligned with many commercial applications. The ability to alter surface chemistry and subsequent properties showed promise for biomedical applications. Poly(ester amide) (PEA) copolymer also exhibited biocompatibility and biodegradable rates desirable for various biomedical applications. The biodegradability, in conjunction with good physical toughness, provides a strong platform for further investigation into the structure-property relations of novel PEA copolymers.

Poly(oxamide) segmented copolymers represent a relatively unexplored family of polymers, and demonstrate excellent elastomeric properties derived from unique structural aspects. Recent studies into the structure-property relationship of poly(oxamide) copolymers reported excellent thermoplastic elastomer behavior with the ability to tune elastomeric properties through polymer structural modifications. Examples of current applications are limited because of their relatively recent discovery, but many emerging technologies could benefit from the persistent oxamide structure. Poly(oxamide) segmented copolymers demonstrate processability, however, a thorough investigation into the extent these copolymers can be processed is needed.

Poly(dimethyl siloxane) (PDMS) segmented copolymers offer excellent properties with well understood polymerization chemistry. The unique properties of PDMS imparts enhanced

physical properties including flexibility, gas permeation, and chemical resistance, which are useful for many commercial applications including thermoplastic adhesives, textiles, separation membranes, and coatings. New HS structures are needed for PDMS segmented copolymers to develop the next generation of PDMS-based high performance materials. Amide-containing segmented copolymers composed of multiple hydrogen bonding groups in conjunction with amides proved useful in developing novel segmented copolymers with unique and tunable physical properties. Many of these copolymers, which include esters, urethanes, ureas, and imides, exemplify the copolymer structural possibilities, and several combinations of polymerization chemistries have resulted in advantageous material properties. As a result, new hydrogen bonding sequences, and topological variations (e.g., branching) developed under alternate reaction scenarios will influence phase separation and improve mechanical properties. Despite the extensive research reported on amide-containing segmented copolymers, there still exist a plethora of research avenues to be explored. For example, more rheological analysis and variable-temperature FTIR spectroscopy to probe the kinetics of phase separation would build a stronger understanding of the influence of hydrogen bonding on phase behavior. Collectively, the current understanding of the structure-property relations for amide-containing segmented copolymers provides a large toolbox for future development of new segmented copolymers with properties easily tuned for specific applications.

2.11 References

1. Castagna, A. M.; Pangon, A.; Choi, T.; Dillon, G. P.; Runt, J. The Role of Soft Segment Molecular Weight on Microphase Separation and Dynamics of Bulk Polymerized Polyureas, *Macromolecules* **2012,** 45, (20), 8438-8444.

2. Chakrabarty, S.; Nisenholt, M.; Wynne, K. J. PDMS-Fluorous Polyoxetane-PDMS Triblock Hybrid Elastomers: Tough and Transparent with Novel Bulk Morphologies, *Macromolecules* **2012,** 45, (19), 7900-7913.
3. ten Cate, A. T.; Sijbesma, R. P. Coils, rods and rings in hydrogen-bonded supramolecular polymers, *Macromol. Rapid. Comm.* **2002,** 23, (18), 1094-1112.
4. van der Schuur, M. J.; Gaymans, R. J. Influence of morphology on the properties of segmented block copolymers, *Polymer* **2007,** 48, (7), 1998-2006.
5. Camberlin, Y.; Pascault, J. P. Phase segregation kinetics in segmented linear polyurethanes - relations between equilibrium time and chain mobility and between equilibrium degree of segregation and interaction parameter, *J. Polym. Sci. Pol. Phys.* **1984,** 22, (10), 1835-1844.
6. Versteegen, R. M.; Sijbesma, R. P.; Meijer, E. W. Synthesis and characterization of segmented copoly(ether urea)s with uniform hard segments, *Macromolecules* **2005,** 38, (8), 3176-3184.
7. Fang, J.; Tanaka, K.; Kita, H.; Okamoto, K.-I.; Ito, Y. Positron annihilation properties of copolyimides and copolyamides with microphase-separated structures, *J. Polym. Sci. Pol. Phys.* **2000,** 38, (9), 1123-1132.
8. Mallakpour, S.; Rafiemanzelat, F. Study of the Miscibility of Hard and Soft Segments of Optically Active Poly(amide-imide-ether-urethane) Copolymers based-L-Leucine with Different Soft Segments, *Polym. Bull. (Heidelberg, Ger.)* **2006,** 56, (1), 9-18.
9. Okoroafor, E.; Rault, J. Cryodilation of thermoplastic PEBA elastomers, *J. Polym. Sci. Pol. Phys.* **1991,** 29, (11), 1427-1436.

10. Tavernier, B.; Mewis, J.; Van Puyvelde, P.; Takenaka, M.; Ernst, B.; Hashimoto, T. Effect of thermomechanical history on the crystallization of poly(ether-block-amide), *Polym. Eng. Sc.* **2008,** 48, (12), 2418-2425.
11. Dodge, J., Polyurethanes and polyureas. In *Synthetic Methods in Step-growth Polymers*, Rodgers, M., Long, TE, Ed. John Wiley & Sons, Inc.: Hoboken, NJ, 2003; pp 197-263.
12. Yilgor, I.; Eynur, T.; Bilgin, S.; Yilgor, E.; Wilkes, G. L. Influence of soft segment molecular weight on the mechanical hysteresis and set behavior of silicone-urea copolymers with low hard segment contents, *Polymer* **2011,** 52, (2), 266-274.
13. Mark, J. E. Some interesting things about polysiloxanes, *Accounts. Chem. Res.* **2004,** 37, (12), 946-953.
14. Das, S.; Yilgor, I.; Yilgor, E.; Wilkes, G. L. Probing the urea hard domain connectivity in segmented, non-chain extended polyureas using hydrogen-bond screening agents, *Polymer* **2008,** 49, (1), 174-179.
15. Krijgsman, J.; Feijen, J.; Gaymans, R. J. Segmented copolymers of uniform tetra-amide units and poly(phenylene oxide): 3. Influence of tetra-amide content, *Polymer* **2004,** 45, (25), 8523-8530.
16. Korley, L. T. J.; Pate, B. D.; Thomas, E. L.; Hammond, P. T. Effect of the degree of soft and hard segment ordering on the morphology and mechanical behavior of semicrystalline segmented polyurethanes, *Polymer* **2006,** 47, (9), 3073-3082.
17. Pukánszky Jr, B.; Bagdi, K.; Tóvölgyi, Z.; Varga, J.; Botz, L.; Hudak, S.; Dóczi, T.; Pukánszky, B. Nanophase separation in segmented polyurethane elastomers: Effect of specific interactions on structure and properties, *Eur. Polym. J.* **2008,** 44, (8), 2431-2438.

18. Jewrajka, S. K.; Yilgor, E.; Yilgor, I.; Kennedy, J. P. Polyisobutylene-based segmented polyureas. I. Synthesis of hydrolytically and oxidatively stable polyureas, *J. Polym. Sci. Pol. Chem*. **2008,** 47, (1), 38-48.
19. Tang, D.; Mulder, D.-J.; Noordover, B. A. J.; Koning, C. E. Well-defined Biobased Segmented Polyureas Synthesis via a TBD-catalyzed Isocyanate-free Route, *Macromol. Rapid Commun.* **2011,** 32, (17), 1379-1385.
20. June, S. M.; Suga, T.; Heath, W. H.; Long, T. E.; Lin, Q.; Puligadda, R. Photo-Reactive Polyimides and Poly(siloxane imide)s as Reversible Polymeric Interfaces, *J. Adhesion.* **2010,** 86, (10), 1012-1028.
21. Xi, K.; Meng, Z.; Heng, L.; Ge, R.; He, H.; Yu, X.; Jia, X. Polyimide–polydimethylsiloxane copolymers for low-dielectric-constant and moisture-resistance applications, *J. Appl. Polym. Sci.* **2009,** 113, (3), 1633-1641.
22. June, S. M.; Bissel, P.; Long, T. E. Segmented block copolyesters using click chemistry, *J. Polym. Sci. Pol. Chem*. **2012,** 50, (18), 3797-3805.
23. Zhang, M.; Moore, R. B.; Long, T. E. Melt transesterification and characterization of segmented block copolyesters containing 2,2,4,4-tetramethyl-1,3-cyclobutanediol, *J. Polym. Sci., Part A: Polym. Chem*. **2012,** 50, (Copyright (C) 2013 American Chemical Society (ACS). All Rights Reserved.), 3710-3718, S3710/1-S3710/2.
24. Oprea, S.; Potolinca, V. O. Synthesis and characterization of linear and crosslinked poly(urethane urea) elastomers with triazine moieties in the main chain, *Des. Monomers Polym*. **2013,** 16, 47-55.
25. Niesten, M.; ten Brinke, J. W.; Gaymans, R. J. Segmented copolyetheresteraramids with extended poly(tetramethyleneoxide) segments, *Polymer* **2001,** 42, (4), 1461-1469.

26. Strawhecker, K. E.; Hsieh, A. J.; Chantawansri, T. L.; Kalcioglu, Z. I.; Van, V. K. J. Influence of microstructure on micro-/nano-mechanical measurements of select model transparent poly(urethane urea) elastomers, *Polymer* **2013,** 54, (Copyright (C) 2013 American Chemical Society (ACS). All Rights Reserved.), 901-908.
27. Sheth, J. P.; Klinedinst, D. B.; Wilkes, G. L.; Iskender, Y.; Yilgor, I. Role of chain symmetry and hydrogen bonding in segmented copolymers with monodisperse hard segments, *Polymer* **2005,** 46, (18), 7317-7322.
28. Sheth, J. P.; Yilgor, E.; Erenturk, B.; Ozhalici, H.; Yilgor, I.; Wilkes, G. L. Structure–property behavior of poly(dimethylsiloxane) based segmented polyurea copolymers modified with poly(propylene oxide), *Polymer* **2005,** 46, (19), 8185-8193.
29. Yilgor, I.; Yilgor, E. Structure-morphology-property behavior of segmented thermoplastic polyurethanes and polyureas prepared without chain extenders, *Polymer Reviews* **2007,** 47, (4), 487-510.
30. Mallakpour, S.; Kowsari, E. Polycondensation reaction of N,N′-(4,4′-oxydiphthaloyl)-bis-L-methionine diacid chloride with aromatic diamines: Synthesis and properties, *J. Appl. Polym. Sci.* **2006,** 99, (3), 1038-1044.
31. Pattabiraman, V. R., Bode Jeffrey W. Rethinking amide bond synthesis, *Nature* **2011,** 480, (7378), 471-479.
32. Shabbir, S.; Zulfiqar, S.; Ahmad, Z.; Sarwar, M. I. Pyrimidine based carboxylic acid terminated aromatic and semiaromatic hyperbranched polyamide-esters: synthesis and characterization, *Tetrahedron* **2010,** 66, (35), 7204-7212.

33. Poulhès, F.; Mouysset, D.; Gil, G.; Bertrand, M. P.; Gastaldi, S. Novozym 435-catalyzed synthesis of polyetheramides from amino-esters, or diesters and diamines built on ethylene- and diethylene- glycol moieties, *Polymer* **2012,** 53, (6), 1172-1179.
34. Yi, C.; Peng, Z.; Wang, H.; Li, M.; Wang, C. Synthesis and characteristics of thermoplastic elastomer based on polyamide-6, *Polym. Int.* **2011,** 60, (12), 1728-1736.
35. Arsenault, S., "New technological developments with PEBAX". In *Annu. Tech. Conf. - Soc. Plast. Eng.*, Society of Plastics Engineers: 2008; Vol. 66th, pp 775-788.
36. Choi, M.-C.; Jung, J.-Y.; Yeom, H.-S.; Chang, Y.-W. Mechanical, thermal, barrier, and rheological properties of poly(ether-block-amide) elastomer/organoclay nanocomposite prepared by melt blending, *Polym. Eng. Sci.* **2012,** 53, (5), 982-991.
37. Gugliuzza, A., Poly(ether-block-amide) copolymers synthesis, properties and applications. In *Handbook of Engineering and Specialty Thermoplastics*, Thomas, S., Visakh, PM, Ed. John Wiley & Sons, Inc.: Hoboken, NJ, 2012; Vol. 4, pp 111-140.
38. Wang, Y.; Alhassan, S. M.; Yang, V. H.; Schiraldi, D. A. Polyether-block-amide copolymer/clay films prepared via a freeze-drying method, *Compos. Part B-Eng.* **2013,** 45, (1), 625-630.
39. Huoli; Lihua. Synthesis of segmented block copolymers based on Polyamide-1010 and polytetramethylene glycol, *Adv. Mater. Res. (Durnten-Zurich, Switz.)* **2012,** 512-515, (Copyright (C) 2012 American Chemical Society (ACS). All Rights Reserved.), 2185-2190.
40. Yoshino, M.; Ito, K.; Kita, H.; Okamoto, K.-I. Effects of hard-segment polymers on CO2/N2 gas-separation properties of poly(ethylene oxide)-segmented copolymers, *Journal of Polymer Science Part B: Polymer Physics* **2000,** 38, (13), 1707-1715.

41. Kim, J. H.; Ha, S. Y.; Lee, Y. M. Gas permeation of poly(amide-6-b-ethylene oxide) copolymer, *J. Membrane. Sci.* **2001,** 190, (2), 179-193.
42. Armstrong, S.; Freeman, B.; Hiltner, A.; Baer, E. Gas permeability of melt-processed poly(ether block amide) copolymers and the effects of orientation, *Polymer* **2012,** 53, (6), 1383-1392.
43. Wang, G.; Xue, B. Synthesis and characterization of poly(ether-block-amide) and application as permanent antistatic agent, *J. Appl. Polym. Sci.* **2010,** 118, (4), 2448-2453.
44. Boulares, A.; Tessier, M.; Maréchal, E. Synthesis and characterization of poly(copolyethers-block-polyamides) II. Characterization and properties of the multiblock copolymers, *Polymer* **2000,** 41, (10), 3561-3580.
45. Peyravi, M.; Babaluo, A. A.; Ardestani, M. A.; Aghjeh, M. K. R.; Pishghadam, S. R.; Hadi, P. Study on the synthesis of poly(ether-block-amide) copolymer based on nylon6 and poly(ethylene oxide) with various block lengths, *J. Appl. Polym. Sci.* **2010,** 118, (2), 1211-1218.
46. Sauer, B. B.; McLean, R. S.; Thomas, R. R. Nanometer resolution of crystalline morphology using scanning probe microscopy, *Polym. Int.* **2000,** 49, (5), 449-452.
47. Hatfield, G. R.; Guo, Y.; Killinger, W. E.; Andrejak, R. A.; Roubicek, P. M. Characterization of structure and morphology in two poly(ether-block-amide) copolymers, *Macromolecules* **1993,** 26, (24), 6350-6353.
48. Begenir, A.; Michielsen, S.; Pourdeyhimi, B. Crystallization behavior of elastomeric block copolymers: Thermoplastic polyurethane and polyether-block-amide, *J. Appl. Polym. Sci.* **2009,** 111, (3), 1246-1256.

49. Sauer, B. B.; McLean, R. S.; Brill, D. J.; Londono, D. J. Morphology and orientation during the deformation of segmented elastomers studied with small-angle X-ray scattering and atomic force microscopy, *J. Polym. Sci. Pol. Phys.* **2002,** 40, (16), 1727-1740.
50. Song, Y.; Yamamoto, H.; Nemoto, N. Segmental Orientations and Deformation Mechanism of Poly(ether-block-amide) Films†, *Macromolecules* **2004,** 37, (16), 6219-6226.
51. Konyukhova, E. V.; Buzin, A. I.; Godovsky, Y. K. Melting of polyether block amide (Pebax): the effect of stretching, *Thermochim. Acta.* **2002,** 391, (1–2), 271-277.
52. Yang, I. K.; Tsai, P. H. Rheological characterization and microphase-separated structure of a poly(ether-block-amide) segmented block copolymer, *J. Polym. Sci. Pol. Phys.* **2005,** 43, (18), 2557-2567.
53. Sheth, J. P.; Xu, J.; Wilkes, G. L. Solid state structure–property behavior of semicrystalline poly(ether-block-amide) PEBAX® thermoplastic elastomers, *Polymer* **2003,** 44, (3), 743-756.
54. Alberola, N.; Vassel, A.; Christophe Helluin, J. Mechanical relaxation processes in polyether block amide copolymers (PEBA), *Makromol. Chem-M. Symp.* **1989,** 23, (1), 219-224.
55. Hucher, C.; Eustache, R. P.; Beaume, F.; Tekely, P. Motional heterogeneity in poly(ether-block-amide) copolymers as revealed by solid-state NMR, *Macromolecules* **2005,** 38, (22), 9200-9209.
56. Sheth, J. P.; Aneja, A.; Wilkes, G. L.; Yilgor, E.; Atilla, G. E.; Yilgor, I.; Beyer, F. L. Influence of system variables on the morphological and dynamic mechanical behavior of polydimethylsiloxane based segmented polyurethane and polyurea copolymers: a comparative perspective, *Polymer* **2004,** 45, (20), 6919-6932.

57. Klinedinst, D. B.; Yilgör, E.; Yilgör, I.; Beyer, F. L.; Wilkes, G. L. Structure–property behavior of segmented polyurethaneurea copolymers based on an ethylene–butylene soft segment, *Polymer* **2005,** 46, (23), 10191-10201.

58. Versteegen, R. M.; Kleppinger, R.; Sijbesma, R. P.; Meijer, E. W. Properties and morphology of segmented copoly(ether urea)s with uniform hard segments, *Macromolecules* **2006,** 39, (2), 772-783.

59. Wisse, E.; Spiering, A. J. H.; van Leeuwen, E. N. M.; Renken, R. A. E.; Dankers, P. Y. W.; Brouwer, L. A.; van Luyn, M. J. A.; Harmsen, M. C.; Sommerdijk, N.; Meijer, E. W. Molecular recognition in poly(epsilon-caprolactone)-based thermoplastic elastomers, *Biomacromolecules* **2006,** 7, (12), 3385-3395.

60. Guang, L.; Gaymans, R. J. Polyesteramides with mixtures of poly(tetramethylene oxide) and 1,5-pentanediol, *Polymer* **1997,** 38, (19), 4891-4896.

61. Niesten, M. C. E. J.; Tol, R.; Gaymans, R. J. Influence of type of uniform aromatic amide units on segmented copolyetheresteramides, *Polymer* **2001,** 42, (3), 931-939.

62. Quaglia, F.; Vignola, M. C.; De Rosa, G.; La Rotonda, M. I.; Maglio, G.; Palumbo, R. New segmented copolymers containing poly(ϵ-caprolactone) and etheramide segments for the controlled release of bioactive compounds, *J. Control. Release.* **2002,** 83, (2), 263-271.

63. D'Angelo, S.; Galletti, P.; Maglio, G.; Malinconico, M.; Morelli, P.; Palumbo, R.; Vignola, M. C. Segmented poly(ether–ester–amide)s based on poly(l,l-lactide) macromers, *Polymer* **2001,** 42, (8), 3383-3392.

64. Deschamps, A. A.; Grijpma, D. W.; Feijen, J. Phase separation and physical properties of PEO-containing poly(ether ester amide)s, *J. Biomater. Sci. Polym. Ed.* **2002,** 13, (12), 1337-1352.

65. Krijgsman, J.; Feijen, J.; Gaymans, R. J. Synthesis and properties of segmented copolymers of polyphenylene ether and tetra-amide units, *Macromol. Sy.* **2003,** 199, (1), 135-146.

66. Krijgsman, J.; Biemond, G. J. E.; Gaymans, R. J. Segmented copolymers of uniform tetra-amide units and poly(phenylene oxide) by direct coupling, *J. Appl. Polym. Sci.* **2007,** 103, (1), 512-518.

67. Ghosh, S.; Bhattacharyya, A. K.; Khastgir, D.; Bhowmick, A. K. Melt rheology of segmented polyamides: Effect of block molecular weight, *J. Appl. Polym. Sci.* **1999,** 71, (11), 1739-1747.

68. van Hutten, P. F.; Mangnus, R. M.; Gaymans, R. J. Segmented copolymers with polyesteramide units of uniform length: structure analysis, *Polymer* **1993,** 34, (20), 4193-4202.

69. Krijgsman, J.; Biemond, G. J. E.; Gaymans, R. J. Segmented copolymers of uniform tetra-amide units and poly(phenylene oxide). Part 4. Influence of the extender, *Polymer* **2005,** 46, (19), 8250-8257.

70. Biemond, G. J. E.; Feijen, J.; Gaymans, R. J. Segmented Block Copolymers with Monodisperse Hard Segments: The Influence of H-Bonding on Various Properties, *Macromolecular Materials and Engineering* **2009,** 294, (8), 492-501.

71. Krijgsman, J.; Feijen, J.; Gaymans, R. J. Segmented copolymers of uniform tetra-amide units and poly(phenylene oxide): 1. Synthesis and thermal-mechanical properties, *Polymer* **2004,** 45, (14), 4677-4684.

72. Niesten, M. C. E. J.; Feijen, J.; Gaymans, R. J. Synthesis and properties of segmented copolymers having aramid units of uniform length, *Polymer* **2000,** 41, (24), 8487-8500.

73. Arun, A.; Gaymans, R. J. Tensile and elastic properties of triblock copolymer based on aramide end-segments and polyether mid-segments, *J. Appl. Polym. Sci.* **2009,** 111, (4), 1780-1785.

74. Sauer, B. B.; McLean, R. S.; Gaymans, R. J.; Niesten, M. C. J. E. Crystalline morphologies in segmented copolymers with hard segments of uniform length, *J. Polym. Sci. Pol. Phys.* **2004,** 42, (9), 1783-1792.

75. Biemond, G. J. E.; Feijen, J.; Gaymans, R. J. Poly(ether amide) segmented block copolymers with adipic acid based tetraamide segments, *J. Appl. Polym. Sci.* **2007,** 105, (2), 951-963.

76. van der Schuur, M.; Gaymans, R. J. Segmented block copolymers based on poly(propylene oxide) and monodisperse polyamide-6,T segments, *J. Polym. Sci. Pol. Chem.* **2006,** 44, (16), 4769-4781.

77. Biemond, G. J. E.; Feijen, J.; Gaymans, R. J. Influence of polydispersity of crystallizable segments on the properties of segmented block copolymers, *Polym. Eng. Sci.* **2008,** 48, (7), 1389-1400.

78. van der Schuur, M.; Boer, J. d.; Gaymans, R. J. Structure-property relations of poly(propylene oxide) block copolymers with monodisperse and polydisperse crystallisable segments, *Polymer* **2005,** 46, (22), 9243-9256.

79. Husken, D.; Feijen, J.; Gaymans, R. J. Surface properties of poly(ethylene oxide)-based segmented block copolymers with monodisperse hard segments, *J. Appl. Polym. Sci.* **2009,** 114, (2), 1264-1269.

80. Krijgsman, J.; Feijen, J.; Gaymans, R. J. Segmented copolymers of uniform tetra-amide units and poly(phenylene oxide): 2. Crystallisation behaviour, *Polymer* **2004,** 45, (14), 4685-4691.

81. Bouma, K.; Wester, G. A.; Gaymans, R. J. Polyether-amide segmented copolymers based on ethylene terephthalamide units of uniform length, *J. Appl. Polym. Sci.* **2001,** 80, (8), 1173-1180.
82. van der Schuur, M.; van der Heide, E.; Feijen, J.; Gaymans, R. J. Structure–property relations of segmented block copolymers with liquid–liquid demixed morphologies, *Polymer* **2005,** 46, (11), 3616-3627.
83. van der Schuur, M.; Gaymans, R. J. Influence of chemical crosslinks on the elastic behavior of segmented block copolymers, *Polymer* **2005,** 46, (18), 6862-6868.
84. Krijgsman, J.; Husken, D.; Gaymans, R. J. Synthesis and properties of thermoplastic elastomers based on PTMO and tetra-amide, *Polymer* **2003,** 44, (25), 7573-7588.
85. Husken, D.; Krijgsman, J.; Gaymans, R. J. Segmented blockcopolymers with uniform amide segments, *Polymer* **2004,** 45, (14), 4837-4843.
86. Niesten, M. C. E. J.; Gaymans, R. J. Tensile and elastic properties of segmented copolyetheresteramides with uniform aramid units, *Polymer* **2001,** 42, (14), 6199-6207.
87. Biemond, G. J. E.; Feijen, J.; Gaymans, R. J. Tensile properties of segmented block copolymers with monodisperse hard segments, *J. Mater. Sci.* **2008,** 43, (10), 3689-3696.
88. Krijgsman, J.; Gaymans, R. J. Tensile and elastic properties of thermoplastic elastomers based on PTMO and tetra-amide units, *Polymer* **2004,** 45, (2), 437-446.
89. Niesten, M. C. E. J.; Harkema, S.; van der Heide, E.; Gaymans, R. J. Structural changes of segmented copolyetheresteramides with uniform aramid units induced by melting and deformation, *Polymer* **2001,** 42, (3), 1131-1142.

90. Lips, P. A. M.; Broos, R.; van Heeringen, M. J. M.; Dijkstra, P. J.; Feijen, J. Synthesis and characterization of poly(ester amide)s containing crystallizable amide segments, *Polymer* **2005,** 46, (19), 7823-7833.

91. Deshayes, G.; Delcourt, C.; Verbruggen, I.; Trouillet-Fonti, L.; Touraud, F.; Fleury, E.; Degee, P.; Destarac, M.; Willem, R.; Dubois, P. Novel Polyesteramide-Based Diblock Copolymers: Synthesis by Ring-Opening Copolymerization and Characterization, *Macromol. Chem. Physic.* **2009,** 210, (12), 1033-1043.

92. Luckachan, G. E.; Pillai, C. K. S. Random multiblock poly(ester amide)s containing poly(L-lactide) and cycloaliphatic amide segments: Synthesis and biodegradation studies, *J. Polym. Sci. Pol. Chem.* **2006,** 44, (10), 3250-3260.

93. Lips, P. A. M.; van Luyn, M. J. A.; Chiellini, F.; Brouwer, L. A.; Velthoen, I. W.; Dijkstra, P. J.; Feijen, J. Biocompatibility and degradation of aliphatic segmented poly(ester amide)s: In vitro and in vivo evaluation, *J. Biomed. Mater. Res. A.* **2006,** 76A, (4), 699-710.

94. Pang, X.; Wu, J.; Reinhart-King, C.; Chu, C.-C. Synthesis and characterization of functionalized water soluble cationic poly(ester amide)s, *J. Polym. Sci. Pol. Chem.* **2010,** 48, (17), 3758-3766.

95. Gaymans, R. J.; van Swaaij, A. W. Enhancing the drawability of a polyester by copolymerization with a second type of crystallizable block, *J. Appl. Polym. Sci.* **2011,** 119, (1), 23-30.

96. Jeong, H. M.; Moon, S. W.; Jho, J. Y.; Ahn, T. O. Phase structure and properties of some thermoplastic polyesteramide elastomers, *Polymer* **1998,** 39, (2), 459-465.

97. Palsule, A. S.; Poojari, Y. Enzymatic synthesis of silicone fluorinated aliphatic polyesteramides, *Polymer* **2010,** 51, (26), 6161-6167.

98. Sharma, B.; Azim, A.; Azim, H.; Gross, R. A.; Zini, E.; Focarete, M. L.; Scandola, M. Enzymatic Synthesis and Solid-State Properties of Aliphatic Polyesteramides with Polydimethylsiloxane Blocks, *Macromolecules* **2007,** 40, (22), 7919-7927.

99. Chromcova, D.; Baslerova, L.; Roda, J.; Brozek, J. Polymerization of lactams. 99 Preparation of polyesteramides by the anionic copolymerization of epsilon-caprolactam and epsilon-caprolactone, *Eur. Polym. J.* **2008,** 44, (6), 1733-1742.

100. Bernaskova, A.; Chromcova, D.; Brozek, J.; Roda, J. Polymerization of lactams, 95 - Part 94 - Preparation of polyesteramides by the anionic polymerization of epsilon-caprolactam in the presence of poly(epsilon-caprolactone), *Polymer* **2004,** 45, (7), 2141-2148.

101. Bera, S.; Jedlinski, Z. Block/segmented polymers. A new method of synthesis of copoly(amide-ester)-ester polymer, *J. Polym. Sci. Pol. Chem.* **1993,** 31, (3), 731-739.

102. Liu, S.; Li, C.; Zhao, J.; Zhang, Z.; Yang, W. Synthesis and characterization of polyesteramides having short Nylon-6 segments in the main chains through polycondensation and chain extension, *Polymer* **2011,** 52, (26), 6046-6055.

103. Deshayes, G.; Delcourt, C.; Verbruggen, I.; Trouillet-Fonti, L.; Touraud, F.; Fleury, E.; Degee, P.; Destarac, M.; Willem, R.; Dubois, P. Novel polyesteramide-based di- and triblock copolymers From thermo-mechanical properties to hydrolytic degradation, *Eur. Polym. J.* **2011,** 47, (1), 98-110.

104. Coe, S.; Kane, J. J.; Nguyen, T. L.; Toledo, L. M.; Wininger, E.; Fowler, F. W.; Lauher, J. W. Molecular Symmetry and the Design of Molecular Solids: The Oxalamide Functionality as a Persistent Hydrogen Bonding Unit, *Journal of the American Chemical Society* **1997,** 119, (1), 86-93.

105. Nguyen, T. L.; Fowler, F. W.; Lauher, J. W. Commensurate and Incommensurate Hydrogen Bonds. An Exercise in Crystal Engineering, *Journal of the American Chemical Society* **2001,** 123, (44), 11057-11064.

106. Schulze, H. Thermoplastic adhesive polyoxamide from polyoxypropylene polyamine. US4119615A, 1978.

107. Benson, K. E.; Hansen, R. G.; Johnson, S. A.; Leir, C. M.; Liu, R. Y.; Purgett, M. D.; Schneider, H. M.; Sherman, A. A. Multilayer films including thermoplastic polyamide-silicone block copolymers. WO2007075900A2, 2007.

108. Benson, K. E.; Hansen, R. G.; Johnson, S. A.; Leir, C. M.; Liu, R. Y.; Purgett, M. D.; Schneider, H. M.; Sherman, A. A. Films including thermoplastic polyamide-silicone block copolymers. WO2007073502A2, 2007.

109. Leir, C. M.; Benson, K. E.; Hansen, R. G.; Purgett, M. D.; Everaerts, A. I. Polydiorganosiloxane-containing materials with oxalylamino groups. US20070149745A1, 2007.

110. Leir, C. M.; Benson, K. E.; Hansen, R. G.; Purgett, M. D.; Everaerts, A. I.; Sherman, A. A. Polydiorganosiloxane polyoxamide copolymers. US20070148474A1, 2007.

111. Sijbrandi, N. J.; Kimenai, A. J.; Mes, E. P. C.; Broos, R.; Bar, G.; Rosenthal, M.; Odarchenko, Y.; Ivanov, D. A.; Dijkstra, P. J.; Feijen, J. Synthesis, Morphology, and Properties of Segmented Poly(ether amide)s with Uniform Oxalamide-Based Hard Segments, *Macromolecules* **2012,** 45, (9), 3948-3961.

112. Sijbrandi, N. J.; Kimenai, A. J.; Mes, E. P. C.; Broos, R.; Bar, G.; Rosenthal, M.; Odarchenko, Y. I.; Ivanov, D. A.; Jan, F. J.; Dijkstra, P. J. Synthesis, morphology and

properties of segmented poly(ether ester amide)s comprising uniform glycine or beta-alanine extended bisoxalamide hard segments, *Polymer* **2012,** 53, (19), 4033-4044.

113. Buckwalter, D. J.; Hudson, A. G.; Moore, R. B.; Long, T. E. Synthesis and Characterization of Poly(propylene glycol) Poly(trioxamide) and Poly(urea oxamide) Segmented Copolymers, *Polym. Int.* **2013,** 63, (7), 1184-1191.

114. Buckwalter, D. J.; Inglefield, D. L.; Enokida, J. S.; Hudson, A. G.; Moore, R. B.; Long, T. E. Effects of Copolymer Structure on the Mechanical Properties of Poly(dimethyl siloxane) Poly(oxamide) Segmented Copolymers, *Macromol. Chem. Physic.* **2013,** 214, (18), 2073-2082.

115. Buckwalter, D. J.; Zhang, M.; Inglefield, D. L.; Moore, R. B.; Long, T. E. Synthesis and Characterization of Poly(dimethyl siloxane) Poly(urea oxamide) Segmented Copolymers *Polymer* **2013,** 54, (18), 4849-4857.

116. Henkensmeier, D.; Abele, B. C.; Candussio, A.; Thiem, J. Synthesis, characterisation and degradability of polyamides derived from aldaric acids and chain end functionalised polydimethylsiloxanes, *Polymer* **2004,** 45, (21), 7053-7059.

117. Kang, B. M.; Park, Y. W. A Study on Phase Separation of PA-PDMS Composites Dependent on Molecular Weight, *Polym. Plast. Technol. Eng.* **2010,** 49, 223-227.

118. Kishida, A.; Furuzono, T.; Ohshige, T.-a.; Maruyama, I.; Matsumoto, T.; Itoh, H.; Murakami, M.; Akashi, M. Study of the surface properties of ultrathin films of poly(dimethylsiloxane)-polyamide multiblock copolymers, *Angew. Makromol. Chem.* **1994,** 220, (1), 89-97.

119. Matsumoto, T.; Uchida, T.; Kishida, A.; Furuzono, T.; Maruyama, I.; Akashi, M. Novel functional polymers: Poly(dimethylsiloxane)-polyamide multiblock copolymer. VII. Oxygen

permeability of aramid-silicone membranes in a gas-membrane-liquid system, *J. Appl. Polym. Sci.* **1997,** 64, (6), 1153-1159.

120. Furuzono, T.; Kishida, A.; Yanagi, M.; Matsumoto, T.; Kanda, T.; Nakamura, T.; Aiko, T.; Maruyama, I.; Akashi, M. Novel functional polymers: Poly(dimethylsiloxane)polyamide multiblock copolymer .5. The interaction between biomolecules and the surface of aramid-silicone resins, *J. Biomat. Sci-Polym. E.* **1996,** 7, (10), 871-880.

121. Furuzono, T.; Yashima, E.; Kishida, A.; Maruyama, I.; Matsumoto, T.; Akashi, M. A novel biomaterial - Poly(dimethylsiloxane)-polyamide multiblock copolymer .1. synthesis and evaluation of blood compatibility, *J. Biomat. Sci-Polym. E.* **1993,** 5, (1-2), 89-98.

122. Gill, R.; Mazhar, M.; Siddiq, M. Structural characterization and thermal behaviour of block copolymers of polydimethylsiloxane and polyamide having trichlorogermyl pendant groups, *Polym. Int.* **2010,** 59, (12), 1598-1605.

123. Saif Ullah Khan, M.; Akhter, Z.; Naz, T.; Bhatti, A. S.; Siddiqi, H. M.; Siddiq, M.; Khan, A. Study on the preparation and properties of novel block copolymeric materials based on structurally modified organometallic as well as organic polyamides and polydimethylsiloxane, *Polym. Int.* **2012,** 62, (2), 319-334.

124. Kajiyama, M.; Kakimoto, M. A.; Imai, Y. Synthesis and characterization of new multiblock copolymers based on poly(dimethylsiloxane) and aromatic polyamides, *Macromolecules* **1989,** 22, (11), 4143-4147.

125. Yilgor, I.; Lee, B.; Steckle, W. P., Jr.; Riffle, J. S.; Tyagi, D.; Wilkes, G. L.; McGrath, J. E. Segmented polysiloxane-polyamide copolymers, *Polym. Prepr. (Am. Chem. Soc., Div. Polym. Chem.)* **1983,** 24(2), (Copyright (C) 2013 American Chemical Society (ACS). All Rights Reserved.), 35-6.

126. Policastro, P. P.; Hernandez, P. K. Synthesis of new polydimethylsiloxane-polyamide copolymers from phenylene-bis-5-oxazolones and aminopropyl-terminated polydimethylsiloxane oligomers, *J. Polym. Sci. Pol. Chem.* **1987,** 25, (10), 2819-2826.

127. Furuzono, T.; Seki, K.; Kishida, A.; Ohshige, T.-A.; Waki, K.; Maruyama, I.; Akashi, M. Novel functional polymers: Poly(dimethylsiloxane)–polyamide multiblock copolymer. III. Synthesis and surface properties of disiloxane–aromatic polyamide multiblock copolymer, *J. Appl. Polym. Sci.* **1996,** 59, (7), 1059-1065.

128. Oishi, Y.; Nakata, S.; Kajiyama, M.; Kakimoto, M. A.; Imai, Y. Preparation and properties of new random and block copolyamides derived from 1,3-bis(3-aminopropyl)tetramethyldisiloxane, aromatic diamines, and isophthaloyl chloride, *J. Polym. Sci. Pol. Chem.* **1992,** 30, (11), 2357-2364.

129. Kishida, A.; Kanda, T.; Furuzono, T.; Maruyama, I.; Akashi, M. Novel functional polymers: Poly(dimethylsiloxane)-polyamide multiblock copolymer. IX. Surface properties of blend film of aramid–silicone resins with aramid, *J. Appl. Polym. Sci.* **2000,** 78, (12), 2198-2205.

130. Furuzono, T.; Senshu, K.; Kishida, A.; Matsumoto, T.; Akashi, M. Novel functional polymers: Poly(dimethylsiloxane)-polyamide multiblock copolymer .6. A transmission electron microscopic study on microphase-separated structure in aramid-silicone resin, *Polym J* **1997,** 29, (2), 201-203.

131. Senshu, K.; Furuzono, T.; Koshizaki, N.; Yamashita, S.; Matsumoto, T.; Kishida, A.; Akashi, M. Novel Functional Polymers: Poly(dimethylsiloxane)−Polyamide Multiblock Copolymer. 8.1 Surface Studies of Aramid−Silicone Resin by Means of XPS, Static SIMS, and TEM, *Macromolecules* **1997,** 30, (15), 4421-4428.

132. Kang, E.-C.; Kaneko, T.; Shiino, D.; Akashi, M. Novel functional polymers: Poly(dimethyl siloxane)–polyamide multiblock copolymers. XI. The effects of sequence regularity on the thermal and mechanical properties, *J. Polym. Sci. Pol. Chem*. **2003,** 41, (6), 841-852.

133. Matsumoto, T.; Koinuma, Y.; Waki, K.; Kishida, A.; Furuzono, T.; Maruyama, I.; Akashi, M. Novel functional polymers: Poly(dimethylsiloxane)–polyamide multiblock copolymer. IV. Gas permeability and thermomechanical properties of aramid–silicone resins, *J. Appl. Polym. Sci.* **1996,** 59, (7), 1067-1071.

134. Kolahdoozan, M.; Mirsafaei, R.; Mallakpour, S. Synthesis and properties of new highly soluble poly(amide-ester-imide)s containing poly(ethylene glycol) as a soft segment, *Polym. Bull. (Heidelberg, Ger.)* **2012,** 68, (5), 1239-1254.

135. Mallakpour, S.; Rafiemanzelat, F. Synthesis and characterization of new optically active poly(amide–imide–urethane) thermoplastic elastomers, derived from bis(p-amido benzoic acid)-N-trimellitylimido-l-leucine and polyoxyethylene-MDI, *React. Funct. Polym*. **2005,** 62, (2), 153-167.

136. Chapman, T. M.; Marra, K. G. Determination of Low Critical Surface Tensions of Novel Fluorinated Poly(amide urethane) Block Copolymers. 2. Fluorinated Soft-Block Backbone and Side Chains, *Macromolecules* **1995,** 28, (6), 2081-2085.

137. van der Schuur, M.; Noordover, B.; Gaymans, R. J. Polyurethane elastomers with amide chain extenders of uniform length, *Polymer* **2006,** 47, (4), 1091-1100.

138. Park, Y. W.; Lee, D. S. Surface and electrical characteristics of poly(amide imide)-poly(dimethylsiloxane) nanocomposites, *J. Appl. Polym. Sci.* **2004,** 93, (1), 342-347.

139. Mallakpour, S.; Rafiemanzelat, F. Synthesis, characterization and properties of a series of copoly(amide-imide-ether-urethane)s with a new hard segment constituent: study of the effect of hard segment content, *High Perform. Polym.* **2008,** 20, (2), 146-165.

140. Báez, J. E.; Ramírez, D.; Valentín, J. L.; Marcos-Fernández, Á. Biodegradable Poly(ester–urethane–amide)s Based on Poly(ε-caprolactone) and Diamide–Diol Chain Extenders with Crystalline Hard Segments. Synthesis and Characterization, *Macromolecules* **2012,** 45, (17), 6966-6980.

141. Nojima, K.; Sanui, K.; Ogata, N.; Yui, N.; Kataoka, K.; Sakurai, Y. Material characterization of segmented polyether poly(urethane-urea-amide)s and its implication in blood compatibility, *Polymer* **1987,** 28, (6), 1017-1024.

142. Mallakpour, S.; Khani, M.; Rafiemanzelat, F. Synthesis and characterization of new optically active segmented poly(amide imide urethane)s based on different diacids via an isocyanate route, *J. Appl. Polym. Sci.* **2008,** 108, (5), 2975-2982.

143. Mallakpour, S.; Khoee, S. Synthesis and characterization of new optically active poly(amide-imide-urethane) thermoplastic elastomers, derived from 4,4′-(hexafluoroisopropylidene)-N,N′-bis(phthaloyl-L-leucine-p-aminobenzoic acid) and PEG-MDI, *J. Appl. Polym. Sci.* **2004,** 91, (4), 2288-2294.

144. Yui, N.; Nojima, K.; Sanui, K.; Ogata, N. Morphology and properties of segmented polyether poly(urethane-urea-amide), *Polym. J. (Tokyo)* **1985,** 17, (Copyright (C) 2012 American Chemical Society (ACS). All Rights Reserved.), 969-75.

Chapter 3: Synthesis and Characterization of Polysulfone-Containing Poly(butylene terephthalate) Segmented Block Copolymers

(Published in *Macromolecules* **2014,** 47, (23), 8171-8177.)

Joseph M. Dennis, Gregory B. Fahs, Robert B. Moore, S. Richard Turner, and Timothy E. Long

Department of Chemistry, Macromolecules and Interfaces Institute

Virginia Tech, Blacksburg, VA 24061

3.1 Abstract

A facile synthetic approach to segmented polysulfone-containing polyesters affords a versatile family of high temperature thermoplastics with tunable thermomechanical properties. End-capping of phenol-terminated polysulfone (PSU) using ethylene carbonate generated telechelic oligomers with primary alcoholic functionality. Melt transesterification of dimethyl terephthalate and 1,4-butanediol in the presence of PSU oligomers yielded high molecular weight segmented block copolymers with alternating PSU and poly(butylene terephthalate) (PBT) sequences. Systematic variation in PSU incorporation resulted in tunable PBT segment length and accompanying thermal properties. DSC and SAXS elucidated a miscible, amorphous PSU and PBT phase, and PBT crystallinity remained below an 80 wt.% incorporation of PSU. Dynamic mechanical analysis (DMA) revealed a crystallinity-dependent plateau regime above the copolymers glass transition temperature (T_g), while SAXS and WAXD confirmed a semi-crystalline morphology below 80 wt.% PSU. Incorporation of PSU segments significantly affected the crystallization and thermomechanical properties of PBT, and as a result these

copolymers offer impact as chemically-resistant, high-temperature thermoplastics due to their crystallinity, thermal stability, and high temperature operating window.

3.2 Introduction

Segmented block copolymers receive significant attention in the literature for their unique physical properties, which address many needs of emerging technologies. Numerous examples demonstrate enhanced physical properties due to the presence of self-assembling segments.[1-3] The self-assembly of covalently-bound immiscible polymer segments in the absence of specific interactions provides a common route for enhanced material properties.[2,4,5] This approach has primarily focused on phase behavior and physical properties of di- and triblock copolymers. However, as synthetic methods for controlled polymerizations improve, exploration into multiblock copolymers with low polydispersity will elucidate fundamental understanding of more complex architectures.[6] The strong dependence of segment length (N), Flory-Huggins interaction parameter (χ), dispersity, and number of repeating segments arise as important parameters in the design of microphase separated block copolymers.[2,6-9]

Specific interactions, such as hydrogen bonding, crystallization, or ionic aggregation, allow for the improvement of elastomeric properties and controlled morphologies at relatively short segment lengths.[1,3,10-13] For example, functionalized siloxane oligomers afforded segmented copolymers with monodisperse urea-oxamide hard segments. The hydrogen bonding between urea-oxamide segments provided an enhanced elastomeric window, as well as lower extensional hysteresis compared to analogous urea-containing siloxanes.[3] Utilizing a similar approach, Gaymans et al. employed short amide segments that enabled enhanced mechanical integrity with rapidly crystallizing nanoribbons.[13] Furthermore, the design of charge-containing polyesters provided platforms for achieving phase separation without a significant change in

polymerization conditions. Association of ionic species into ion-rich domains extends the upper operating temperature as well as introduces ion carriers for energy applications.[10]

Recently, sulfonated polysulfone segmented block copolymers have received significant attention as water separation and proton exchange membranes.[14,15] The thermal and hydrolytic stability of polysulfones with chlorine resistance allows for extended membrane life under the harsh use conditions.[16] However, poor solvent resistance arising from the lack of crystallinity hinders the use of polysulfone membranes in the presence of solvents.[17] Semi-crystalline polyesters exhibit superior solvent resistance compared to polysulfones, and consequently, copolymerization of polysulfones and polyesters has received modest attention.[18-24] The thermal stability of polysulfone advantageously allows for processing at elevated temperatures, which are required for the melt phase synthesis of polyesters.[20,22] Previously, acidolysis has been utilized to prepare poly(ether ether ketone)-polysulfone segmented copolymers,[21] and liquid crystalline, polyester-polysulfone copolymers.[20,22] Other reports have shown success in incorporating soft, poly(dimethyl siloxane) segments with polysulfone oligomers to form elastomeric materials.[19,24] Also, successful incorporation of short, crystallizable segments through condensation of phenol-terminated polysulfone with acid chloride-functionalized, small molecules improved tensile properties over commercial polysulfones.[18] However, the synthesis of segmented copolymers containing polysulfone and semi-crystalline polyester sequences remains unprecedented and will provide a new family of semi-crystalline polysulfones with enhanced thermomechanical properties and chemical resistance. This synergy of physical and chemical properties will offer immediate impact as high performance engineering thermoplastics for emerging automotive and electronic industries.

This report describes a novel, and facile synthesis of segmented block copolymers utilizing primary alcohol end-functionalized polysulfone oligomers as a segment precursor. This synthetic route is amenable to conventional melt phase polytransesterification chemistry and yields polysulfone-polyester segmented block copolymers. Post-polymerization functionalization of phenol-terminated polysulfone with ethylene carbonate afforded primary alcohol telechelic oligomers. Melt transesterification of the oligomers in the presence of dimethyl terephthalate and 1,4-butanediol resulted in segmented block copolymers with varying polyester segment lengths. Varying the weight percent incorporation of polysulfone allowed a detailed study of crystallinity on thermal and morphological behavior.

3.3 Experimental

Materials. 1,4-butanediol (99%), bisphenol-A (≥99%), dimethyl terephthalate (99%), potassium carbonate (≥99%), ethylene carbonate (98%), Celite 545, and titanium tetraisopropoxide (99.999%) were purchased from Sigma Aldrich and used as received. 4,4'-dichlorodiphenyl sulfone (98%) was purchased from Sigma Aldrich and recrystallized twice from toluene. All solvents were used as received.

Analytical Methods. ^{1}H nuclear magnetic resonance spectroscopy (^{1}H NMR) was performed using a Varian Unity 400 MHz spectrometer with either $CDCl_3$ or a 9:1 $CDCl_3$:CF_3COOD solvent mixture at 23 °C. Thermogravimetric analysis (TGA) utilized a TA Instruments TGA Q500 from room temperature to 600 °C at a heating rate of 10 °C/min under constant N_2 purge. Differential scanning calorimetry (DSC) was completed using a TA Instruments DSC Q2000 under N_2 atmosphere with heat/cool/heat cycle performed at designated rates described later. Dynamic mechanical analysis (DMA) was accomplished using a TA Instruments DMA Q800 in oscillatory tension mode at 1 Hz and 3 °C/min. Intrinsic viscosity

was determined utilizing a binary mixture of 1:1 (v:v %) Phenol:*o*-dichlorobenzene and AVS Pro viscometer with a Micro-Ubbelohde II capillary following ISO 1628-1. Films were compression molded at 270 °C between steel plates using a PHI hydraulic press and allowed to cool in air over 1 h.

Small Angle X-Ray Scattering (SAXS). A Rigaku S-Max 3000 3 pinhole small-angle X-ray scattering instrument adapted with a rotating anode produced Cu K_α irradiation at a wavelength of 1.54 Å to analyze bulk morphology on the segmented block copolymer films. The instrument was calibrated with a silver behenate standard and the sample-to-detector distance was 1.5 m. Two-dimensional data sets were collected using a fully integrated 2D multiwire area detector with one hour exposure time. The data was then corrected for detector noise, background scattering, and sample absorption. All data processing and analysis were completed with the SAXSGUI software package to obtain intensity versus scattering vector q plots, where $q=4\pi \sin(\theta)/\lambda$ and 2θ is the scattering angle.

Wide Angle X-Ray Diffraction (WAXD). WAXD was performed using a Rigaku S-Max 3000 3 pinhole SAXS system, equipped with a rotating anode emitting X-rays with a wavelength of 0.154 nm (Cu Kα). Scattering from a silver behenate standard was used to calibrate a sample-to-detector distance of 80.0 mm. WAXD two-dimensional diffraction patterns were obtained using an image plate, with an exposure time of 2 hours. All WAXD data were analyzed using the SAXSGUI software package to obtain azimuthal averaged WAXD intensity versus 2θ profiles, where θ is one half of the scattering angle.

Phenol-terminated Polysulfone Synthesis. Syntheses of polysulfone oligomers were performed following established procedures[25], and the typical synthesis of a 6 kg/mol polysulfone is summarized. 4,4'-dichlorodiphenyl sulfone (36.11 g, 0.126 mol), bisphenol-A

(34.17 g, 0.150 mol), potassium carbonate (24.8 g, 0.179 mol), toluene (150 mL) and anhydrous *N,N*-dimethylacetamide (300 mL) were charged to a three-necked, round-bottomed flask. The resulting heterogeneous solution was purged with argon and then heated to 160 °C for 4 h. Collection of water in a Dean-Stark trap under toluene reflux monitored reaction progress. When the rate of water collection deceased, the reaction temperature was increased to 180 °C and toluene was removed. The reaction was allowed to proceed under these conditions for 12 h. After 12 h, the resulting green heterogeneous solution was cooled and filtered through Celite to remove undesired salts. Dilute hydrochloric acid was then titrated into the clear solution and neutralization was monitored colorimetrically until a pale yellow solution was obtained. The product was precipitated dropwise into 4 L water, filtered, and dried *in vacuo* at 120 °C for 24 h.

Hydroxyethyl End-group Functionalization of Polysulfone (HE-PSU-6k). The functionalization of phenol-terminated polysulfone was performed according to earlier literature,[26] and the functionalization of 6 kg/mol polysulfone follows as an example. 6 kg/mol phenol-terminated polysulfone (46.13 g, 9.22 mmol), potassium carbonate (3.82 g, 0.028 mol), ethylene carbonate (4.06 g, 0.046 mol), and dimethylformamide (125 mL) were added to a single-necked, round-bottomed flask with magnetic stir bar. After purging with argon, the heterogeneous mixture was heated to 120 °C for 24 h. The resulting polymer solution was filtered through a Celite column and neutralized with dilute hydrochloric acid. Precipitation into water afforded a white solid that was filtered and dried *in vacuo* at 120 °C for 24 h (>99% yield).

Polysulfone-Poly(butylene terephthalate) Segmented Block Copolymer Synthesis. All segmented block copolymer polymerizations were achieved using conventional melt transesterification methods, and the synthesis of 20PSU-80PBT is described. HE-PSU-6k (1.1 g, 0.22 mmol), 1,4-butanediol (2.16 g, 0.024 mol), dimethyl terephthalate (3.88 g, 0.20 mol) were

charged to a dry, 100-mL round-bottomed flask. Titanium tetraisopropoxide (100 ppm) was added to facilitate transesterification. The flask was equipped with an overhead stir rod, nitrogen inlet, and condenser. The contents were sequentially degassed under vacuum then purged with argon three times. Under constant argon purge, the flask was heated from 220 to 250 °C over 2.5 h and the pressure was subsequently reduced (>0.1 mmHg) at 270 °C for an additional 2 h. The resulting polymer products were used directly without further purification.

3.4 Results and Discussion

Oligomer and Segmented Block Copolymer Synthesis. Stoichiometric imbalance produces telechelic polymers with specific end-group functionality.[20,21,24,26] For polysulfones, excess bisphenol-A resulted in a telechelic polymer with phenolic reactive end-groups. This method proved quantitative and allowed for molecular weight determination with end-group analysis.[26] However, the phenolic functionality is not sufficiently nucleophilic for quantitative transesterification polymerizations, and consequently post-polymerization functionalization is necessary to activate these telechelic oligomers.[13,19,20,24] For subsequent polycondensation, high end group functionality is necessary to achieve high conversion and high molecular weight formation. Quantitative functionalization with ethylene carbonate addresses the required purity for polycondensation.[26]

Scheme 1 illustrates the synthesis of a segmented block copolymer using melt transesterification polymerization. 1,4-butanediol and dimethyl terephthalate afforded poly(butylene terephthalate) (PBT) segments upon chain extension of the polysulfone (PSU) oligomer. Because bulk transesterification proceeds in the absence of solvent, the solubility of the PSU oligomer in the starting materials is crucial. The low molar mass monomers promoted solvation of the PSU oligomer, ensuring a homogeneous polymerization. However, a limiting

number-average molecular weight of *ca.* 6 kg/mol was observed for the PSU oligomer, consistent with previous literature observations.[20] Furthermore, faster reaction kinetics favor copolymerization of short-chain oligomers over high molecular weight polymers due to the higher concentration of reactive end-groups. As a result, the PSU oligomer incorporates into the growing polymer chain, preventing macrophase separation at the later stages of the polymerization.

Scheme 1. Synthesis of PSU-PBT segmented block copolymers.

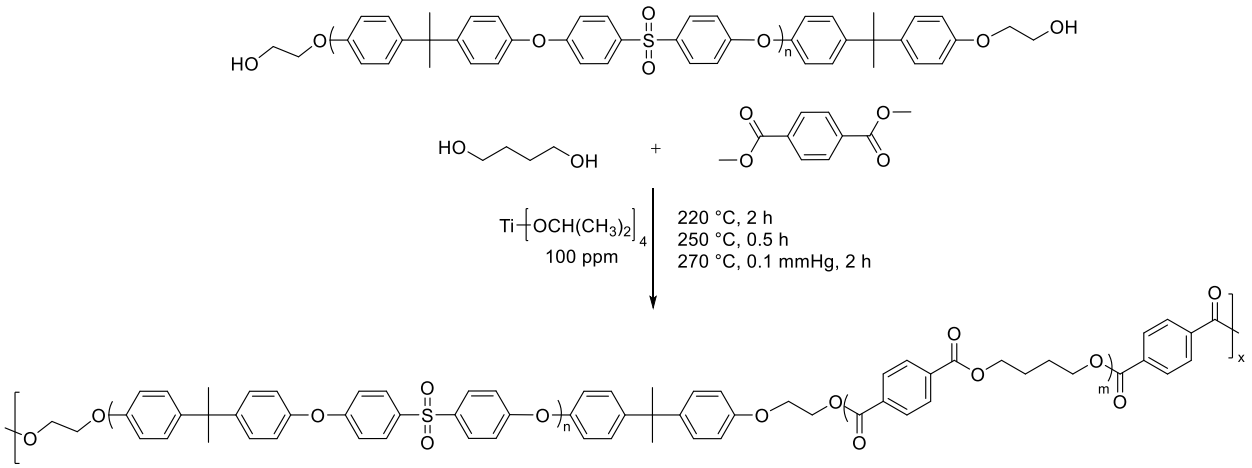

Successful chain extension of the hydroxyl-terminated PSU with dimethyl terephthalate and 1,4-butanediol was confirmed with a chemical shift of the ethylene end group protons from 3.92 and 4.04 ppm to 4.39 and 4.74 ppm, respectively **(Figure S.1)**. Although this shift only suggests the addition of a single monomeric unit at the chain ends, the resulting polymer films were mechanically robust. Optical clarity throughout the melt polymerization suggested the absence of macrophase separation and solubility of growing polyester chains. Increase in melt viscosity near the end of the reaction and the absence of discoloration due to degradation suggested high molecular weight formation. The insolubility of these semi-crystalline, PBT-PSU copolymers in most organic solvents renders direct characterization of molecular weight

challenging. However, the comparison of intrinsic viscosity (IV) of the PSU-PBT block copolymers with commercial homopolymers of PSU (Ultrason S2010, M_n = 15,600 g/mol) and PBT (Ultradur B2550, M_n = 16,600 g/mol) indicates the copolymers are comparable, and high molecular weight (Table S.1).

Herein, the segmented block copolymers are defined as xPSU-yPBT where x corresponds to the charged weight percent polysulfone oligomer and y corresponds to the charged weight percent PBT. Integration of aromatic peaks in ^{1}H NMR spectrum elucidated both relative segment block lengths as well as polyester and polysulfone weight percent. Table 1 highlights agreement between charged and actual weight percent in the copolymers as determined with ^{1}H NMR spectroscopy. The polysulfone block does not degrade due to its inherent thermal stability, resulting in retention of the sulfone segments upon post-polymerization **(Table 1)**.

Table 1. Summary of thermal, mechanical, and morphological analysis of PSU-PBT segmented copolymers

Weight Percent Polysulfone (%)			Segment Length[c] (kDa)		T_g (°C)		T_m (°C)	Crystallinity[f] (%)	Domain Spacing[g] (nm)	
Charged	Experimental		PSU	PBT					Annealing?	
	^{1}H NMR[a]	TGA[b]	^{1}H NMR[a]		DSC[d]	DMA[e]	DSC[d]	DSC[d]	No	Yes
5	5.0	9.0	--	--	51	70	223	23	14	13
20	19	19	5.8	25	66	93	217, 225	18	18	17
40	38	39	5.8	9.3	65	84	206, 217	2.8	--	16

50	49	50	5.8	6.0	87	95	202*	--	--	21
60	53	54	5.8	5.1	95	101	--	--	--	29
80	78	75	5.8	1.6	144	143	--	--	--	--
95	93	95	5.8	0.63	164	163	--	--	--	--
PSU_{6k}	--	--	5.8	--	147	--	--	--	--	--
PBT	--	--	--	--	42	54	222	22	12	12

[a] 9:1 $CDCl_3$: CF_3COOD solvent mixture, ambient conditions.

[b] TGA: 10 °C/min, N_2, weight percent determined by first step change.

[c] Determined by ^1H NMR analysis using PSU end group protons and peak integration

[d] DSC: heat/cool/heat, second heat; N_2, 10 °C/min. T_g reported as inflection point of step transition, T_m reported as peak maximum of endothermic event.

[e] DMA: tension mode, 1 Hz, 3 °C/min. T_g reported as peak maximum in tan delta curve, T_{flow} reported as temperature just prior to inconsistent data.

[f] Determined by area under melting endotherm using $\Delta H_f° = 142$ J/g.

[g] Spacing calculated using $D = 2\pi/q^*$.

* At heating rate of 3 °C/min.

A correlation existed between the resulting average PBT segment length and charged PSU. ^1H NMR spectroscopy determined PBT segment length through comparative integration between the PSU end-group protons and the aromatic and butyl protons of PBT. **Table 1** indicates that the introduction of the transesterification resistant PSU segments results in a decrease in PBT segment length. Furthermore, a transition from opaque to optically transparent films qualitatively

described the reduction in crystallization resulting from the decrease in PBT segment length. Control of the polyester segment length through weight percent polysulfone incorporation advantageously generated a wide range of copolymers with tailored physical properties.

Thermogravimetric Analysis. TGA confirmed the thermal stability of the PSU-PBT segmented block copolymers **(Figure 1)**. All block copolymers had an onset of degradation above 350 °C and displayed a two-step, weight loss profile under a nitrogen purge. Each step correlated well with the $T_{d,5\%}$ of PSU and PBT at approximately 400 °C and 500 °C, respectively. The significant difference in $T_{d,5\%}$ between the two segments permitted a determination of the weight percent incorporation, which correlated well with ^{1}H NMR spectroscopy **(Table 1)**.

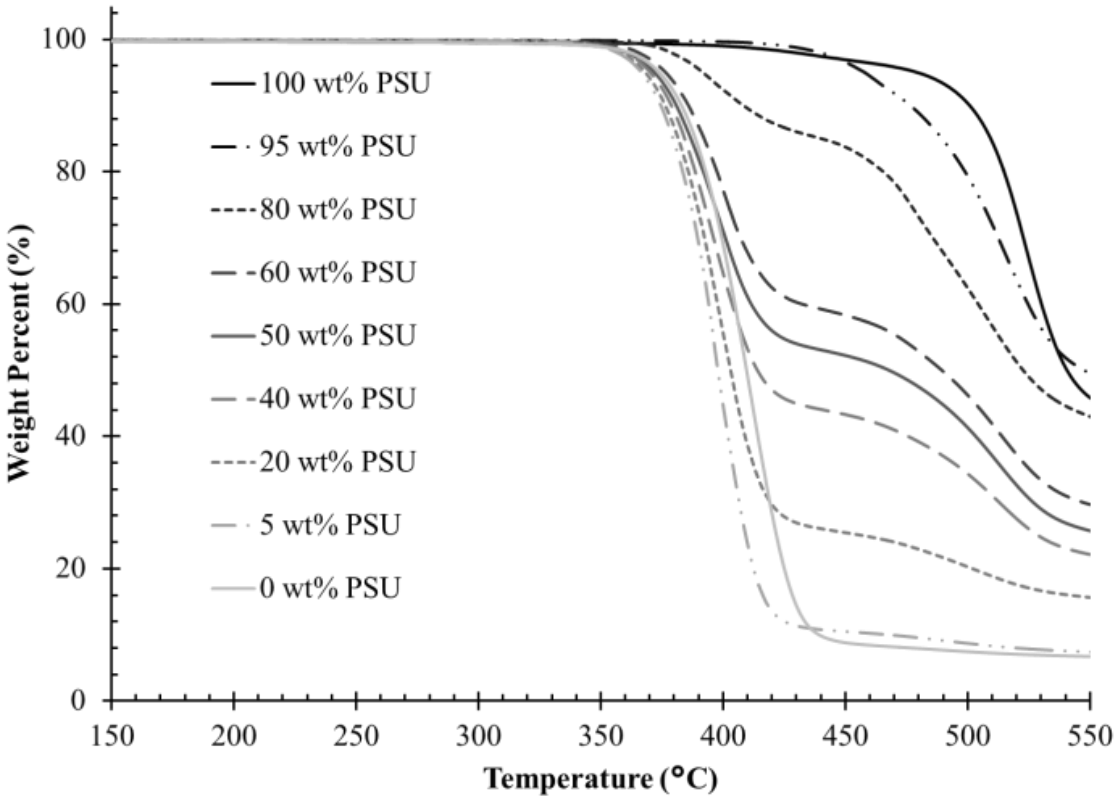

Figure 1. TGA thermograms displaying two-step degradation dependent on polysulfone incorporation into polyester block copolymers. TGA analysis performed at 10 °C/min under nitrogen purge.

Dynamic Scanning Calorimetry. Below 50 wt.% PSU, the block copolymers exhibited a melting transition similar to the melting temperature of pure PBT **(Figure 2)**. At 50 wt.% PSU and above, a single-step transition was observed and reported as the glass transition (T_g) **(Table 1)**. Phase separation would give rise to two T_g's, however, the observation of a single T_g suggested randomly dispersed segments in an amorphous phase.

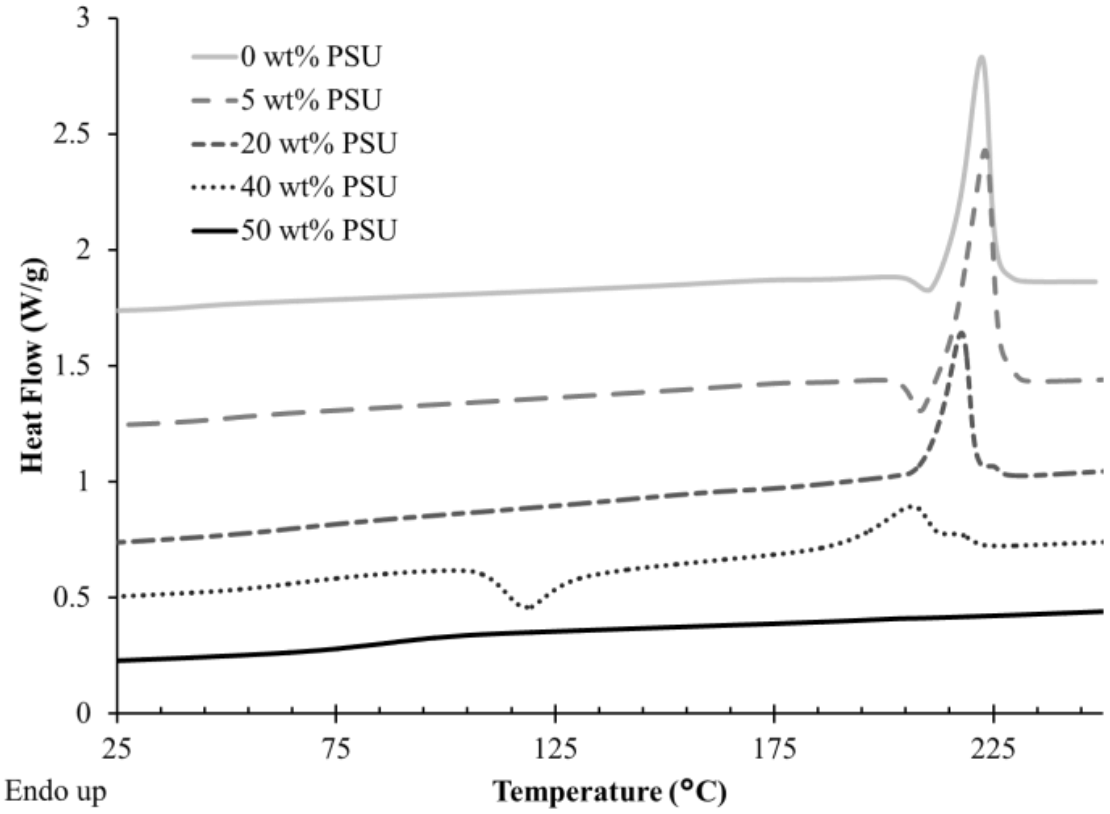

Figure 2. Representative DSC traces of PSU-PBT segmented copolymers. Melting endotherms only observed below 50 wt.% polysulfone incorporation. Second heat reported with a heat rate of 10 °C/min after quench cooling from 250 °C.

Self-consistent mean field theory (SCFT) derived phase diagrams for infinitely long $(AB)_n$ polymers were developed elsewhere.[9] Both SCFT predictions and experimental results demonstrated a reduction in the critical χN requirement for phase separation in multiblock polymers compared to analogous di- or triblock polymers.[6,8,9] Furthermore, polydispersity in segment length reduces the χN order-disorder transition; however, a "swelling" of domains from chain relaxations results in asymmetric phase behavior.[5] We propose that the combination of disperse block lengths and relatively low average polysulfone segment length contributes to the random mixing of the segmented PSU-PBT copolymers in the amorphous phase. Unfortunately,

limited bulk compatibility of PSU with PBT prevents the investigation of longer PSU segment lengths through melt transesterification polymerization. Analysis of the compositional dependence of T_g further justified the random mixing in the amorphous fraction **(Figure 3)**. Increasing PSU content increased the T_g according to the theoretical Fox relationship for random copolymers.[27,28]

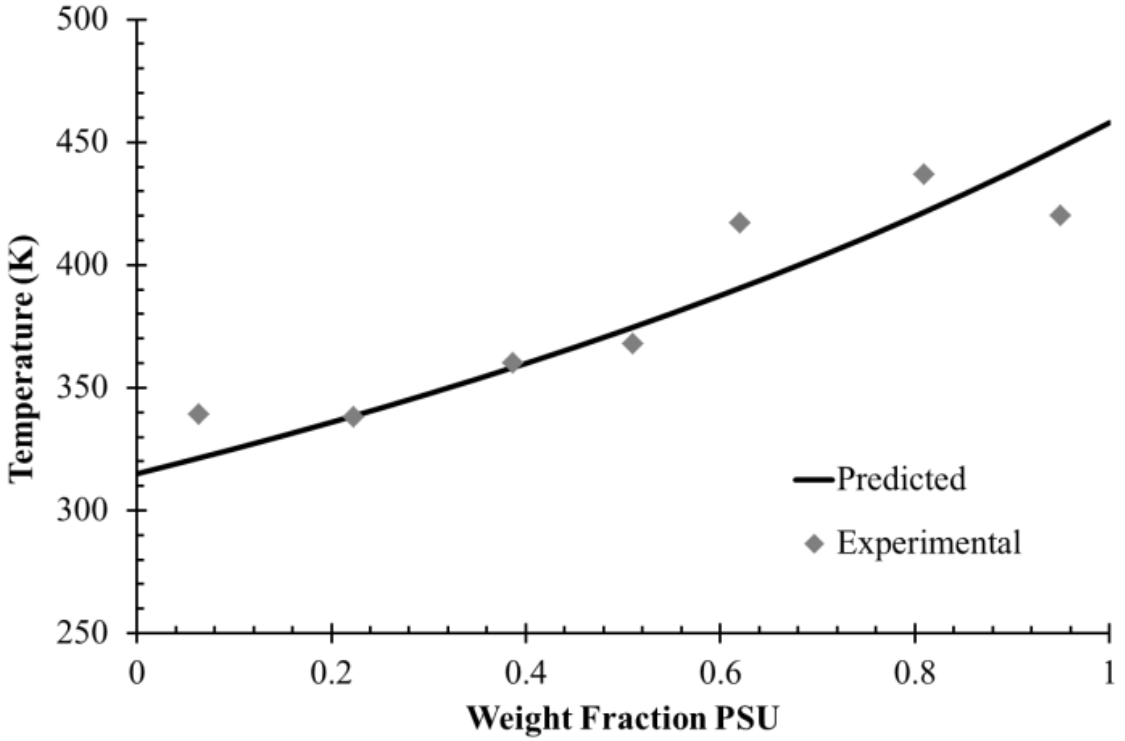

Figure 3. Composition dependence of glass transition observed in DSC. Weight fraction adjusted by percent crystallinity determined from the melting endotherm. Fox prediction shown as solid line. Error bars are within the range of the marker.

For semi-crystalline copolymers, the amorphous weight fractions are typically corrected using percent crystallinity as determined with DSC according to previous reports for PBT (ΔH_f° = 142 J/g).[29] Deviations at compositions 5PSU-95PBT and 95PSU-5PBT resulted from loss of resolution in ^{1}H NMR resonances, leading to difficulty in determining exact copolymer

compositions. Furthermore, the deviation observed at 60PSU-40PBT resulted from unaccounted crystallites, skewing the amorphous weight fraction calculation. Wide-angle x-ray diffraction enabled more precise measurements of crystallinity and will be discussed in a future publication.

Dynamic Mechanical Analysis. Figures 4 and 5 depict the effects of crystallinity on the thermal mechanical behavior of the PSU-PBT segmented block copolymers. **Figure 4** presents an overlay of the DMA for copolymers with compositions ≥ 60% PSU. Importantly, the compositions in Figure 4 do not exhibit any crystallinity observed from DSC. However the 60PSU-40PBT and 80PSU-20PBT had a plateau region above the T_g **(Figure 4)**. Observation of the plateau region presumably resulted from small crystallites serving as physical crosslinks, which prolong terminal flow until reaching temperatures close to the melting temperature of PBT *ca.* 225 °C. The absence of a melting transition in the DSC for these products resulted from a weak endothermic event, and was indistinguishable above the base line.

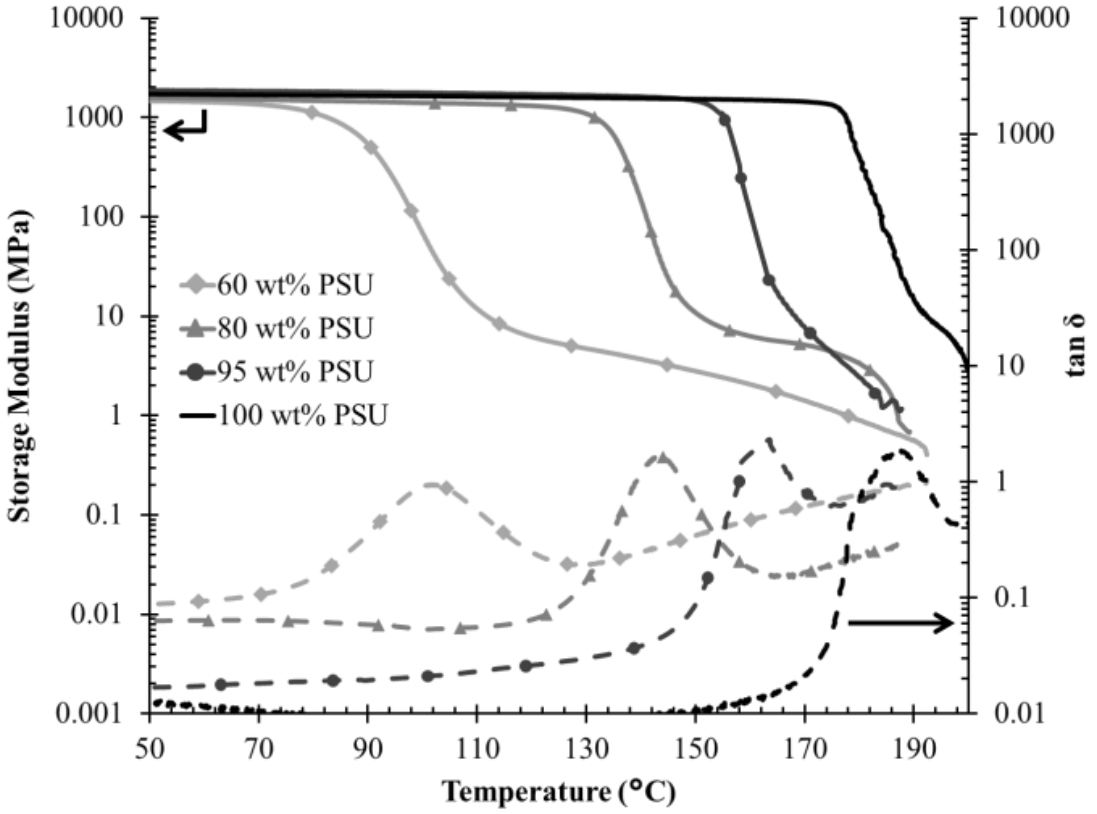

Figure 4. Dynamic mechanical comparison of polysulfone incorporation above 50 wt.% in segmented copolymers. Control (black) is polysulfone (M_n 50 kg/mol). Analyzed in tension mode: 1 Hz and 3 °C/min.

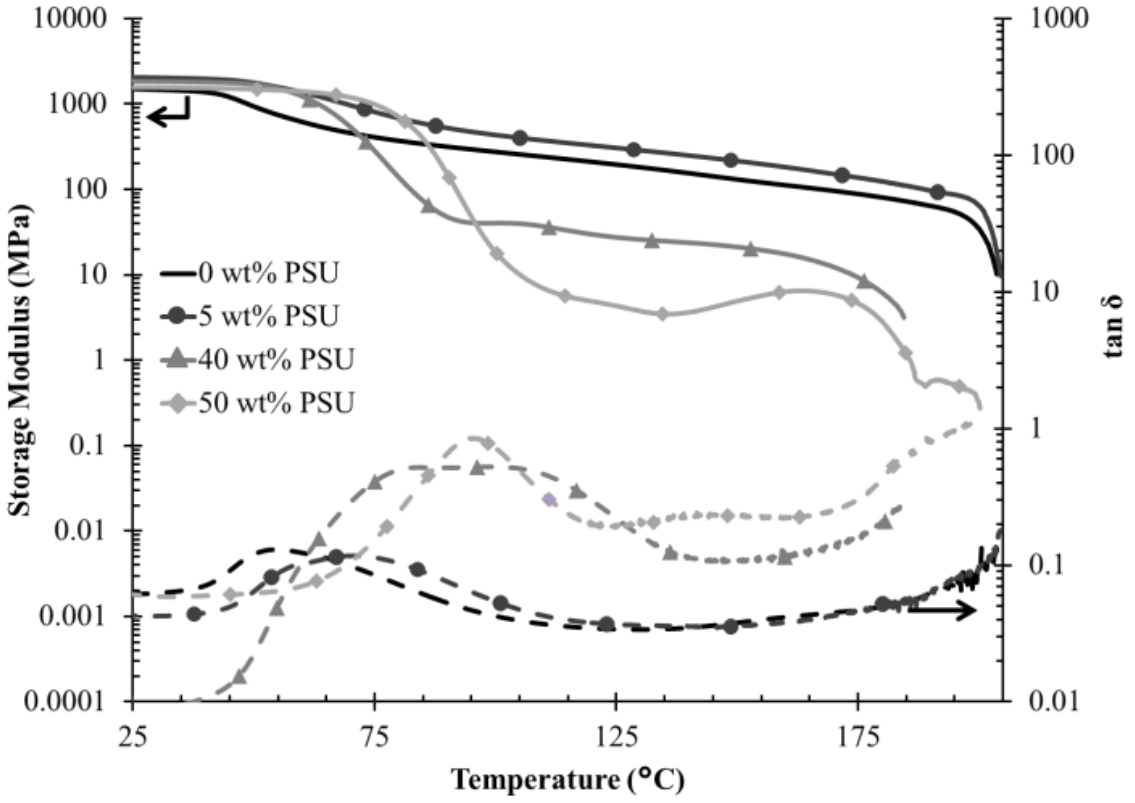

Figure 5. Dynamic mechanical comparison of polysulfone incorporation below 50 wt.% in PSU-PBT segmented copolymers. Control (black) is PBT (M_v 38 kg/mol). Analyzed in tension mode: 1 Hz and 3 °C/min.

As the amount of PSU decreases (**Figure 5**), the plateau modulus increased in tandem with percent crystallinity. For example, 5PSU-95PBT had approximately two orders-of-magnitude increase in storage modulus compared to 50PSU-50PBT. Furthermore, asymmetry in the tan δ peak for these products follows as a result of crystallization occurring after the T_g.[30] The physical barrier with the high T_g PSU segment exaggerated the asymmetry as the rate of crystallinity was retarded and the accompanying crystallization relaxation was delayed. At a composition of 40PSU-60PBT, the broad relaxation in tan δ resulted from a combination of long-range segmental motion and crystallization. Accompanying the broad peak, an increase in the

storage modulus following the T_g suggested crystallization accounted for asymmetry in tan δ. To further illustrate this observation, a reduced heating rate of 3 °C/min for DSC was superimposed with the mechanical analysis of 50PSU-50PBT confirms crystallization **(Figure 6)**. Upon heating at 3 °C/min in the DSC, both the crystallization exothermic and melting endothermic events occurred and complemented the transitions observed in DMA. **Figure S.2** displays similar results for 40PSU-60PBT.

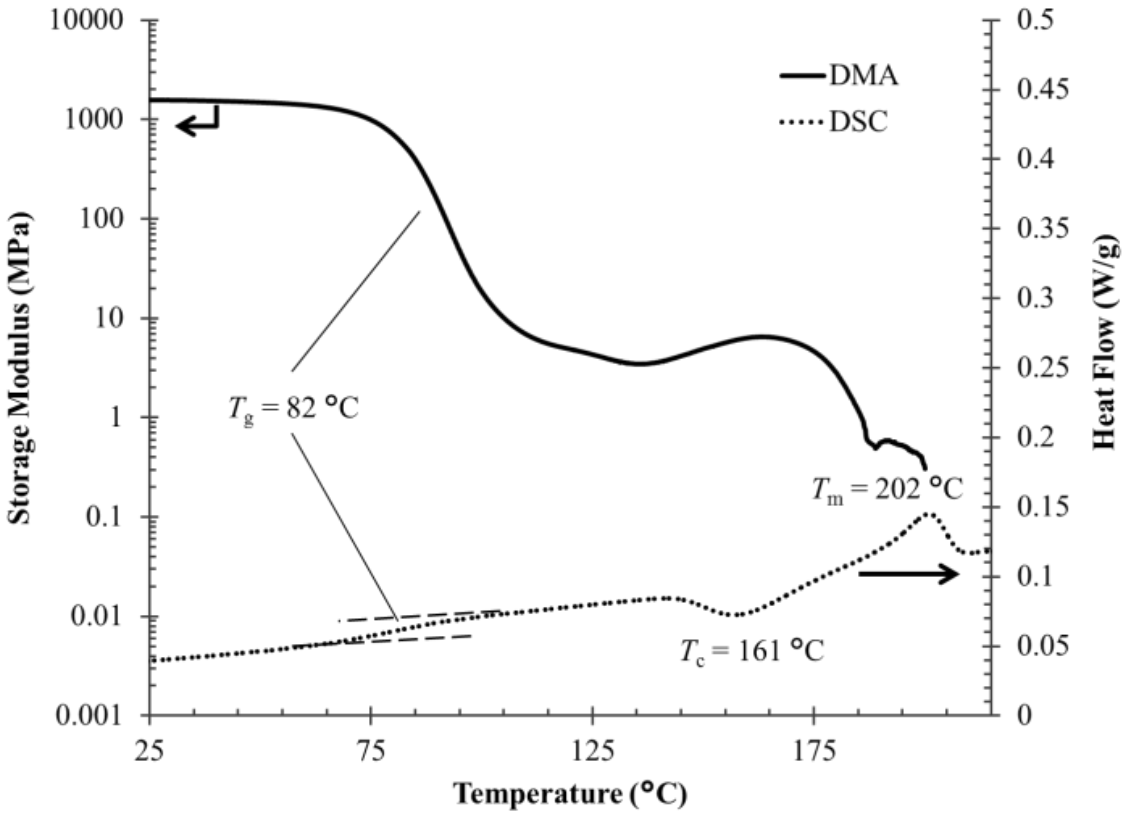

Figure 6. DSC and DMA overlay of 50PSU-50PBT at equivalent heating rates. DMA in tension mode, 1 Hz and 3 °C/min. Second heat at 3 °C/min reported for DSC.

Polysulfones are well established as high-impact materials, and they exhibit relaxations at sub-ambient temperatures, c.a. -100 °C, associated with structural relaxations.[31] **Figure 7**

displays relaxations in the glassy state of the PSU-PBT copolymers. Across the compositional range, a single beta relaxation near -100 °C coincided with the beta transitions of the homopolymers. Studies of impact-resistance dependence on crystallinity for polycarbonate showed significant reduction in impact properties as a result of reduction in beta transition intensity. The authors contributed this reduction in intensity to restriction of amorphous chains from crystalline domains.[32] Interestingly, the intensities of the beta relaxations in **Figure 7** show little variation across the compositional range despite increases in crystallinity with PBT content. As a result, further experiments are ongoing to evaluate the impact-resistance of PSU-PBT copolymers.

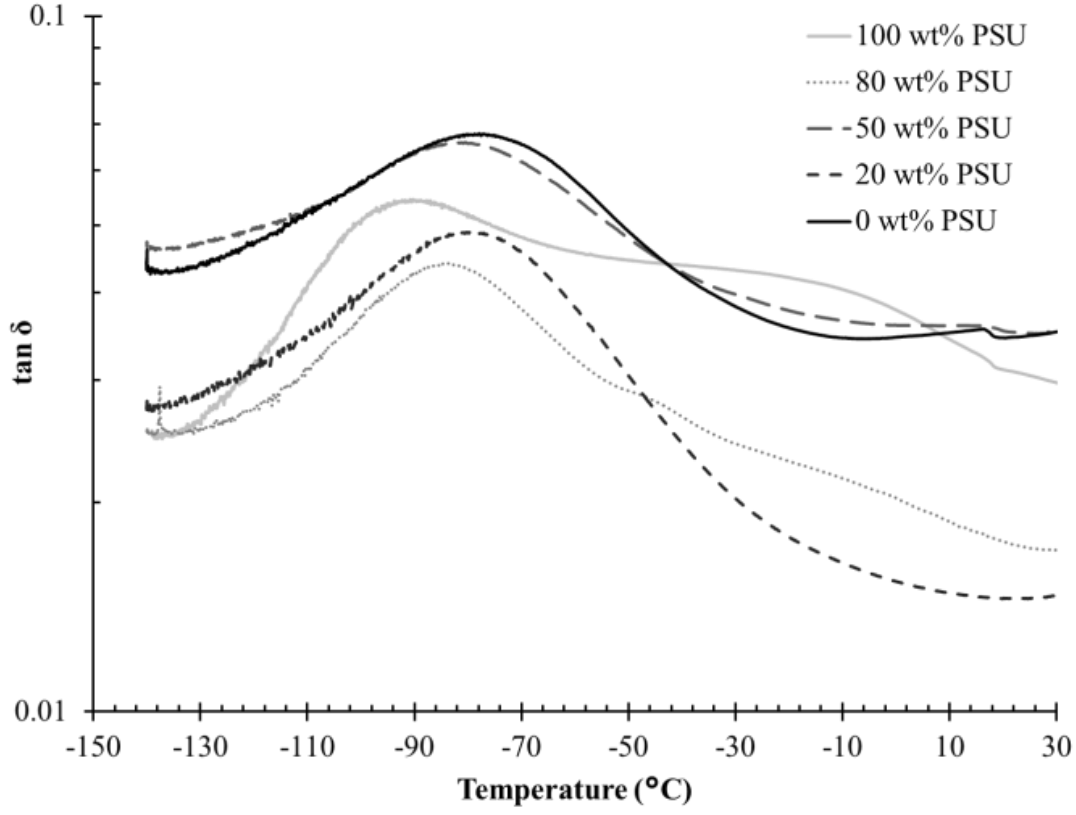

Figure 7. Dynamic mechanical comparison of secondary (beta) transitions at sub-ambient temperatures. DMA in tension mode, 1 Hz and 3 °C/min

Small Angle X-Ray Scattering. Small angle x-ray scattering (SAXS) provides insight into the bulk morphology and reveals a phase ordering consistent with crystallinity.[33,34] **Figure 8** compares the scattering profiles of quench-cooled films, where compositions of less than 40% PSU exhibited a distinct Bragg's reflection. The domain spacing determined from the peak maximum increases with increasing PSU. This observation complements an exclusion of the PSU to the edge of the growing lattice, leading to an increase in spacing between crystallized PBT. As a result, PSU acts as an impurity during crystallization and remains excluded from the crystal structure of PBT.

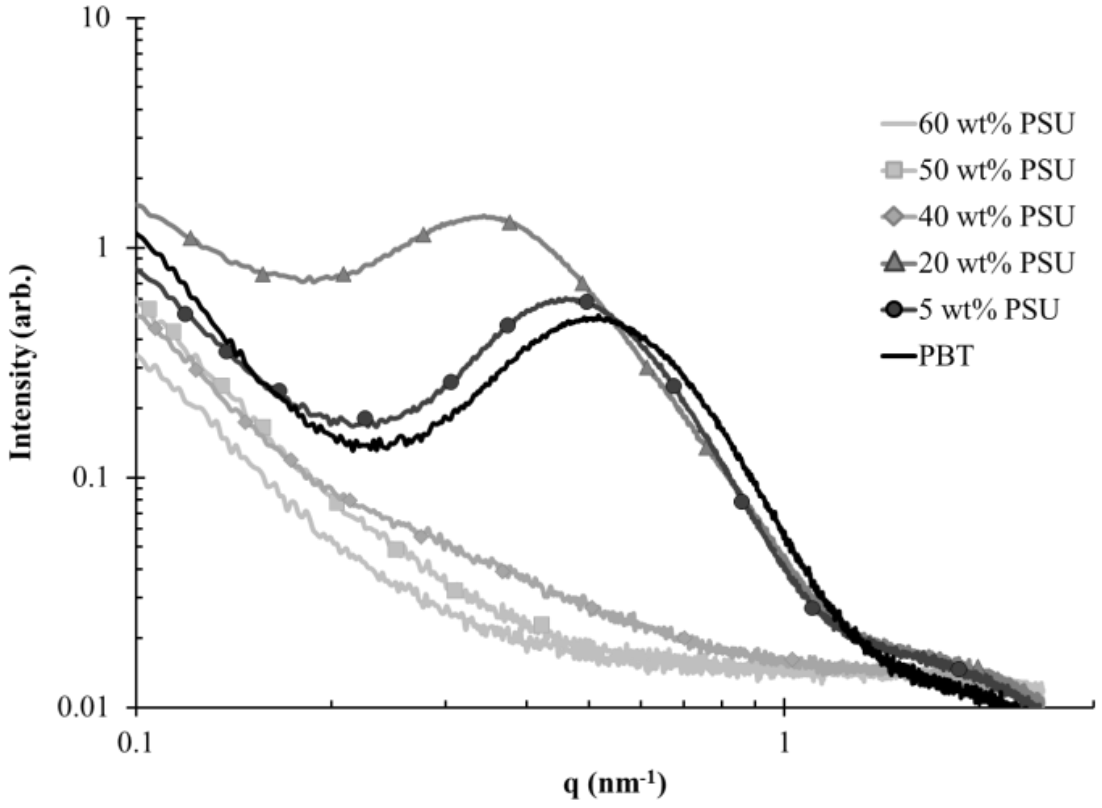

Figure 8. SAXS intensity plots of PSU-PBT segmented copolymers varying in polysulfone incorporation before annealing.

The thermal history of these polymer films significantly impacts their mechanical analyses due to restricted crystallization of the PBT segments. As such, the polymer films were annealed at 160 °C *in vacuo* for 3 d. A temperature was chosen above the T_g of the oligomeric PSU (T_g = 147 °C) to promote long range segmental motion and was used consistently for all compositions. **Figure 9** overlays the resulting scattering profiles for the polymer films. As expected from the DMA results, the annealed films show a single Bragg's reflection at values similar to those observed in the non-annealed, semi-crystalline copolymers. Furthermore, the non-annealed, semi-crystalline copolymers showed a reduction in the domain spacing post-annealing and approached the crystallite spacing of neat PBT **(Table 1)**.

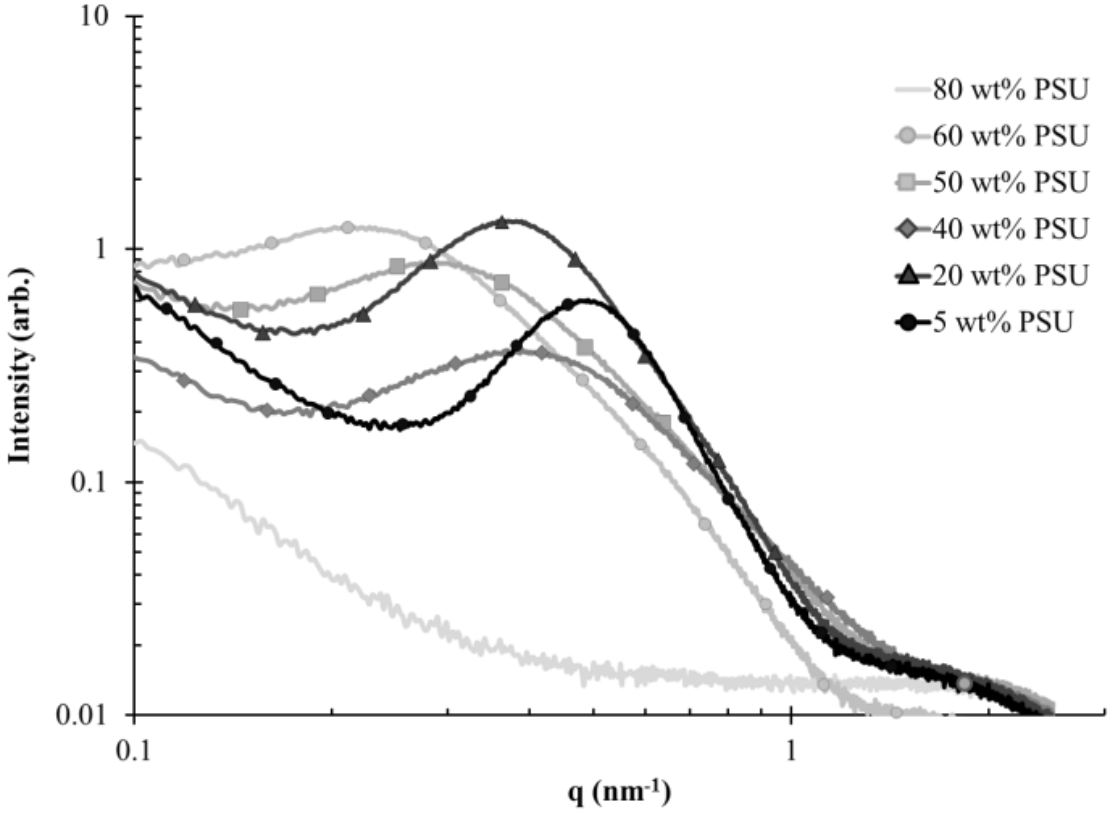

Figure 9. SAXS intensity plots of PSU-PBT segmented copolymers varying in polysulfone incorporation after annealing at 160 °C for 3 days.

The domain spacing correlated to the wt.% PSU incorporation. Similar to the non-annealed samples, the annealed crystallite spacing increased with increasing PSU content **(Table 1)**. Utilizing wide angle x-ray diffraction (WAXD) the resulting crystalline structure of the copolymers is determined to be independent of PSU incorporation **(Figures S.3-S.8)**. The Bragg's reflections correlate strongly with reported literature of semi-crystalline PBT, and only line broadening is observed with incorporation of the PSU segments.[35] Furthermore, from WAXD, crystallinity is verified up to 60 wt.% PSU incorporation. As a result, the PSU segments are restricted to the amorphous domain, increasing the intercrystallite spacing. Simultaneously, the average segment length of the PBT decreases with increasing PSU content **(Table 1)**. As the PBT segment shortens, the available length of crystallizable segments decreases, resulting in a smaller crystallite size. The crystallite size decrease contributes to both an increase in intercrystallite distance and a decrease in T_m **(Table 1)**.

3.5 Conclusions

Melt transesterification of functionalized PSU oligomers generated segmented block copolymers of polysulfone and poly(butylene terephthalate) for the first time. TGA and ^{1}H NMR spectroscopy confirmed compositions of the resulting segmented block copolymers were consistent with the charged weight percent. Also, chemical shifts in ^{1}H NMR spectroscopy highlight extension of the reactive PSU oligomer with PBT formed *in-situ* with dimethyl terephthalate and 1,4-butanediol. A single T_g in DSC suggested a randomly mixed amorphous fraction, indicating that phase separation into ordered morphologies required higher molecular weights between segments. Compositions with ≥ 50 wt.% PBT displayed a T_m relative to the average PBT segment length determined by ^{1}H NMR spectroscopy. Increasing PSU content

resulted in a decrease in the average segment length of PBT, which reduced the percent crystallinity and the melting temperature.

SAXS confirmed the presence of crystallites, which serve as physical crosslinks in the segmented copolymers, resulting in a plateau region in DMA. Tailoring of the percent crystallinity with thermal annealing and PSU content directly impacted the plateau modulus. Furthermore, the retention of the sub-ambient beta transition suggested high impact properties, as typical of polysulfones. Finally, SAXS directly confirmed bulk morphology dependence on the crystallization of the segmented copolymers, not phase ordering. The domain spacing depended on both thermal history and PSU content, and correlated to the amorphous dimension between crystallites. Future work will probe the rheological characteristics as well as further elucidate crystallization kinetics.

3.6 Acknowledgements

The material presented here is based upon work supported in part by the U.S. Army Research Laboratory and the U.S. Army Research Office under the Army Materials Center of Excellence Program, contract W911NF-06-2-0014. Also, the material is partially based upon work supported by the National Science Foundation under Grant No. DMR-0923107. The authors would like to acknowledge Arnold Schneller and Axel Wilms at BASF for insightful discussion and IV analysis.

3.7 References

1. Buckwalter, D. J.; Inglefield, D. L.; Enokida, J. S.; Hudson, A. G.; Moore, R. B.; Long, T. E. Effects of Copolymer Structure on the Mechanical Properties of Poly(dimethyl siloxane) Poly(oxamide) Segmented Copolymers, *Macromol. Chem. Phys.* **2013,** 214, (18), 2073-2082.

2. Bates, F. S.; Hillmyer, M. A.; Lodge, T. P.; Bates, C. M.; Delaney, K. T.; Fredrickson, G. H. Multiblock Polymers: Panacea or Pandora's Box?, *Science* **2012,** 336, (6080), 434-440.
3. Buckwalter, D. J.; Zhang, M.; Inglefield Jr, D. L.; Moore, R. B.; Long, T. E. Synthesis and characterization of siloxane-containing poly(urea oxamide) segmented copolymers, *Polymer* **2013,** 54, (18), 4849-4857.
4. Widin, J. M.; Kim, M.; Schmitt, A. K.; Han, E.; Gopalan, P.; Mahanthappa, M. K. Bulk and Thin Film Morphological Behavior of Broad Dispersity Poly(styrene-b-methyl methacrylate) Diblock Copolymers, *Macromolecules* **2013,** 46, (11), 4472-4480.
5. Widin, J. M.; Schmitt, A. K.; Schmitt, A. L.; Im, K.; Mahanthappa, M. K. Unexpected Consequences of Block Polydispersity on the Self-Assembly of ABA Triblock Copolymers, *J. Amer. Chem. Soc.* **2012,** 134, (8), 3834-3844.
6. Wu, L.; Cochran, E. W.; Lodge, T. P.; Bates, F. S. Consequences of Block Number on the Order−Disorder Transition and Viscoelastic Properties of Linear (AB)n Multiblock Copolymers, *Macromolecules* **2004,** 37, (9), 3360-3368.
7. Bates, F. S. Polymer-Polymer Phase Behavior, *Science* **1991,** 251, (4996), 898-905.
8. He, P.; Shen, W.; Yu, W.; Zhou, C. Mesophase Separation and Rheology of Olefin Multiblock Copolymers, *Macromolecules* **2014,** 47, (2), 807-820.
9. Matsen, M. W. Effect of Architecture on the Phase Behavior of AB-Type Block Copolymer Melts, *Macromolecules* **2012,** 45, (4), 2161-2165.
10. Zhang, M.; Zhang, M.; Moore, R. B.; Long, T. E. Influence of charge placement on the thermal and morphological properties of sulfonated segmented copolyesters, *Polymer* **2013,** 54, (14), 3521-3528.

11. Matsushita, Y. Creation of Hierarchically Ordered Nanophase Structures in Block Polymers Having Various Competing Interactions, *Macromolecules* **2007,** 40, (4), 771-776.
12. Gaymans, R. J. Segmented copolymers with monodisperse crystallizable hard segments: Novel semi-crystalline materials, *Prog. Polym. Sci.* **2011,** 36, (6), 713-748.
13. Stephen, R.; Gibon, C. M.; Weber, M.; Gaymans, R. J. Modifying an amorphous polymer to a fast crystallizing semi-crystalline material by copolymerization with monodisperse amide segments, *J. Polym. Sci., Part A: Polym. Chem.* **2010,** 48, (1), 63-73.
14. Chen, Y.; Lee, C. H.; Rowlett, J. R.; McGrath, J. E. Synthesis and characterization of multiblock semi-crystalline hydrophobic poly(ether ether ketone)–hydrophilic disulfonated poly(arylene ether sulfone) copolymers for proton exchange membranes, *Polymer* **2012,** 53, (15), 3143-3153.
15. Hickner, M. A.; Ghassemi, H.; Kim, Y. S.; Einsla, B. R.; McGrath, J. E. Alternative polymer systems for proton exchange membranes (PEMs), *Chem. Rev. (Columbus)* **2004,** 104, (10), 4587-4612.
16. Xie, W.; Ju, H.; Geise, G. M.; Freeman, B. D.; Mardel, J. I.; Hill, A. J.; McGrath, J. E. Effect of Free Volume on Water and Salt Transport Properties in Directly Copolymerized Disulfonated Poly(arylene ether sulfone) Random Copolymers, *Macromolecules* **2011,** 44, (11), 4428-4438.
17. Kambour, R. P.; Romagosa, E. E.; Gruner, C. L. Swelling, Crazing, and Cracking of an Aromatic Copolyether-Sulfone in Organic Media, *Macromolecules* **1972,** 5, (4), 335-340.
18. Zhang, B.; Turner, S. R. Synthesis and characterization of poly(arylene ether sulfone)s with trans-1,4-cyclohexylene ring containing ester linkages, *J. Polym. Sci., Part A: Polym. Chem.* **2011,** 49, (20), 4316-4324.

19. Cureton, L. T.; Turner, S. R. Synthesis and properties of bisphenol A–terphenol poly(arylene ether sulfone)–polydimethylsiloxane segmented block copolymers, *Eur. Polym. J.* **2011,** 47, (12), 2303-2310.
20. Auman, B. C.; Percec, V. Synthesis and characterization of segmented copolymers of aromatic polyether sulphone and a thermotropic liquid crystalline polyester, *Polymer* **1988,** 29, (5), 938-949.
21. Hoffmann, T.; Pospiech, D.; Häußler, L.; John, A.; Friedel, P.; Komber, H.; Voigt, D.; Werner, P.; Altstädt, V. Synthesis of PEEK/PSU Multiblock Copolymers, *High Performance Polymers* **2004,** 16, (1), 3-20.
22. Pospiech, D.; Häubler, L.; Komber, H.; Voigt, D.; Jehnichen, D.; Janke, A.; Baier, A.; Eckstein, K.; Böhme, F. LC multiblock copolymers containing polysulfone segments. I. Synthesis and morphology, *J. Appl. Polym. Sci.* **1996,** 62, (11), 1819-1833.
23. Pospiech, D.; Häußler, L.; Eckstein, K.; Komber, H.; Voigt, D.; Jehnichen, D.; Friedel, P.; Gottwald, A.; Kollig, W.; Kricheldorf, H. R. Synthesis and Phase Separation Behaviour of High Performance Multiblock Copolymers, *High Perform. Polym.* **2001,** 13, (2), S275-S292.
24. Auman, B. C.; Percec, V.; Schneider, H. A.; Cantow, H.-J. Alternating block copolymers of aromatic poly(ether sulphone) and poly(dimethylsiloxane) by hydrosilylation, *Polymer* **1987,** 28, (8), 1407-1417.
25. Viswanathan, R.; Johnson, B. C.; McGrath, J. E. Synthesis, kinetic observations and characteristics of polyarylene ether sulphones prepared via a potassium carbonate DMAC process, *Polymer* **1984,** 25, (12), 1827-1836.
26. Celebi, O.; Lee, C. H.; Lin, Y.; McGrath, J. E.; Riffle, J. S. Synthesis and characterization of polyoxazoline–polysulfone triblock copolymers, *Polymer* **2011,** 52, (21), 4718-4726.

27. Couchman, P. R. Compositional Variation of Glass-Transition Temperatures. 2. Application of the Thermodynamic Theory to Compatible Polymer Blends, *Macromolecules* **1978,** 11, (6), 1156-1161.
28. Schneider, H. The meaning of the glass temperature of random copolymers and miscible polymer blends, *J. Therm. Anal. Calorim.* **1999,** 56, (3), 983-989.
29. Runt, J.; Miley, D. M.; Zhang, X.; Gallagher, K. P.; McFeaters, K.; Fishburn, J. Crystallization of poly(butylene terephthalate) and its blends with polyarylate, *Macromolecules* **1992,** 25, (7), 1929-1934.
30. Cecere, A.; Greco, R.; Ragosta, G.; Scarinzi, G.; Taglialatela, A. Rubber toughened polybutylene terephthalate: influence of processing on morphology and impact properties, *Polymer* **1990,** 31, (7), 1239-1244.
31. Noshay, A.; Robeson, L. M. Sulfonated polysulfone, *J. Appl. Polym. Sci.* **1976,** 20, (7), 1885-1903.
32. Wyzgoski, M. G.; Yeh, G. S. Y. Origin of Impact Strength in Polycarbonate: I. Effect of Crystallization and Residual Solvent, *International Journal of Polymeric Materials and Polymeric Biomaterials* **1974,** 3, (2), 133-148.
33. Mauritz, K. A.; Moore, R. B. State of Understanding of Nafion, *Chem. Rev.* **2004,** 104, (10), 4535-4586.
34. Goderis, B.; Reynaers, H.; Koch, M. H. J.; Mathot, V. B. F. Use of SAXS and linear correlation functions for the determination of the crystallinity and morphology of semi-crystalline polymers. Application to linear polyethylene, *J. Polym. Sci. Part B Polym. Phys.* **1999,** 37, (14), 1715-1738.

35. Hsiao, B.; Wang, Z.-g.; Yeh, F.; Gao, Y.; Sheth, K. Time-resolved X-ray studies of structure development in poly(butylene terephthalate) during isothermal crystallization, *Polymer* **1999,** 40, (12), 3515-3523.

3.8 Supporting Information

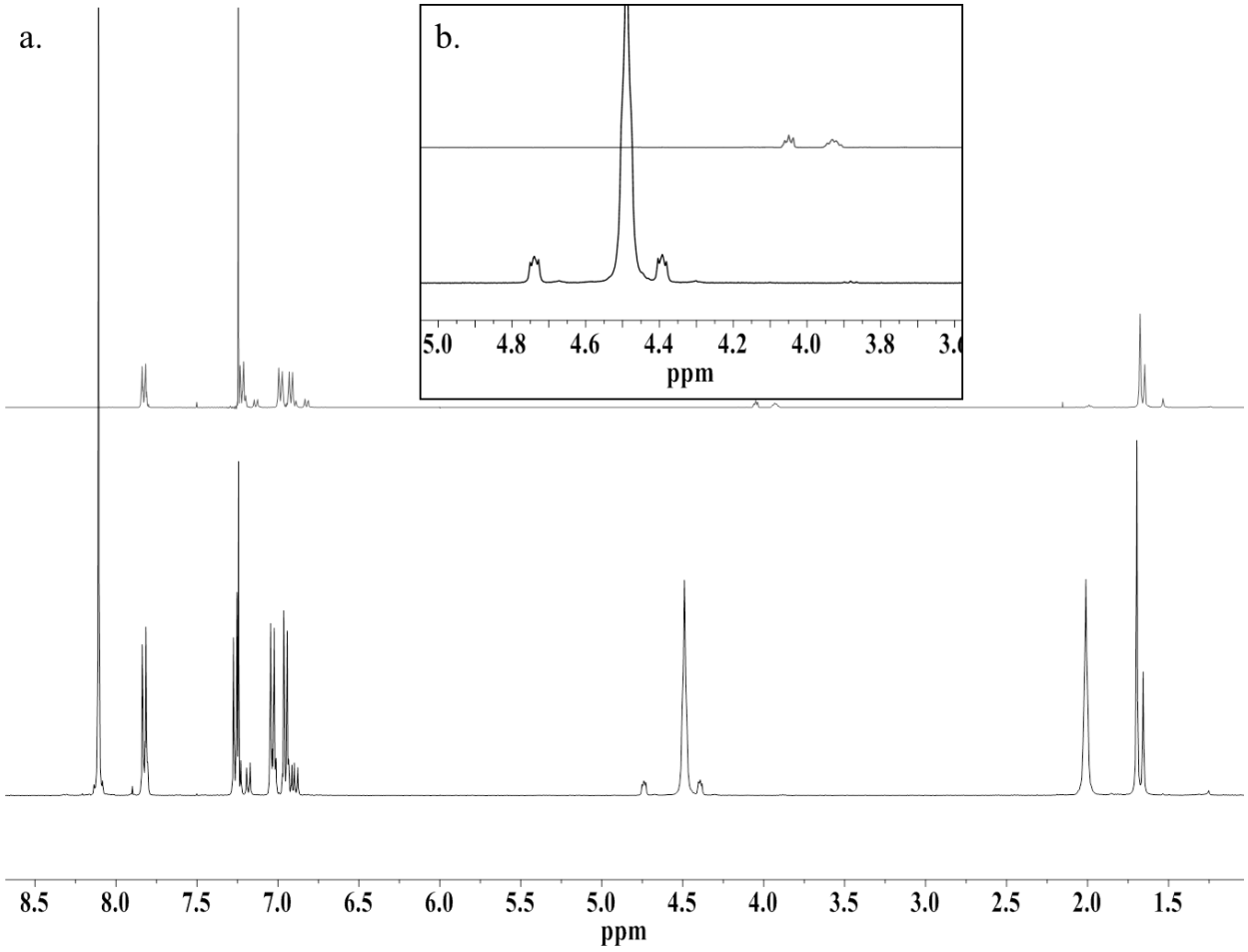

Figure S.1. ^{1}H NMR of functionalized polysulfone oligomer (top) and 50PSU-50PBT segmented copolymer (bottom). Inset spectrum (b) highlights the downfield chemical shift associated with successful polysulfone incorporation.

Table S.1. Intrinsic viscosity of PSU-PBT copolymers in 1:1 (v:v %) Phenol:*o*-dichlorobenzene.

	Intrinsic Viscosity (mL/g)
Ultrason S2010	66
80PSU-20PBT	75
50PSU-50PBT	97
20PSU-80PBT	95
Ultradur B2550	108

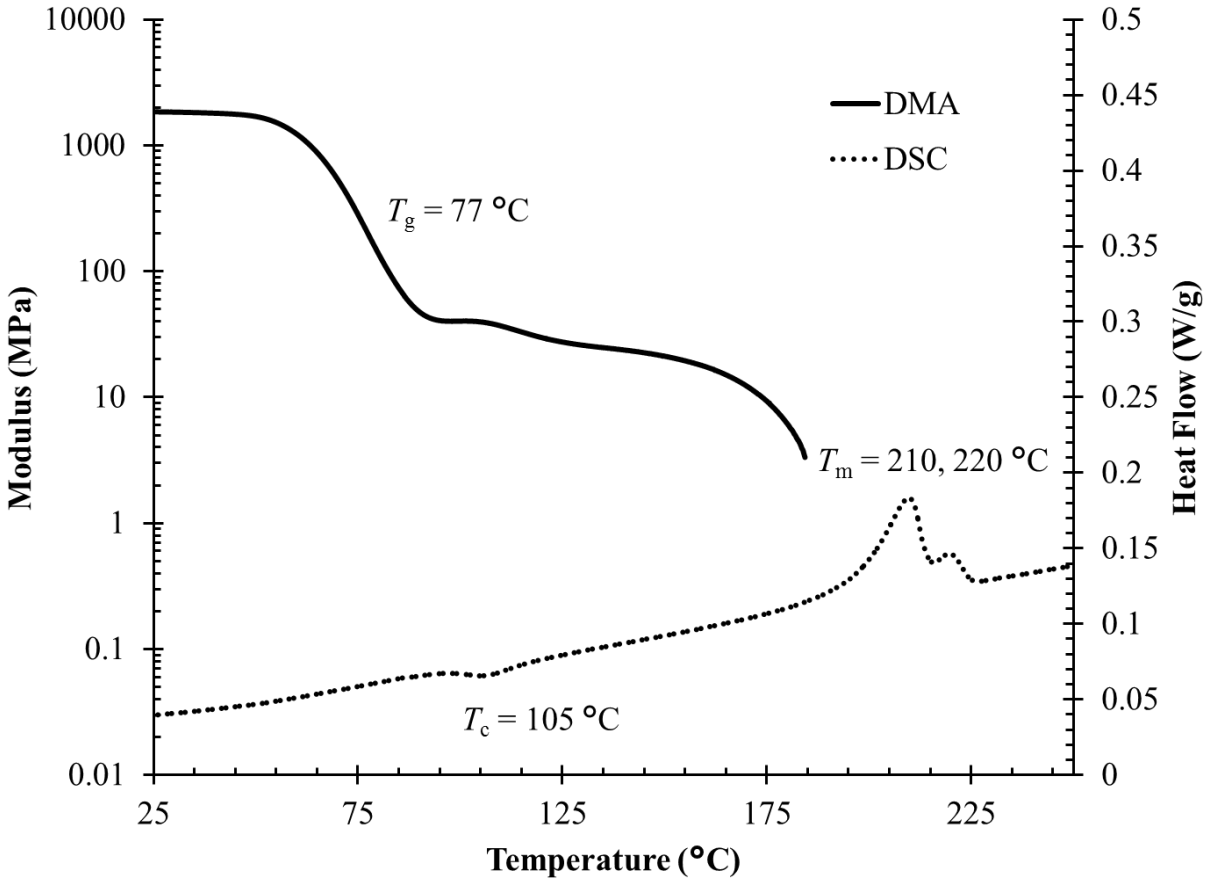

Figure S.2. DSC and DMA overlay of 40PSU-60PBT copolymer at equivalent heating rates. DMA in tension mode, 1 Hz and 3 °C/min. Second heat at 3 °C/min reported for DSC.

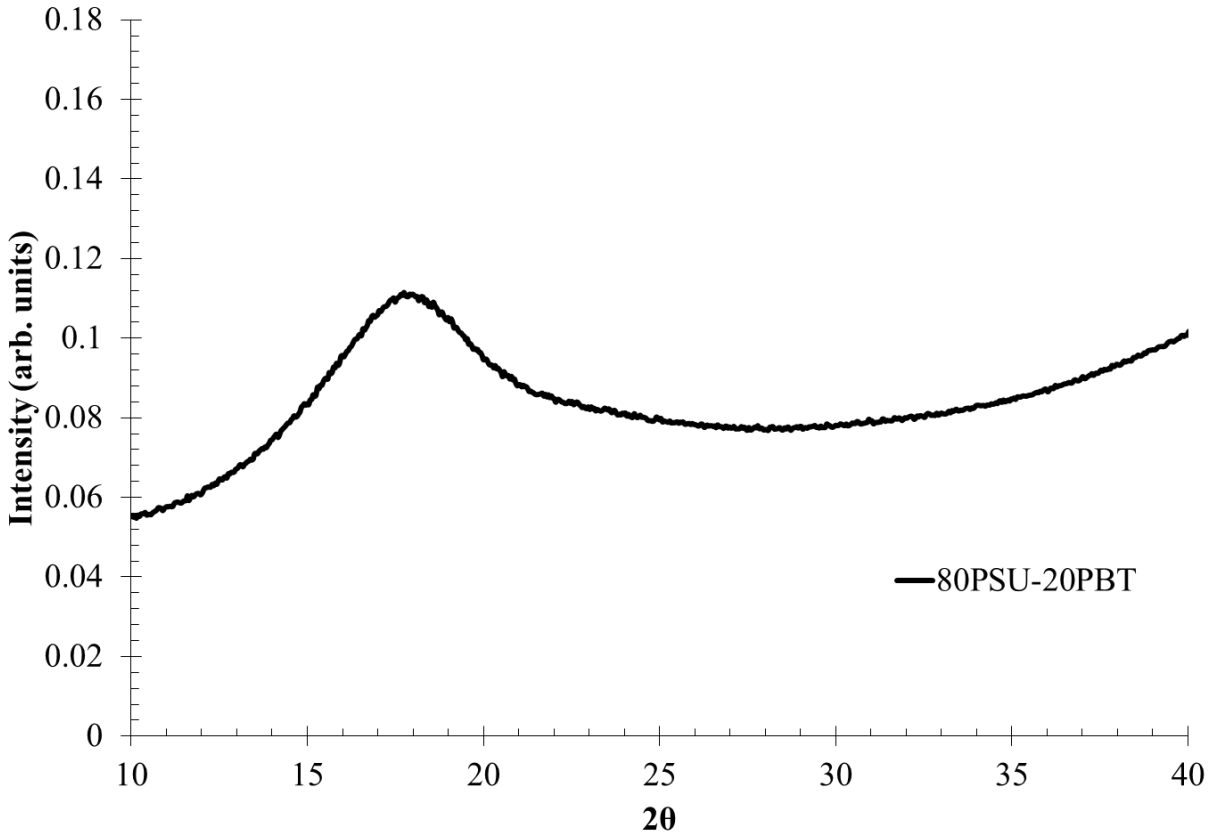

Figure S.3. WAXD intensity plot of annealed 80PSU-20PBT segmented block copolymer.

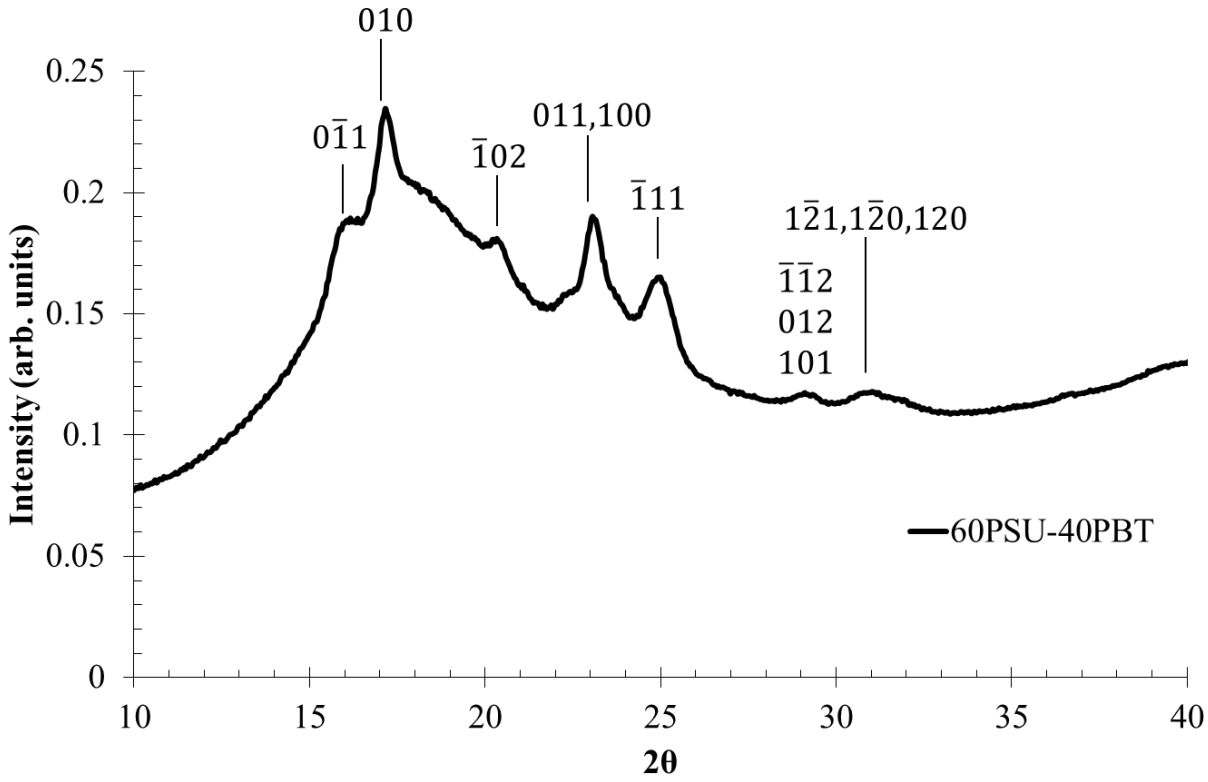

Figure S.4. WAXD intensity plot of annealed 60PSU-40PBT segmented block copolymer.

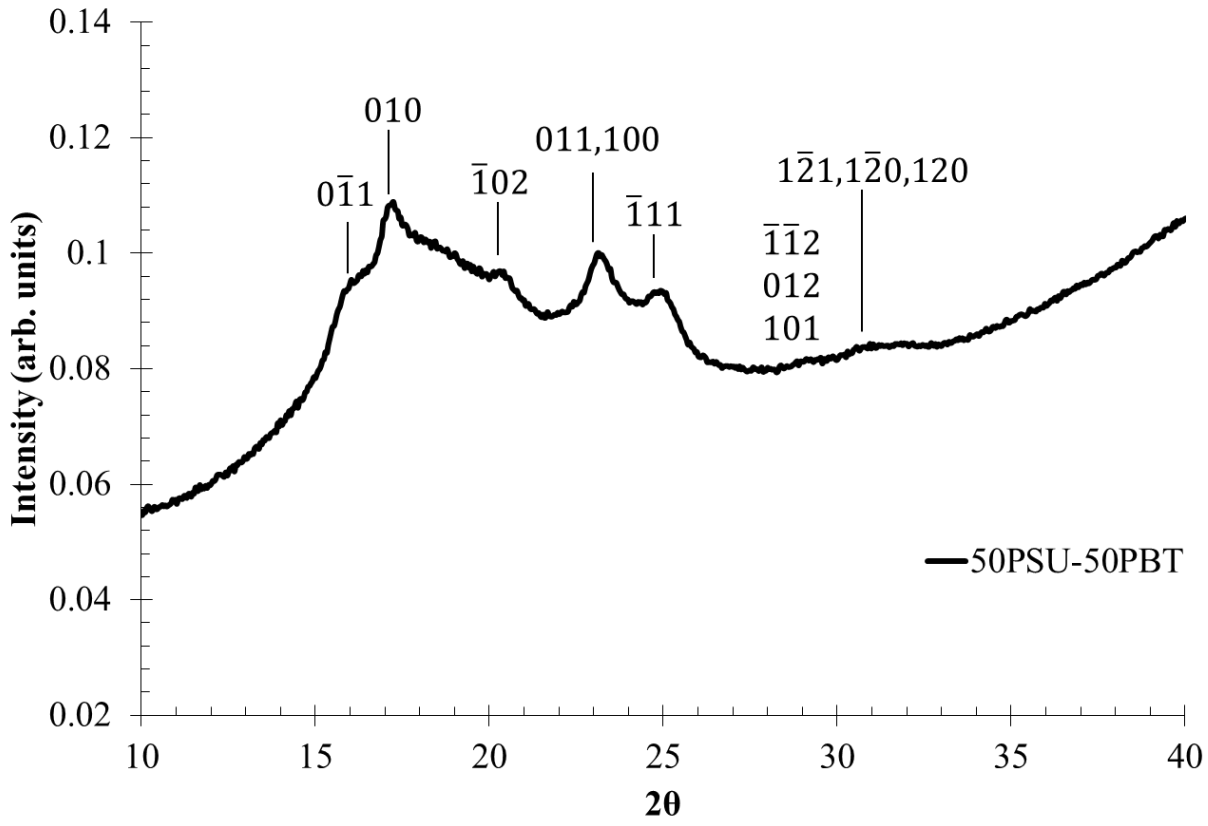

Figure S.5. WAXD intensity plot of annealed 50PSU-50PBT segmented block copolymer.

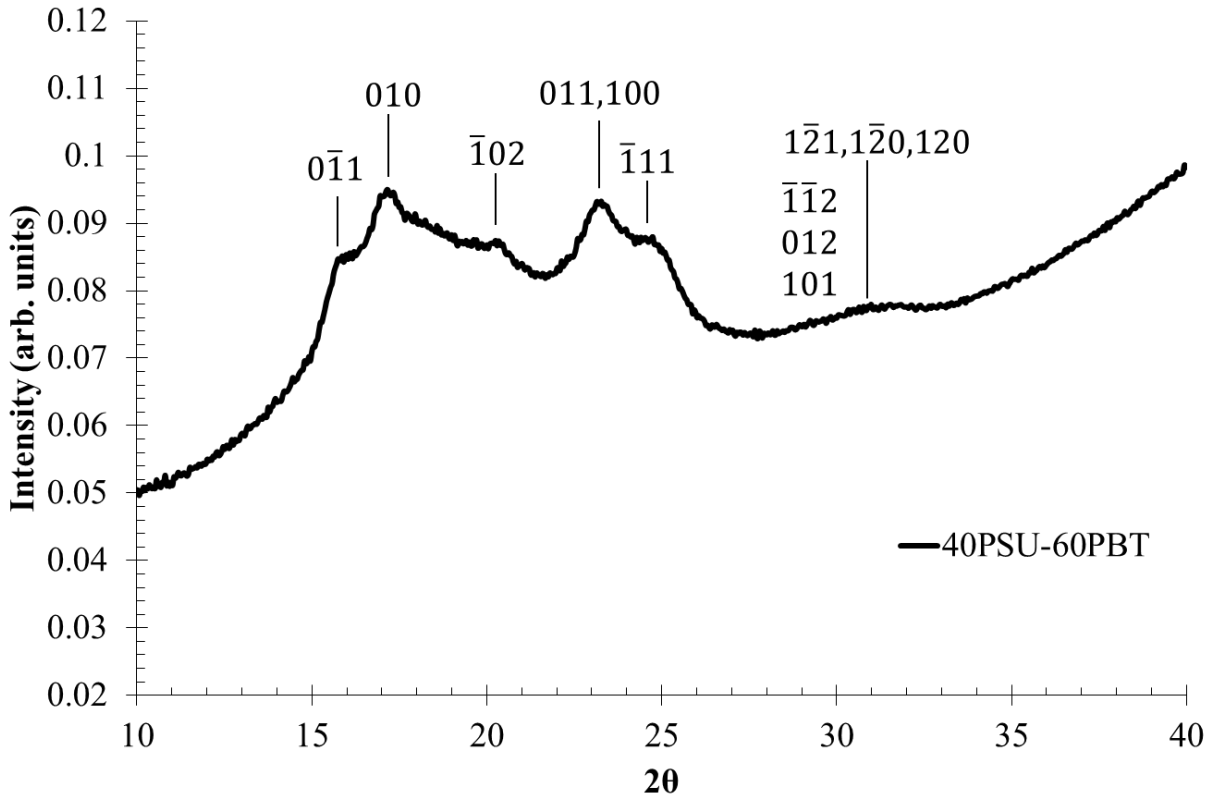

Figure S.6. WAXD intensity plot of annealed 40PSU-60PBT segmented block copolymer.

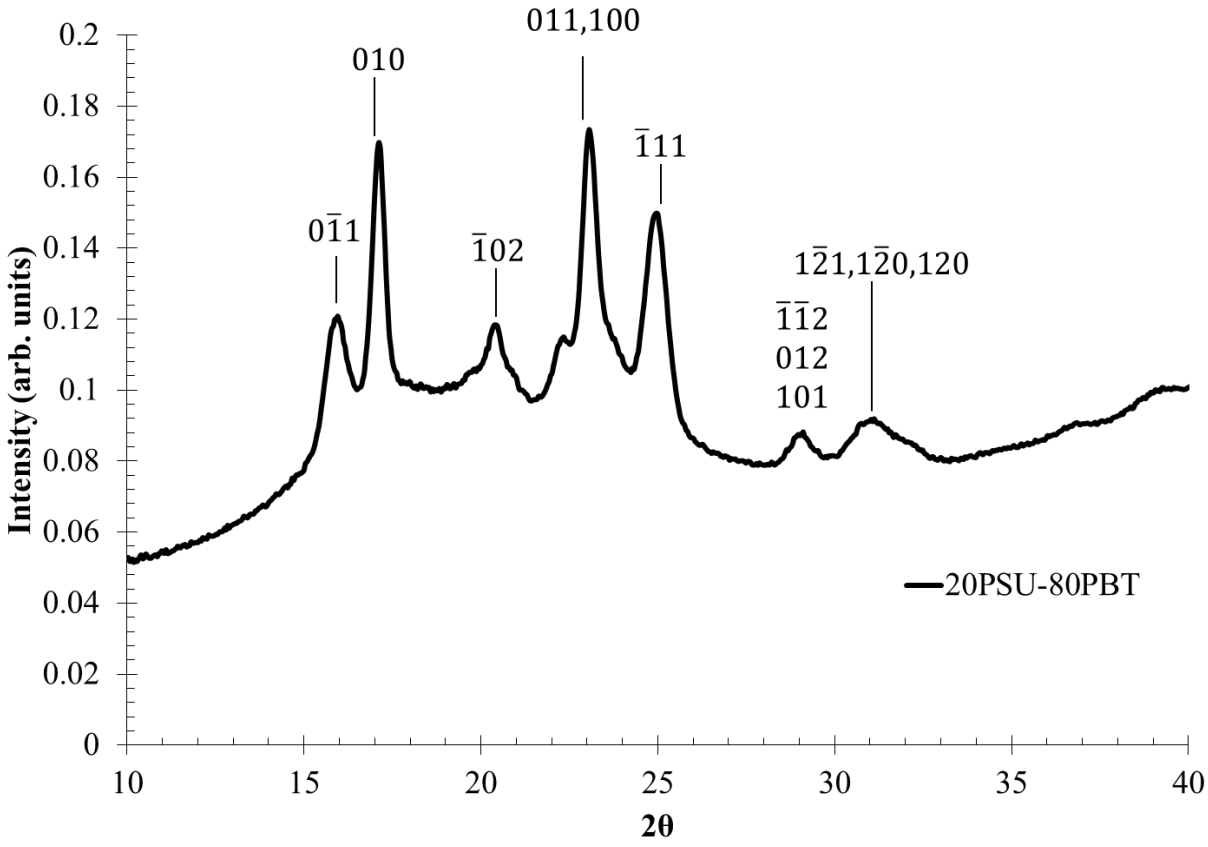

Figure S.7. WAXD intensity plot of annealed 20PSU-80PBT segmented block copolymer.

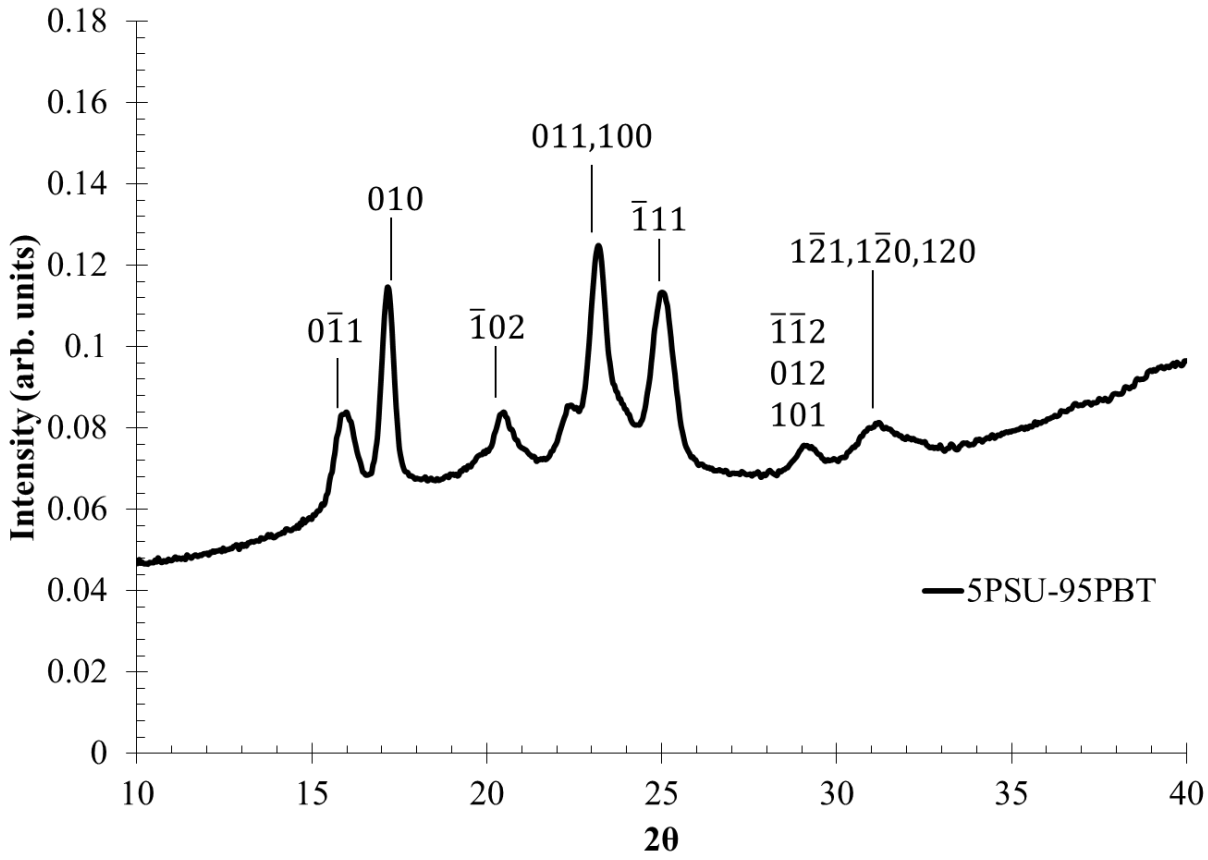

Figure S.8. WAXD intensity plot of annealed 5PSU-95PBT segmented block copolymer.

Chapter 4: Synthesis of Polysulfone-containing Poly(butylene terephthalate) Segmented Block Copolymers: Influence of segment length on thermomechanical performance

(Submitted to *Macromolecules*)

Joseph M. Dennis, Gregory B. Fahs, Nicholas G. Moon, Ryan J. Mondschein, Robert B. Moore, Garth L. Wilkes, and Timothy E. Long

Department of Chemistry, Macromolecules Innovation Institute

Virginia Tech Blacksburg, Virginia 24061 USA

4.1 Abstract

A facile synthesis of hydroxyethyl-functionalized poly(ether sulfone) (PESu) oligomers permitted subsequent melt transesterification into segmented block copolymers with poly(butylene terephthalate). The unique solubility of the PESu oligomers in the melt with 1,4-butanediol and dimethyl terephthalate enabled a systematic study of segment length on thermomechanical properties of the resulting block copolymers. ^{1}H NMR spectroscopy revealed a compositional dependence on the average segment length of the PBT. Additionally, the concert of NMR spectroscopy, DSC, and DMA highlighted critical segment lengths for crystallization and phase separation. In agreement with a relatively constant T_m and phase separation observed with DSC and DMA, respectively, small-angle x-ray scattering identified a compositionally independent lamellar thickness, while the amorphous layer thickness increased with PESu incorporation. As a result, the complementary analytical techniques provided an

understanding of the morphological influence on the thermomechanical behavior of an unprecedented family of high T_g, semi-crystalline, segmented block copolymers.

4.2 Introduction

The self-assembly of covalently bound immiscible polymer segments enables unique physical properties to address many needs of emerging technologies.[1-3] Numerous examples demonstrate the phase behavior and physical properties of di- and triblock copolymers with focus on the interdependence of segment length (N) and the Flory-Huggins interaction parameter (χ).[4-6] Improved synthetic methods for controlled polymerizations continue to elucidate a fundamental understanding of more complex polymer microstructures and architectures.[7] In contrast to the phase behavior of multiblock copolymers (AB, ABA, etc.) with low polydispersity, the number of repeating shorter segments [$(AB)_n$] remains as another important parameter in the design of microphase-separated block copolymers.[8-10]

Specific interactions, such as hydrogen bonding, crystallization, or ionic aggregation impart controlled morphologies at relatively short segment lengths.[1-3, 11, 12] As a result, many thermoplastic elastomers (TPEs) feature segmented copolymers with hydrogen-bonding sequences.[2, 3, 12] The directionality and strength of the hydrogen bond provides enhanced mechanical integrity, including improved elastomeric windows and lower extensional hysteresis.[2, 3] Introducing ion-containing segments provided platforms for achieving phase separation for energy and water purification applications.[13-15] In particular, the thermal and hydrolytic stability of sulfonated polysulfone segmented block copolymers permitted extended water purification membrane life under harsh use conditions.[15] However, poor solvent resistance hinders the use of amorphous polysulfone membranes.[16]

Semicrystalline polyesters exhibit superior solvent resistance compared to amorphous polysulfones. Recently, copolymerization of bisphenol-A (BPA) based, polysulfone-containing polyesters revealed a commercially viable synthetic route to generate segmented block copolymers.[17, 18] The thermal stability of BPA polysulfones advantageously permitted processing at elevated temperatures required for melt phase synthesis of polyesters.[17, 18] Interestingly, the miscibility of short segments of BPA polysulfone in poly(butylene terephthalate) eliminated crystallization of the polyester at high incorporations. However, melt heterogeneity longer segments prevented further investigation into the influence of segment length on physical properties.

Taking advantage of the diversity of commercially available polysulfone structures, this report circumvents melt heterogeneity through optimal solubility parameters to evaluate the influence of polysulfone segment length on physical properties. A facile, one-pot synthesis of telechelic, hydroxyethyl-functionalized poly(ether sulfones) (PESu) reduced waste and improved atom efficiency compared to previous reports. Subsequent melt transesterification of the functional polysulfones in the presence of dimethyl terephthalate and 1,4-butanediol afforded segmented block copolymers with varying polyester segment lengths. Variation of polysulfone and polyester segment lengths generated critical structure-property relationships for this novel family of copolymers. Understanding this synergy of physical and chemical properties offers immediate impact as high performance engineering thermoplastics for emerging automotive and electronic industries.

4.3 Experimental

Materials. 4,4'-dichlorodiphenylsulfone (DCDPS, BASF), and 4,4'-bishydroxydiphenolsulfone (BHDPS, BASF) was used without purification. 1,4-butanediol (99%), dimethyl terephthalate

(99%), potassium carbonate (≥99%), 2-chloroethanol (99%), Celite 545, anhydrous dimethylacetamide, and titanium tetraisopropoxide (99.999%) were purchased from Sigma Aldrich and used as received. All deuterated solvents were purchased from Cambridge Isotope Laboratories, Inc.

Analytical Methods. ^{1}H NMR spectroscopy utilized a Varian Unity 400 spectrometer operating at 399.87 MHz and 23 °C with a either $CDCl_3$ or a binary mixture of 9:1 $CDCl_3$:CF_3COOD (*circa* 8 mg/mL). Thermogravimetric analysis (TGA) exploited a TA Instruments TGA Q500 from room temperature to 600 °C at a heating rate of 10 °C/min under constant N_2 purge. TA Instruments DSC Q2000 with a N_2 atmosphere and heat/cool/heat cycles of 10 °C/min, 100 °C/min, and 10 °C/min, respectively, provided differential scanning calorimetry (DSC). Dynamic mechanical analysis (DMA) revealed modulus versus temperature behavior using a TA Instruments DMA Q800 in oscillatory tension mode at 1 Hz and 3 °C/min. Compression molding between Kapton® sheets at 270 °C using a PHI hydraulic press generated free-standing films, which were cooled slowly in air over 1 hour (to facilitate crystallization of the PBT component).

Small Angle X-Ray Scattering (SAXS). Small-angle, x-ray scattering provided bulk morphology on the resulting copolymer films using a Rigaku S-Max 3000, 3-pinhole instrument adapted with a rotating anode producing Cu K_α irradiation at a wavelength of 1.54 Å. Using a constant sample-to-detector distance of 1.6 m, the instrument was calibrated with a silver behenate standard. A 2D multiwire, proportional counting, gas-filled detector was used to collect two-dimensional SAXS patterns with a one-hour exposure time, and then corrected for detector noise, background scattering, and sample absorption. All data processing and analysis were completed with the SAXSGUI software package to obtain radially integrated SAXS

intensity versus scattering vector q, where $q = 4\pi \sin(\theta)/\lambda$ and 2θ is the scattering angle and λ is the x-ray wavelength. SAXS profiles were analyzed using the linear correlation function *via* the following relationship[19] in order to extract characteristic dimensions associated with the lamellar crystallites:

$$\gamma(r) = \frac{\int_0^\infty I(q)\cos(qr)q^2\,dq}{\int_0^\infty I(q)q^2 dq} \qquad Eq.1$$

Although physically limited to a finite scattering angle, extrapolation to high and low-q regions using Porod and Guinier functions, respectively, enabled the application of Equation 1 .

The real space dimension, r, provided the shift factor in the intensity spectrum *via* the cosine transform (Equation 1). The correlation between the shifted and unshifted spectra originated a solution $\gamma(r = 0) = 1$, and behaved as a decaying oscillation about $\gamma(r) = 0$ with increasing r for periodic systems (e.g. stacked lamella). Furthermore, a comparable model system for an "ideal" lamellar lattice, as described by Vonk[19], enabled extraction of the characteristic dimensions. In summary, a linear extrapolation of the initial decay to intersect with the tangent of the first minimum identified the minimum thickness for the minor phase (S) (e.g. crystallite thickness) in nanometers. The long period (L_p) is extractable as the first maxima away from $r = 0$. Using both the minimum crystallite thickness and the long period, the local crystallinity (L_c) is defined as follows:

$$L_c = \frac{S}{L_p} \qquad Eq.2$$

Hydroxyethyl-terminated Poly(ether sulfone) Synthesis (HE-PESu$_{8k}$). A novel, one-pot synthesis of a 8 kg/mol, hydroxyethyl-terminated, poly(ether sulfone) summarizes the typical

method. 4,4'-dichlorodiphenyl sulfone (57.012 g, 0.198 mol), 4,4'-bishydroxydiphenyl sulfone (53.879 g, 0.2153 mol), potassium carbonate (89.26 g, 0.646 mol), toluene (230 mL) and anhydrous N,N-dimethylacetamide (475 mL) were charged to a 1000 mL, three-necked, round-bottomed flask. Purging the flask prior to heating to 160 °C for 30 min with N_2 ensured an inert atmosphere. The collection of water in a Dean-Stark trap under toluene reflux monitored the dehydration progress. Once water collection stopped, the reaction temperature was slowly increased to 180 °C with the removal of toluene, and the reaction proceeded under these conditions for 18 h. The resulting green, heterogeneous solution was then cooled to 130 °C and 2-chloroethanol (5.032 g, 0.0625 mol) and potassium iodide (1.04 g, 0.00625 mol) were added directly into the reaction flask. The reaction continued for 2 hours resulting in a pale yellow solution. The heterogenous solution was then cooled to room temperature and filtered through Celite to remove undesired salts. Dropwise addition into 4 L of DI water resulted in a solid precipitate, which was filtered and dried *in vacuo* at 120 °C for 24 hours.

Poly(ether sulfone)-Poly(butylene terephthalate) Segmented Block Copolymer Synthesis. Conventional melt transesterification provided segmented block copolymers, and the synthesis of 80PESu_{8k}-20PBT is described. HE-PESu_{8k} (13.2 g), 1,4-butanediol (1.6 g, 0.018 mol), and dimethyl terephthalate (2.91 g, 0.015 mol) were charged to a dry, 100-mL, round-bottomed flask. Titanium tetraisopropoxide (100 ppm) was added to facilitate transesterification. The flask was equipped with an overhead stir rod, nitrogen inlet, and condenser. Three cycles of sequential degassing under vacuum followed by a nitrogen purge ensured an inert atmosphere for polymerization. Under a constant nitrogen purge, the reaction proceeded at sequential temperature steps from 220 to 250 °C over 2.5 h. The pressure was then subsequently reduced (> 0.1 mmHg) and the temperature raised to 270 °C for an additional 2 h. The resulting polymer

products were isolated directly without further purification. Nomenclature for the copolymer follows *x*PESu$_y$-*z*PBT, where *x* and *z* report the weight percent of poly(ether sulfone) and poly(butylene terephthalate), respectively, and *y* describes the segment length of the poly(ether sulfone).

4.4 Results and Discussion

Previous literature reports the synthesis of hydroxyethyl-terminated polysulfones through ring-opening of ethylene carbonate.[17, 18, 20] Although quantitative, functionalization required isolation of the phenol-terminated oligomers with an excess of solvent. Direct end-capping of phenol-terminated polysulfones with an alkyl halide following polymerization provided commercially viable, quantitative conversions without an intermediate isolation step.[21-23] Following a similar protocol, synthesis of hydroxyethyl-terminated poly(ether sulfone)s (PESu) proceeded through the displacement of chlorine from 1-chloroethanol with phenol-terminated PESu (Scheme 1). This synthetic method provides a facile, one-pot approach to quantitative conversions of a phenol-terminated polysulfone to a primary alcohol. Using unique chemical shifts of the phenol and hydroxyethyl protons, ^{1}H NMR spectroscopy (Figure S.1) provided insight into reaction conversions and enabled optimization of reaction conditions (Table S.1). Importantly, a substochiometric amount of potassium iodide enabled quantitative end-group functionalization.

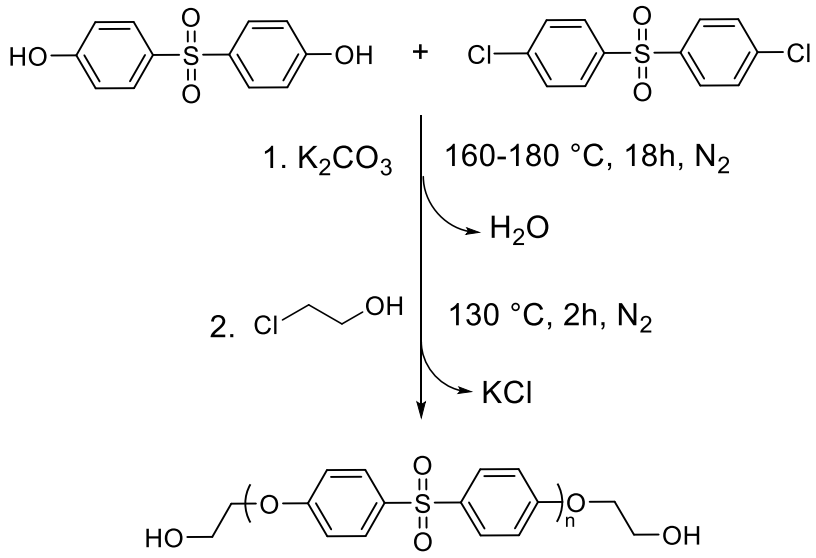

Scheme 1. One-pot, two-step synthesis of hydroxyethyl-terminated PESu oligomers.

Incorporation of polysulfone segments into poly(butylene terephthalate) followed our similar procedures reported earlier (Scheme 2).[17] As a result of the solvent-free polymerization technique, the solubility of the PESu oligomer in the increasing polyester melt viscosity is critical.[17] Interestingly, the change in polarity between PESu and PSU enabled incorporation of higher molecular weight segments of PESu into PESu-PBT segmented block copolymers without the observation of melt heterogeneity. Using van Krevelen's group contribution theory[24], Figure 1 highlights the change in solubility parameters for PBT and PESu at various molecular weights. The intersection of solubility parameter curves of PESu and PBT occurs during the polymerization of PBT, providing accessibility of the PESu end groups at a critical stage in the reaction. At the crossover point, the similar oligomer molecular weights of PBT and PESu enable segment-segment coupling in an ideal step-growth fashion. In contrast, PSU's solubility parameter does not indicate a crossover, corroborating the segmental limitation reported previously.[17]

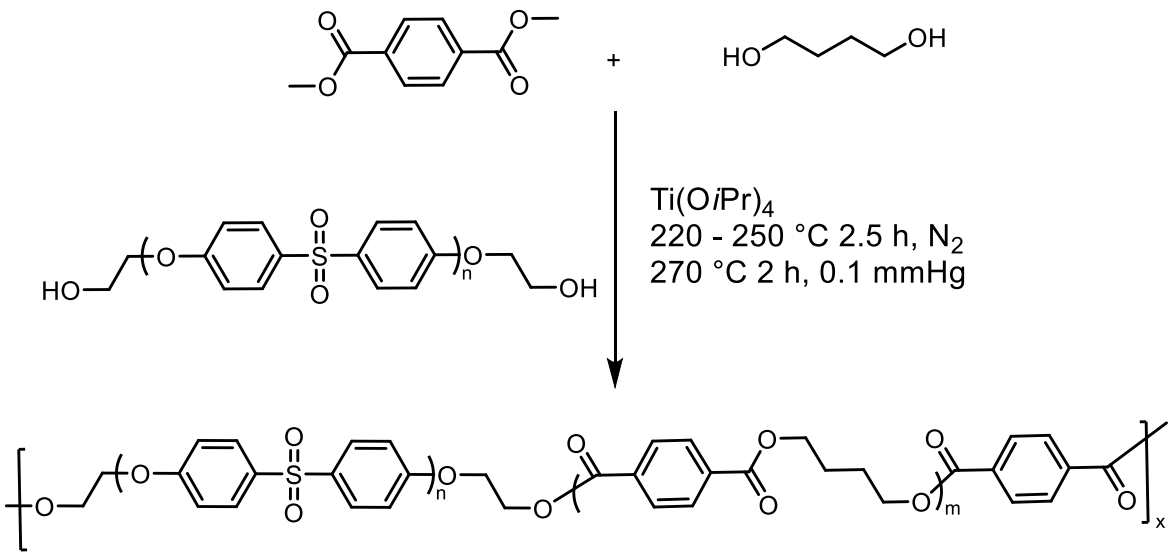

Scheme 2. Synthesis of PESu-PBT segmented block copolymers using melt transesterification.

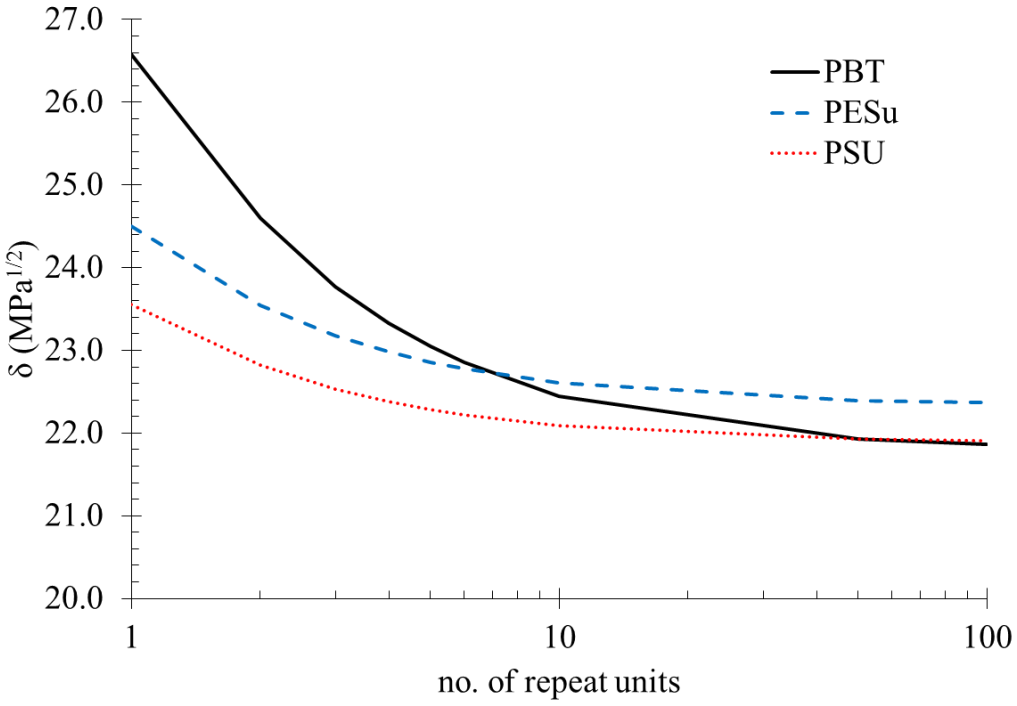

Figure 1. Solubility parameters calculated using van Krevelen group contribution theory of poly(butylene terephthalate), poly(ether sulfone), and bisphenol-A polysulfone at various block lengths, identifying the influence of end groups on chain polarity.

The unique chemical shifts observed in ^{1}H NMR spectroscopy provided insight into the successful incorporation of the PESu oligomer into the PBT chain (Figure S.2). Esterification of the hydroxyethyl-terminated PESu oligomers imparted a quantifiable and complete shift in the proton spectra indicating successful end group conversion. Furthermore, peak integration, relative to the ethyl protons of 4.39 and 4.74 ppm, revealed the average segment lengths of PBT and PESu in the resulting copolymer (Table 1). Consistent with previous literature, the PESu average segment length remained unchanged, suggesting the absence of chain degradation at the reaction conditions.[17, 18]

Table 1. Summary of average segment length and wt.% of segmented block copolymers determined with ^{1}H NMR spectroscopy.

	M_n PESu Seg	M_n PBT Seg	PESu wt.%	PBT wt.%
3 kg/mol PESu				
$80PESu_{3k}$-20PBT	3100	800	80	20
$60PESu_{3k}$-40PBT	3000	2200	58	42
$40PESu_{3k}$-60PBT	2850	5400	35	65
$20PESu_{3k}$-80PBT	2800	13800	17	83
8 kg/mol PESu				
$80PESu_{8k}$-20PBT	7700	1900	80	20
$60PESu_{8k}$-40PBT	7700	5600	58	42
$50PESu_{8k}$-50PBT	7700	8600	47	53
$20PESu_{8k}$-80PBT	7700	34000	19	81
10 kg/mol PESu				
$80PESu_{10k}$-20PBT	9700	2100	82	18
$60PESu_{10k}$-40PBT	9700	6100	61	39
$50PESu_{10k}$-50PBT	9700	8800	52	48
$40PESu_{10k}$-60PBT	9700	13000	43	57
$20PESu_{10k}$-80PBT	9700	35,000	22	78
13 kg/mol PESu				
$90PESu_{13k}$-10PBT	13000	1200	91	9.0
$80PESu_{13k}$-20PBT	13000	3150	81	19
$50PESu_{13k}$-50PBT	13000	14500	47	53

20PESu$_{13k}$-80PBT	13000	53000	20	80

Figure 2 illustrates the compositional dependence of PBT segment length for various PESu oligomers. In summary, the average segment length of PBT decreases as the concentration of PESu end groups increases. This result has two important implications. First, increasing the weight percent at a constant PESu segment length results in a reduction in the PBT segment length and, consequently, the copolymer's ability to crystallize. At a critical PBT segment length (*circa* 3 kg/mol), crystallinity is no longer observed, corroborating previous results.[17] Second, increasing the PESu segment length at a constant weight percent encourages longer PBT segment lengths. Increasing the PESu segment length reduces the concentration of end groups available at a given weight percent, which facilitates PBT growth prior to PESu incorporation. This results in an unprecedented, semi-crystalline polysulfone copolymer.

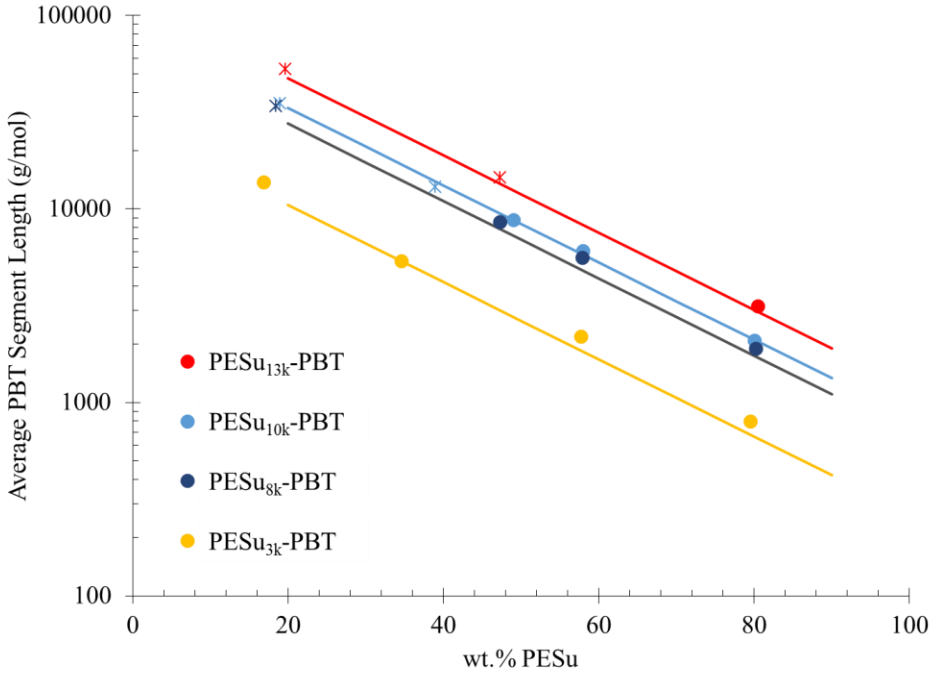

Figure 2. Average PBT segment length determined by ^{1}H NMR spectroscopy. Star indicates a heterogeneous melt occurred.

Figure 2 also outlines the compositions that resulted in heterogeneous melts and brittle materials. At low incorporation of PESu oligomer molecular weights greater than 3 kg/mol, the reaction became heterogeneous at early stages in the polymerization, resulting in a brittle material. These compositions highlight the complexity of melt polymerizations to generate segmented block copolymers. High molecular weight PESu likely does not participate in the early stages of the reaction, and the short, soluble PBT segments couple independently of the PESu oligomer. At the critical time for the PESu chains to participate in the polymerization, the PBT segments macrophase separate due to their substantial molecular weight and exclude the PESu segments. This highlights the importance of the solubility parameters to guide the synthesis of these segmented block copolymers.

Table 2. Summary of thermal transitions observed in DSC and DMA.

	DSC[a]		DMA[b]	
	T_g (°C)	T_m (°C)	T_g (°C)	T_f (°C)
3 kg/mol PESu				
80PESu$_{3k}$-20PBT	155	N/A	N/A	N/A
60PESu$_{3k}$-40PBT	111	N/A	124	162
40PESu$_{3k}$-60PBT	80	207	89	206
20PESu$_{3k}$-80PBT	76	217	62	216
8 kg/mol PESu				
80PESu$_{8k}$-20PBT	172	N/A	177	218
60PESu$_{8k}$-40PBT	157	219	42, 152	199
50PESu$_{8k}$-50PBT	160	217	51, 156	198
20PESu$_{8k}$-80PBT	59	222	53, 175	208
10 kg/mol PESu				
80PESu$_{10k}$-20PBT	168	N/A	161	220
60PESu$_{10k}$-40PBT	162	217	83, 159	205
50PESu$_{10k}$-50PBT	166	220	70, 165	205
40PESu$_{10k}$-60PBT	65	220	68, 173	205
20PESu$_{10k}$-80PBT	55	222	68, 159	215
13 kg/mol PESu				

	$90PESu_{13k}$-10PBT	197	N/A	45, 206	246
	$80PESu_{13k}$-20PBT	179	219	48, 176	201
	$50PESu_{13k}$-50PBT	57	221	65, 184	205
	$20PESu_{13k}$-80PBT	56	222	68, 195	212

[a] DSC: heat/cool/heat, second heat; N_2, 10 °C/min. T_g reported as inflection point of step transition, T_m reported as peak maximum of endothermic event.

[b] DMA: tension mode, 1 Hz, 3 °C/min. T_g reported as peak maximum in tan delta curve, T_f reported as temperature just prior to inconsistent data.

Table 2 summarizes the thermal transitions observed in differential scanning calorimetry (DSC). Similar to previous reports, all copolymers exhibit a single, composition-dependent glass transition temperature (T_g), suggesting a mixed amorphous phase. However, comparing the observed T_g to an expected trend defined by the Fox equation for randomly sequenced copolymers revealed a segment-length dependence on the thermal behavior (Figure 3). At low PESu segment length, the T_g followed the predicted behavior for randomly-sequenced copolymers and indicated a miscibility of the PESu segment in the PBT amorphous phase. However, increasing the PESu segment length resulted in a systematic deviation from the predicted behavior, suggesting a more complex phase behavior. As the PESu segment length increased, the copolymer T_g approached the expected homopolymer T_g of the major phase, with an apparent inflection centered at 50:50 mol.%.

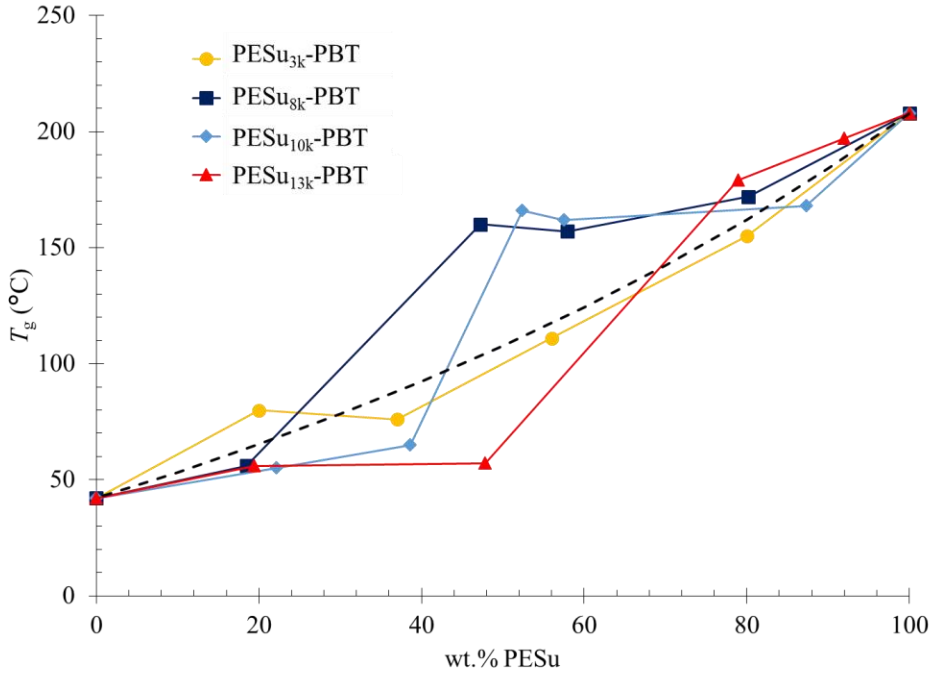

Figure 3. T_gs determined using DSC for the various PESu-PBT segmented block copolymers indicate large deviation from the predicted Fox relationship (black dashed line). Open symbols represent reactions resulting in opaque melts.

Dynamic mechanical analysis (DMA) confirmed the thermal transitions observed in DSC and identified additional thermal events associated with a second T_g for certain compositions (Table 2). Corroborating the DSC results, PESu short segments resulted in a single T_g as predicted with the Fox equation. However, DMA revealed another transition not observed in DSC, at longer PESu segment lengths. Figure 4 illustrates representative storage moduli for 50PESu-50PBT at varying PESu segment lengths. The single step-transition observed in 50PESu$_{3k}$-50PBT correlated well with the T_g observed in DSC. Increasing the PESu segment length to 8 kg/mol promoted phase separation, as indicated with two transitions observed in DMA. This behavior remained unchanged with further increases in PESu segment length up to 13 kg/mol. At 50PESu$_{13k}$-50PBT the macrophase separation in the melt resulted in a

complicated relaxation spectrum at high temperatures, presumably from coupled and uncoupled PESu segments.

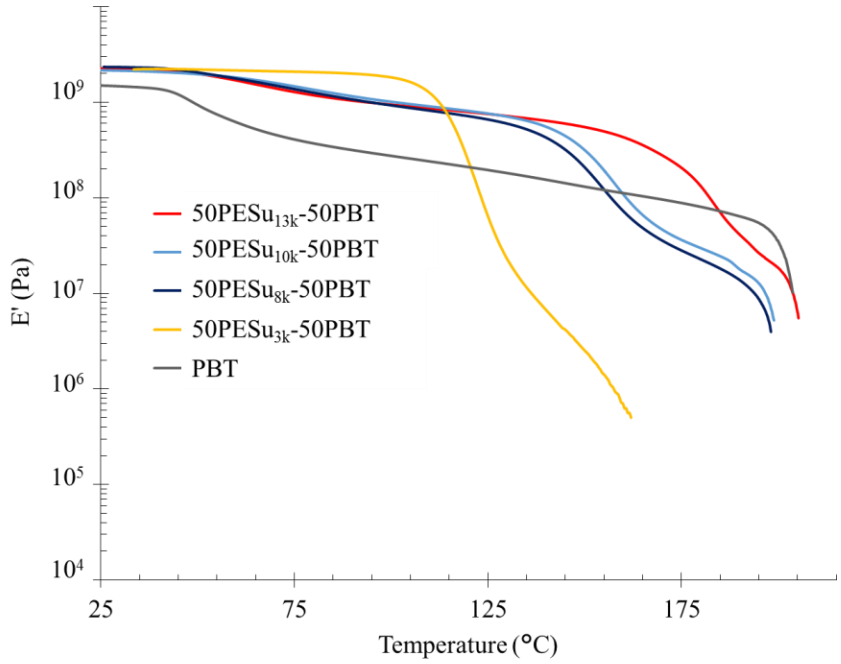

Figure 4. Storage moduli of 50PESu-50PBT segmented block copolymers at varying block lengths.

The compositional influence of the PESu-PBT segmented block copolymers at a single PESu segment length is necessary to evaluate the segment-dependence on the thermal transitions (Figure 5). Increasing the PESu wt.% at a constant segment length reduced the PBT average segment length and promoted a mixed amorphous phase. The transition from two T_gs to a single T_g occurred between 60 and 80 wt.% incorporation of a 10 kg/mol PESu segment and decreased with decreasing PESu segment length.

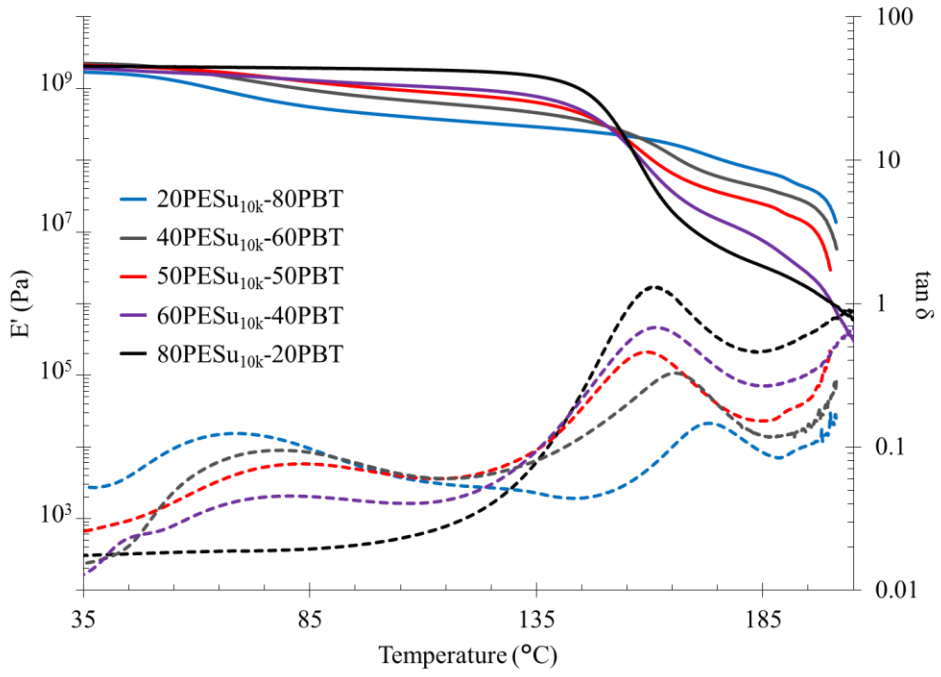

Figure 5. Dynamic mechanical analysis of PESu-PBT segmented block copolymers with 10 kg/mol PESu segments.

Small angle x-ray scattering (SAXS) explored nanoscale order of the novel segmented block copolymers. Figure 6 provides representative *q* scattering plots of copolymers with a constant 10 kg/mol PESu segment length and varying compositions. The single, primary peak across compositions >80 wt.% PESu correlated well with previous literature[25, 26] on the inter-crystallite distance of PBT. In comparison to the PBT homopolymer control, the d-spacing increased from 12.3 to 16.4 nm upon 40 wt.% incorporation of 10 kg/mol PESu, indicating a small fraction of soluble PESu segments in the amorphous PBT phase. Further incorporation of 10 kg/mol PESu resulted in minimal change to the inter-crystallite distance (16.0 ± 0.7 nm). However, the reduction in the PBT segment length inhibited the copolymer's propensity to crystallize and resulted in a lower peak intensity, presumably due to a decrease in the crystallinity. At 80 wt.% incorporation of 10 kg/mol PESu, the material did not display any phase separation.

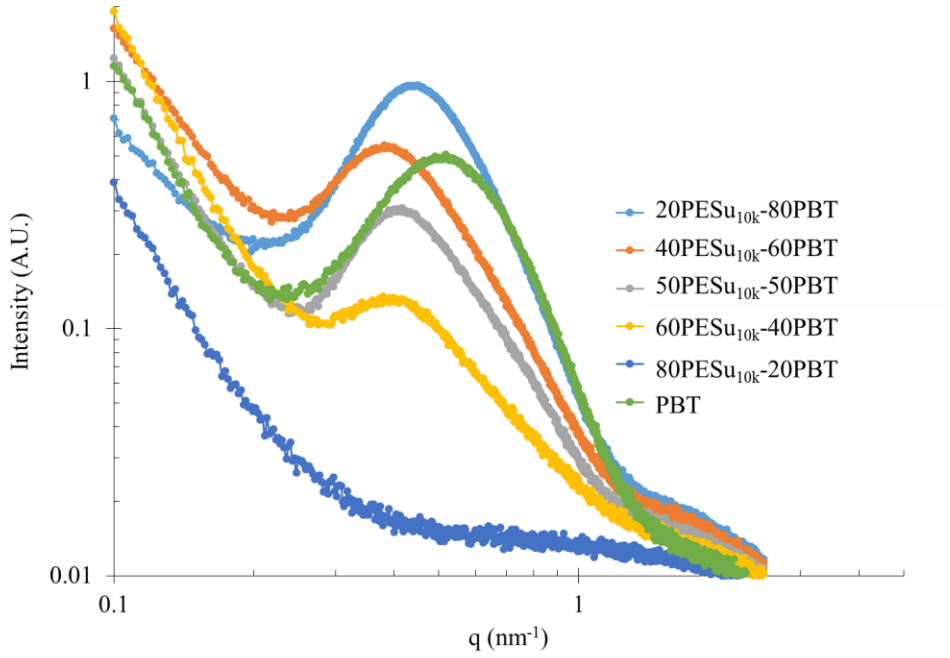

Figure 6. Small angle x-ray scattering of PESu-PBT segmented block copolymers at a constant PESu segment length of 10 kg/mol.

In order to provide a more in-depth comparison of the PBT homopolymer and the PBT-PESu segmented block copolymers, the linear correlation function was computed and analyzed using the method as described by Vonk[19] and later extended upon by Ruland[27]. The correlation function provided estimates of the lamellar thickness, amorphous thickness, long period of crystallites, and local crystallinity (crystallinity within an assembly of stacked crystallites). The lamellar thickness (*circa* 3.0 nm) changed minimally when comparing the PBT homopolymer and each of the $PESu_{10k}$-PBT copolymers, which is consistent with the observed small deviation in melting points for all samples measured. The correlation function analysis also indicated that the amorphous thickness increased from 6.3 nm in the homopolymer to ~9.0 nm for all copolymer compositions of $PESu_{10k}$-PBT. The local crystallinity shows that with increasing PESu content the local crystallinity decreases, indicating that the packing density of crystallites decreases as larger non-crystallizable PESu blocks are incorporated between the crystallizable

PBT blocks. Figure 7 and Table 3 provides plots of the autocorrelation function and the calculated parameters respectively.

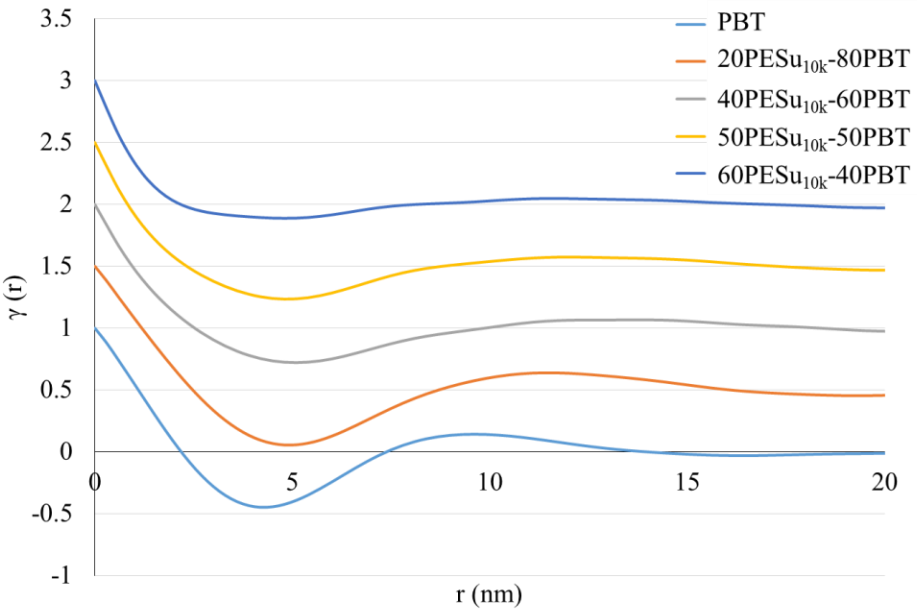

Figure 7. SAXS linear correlation function of PESu-PBT segmented block copolymers with 10 kg/mol PESu segments. Curves have been offset vertically (by 0.5 each) to facilitate comparison.

Table 3. Calculated parameters for the linear correlation function of PESu-PBT segmented block copolymers with 10 kg/mol PESu segments using a paracrystalline (ideal) lattice.

	Crystal Lamellar Thickness (nm)	Amorphous Interlamellar Thickness (nm)	Long Period (Lp) (nm)	Local Crystallinity (%)
PBT	3.3	6.3	9.6	34.0
20PESu$_{10k}$-80PBT	3.6	7.8	11.5	31.7
40PESu$_{10k}$-60PBT	3.3	8.7	12.0	27.8
50PESu$_{10k}$-50PBT	3.2	8.8	12.0	26.4
60PESu$_{10k}$-40PBT	2.5	9.1	11.6	21.3

Figure 8 and 9 illustrate the compositional dependence on the melting temperature (T_m) and crystallinity, respectively. Maintaining a constant composition of 80PESu-20PBT, Figure 8 identifies a transition from an amorphous to a semi-crystalline material, occurring at high PESu segment lengths (*circa* 13 kg/mol). Additionally, the relatively long segment lengths of PESu and PBT for the 80PESu$_{13k}$-20PBT copolymer promoted phase separation as evidenced by the second transition in DMA (Table 2). The combination of segment lengths and phase separation enabled crystallization of the PBT-rich phase at high PESu incorporation. Below the 13 kg/mol PESu segment length, a single T_g occurred, which increased with PESu segment length. The steady increase in the T_g with increasing segment lengths at a constant 80:20 composition suggested restricted segmental mobility, which likely arises from a weakly segregated polymer near the phase boundary.

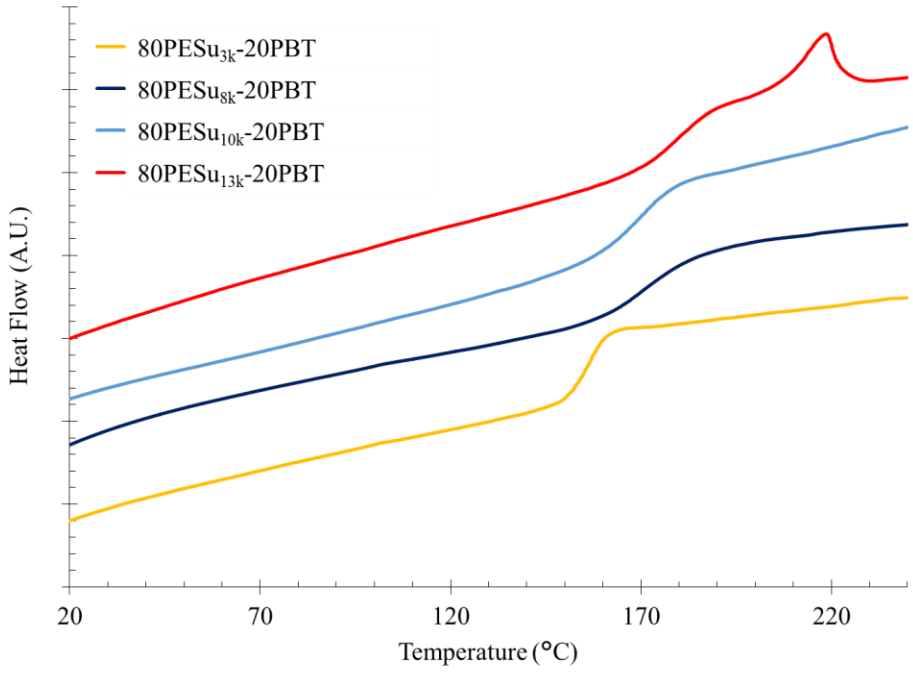

Figure 8. Differential scanning calorimetry of 80PESu-20PBT segmented block copolymers with varying block lengths.

Figure 9 summarizes the percent crystallinity in reference to a PBT homopolymer control using $\Delta H_f°$ = 142 J/g.[28] At low incorporation of PESu, the copolymers crystallized to similar extents as PBT, suggesting little constraint on the crystallization behavior. However, increasing the PESu weight fraction restricted the crystallization of PBT because of segment length and chain heterogeneity. At short PESu segments, the average segment length of PBT remained below the critical molecular weight for crystallization at most compositions. Furthermore, the short segments promoted an intermixed amorphous phase, inhibiting crystallization. Increasing the PESu segment length increased the material's propensity to crystallize. As the PESu segment length increased, the average length of the PBT segment also increased, driving phase separation. As a result of the topological and morphological changes in structure, the copolymers of long PESu segments crystallized at high PESu content.

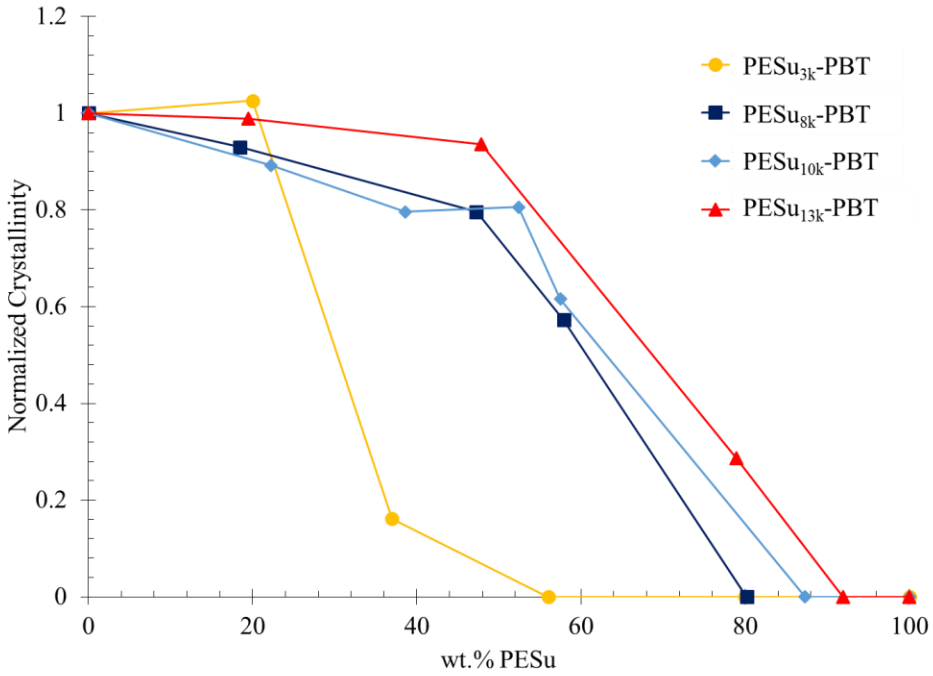

Figure 9. Percent crystallinity normalized to the weight percent of crystallizable content. A value of one represents 28.7% of the PBT fraction crystallized. Lines are there to help guide the eye.

4.5 Conclusions

A facile synthesis of hydroxyethyl-functionalized PESu enabled incorporation into segmented block copolymers through melt transesterification with PBT. The unique solubility of PESu segments in the melt with PBT facilitated a systematic study of segment length on thermomechanical properties. ^{1}H NMR spectroscopy elucidated the compositional dependence of segment length of PBT. DSC and DMA, in concert with ^{1}H NMR spectroscopy, established a critical average segment length for crystallization and phase separation. SAXS has indicated that the lamellar thickness is nearly independent of the PESu block length, indicating a similar thermal stability within all of the semicrystalline copolymers. The correlation analysis also clearly indicates that the amorphous layer thickness between crystallites increased as the size of the non-crystallizable PESu block is increased. The complex interplay between morphology, topology, and solubility enables novel, commercially viable copolymers for emerging automotive and electronic applications.

4.6 Acknowledgements

The authors would like to acknowledge Arnold Schneller and Axel Wilms at BASF for insightful discussions. This material is partially based upon work supported by the National Science Foundation under Grant No. DMR-1507245 and Grant No. DMR-0923107.

4.7 References

1. Buckwalter, D. J.; Dennis, J. M.; Long, T. E. Amide-containing segmented copolymers, *Prog. Polym. Sci.* **2015,** 45, 1-22.

2. Buckwalter, D. J.; Hudson, A. G.; Moore, R. B.; Long, T. E. Synthesis and characterization of poly(propylene glycol) polytrioxamide and poly(urea oxamide) segmented copolymers, *Polym. Int.* **2014,** 63, (7), 1184-1191.
3. Buckwalter, D. J.; Zhang, M.; Inglefield Jr, D. L.; Moore, R. B.; Long, T. E. Synthesis and characterization of siloxane-containing poly(urea oxamide) segmented copolymers, *Polymer* **2013,** 54, (18), 4849-4857.
4. Bates, F. S. Polymer-Polymer Phase Behavior, *Science* **1991,** 251, (4996), 898-905.
5. Widin, J. M.; Schmitt, A. K.; Im, K.; Schmitt, A. L.; Mahanthappa, M. K. Polydispersity-Induced Stabilization of a Disordered Bicontinuous Morphology in ABA Triblock Copolymers, *Macromolecules* **2010,** 43, (19), 7913-7915.
6. Widin, J. M.; Schmitt, A. K.; Schmitt, A. L.; Im, K.; Mahanthappa, M. K. Unexpected Consequences of Block Polydispersity on the Self-Assembly of ABA Triblock Copolymers, *J. Amer. Chem. Soc.* **2012,** 134, (8), 3834-3844.
7. Wu, L.; Cochran, E. W.; Lodge, T. P.; Bates, F. S. Consequences of Block Number on the Order−Disorder Transition and Viscoelastic Properties of Linear (AB)n Multiblock Copolymers, *Macromolecules* **2004,** 37, (9), 3360-3368.
8. He, P.; Shen, W.; Yu, W.; Zhou, C. Mesophase Separation and Rheology of Olefin Multiblock Copolymers, *Macromolecules* **2014,** 47, (2), 807-820.
9. Li, S.; Register, R. A.; Weinhold, J. D.; Landes, B. G. Melt and Solid-State Structures of Polydisperse Polyolefin Multiblock Copolymers, *Macromolecules* **2012,** 45, (14), 5773-5781.
10. Matsen, M. W. Effect of Architecture on the Phase Behavior of AB-Type Block Copolymer Melts, *Macromolecules* **2012,** 45, (4), 2161-2165.

11. Zhang, M.; Zhang, M.; Moore, R. B.; Long, T. E. Influence of charge placement on the thermal and morphological properties of sulfonated segmented copolyesters, *Polymer* **2013,** 54, (14), 3521-3528.
12. Gaymans, R. J. Segmented copolymers with monodisperse crystallizable hard segments: Novel semi-crystalline materials, *Prog. Polym. Sci.* **2011,** 36, (6), 713-748.
13. Lee, H.-S.; Badami, A. S.; Roy, A.; McGrath, J. E. Segmented sulfonated poly(arylene ether sulfone)-b-polyimide copolymers for proton exchange membrane fuel cells. I. Copolymer synthesis and fundamental properties, *J. Polym. Sci., Part A: Polym. Chem.* **2007,** 45, (21), 4879-4890.
14. Xie, W.; Geise, G. M.; Freeman, B. D.; Lee, C. H.; McGrath, J. E. Influence of processing history on water and salt transport properties of disulfonated polysulfone random copolymers, *Polymer* **2012,** 53, (7), 1581-1592.
15. Xie, W.; Ju, H.; Geise, G. M.; Freeman, B. D.; Mardel, J. I.; Hill, A. J.; McGrath, J. E. Effect of Free Volume on Water and Salt Transport Properties in Directly Copolymerized Disulfonated Poly(arylene ether sulfone) Random Copolymers, *Macromolecules* **2011,** 44, (11), 4428-4438.
16. Kambour, R. P.; Romagosa, E. E.; Gruner, C. L. Swelling, Crazing, and Cracking of an Aromatic Copolyether-Sulfone in Organic Media, *Macromolecules* **1972,** 5, (4), 335-340.
17. Dennis, J. M.; Fahs, G. B.; Moore, R. B.; Turner, S. R.; Long, T. E. Synthesis and Characterization of Polysulfone-Containing Poly(butylene terephthalate) Segmented Block Copolymers, *Macromolecules* **2014,** 47, (23), 8171-8177.

18. Chang, Z.; Fahs, G. B.; Zhang, B.; Edling, H. E.; Orler, E. B.; Moore, R. B.; Turner, S. R. New semicrystalline block copolymers of poly(arylene ether sulfone)s and poly(1,4-cyclohexylenedimethylene terephthalate), *Polymer* **2015,** 74, 86-93.
19. Vonk, C. G.; Kortleve, G. X-ray small-angle scattering of bulk polyethylene, *Kolloid-Zeitschrift und Zeitschrift für Polymere* **1967,** 220, (1), 19-24.
20. Celebi, O.; Lee, C. H.; Lin, Y.; McGrath, J. E.; Riffle, J. S. Synthesis and characterization of polyoxazoline–polysulfone triblock copolymers, *Polymer* **2011,** 52, (21), 4718-4726.
21. Weber, M.; Maletzko, C.; Lange, G.; Erbes, J.; Dietrich, M.; Inchaurrondo, N.; Sigwart, C. Method for producing low-halogen polybiphenylsulfone polymers. 20100817, 2011.
22. Caldwell, J. R. Bis (4-beta-hydroxyalkoxyphenyl) sulfones and polyesters prepared therefrom. US2593411, 1952.
23. Lambrech, J. A. Herbicide. US2573769, 1951.
24. Barton, A. F. M., *CRC handbook of solubility parameters and other cohesion parameters*. CRC Press: Boca Raton, 1991.
25. Stribeck, N.; Fakirov, S.; Apostolov, A. A.; Denchev, Z.; Gehrke, R. Deformation Behavior of PET, PBT and PBT-Based Thermoplastic Elastomers as Revealed by SAXS from Synchrotron, *Macromol. Chem. Phys.* **2003,** 204, (7), 1000-1013.
26. Néhmé, O. A.; Gabriel, C. A.; Farris, R. J.; Thomas, E. L.; Malone, M. F. Microstructural investigations of PBT/nylon 6,6 composites, *J. Appl. Polym. Sci.* **1988,** 35, (7), 1955-1965.
27. Ruland, W. Small-angle scattering of two-phase systems: determination and significance of systematic deviations from Porod's law, *J. Appl. Crystallogr.* **1971,** 4, (1), 70-73.

28. Runt, J.; Miley, D. M.; Zhang, X.; Gallagher, K. P.; McFeaters, K.; Fishburn, J. Crystallization of poly(butylene terephthalate) and its blends with polyarylate, *Macromolecules* **1992,** 25, (7), 1929-1934.

4.8 Supporting Information

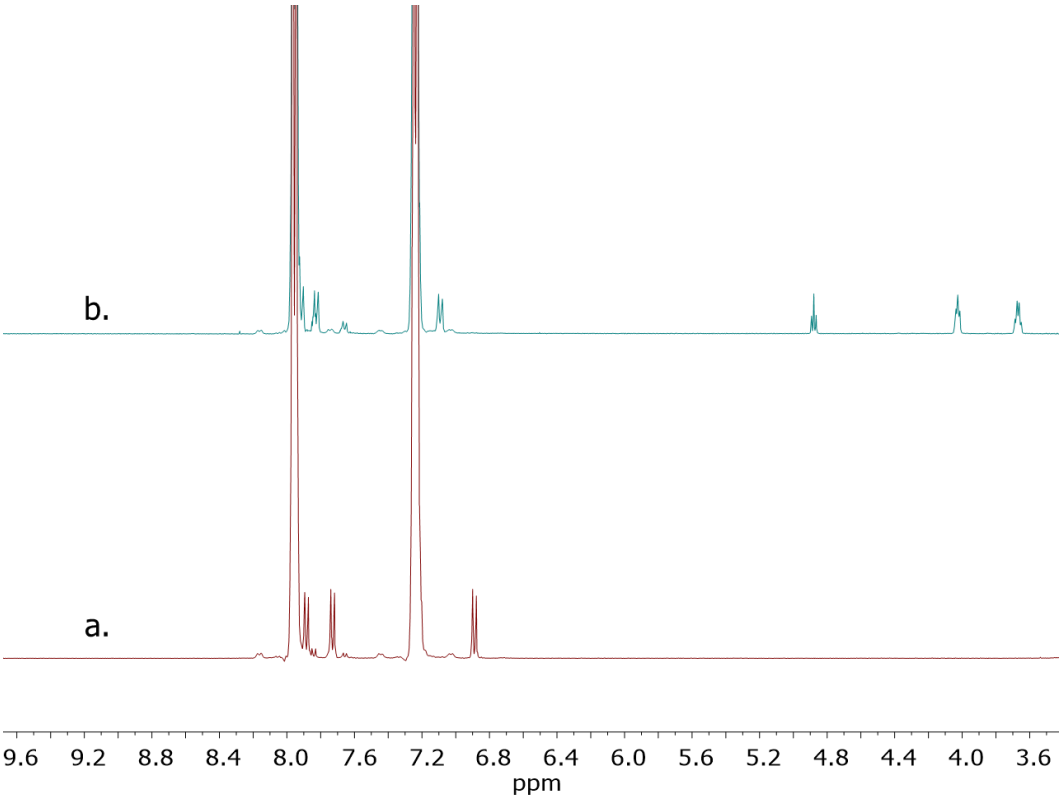

Figure S1. ^{1}H NMR spectrum of a. phenol-terminated poly(ether sulfone) and b. hydroxyethyl-terminated poly(ether sulfone). Quantitative shift of endgroup protons at 6.89 and 7.71 to 7.09 and 7.83 ppm identifies successful functionalization.

Table S1. Various reaction conditions and respective conversions for the endgroup functionalization of phenol-terminated PESu to hydroxyethyl-terminated PESu.

KI	Hours	Solvent	Temperature	Conversion	Side Products
N	24	DMAc	25	0	Y
N	24	DMAc	65	7.4	Y
N	24	DMAc	85	8.3	Y
N	24	DMAc	120	39	Y
Y	1	DMAc	120	>99	N
Y	24	DMAc	120	>99	Y

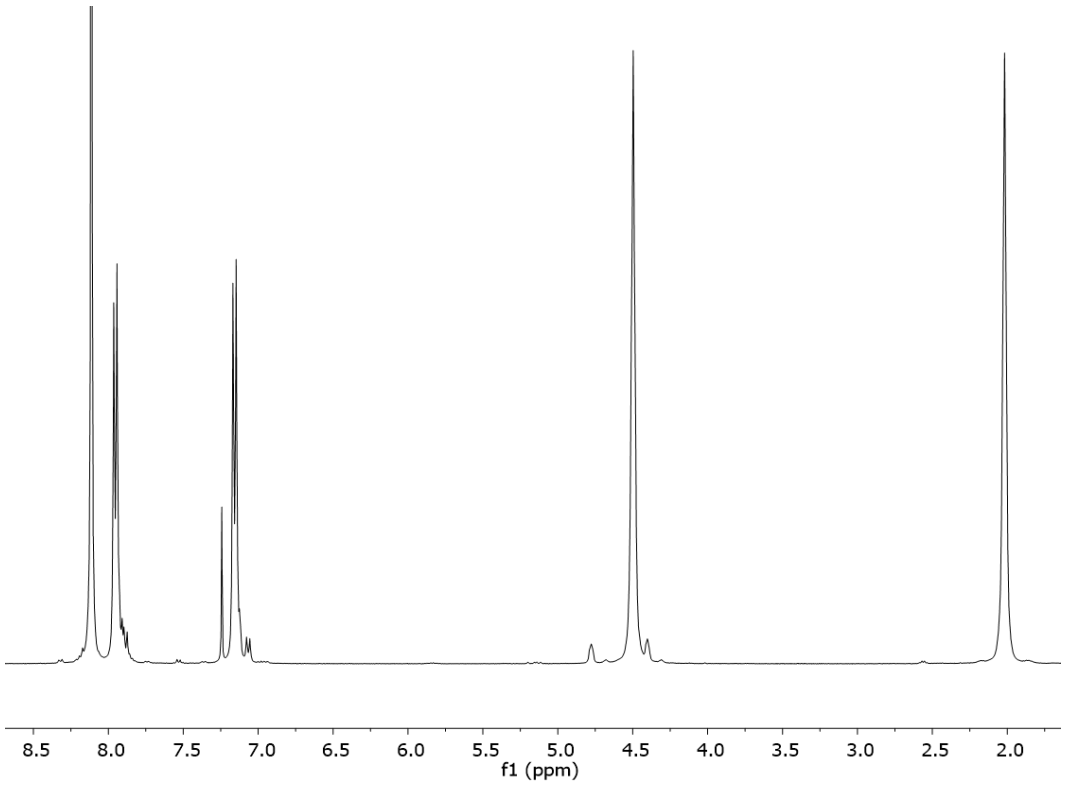

Figure S2. ^{1}H NMR spectrum of 60PESu$_{10k}$-40PBT in 9:1 $CDCl_3$:CF_3COOD.

Chapter 5: Synthesis and Characterization of Decahydronaphthalene-containing Polyesters

(Published in *Macromolecules* **2015,** 48, (24), 8733-8737.)

Joseph M. Dennis, Joshua S. Enokida, and Timothy E. Long

Department of Chemistry, Macromolecules and Interfaces Institute

Virginia Tech, Blacksburg, Virginia 24061 USA

5.1 Abstract

Melt polycondensation of decahydronaphthalate dimethylester with various diols enabled the synthesis of novel polyesters containing hydrogenated naphthalene rings. Decahydronaphthalene-containing polyesters demonstrated thermal stabilities above 350 °C, and compression molding provided ductile, optically clear films. ^{1}H NMR spectroscopy confirmed transesterification, and intrinsic viscosity measurements verified high molecular weights. Differential scanning calorimetry and dynamic mechanical analysis revealed structure-property relationships for glass transition temperatures (T_g) and β-relaxations. Melt rheology examined the effect of chemical structure on flow behavior, and time-temperature superposition revealed two distinct transitions, which correlated to the T_g and chain disentanglement. Furthermore, evaluation of the fractional free volume and flow activation energies suggested a structural dependence associated with regularity along the polymer backbone.

5.2 Introduction

Earlier reports link bisphenol-A (BPA), a synthetic estrogen mimic, with increased risks of cancers, infertility, metabolic disorders, and developmental issues in fetuses and infants.[1] Due

to BPA's widespread use in coatings and food packaging, companies continue to invest much effort into the identification of BPA replacements.[1] A potential hydrolytic degradation of BPA-containing polycarbonates yields the BPA monomer over time.[1-6] Thus, the need for BPA-free, high T_g polymeric packaging emerges as a critical area for future research.[1-9]

Recently, several reports identify copolyesters as potential BPA-free, injection moldable thermoplastics with glass transition temperatures (T_gs) above 110 °C.[2-4, 7-13] The optically clear polyesters offer dimensional stability at elevated temperatures and demonstrate improved weatherability through reduced UV absorbance over BPA-containing polycarbonates.[7] However, the high T_g polyesters suffer from reduced impact strength and melt stability, which prevent utility in many molded polycarbonate structures (e.g. impact-resistant bottles).[7, 10] Furthermore, the aromaticity remaining in these copolyesters results in UV absorption and potential for subsequent chain degradation.[7] Therefore, many opportunities remain for development of potential BPA-replacements.

Previous investigations into the origin of high impact strength of polycarbonates identified low-temperature β-relaxations as an indicator of impact strength.[5, 6, 14-21] The rapid, short-range structural motions, such as methyl spins or ring flips, introduce high-energy relaxations at temperatures well below the T_g.[14-17] As a result, these rapid motions and increases in free volume promote energy absorption during high-speed deformation, and the magnitude of these relaxations correlate strongly to impact resistance.[5, 6, 19-21] Furthermore, crystallinity reduces impact resistance as a result of restricted molecular movement within the crystalline lattice.[6, 22]

This manuscript describes BPA-free, amorphous, high-impact polyester families containing hydrogenated naphthalene dicarboxylate. It is expected that the fused rings will

provide energy absorption, similar to poly(cyclohexylenedimethylene terephthalate).[23, 24] Synthesis of dimethyl decahydronaphthalate-2,6-dicarboxylate involves hydrogenation of dimethyl napthalate-2,6-dicarboxylate, as described previously, and allows for direct incorporation into a melt-processable polyester family.[25, 26] The resulting isomeric mixture advantageously prevents polymer crystallization and provides amorphous polyesters for optimal impact performance. The following report discusses the melt transesterification of dimethyl decahydronaphthalate-2,6-dicarboxylate with various diols to achieve tough, ductile polyesters. Complementary analytical techniques provide a detailed analysis of structural effects on thermal and rheological properties. Decahydronaphthalene-containing polyesters, with T_gs approaching 100 °C and multiple β-relaxations, provide a viable avenue toward replacing BPA-containing polycarbonates.

5.3 Experimental

Materials. 1,4-Butanediol (99%) and 1,4-cyclohexanedimethanol (99%, mixture of isomers) were purchased from Sigma-Aldrich and used as received. Titanium tetraisopropoxide (99.999%) was purchased from Sigma-Aldrich and diluted to 10.18 mg/mL in *n*-butanol. 2,6-Dimethyldecahydronaphthalene dicarboxylate, *trans*-1,4-cyclohexanedimethanol, and 1,3-cyclohexanedimethanol were used as received. 1,1,1,3,3,3-Hexafluoro-2-propanol (99.5+%, HFIP) was purchased from Acros Organics and used as received. All deuterated solvents were purchased from Cambridge Isotope Laboratories, Inc.

Analytical Methods. ^{1}H NMR spectroscopy was performed using a Varian Unity 400 spectrometer operating at 399.87 MHz and 23 °C with a binary mixture of 9:1 $CDCl_3$:CF_3COOD (ca. 8 mg/mL). Thermogravimetric analysis (TGA) employed a TA Instruments TGA Q500 from room temperature to 600 °C with a heating rate of 10 °C/min under constant N_2 purge.

Differential scanning calorimetry (DSC) utilized a TA Instruments DSC Q2000 under a N_2 atmosphere with heat/cool/heat cycles of 10 °C/min, 100 °C/min, and 10 °C/min, respectively. Dynamic mechanical analysis (DMA) with a TA Instruments DMA Q800 in oscillatory tension mode at 1 Hz and 3 °C/min revealed modulus versus temperature behavior. Compression molding at 270 °C between steel plates using a PHI hydraulic press generated freestanding films, which were cooled in air over 1 h. A Cannon-Ubbelohde 75 capillary viscometer provided intrinsic viscosity measurements following ISO 1628-1 in hexafluoroisopropanol (HFIP).

Melt rheological experiments utilized a TA Instruments AR-G2 rheometer with an 8-mm, parallel-plate geometry. Initial strain sweep experiments (0.01 to 10 % oscillatory strain at 1 Hz) determined the linear viscoelastic region for these polyesters. Temperature step and frequency sweep experiments at 10 °C/step (1.2% oscillatory strain, 0.1-100 rad/s) provided storage and loss moduli and viscosity responses over a wide range of frequency. Curve shifting using the TA Instruments TRIOS software generated master curves for each polyester. Evaluation of melt flow properties involved fitting of corresponding shift factors to the WLF equation using TA Instruments TRIOS software.

Synthesis of Decahydronaphthalate-2,6-dicarboxylate-containing Polyesters. Melt transesterification generated decahydronaphthalate-2,6-dicarboxylate-containing polyesters, and the synthesis of poly(cyclohexanedimethylene decahydronaphthalate) (Poly(CHDN)) is described. Dimethyl 2,6-decahydronaphthalate dicarboxylate (10.0 g, 0.0393 mol) and 1,4-cyclohexandimethanol (6.80 g, 0.0472 mol) were charged to a dry, 100-mL round-bottomed flask. Titanium tetraisopropoxide in *n*-butanol was added (0.06 mL, 100 ppm titanium tetraisopropoxide) to facilitate transesterification. Equipped with an overhead stir rod, nitrogen inlet, condensing tube, and collection flask, the contents were sequentially degassed under

vacuum and purged with nitrogen three times. Under constant nitrogen purge, the flask was heated from 220 to 280 °C over 2 h and the pressure was subsequently reduced (<0.1 mmHg) at 280 °C for an additional 2 h. Collection of methanol distillate in a dry ice-cooled, round-bottomed flask monitored the reaction progress. The resulting products were used directly without further purification.

5.4 Results and Discussion

Scheme 1 illustrates the synthesis of decahydronaphthalene-containing polyesters utilizing melt transesterification with a titanium tetraisopropoxide catalyst. Commonly, a slight excess of diol facilitates transesterification of the dimethyl ester.[7, 11, 12, 27] Following the completion of methanol generation, a combination of higher temperatures and reduced pressure removes excess diol and drives the reaction to high conversions (>99.9%). The reaction is complete when the melt viscosity increases substantially and remains visibly constant. Methanol generation and diol boiling points guided the reaction times and designated the final reaction temperature. In all cases, transesterification of the dimethyldecahydronapthalate dicarboxylate with the diol was complete within 2 h at 220 °C, and overall reaction times did not exceed 5 h. Polymerization resulted in pale yellow, optically clear products.

Scheme 1. Melt transesterification synthesis of decahydronaphthalene-containing polyesters.

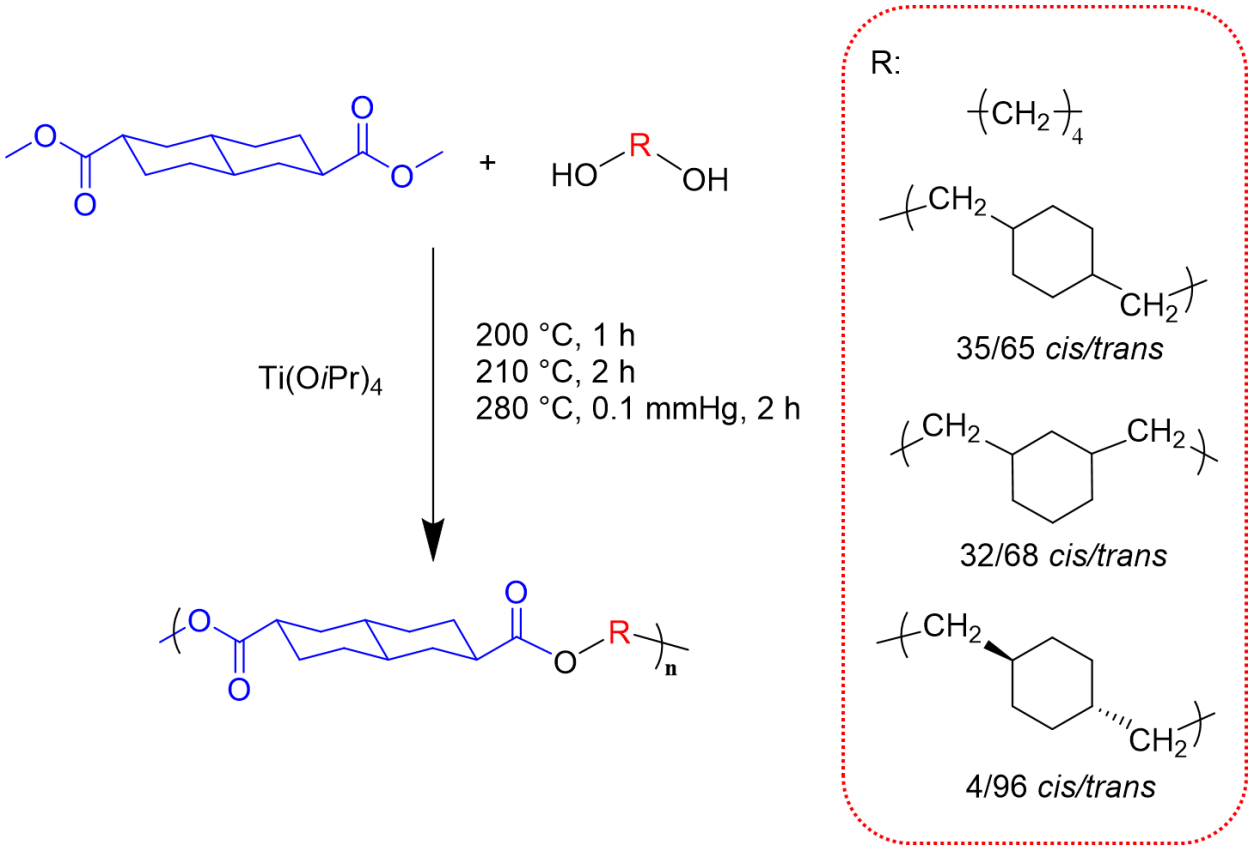

Size exclusion chromatography (SEC) was not reliable due to poor solubility of the polyesters in most organic solvents. Although the polymers produced optically clear solutions in chloroform, tetrahydrofuran, and *N*-methylpyrrolidinone, dynamic light scattering (DLS) revealed aggregated structures that were unsuitable for accurate SEC analysis. Hexafluoroisopropanol is a well-known solvent for polyesters;[7] however, its corrosive behavior prevented use on current SEC columns. Alternatively, comparison of intrinsic viscosity ([η]) of HFIP solutions to literature suggested high molecular weight polyesters. **Table 1** summarizes [η] values and ranged from 0.33-0.66 dL/g, which correlated well with literature values for other commercially available, high molecular weight polyesters at similar reaction conditions (*c.a.* 0.3-0.8 dL/g).[7]

Table 1. Physical properties of decahydronaphthalene-containing polyesters.

	$T_{d,5\%}$[a] (°C)	T_g[b] (°C)	[η][c] (dL/g)	*cis/trans*[d]
Poly(BDN)	386	22	0.33	N/A
Poly(1,4-CHDN)	407	89	0.66	33/67
Poly(*t*-1,4-CHDN)	398	93	0.57	4/96
Poly(1,3-CHDN)	397	78	0.53	32/78

[a] TGA: 10 °C/min, N_2.
[b] DSC: heat/cool/heat, second heat; 10 °C/min, N_2
[c] Intrinsic Viscosity: HFIP, 35 °C, Cannon-Ubbelohde 75 viscometer
[d] *cis/trans* ratio of cyclohexanedimethanol as determined by ^{1}H NMR spectroscopy

^{1}H NMR spectroscopy confirmed the structure of the polyesters **(Figures S1-S4).** Distinct proton shifts enabled characterization of the *cis/trans* ratio for both decahydronaphthalate and cyclohexyldimethylene. An 18/82 *cis/trans* isomeric ratio of decahydronaphthalate was consistent throughout all polymerizations. For the 1,4-cyclohexanedimethanol, an initial *cis*/*trans* ratio of 35/65 correlated well with the 33/67 *cis*/*trans* ratio observed in the polymer. Similarly, the 1,3-cyclohexanedimethanol *cis*/*trans* ratio remained unchanged at 32/68 after polymerization. As a result, no observable isomerization occurred at the elevated polymerization temperatures, which was consistent with previous reports.[7]

Thermogravimetric analysis (TGA) identified a single-step weight loss at temperatures greater than 350 °C for all polyesters **(Figure S5). Table 1** also reports the temperatures at 5 % weight loss ($T_{d,5\%}$). **Figure 1** displays the thermograms from dynamic scanning calorimetry (DSC) with the T_gs listed in **Table 1**. DSC showed a single-step transition in the temperature range of -10 to 250 °C, and optical clarity suggested the absence of crystallinity in these polyesters. The mixture of isomers in the naphthalate and cyclohexyl rings prevented crystallization and maintained optical clarity. Diol selection resulted in a T_gs ranging from 22-93 °C, demonstrating the utility of decahydronaphthalene-containing polyesters as a promising new

family of all aliphatic, high-T_g polyesters. Previous literature reported the incorporation of more rigid diols, such as 2,2,4,4-tetramethylcyclobutane diol, to raise the T_g.[7, 12]

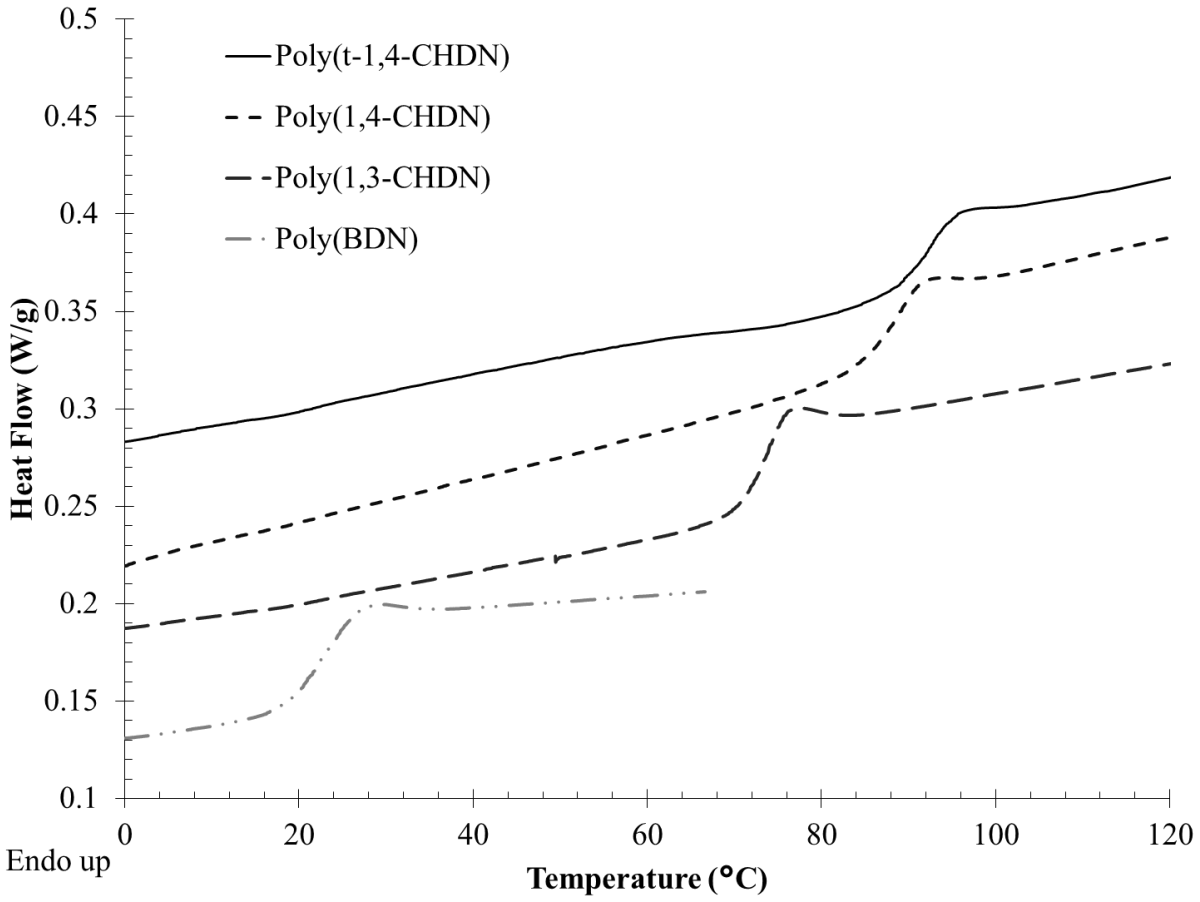

Figure 1. DSC thermograms of decahydronaphthalene-containing polyesters. Second heat reported with a heating rate of 10 °C/min after quench cooling from 250 °C.

Dynamic mechanical analysis (DMA) highlighted the thermomechanical response of the decahydronaphthalene-containing polyesters **(Figures 2 and 3).** In the temperature range from -140 to 250 °C, all the polyesters indicated a temperature-insensitive glassy modulus at low temperatures, with a precipitous drop in modulus corresponding to the T_g, as determined by DSC. All the polyesters have multiple relaxations spanning a large temperature range below the

T_g. With minimal change in storage modulus, the distinct tan δ maxima arise from complex local relaxations.

As highlighted in **Figure 3**, a strong correlation exists between specific structural units and the resulting maxima. Peak I, centered near -120 °C, corresponds well with previous reports of a "crankshaft" relaxation resulting from rotation about the butylene chain.[28] Peaks II and III are consistent throughout all the polyesters presumably due to the decahydronaphthalate rings. A slight shift of II to II_b in the *trans* isomer of poly(*t*-cyclohexyldimethylene decahydronapthalate) (Poly(*t*-CHDN)) from the *cis*/*trans* mixture requires further studies, such as molecular modeling and solid-state NMR spectroscopy. The absorption of mechanical energy through relaxation mechanisms in the glassy state provides toughness and fracture resistance.[29, 30] More specifically, the intensity of these peaks correlate strongly with impact performance.[29] In comparison to BPA-containing polycarbonates, the relative intensities of β-relaxations in the decahydronaphthalene-containing polyesters are significantly larger, and suggests the possibility for more high-energy absorption.

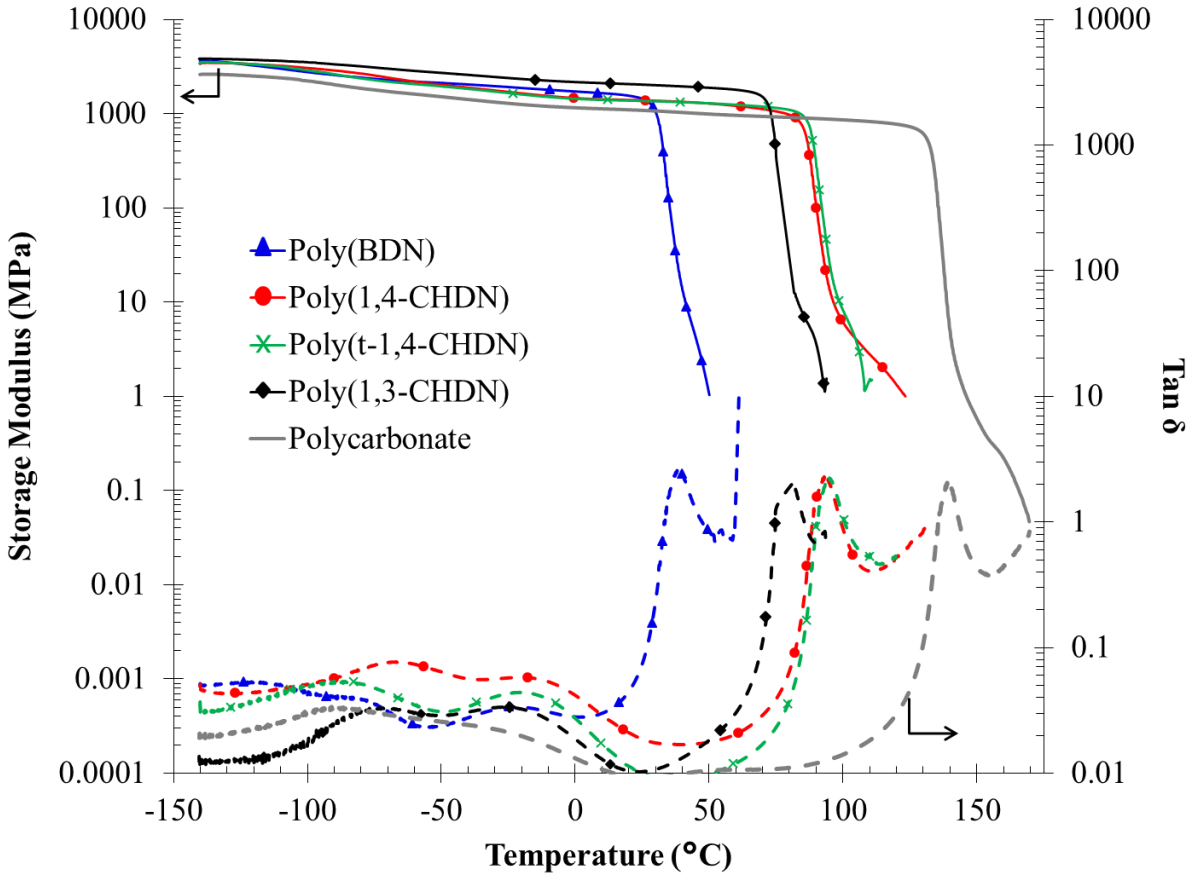

Figure 2. Dynamic mechanical analysis of decahydronaphthalene-containing polyesters. Analyzed in tension mode at a frequency of 1 Hz and a heating rate of 3 °C/min.

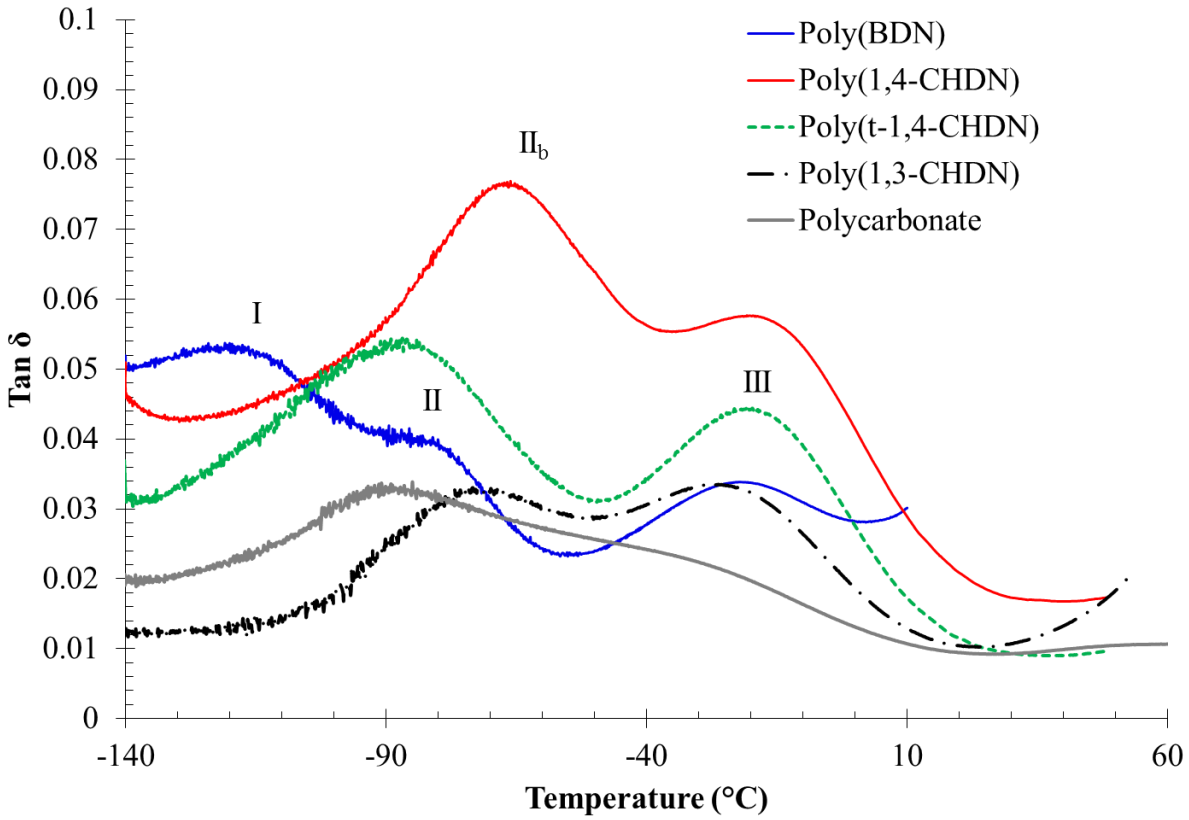

Figure 3. Low-temperature dynamic mechanical analysis of decahydronaphthalene-containing polyesters. Analyzed in tensile mode at a frequency of 1 Hz and a heating rate of 3 °C/min.

Typical post-polymerization processing of polyesters include melt spinning, molding, and extrusion.[31] As a result, the melt stability and flow behavior of these polyesters are of particular interest. Melt rheology of the decahydronaphthalene-containing polyesters directly examined the impact of chemical structure on flow characteristics. Time-temperature superposition (TTS) identified a broad viscoelastic region for desirable melt processability.

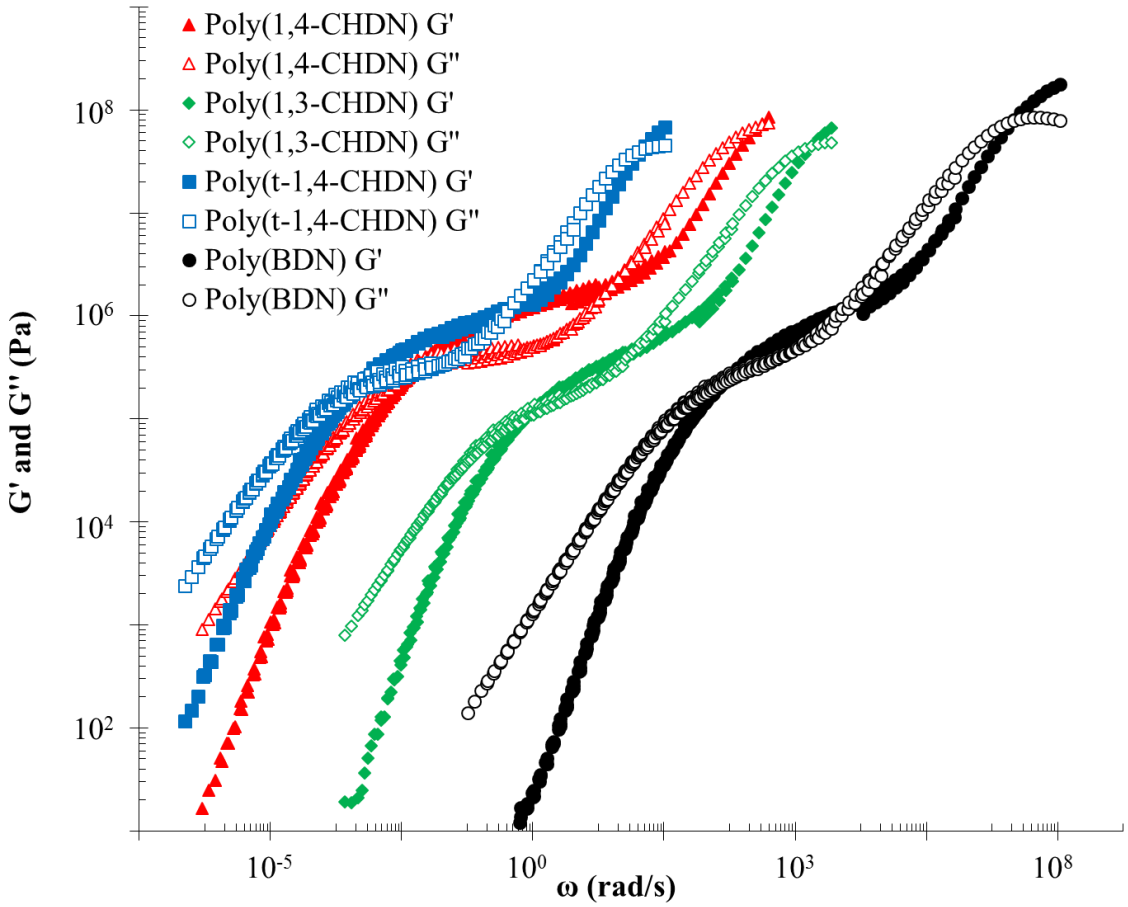

Figure 4. Storage and loss moduli master curves for decahydronaphthalene-containing polyesters at T_r = 100 °C.

Figure 4 highlights storage (*G'*) and loss moduli (*G"*) master curves, and **Figure 5** depicts viscosity master curves. Shifting to a common reference temperature (T_r) of 100 °C for TTS facilitates a direct comparison between each polyesters. The master curves exhibit acceptable overlap across several decades of angular frequency, indicating predictable processing. Furthermore, the decahydronaphthalene-containing polyesters observed two distinct relaxations. The first relaxation, at relatively high frequencies, isolates the onset of long-range segmental motion. The second relaxation at lower frequencies was indicative of chain entanglements and the transient network of enchained molecules. After this second relaxation,

long-range motions dominated resulting in terminal flow. Slopes of 0.98 and 1.82 for *G'* and *G"* agreed well with the expected slopes for typical polymer melts of *G'*~1.0 and *G"*~2.0. Importantly, the observation of the second relaxation indicated sufficient molecular weights for entanglements and further justified the intrinsic viscosity measurements.

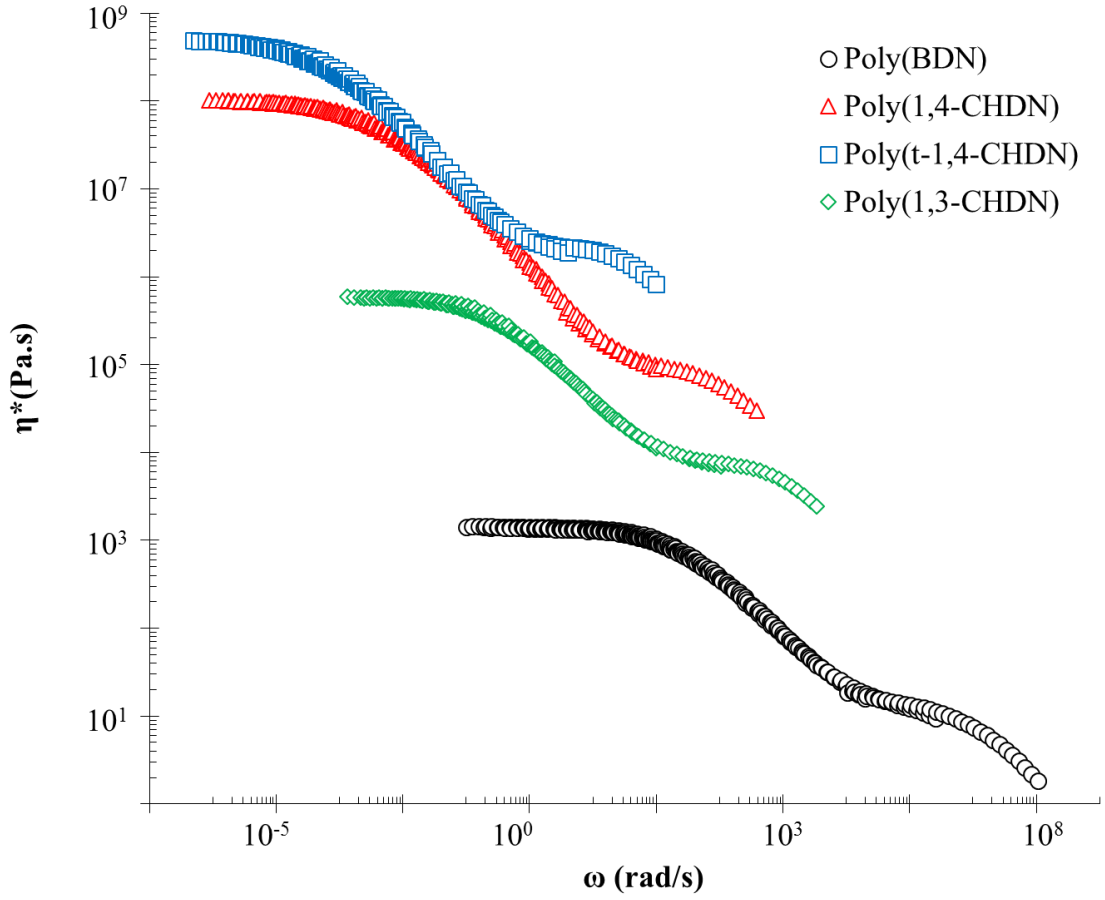

Figure 5. Complex viscosity master curves of decahydronaphthalene-containing polyesters at T_r = 100 °C.

These observations corroborated the findings illustrated with the viscosity master curves (Figure 5). At low frequencies, beyond the entanglement relaxation of G' and G", the viscosity was frequency-independent and behaved as a Newtonian fluid. Increasing the oscillation frequency resulted in shear thinning as the chain entanglement relaxation is traversed. Another

slope change occurred as the dominant relaxation changed near the T_g, but shear thinning resumed after transitioning below the onset of segmental motion.

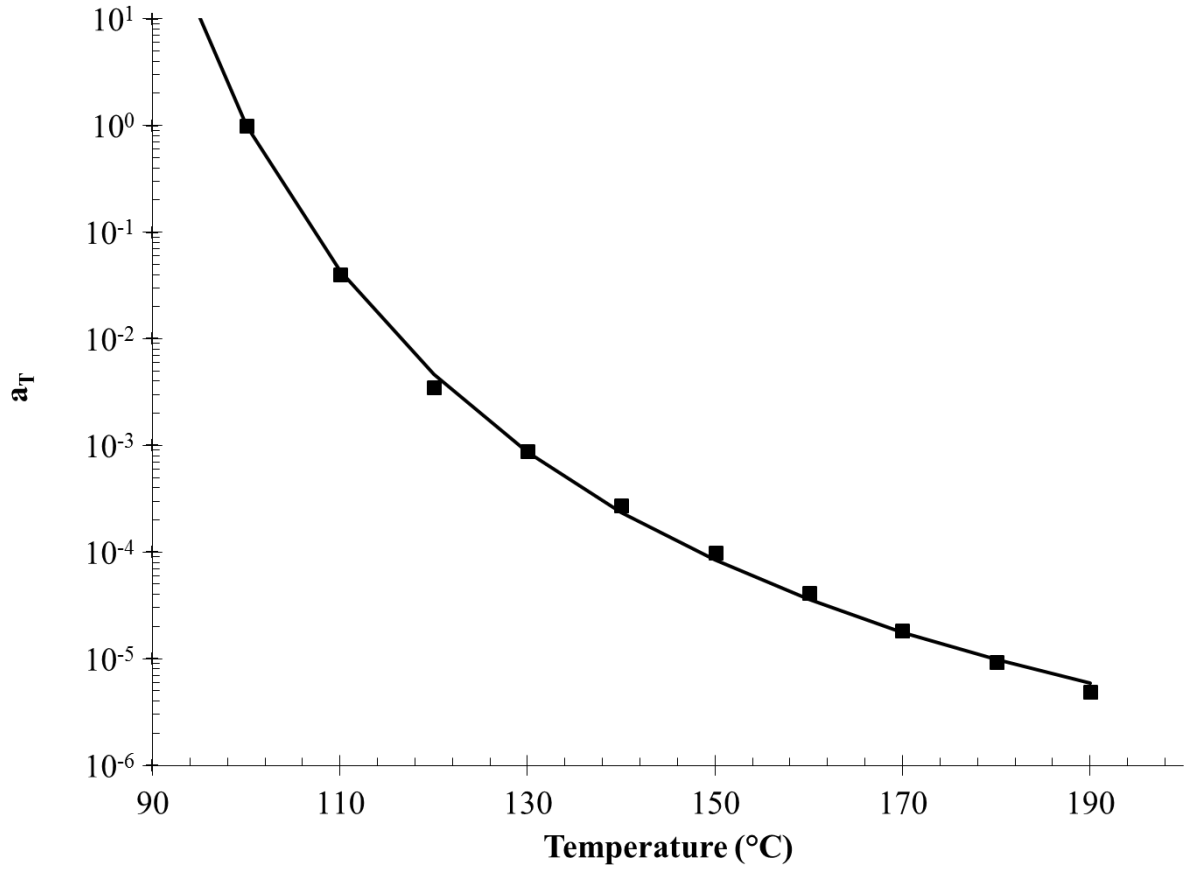

Figure 6. Representative WLF fitting of shift factors (a_T) *versus* temperature for Poly(*t*-1,4-CHDN). T_r = 100 °C.

All decahydronaphthalene-containing polyesters obeyed the Williams-Landel-Ferry (WLF) equation, where shift factors (a_T) as a function of temperature follow:

$$\log(a_T) = \frac{-C_1(T - T_r)}{C_2 + (T - T_r)} \quad (1)$$

T_r refers to the reference temperature chosen, and C_1 and C_2 are polymer-specific constants determined by least-squares regression. **Figure 6** illustrates a representative WLF fit for the shift

factors of Poly(*t*-1,4-CHDN). Since C_1 and C_2 are dependent on the reference temperature chosen, an established conversion to C_1^g and C_2^g (eq. 2 and 3) enables direct comparison to other C_1^g and C_2^g literature values.[32]

$$C_1^g = \frac{C_1 C_2}{C_2 + (T_g - T_r)} \quad (2)$$

$$C_2^g = C_2 + (T_g - T_r) \quad (3)$$

Table 2 summarizes the C_1^g and C_2^g values for the decahydronaphthalene polyesters, and correlate well with reported values for neutral, non-associating polymers.[32] Furthermore, equations 4 and 5 enabled calculations of fractional free volume at T_g (f_g) and the thermal expansion coefficient (α_f).[32]

$$f_g = \frac{B}{2.303 C_1^g} \quad (4)$$

$$\alpha_f = \frac{B}{2.303 C_1^g C_2^g} \quad (5)$$

The fractional free volume, detailed in **Table 2** provides insight into the rate of molecular rearrangements and diffusive transport.[32] The replacement of a linear, aliphatic chain with the stiffer aliphatic ring reduced chain mobility and f_g. Also, introduction of the 1,3-cyclohexanedimethanol increased f_g over the *para*-substituted isomer. The odd-spaced carbon linkage reduced chain regularity and increased molecular mobility. The 4/96 *cis*/*trans* cyclohexandimethanol-containing polyester had the lowest free volume, and indicated the highest amount of chain regularity.

Table 2. WLF parameters, fractional free volume (f_g), flow activation energy (E_a), and thermal expansion coefficient (α_f) of decahydronaphthalene-containing polyesters.

Polymer	C_1	C_2 (K)	C_1^g	C_2^g (K)	f_g	E_a (kJ/mol)	α_f (x 10^{-4} K^{-1})
Poly(BDN)	3.48	110.8	3.75	102.8	0.118	152	11.3
Poly(1,4-CHDN)	6.69	55.8	7.98	46.8	0.054	188	11.6
Poly(*t*-1,4-CHDN)	7.19	48.8	9.53	36.8	0.046	201	12.4
Poly(1,3-CHDN)	5.22	51.6	6.04	44.6	0.072	161	16.1

Detailed investigation into the terminal flow regime (T >> T_g) enabled calculation of the melt flow activation energy (E_a) through an Arrhenius relationship.[32] In this case, the activation energy referred to the energy barrier for hole formation and chain flow. Similar to the fractional free volume, introduction of 1,4-cyclohexanedimethanol resulted in an increase in the flow activation energy over Poly(BDN) **(Table 2)**. The activation energy of the different cyclohexanedimethanol isomers also followed the f_g trends with the highest energy associated with the *t*-1,4-cyclohexanedimethanol isomer.

5.5 Conclusions

Melt polycondensation of a decahydronapthalate dimethylester with various diols generated optically clear, melt-processable polyesters. A systematic thermal analysis resulted in a range of T_gs approaching 100 °C, and thermal stabilities above 350 °C. All decahydronaphthalene-containing polyesters demonstrated several β-relaxations indicating possible impact resistance. Melt rheology directly probed processing ability and highlights melt stability. TTS evaluated a broad range of angular frequencies and established two relaxations attributed to the T_g and chain entanglements. Using WLF parameters, the fractional free volume and flow activation energies indicated a direct correlation to structural regularity, with increasing

regularity decreasing fractional free volume and increasing flow activation energy. Future studies will focus on enhancing T_gs for thermally stable, BPA-free plastic alternatives.

5.6 References

1. Nelson, A. M.; Long, T. E. A perspective on emerging polymer technologies for bisphenol-A replacement, *Polym. Int.* **2012,** 61, (10), 1485-1491.
2. Crawford, E. D.; Pecorini, T. J.; McWilliams, D. S.; Porter, D. S.; Connell, G. W.; Germroth, T. C.; Barton, B. F.; Shackelford, D. B. Polyester Compositions Containing Cyclobuntanediol Having a Certain Combination of Inherent Viscosity and Moderate Glass Transition Temperature and Articles Made Therefrom. US2006042292, 2007.
3. Scott, C. E.; Morris, J. C.; Bradley, J. R. Clear polycarbonate and polyester blends. US6043322 A, 1997.
4. Scott, C. E.; Morris, J. C.; Bradley, J. R. Clear blends of polycarbonates and polyesters. US6037424 A, 1997.
5. Wyzgoski, M.; Yeh, G. Origin of Impact Strength in Polycarbonate: II. Effect of Thermal Treatments, *Int. J. Polym. Mater.* **1974,** 3, (2), 149-163.
6. Wyzgoski, M.; Yeh, G. Origin of Impact Strength in Polycarbonate: I. Effect of Crystallization and Residual Solvent, *Int. J. Polym. Mater.* **1974,** 3, (2), 133-148.
7. Kelsey, D. R.; Scardino, B. M.; Grebowicz, J. S.; Chuah, H. H. High Impact, Amorphous Terephthalate Copolyesters of Rigid 2,2,4,4-Tetramethyl-1,3-cyclobutanediol with Flexible Diols, *Macromolecules* **2000,** 33, (16), 5810-5818.
8. Scott, C. E.; Morris, J. C.; Bradley, J. R. Clear polycarbonate and polyester blends. US6005059 A, 1997.

9. Scott, C. E.; Stewart, M. E.; Wilmoth, D. S.; Morris, J. C.; Bradley, J. R. Polycarbonate and polyester blends. US5942585 A, 1997.
10. Barton, B. F.; Shackelford, D. B. Process for the Preparation of Copolyesters Based on 2,2,4,4-Tetramethyl-1,3-Cylclobutanediol and 1,4-Cyclohexanedimethanol US2008005799, 2007.
11. Beall, G. W.; Powell, C. E.; Hancock, J.; Kindinger, M.; McKenzie, H. R.; Bray, A. V.; Booth, C. J. Physical properties of CBDO based co-polyterephthalate nanocomposites, *Appl. Clay Sci.* **2007,** 37, (3–4), 295-306.
12. Booth, C. J.; Kindinger, M.; McKenzie, H. R.; Handcock, J.; Bray, A. V.; Beall, G. W. Copolyterephthalates containing tetramethylcyclobutane with impact and ballistic properties greater than bisphenol A polycarbonate, *Polymer* **2006,** 47, (18), 6398-6405.
13. Crawford, E. D.; Porter, D. S.; Connel, G. W. Polyester compositions which comprise cyclobutanediol having certain cis/trans ratios. EP20090012051, 2011.
14. Heijboer, J. Modulus and damping of polymers in relation to their structure, *Brit. Polym. J.* **1969,** 1, (1), 3-14.
15. Heijboer, J. Molecular Origin of Relaxations in Polymers, *Ann. NY Acad. Sci.* **1976,** 279, (1), 104-116.
16. Heijboer, J. Secondary loss peaks in glassy amorphous polymers, *Int. J. Polym. Mater.* **1977,** 6, (1-2), 11-37.
17. Heijboer, J.; Baas, J. M. A.; van de Graaf, B.; Hoefnagel, M. A. A molecular mechanics study on rotational motions of side groups in poly(methyl methacrylate), *Polymer* **1987,** 28, (3), 509-513.

18. Perkins, W. G. Polymer toughness and impact resistance, *Polym. Eng. Sci.* **1999,** 39, (12), 2445-2460.
19. Turley, S. G.; Keskkula, H. A survey of multiple transitions by dynamic mechanical methods, *J. Polym. Sci., Part C: Polym. Symp.* **1966,** 14, (1), 69-87.
20. Turley, S. G.; Keskkula, H. Effect of rubber-phase volume fraction in impact polystyrene on mechanical behaviour, *Polymer* **1980,** 21, (4), 466-468.
21. Wyzgoski, M. G.; Yeh, G. S.-Y. Relation between Free Volume and the Low-Temperature [ldquo]Beta[rdquo] Transition in Glassy Polycarbonate, *Polym J* **1973,** 4, (1), 29-34.
22. Roe, J.; Baer, E. Correlation of Tensile Properties of Tough Amorphous Polymers with Internal Friction, *Int. J. Polym. Mater.* **1972,** 1, (2), 133-146.
23. Chen, L. P.; Yee, A. F.; Goetz, J. M.; Schaefer, J. Molecular Structure Effects on the Secondary Relaxation and Impact Strength of a Series of Polyester Copolymer Glasses, *Macromolecules* **1998,** 31, (16), 5371-5382.
24. Chen, L. P.; Yee, A. F.; Moskala, E. J. The Molecular Basis for the Relationship between the Secondary Relaxation and Mechanical Properties of a Series of Polyester Copolymer Glasses, *Macromolecules* **1999,** 32, (18), 5944-5955.
25. M, P. F. Decahydro-bis (hydroxymethyl) naphthalenes. 1966.
26. Storms, P. W.; Farrar, G. L. Hydrogenation of naphthalene esters to tetralin esters, *J. Chem. Eng. Data* **1969,** 14, (4), 489-490.
27. Zhang, M.; Zhang, M.; Moore, R. B.; Long, T. E. Influence of charge placement on the thermal and morphological properties of sulfonated segmented copolyesters, *Polymer* **2013,** 54, (14), 3521-3528.

28. Illers, V. K.-H. Der einfluß von wasser auf die molekularen beweglichkeiten von polyamiden, *Makromolekul. Chem.* **1960,** 38, (1), 168-188.
29. Wada, Y.; Kasahara, T. Relation between impact strength and dynamic mechanical properties of plastics, *J. Appl. Polym. Sci.* **1967,** 11, (9), 1661-1665.
30. Boyer, R. Dependence of mechanical properties on molecular motion in polymers, *Polym. Eng. Sci.* **1968,** 8, (3), 161-185.
31. Pang, K.; Kotek, R.; Tonelli, A. Review of conventional and novel polymerization processes for polyesters, *Prog. Polym. Sci.* **2006,** 31, (11), 1009-1037.
32. Ferry, J. D., *Viscoelastic properties of polymers*. John Wiley & Sons: 1980.

5.7 Supporting Information

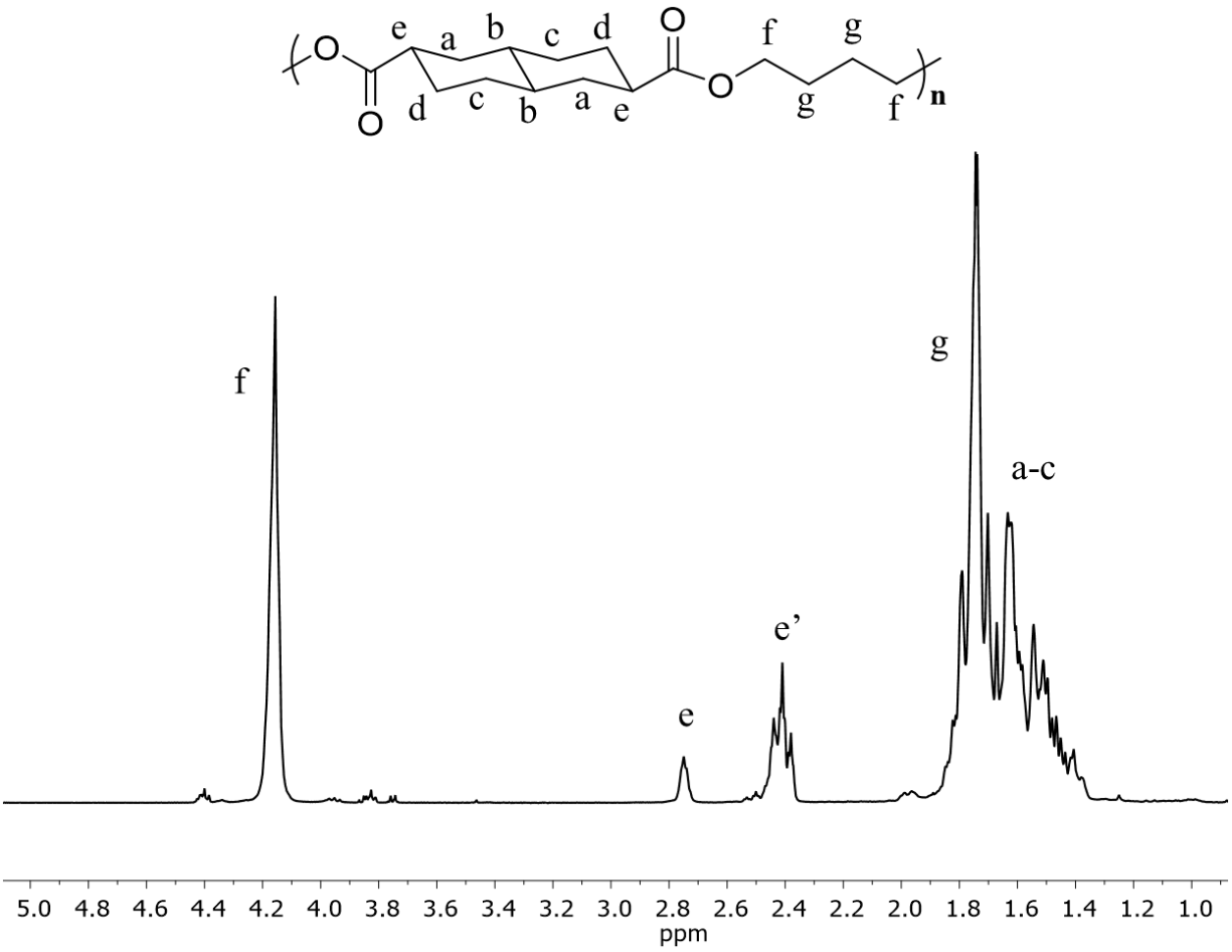

Figure S1. 1H NMR spectrum of Poly(BDN) in 9:1 CDCl3:CDCOOF3. Prime designates isomeric protons.

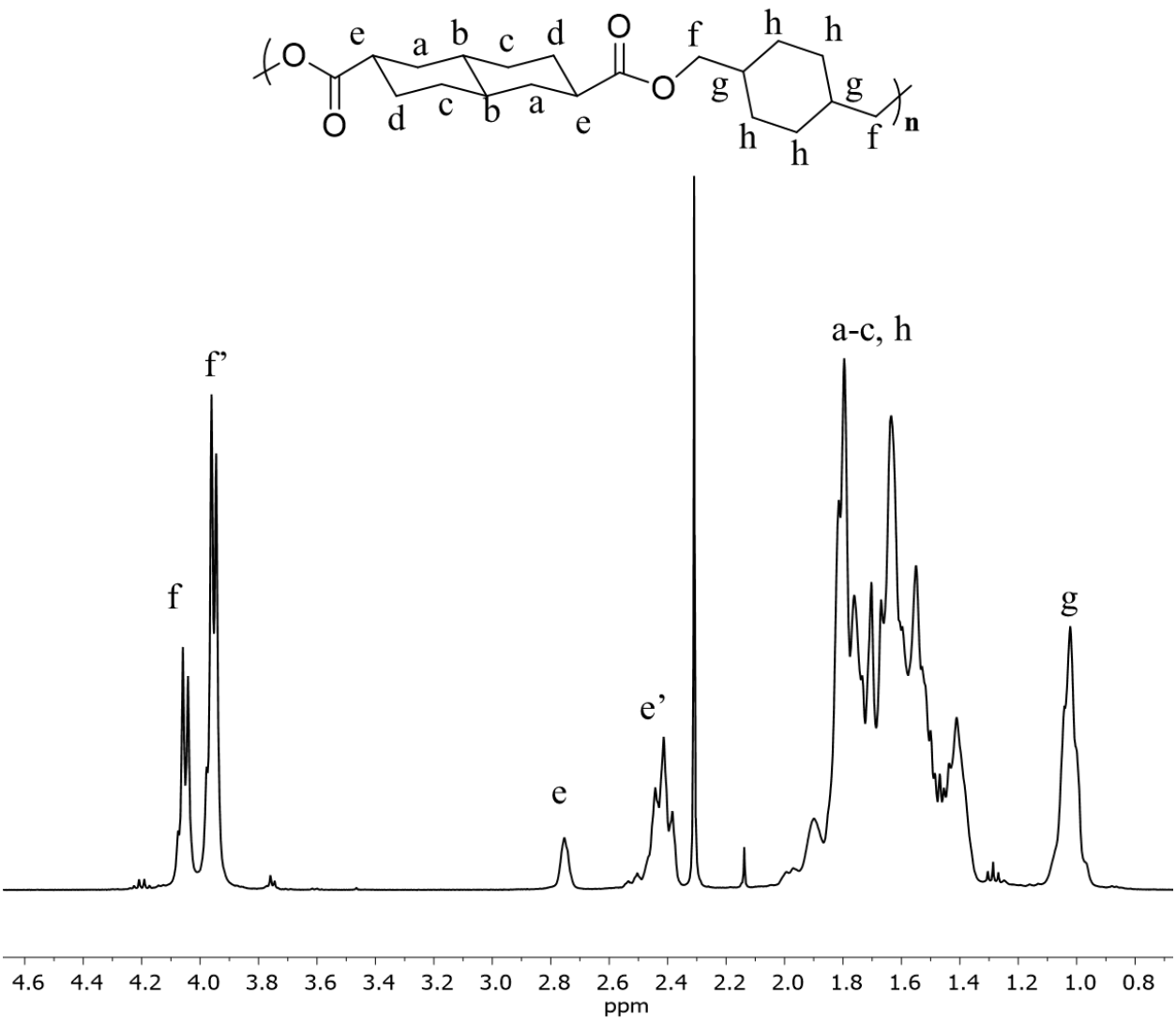

Figure S2. ^{1}H NMR spectrum of Poly(1,4-CHDN) in 9:1 $CDCl_3$:$CDCOOF_3$. Prime designates isomeric protons.

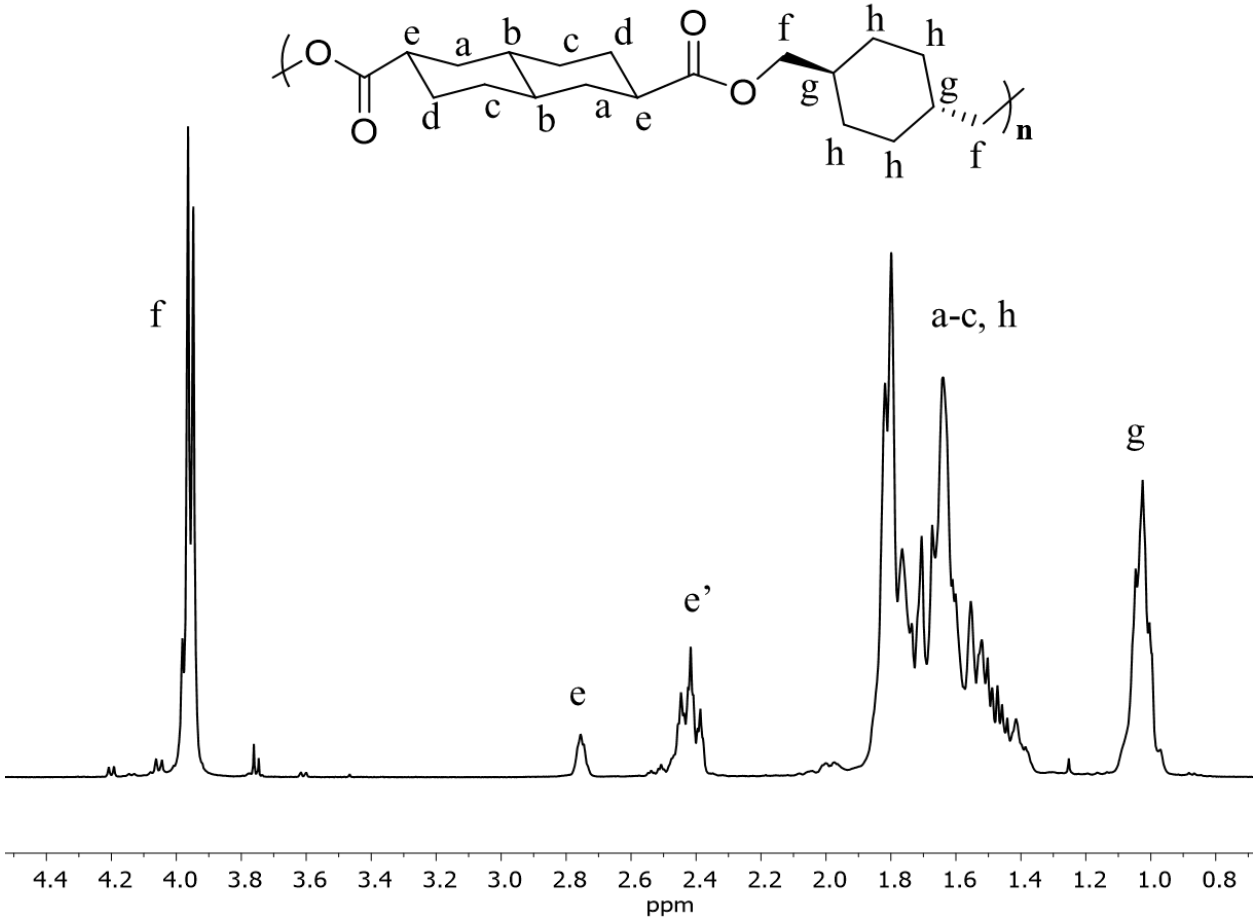

Figure S3. ^{1}H NMR spectrum of Poly(t-1,4-CHDN) in 9:1 $CDCl_3$:$CDCOOF_3$. Prime designates isomeric protons.

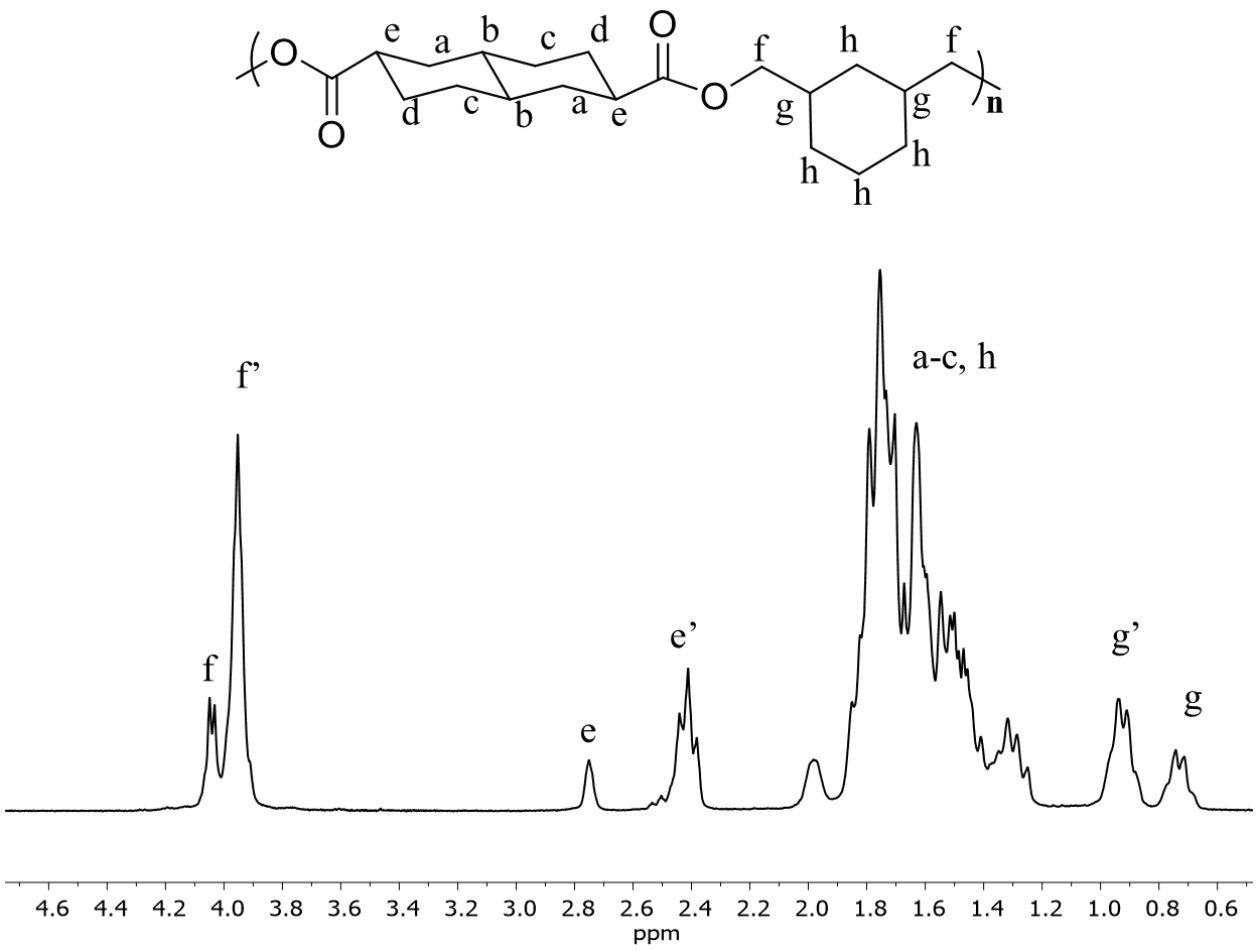

Figure S4. ^{1}H NMR spectrum of Poly(1,3-CHDN) in 9:1 $CDCl_3$:$CDCOOF_3$. Prime designates isomeric protons.

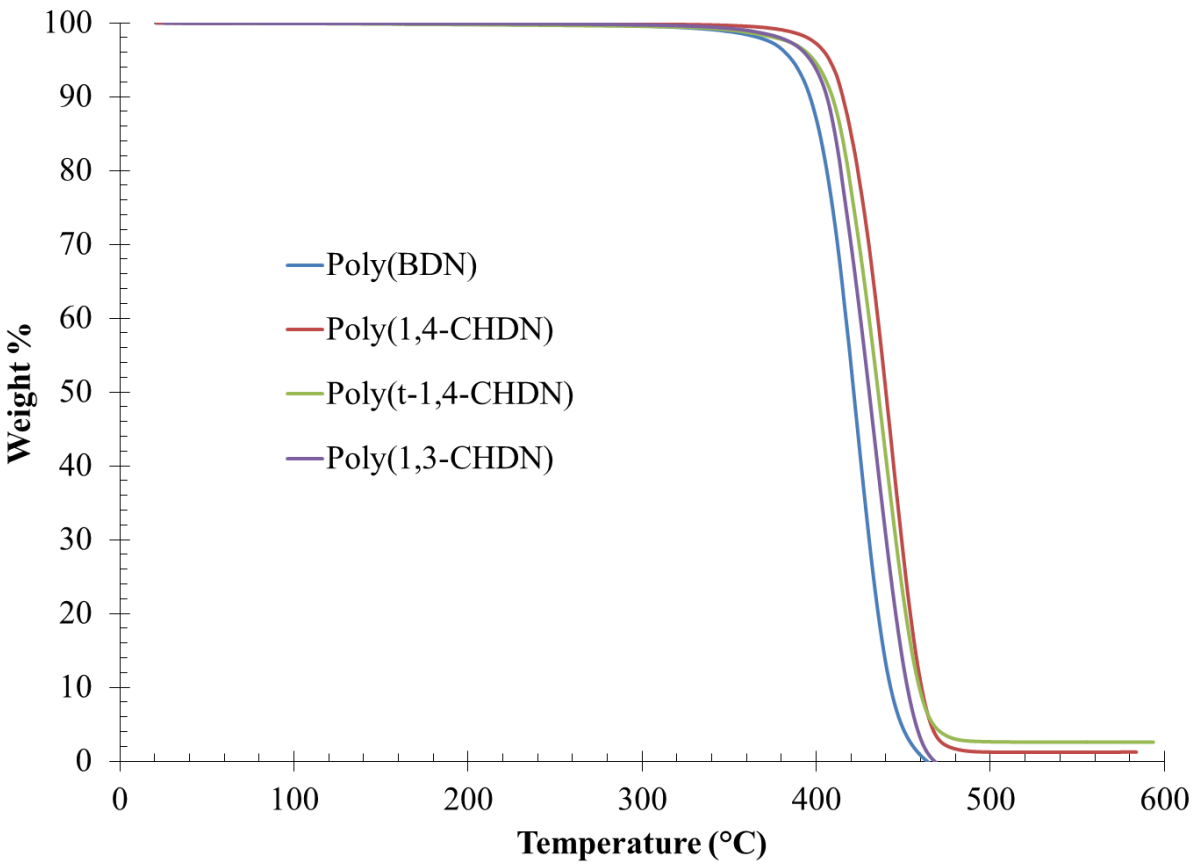

Figure S5. Thermogravimetric analysis of decahydronaphthalene-containing polyesters. 10°C/min, N_2.

Chapter 6: Influence of Cyclobutane Segments in Cycloaliphatic Decahydronaphthalene-containing Copolyesters

(Accepted to *High Performance Polymers*)

Joseph M. Dennis[1], Nicole A. Fazekas[1], Ryan J. Mondschein[1], Ramesh Ramakrishnan[2], Sergei Nazarenko[2], and Timothy E. Long[1]

[1]*Department of Chemistry, Macromolecules Innovation Institute (MII)*

Virginia Tech, Blacksburg, Virginia 24061 USA

[2]*School of Polymers and High Performance Materials*

University of Southern Mississippi, Hattiesburg, Mississippi 39406 USA

6.1 Abstract

Melt transesterification polycondensation enabled the incorporation of rigid, cycloaliphatic diols (2,2,4,4-tetramethylcyclobutane-1,3-diol) into decahydronaphthalene-containing copolyesters, which resulted in amorphous, optically clear materials. Glass transition temperatures approached 155 °C and followed predictable trends using the Fox equation for randomly sequenced copolymers. Dynamic mechanical analysis identified several low-temperature relaxations attributed to the complex motions of the decahydronaphthalate and cyclohexyl rings within the polymer backbone. Furthermore, incorporating cyclobutane rings suppressed the low-temperature local mobility, revealing a strong structural dependence on these relaxations. The rheological simplicity of these non-associating chains permitted analysis over a large frequency window using time-temperature superposition. As a result, the characteristic relaxation times provided insight into chain dynamics and the propensity for chain

entanglements. Finally, positron annihilation lifetime spectroscopy probed hole free volume and reinforced the trends observed with oxygen permeability measurements.

6.2 Introduction

The potential release of bisphenol-A (BPA) through the hydrolytic degradation of BPA-containing polycarbonates encourages investigation into BPA-free materials.[1] BPA is often linked to increased risk of cancers, infertility, metabolic disorders, and developmental issues in fetuses and infants. Thus, companies continue to invest in novel materials for BPA replacement.[1] Earlier reports evaluated copolyesters as potential BPA-free thermoplastics with glass transition temperatures (T_gs) above 110 °C.[2-9] The cycloaliphatic, isomeric mixtures of diols imparted optical clarity and demonstrated improved weatherability through reduced UV absorbance over BPA-based polycarbonates.[6] However, the high T_g polyesters suffered from reduced impact strength and melt stability, inhibiting utility in many BPA-based polycarbonate applications.[6, 7]

Recently, our research group established a novel family of polyesters based on a fused cycloaliphatic monomer derived from dimethylnaphthalate as potential BPA-based polycarbonate replacements.[10] The isomeric mixture of the cycloaliphatic monomers prevented crystallization and generated optically clear polyesters. Although T_gs remained below 100 °C, dynamic mechanical analysis revealed low-temperature relaxations that are ideal for high-impact resistance. These rapid, short-range structural motions are associated with aliphatic ring flips and correlate strongly to impact resistance.[11-16]

This manuscript describes a family of amorphous, high-T_g copolyesters containing a complement of cycloaliphatic groups. The introduction of tetramethylcyclobutane diol (CBDO) increases the T_g, while the decahydronaphthalate promotes energy absorption. Earlier literature

demonstrated the synthesis of dimethyl decahydronaphthalate-2,6-dicarboxylate from the hydrogenation of dimethyl naphthalate-2,6-dicarboxylate, and enables direct incorporation into a melt-processable polyester family.[10, 17, 18] Complementary analytical techniques provide a detailed evaluation of structural effects on thermal and rheological properties. In addition, correlations between structure, entanglements, and free volume reveal important characteristics for target applications such as food packaging.

6.3 Experimental

Materials. 1,4-cyclohexanedimethanol (99%, mixture of isomers), and dibutyltin(II) oxide (97%) were purchased from Sigma-Aldrich and used as received. Titanium tetraisopropoxide (99.999%) was purchased from Sigma-Aldrich and diluted to 13.4 mg/mL in *n*-butanol. Dimethyl decahydronaphthalate-2,6-dicarboxylate, 1,1,3,3-tetramethylcyclobutane-2,4-diol (CBDO) were used as received. 1,1,1,3,3,3-hexafluoro-2-propanol (99.5+%, HFIP) was purchase from Acros Organics and used as received. All deuterated solvents were purchased from Cambridge Isotope Laboratories, Inc.

Analytical Methods. ^{1}H NMR spectroscopy utilized a Varian Unity 400 spectrometer operating at 399.87 MHz and 23 °C with a binary mixture of 9:1 $CDCl_3$:CF_3COOD (*circa* 8 mg/mL). A TA Instruments TGA Q500 with a heating rate of 10 °C/min from room temperature to 600 °C under constant N_2 purge provided thermogravimetric analysis (TGA). Differential scanning calorimetry (DSC) exploited a TA Instruments DSC Q2000 under a N_2 atmosphere with heat/cool/heat cycles of 10 °C/min, 100 °C/min, and 10 °C/min, respectively. Dynamic mechanical analysis (DMA) with a TA Instruments DMA Q800 in oscillatory tension mode at 1 Hz and 3 °C/min revealed modulus versus temperature behavior. Compression molding between Kapton® sheets at 50 °C above T_g using a PHI hydraulic press generated free-standing films,

which were cooled in air over 1 hour. A Cannon-Ubbelohde 75 capillary viscometer provided intrinsic viscosity measurements, following ISO 1628-1 hexafluoroisopropanol (HFIP). A Systech Illinois 8001 Oxygen Permeation Analyzer operating at 23 °C and 0% relative humidity with oxygen and nitrogen flows of 20 cc/min and 10 cc/min, respectively, achieved oxygen transmission rates (OTR).

Melt rheological experiments employed a TA Instruments AR-G2 rheometer with an 8-mm parallel-plate geometry. Initial strain-sweep experiments (0.01 to 10 % oscillatory strain at 1 Hz) determined the linear viscoelastic region for these polyesters. Isothermal, time-sweep experiments at 1 % oscillatory strain under air identified the thermal stability at relevant processing conditions. Temperature-step and frequency-sweep experiments at 10 °C/step (1.0% oscillatory strain, 1-100 rad/s) provided storage and loss moduli and viscosity responses over a wide range of frequency. Curve shifting using the TA Instruments TRIOS software generated master curves for each polyester. Fitting of the Williams-Landel-Ferry (WLF) and Arrhenius equations using TA Instruments TRIOS software further evaluated melt flow properties.

Positron annihilation lifetime spectroscopy (PALS) probed average hole volume, $<V_h>$. A detailed background on PALS methodology is available elsewhere.[19, 20] Compression-molded, thin films were stacked to a total thickness of about 1 mm and a 30 μCi ^{22}Na positron source was sandwiched between two thick pieces. The sample-source assembly was placed between two photomultiplier tubes (PMT) each equipped with BaF_2 gamma radiation sensitive scintillators and tuned so one PMT can differentiate and convert into a signal the absorbed gamma quanta associated with a positron emission and another PMT with its annihilation. Determining the time difference between a positron 'birth' and 'death' events (the lifetime) is at the core of these measurements. The data were collected using a fast-fast coincidence system with a time

resolution of 290 ps. An Ortec Positron Lifetime System (Advanced Measurement Technology Oak Ridge, TN) collected greater than 10^6 incidences for each sample over 1 h at 23 °C and 45 % relative humidity. A multichannel analyzer compiled coincidences and PATFIT-88 software analyzed the annihilation spectra assuming three components.[21] The characteristic lifetime, τ_3, of the orthopositronium (o-Ps) annihilation component acquired from PALS spectra was first related to the average spherical hole radius, $<R_h>$, via the Tao-Eldrup equation and then to the average hole volume $<V_h> = 4\pi(<R_h>)^3/3$.[22]

Synthesis of Poly(Cyclohexanedimethyl decahydronaphthalate)-*co*-Poly(cyclobutyl decahydronaphthalate) Copolyesters [Poly(CHDN)-*co*-Poly(CBDN)]. A two-step, melt transesterification polymerization enabled synthesis of all copolyesters. The synthesis of poly(CHDN)$_{70}$-*co*-poly(CBDN)$_{30}$ is described as an example. Dimethyl 2,6-decahydronaphthalate dicarboxylate (6.104 g, 0.8 mol), 1,1,3,3-tetramethylcyclobutane-2,4-diol (1.557 g, 0.36 mol), and dibutyltin(II) oxide (3.06 mg, 400 ppm) were charged to a dry, 100-mL, round-bottomed flask. The flask was equipped with an overhead stir rod, nitrogen inlet, condensing tube, and collection flask. Sequential vacuum and purge cycles (3x) ensured an inert atmosphere. Transesterification of the dimethylester with the sterically hindered CBDO required a reaction time of 5 h at 240 °C under a constant nitrogen purge. Collection of methanol distillate in a dry-ice-cooled, round-bottomed flask evaluated the extent of transesterification. After removal of methanol ceased, the reaction flask was cooled and cyclohexanedimethanol (2.769 g, 0.64 mol) and titanium tetraisopropoxide in *n*-butanol was added (0.73 mg, 70 ppm) to facilitate polycondensation. Again, a sequential vacuum and nitrogen purge (3x) provided an inert atmosphere. Under constant nitrogen purge, the flask was heated at 240 °C for 2 h. Finally, the temperature was increased to 270 °C over 1 h under vacuum and the reaction

proceeded at 270 °C for 2 h. The resulting products were used directly without further purification.

6.4 Results and Discussion

A two-step, melt transesterification of tetramethylcyclobutane diol (CBDO) and cyclohexyldimethanol (CHDM) with dimethyl-2,6-decahydronaphthalate dicarboxylate afforded copolyesters with diverse composition (Scheme 1). Due to the difference in reactivity of CBDO and CHDM, a sequential addition was necessary to prevent homopolymerization of CHDM.[6, 23] Furthermore, previous reports identified dibutyltin(II) oxide as an active catalyst to assist in transesterification.[6] Monitoring methanol generation provided insight into reaction conditions, and the transesterification of CBDO with dimethyl-2,6-decahydronaphthate dicarboxylate required 240 °C and 5 h before methanol generation ceased. Addition of CHDM followed the initial transesterification, and titanium(IV) tetraisopropoxide facilitated transesterification and high molecular weight growth. The reaction proceeded by a step-wise temperature ramp from 240 °C to 280 °C over 3 h. In the final 2 h, reduced pressures removed excess diols and afforded high molecular weight product, as evidenced by high melt viscosities and intrinsic viscosities (Table 1).

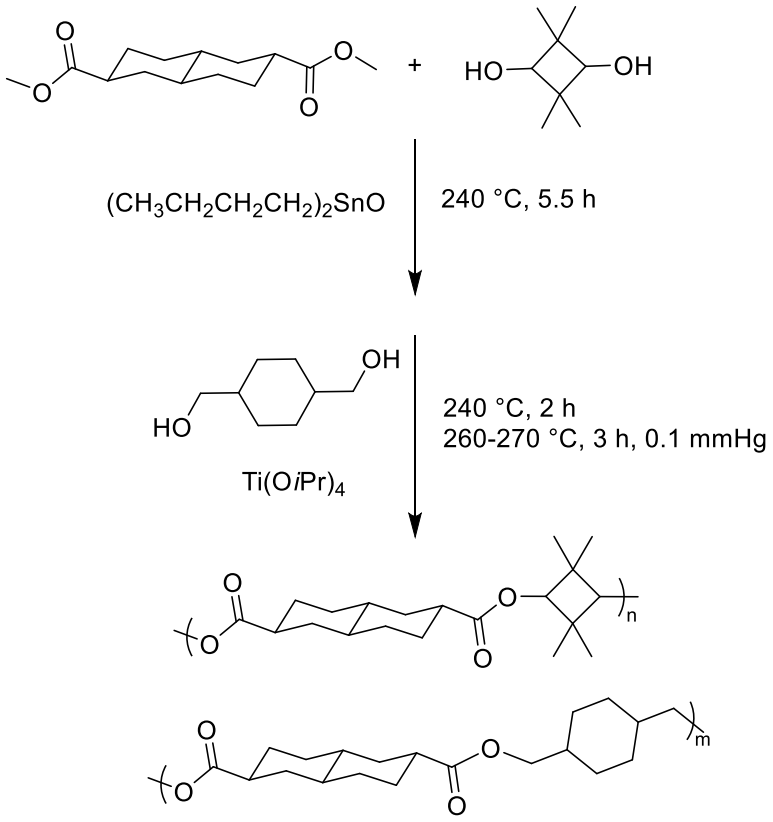

Scheme 1: Synthesis of decahydronaphthalene-containing copolyesters utilizing a two-step melt polymerization method.

The poor solubility of the copolyesters in typical organic solvents prevented molecular weight determination with size exclusion chromatography, and thus intrinsic viscosity ([η]) measurements in hexafluoroisopropanol (HFIP) as a common solvent revealed relative molecular weights (Table 1).[6, 10] Consistent intrinsic viscosities across the compositional range highlighted comparable molecular weights of the copolymers, and permitted direct mechanical and rheological comparison. Furthermore, these values were consistent with previous literature of high molecular weight polyesters.[2, 6, 10]

Table 1: Summary of thermal transitions and intrinsic viscosity

Sample	$T_{d,5\%}$	T_g	[η]	M_e

	(°C)[a]	(°C)[b]	(dL/g)[c]	(g/mol)
Poly(1,4-CHDN)	396	87	0.66	3500
Poly(1,4-CHDN)$_{89}$-*co*-Poly(CBDN)$_{11}$	395	98	0.55	4200
Poly(1,4-CHDN)$_{69}$-*co*-Poly(CBDN)$_{31}$	404	107	0.36	4400
Poly(1,4-CHDN)$_{60}$-*co*-Poly(CBDN)$_{40}$	399	114	0.60	5200
Poly(1,4-CHDN)$_{35}$-*co*-Poly(CBDN)$_{65}$	400	124	0.58	5600

[a] TGA: 10 °C/min, N_2
[b] DSC: heat/cool/heat, second heat; 10 °C/min, N_2
[c] Intrinsic Viscosity: HFIP, 35 °C, Cannon-Ubbelohde 75 viscometer

Manipulating the ratio of CBDO to CHDM provided novel, optically clear copolyesters containing decahydronapthalate and CBDO. Introduction of the rigid cyclobutane ring systematically increased the glass transition temperature (T_g) following the Fox equation, confirming a random sequence in the copolymer (Figure 1). Although, the poor reactivity of CBDO prevented synthesis of a high molecular weight homopolymer of CBDO-decahydronaphthalate, extrapolation of the Fox equation to 100 % CBDO identified a potential polyester with an estimated T_g of 155 °C, an important benchmark for a BPA-polycarbonate replacement. The poor solubility restricted ^{1}H NMR spectroscopy to a 9:1 v:v mixture of $CDCl_3$:CF_3COOD. Unique chemical shifts of CBDO and CHDM verified target compositions, and confirmed retention of *cis*/*trans* ratios of all starting materials, which correlated well to previous literature (Table 2).[6, 10] Maintaining the isomeric mixtures enhanced conformational complexity and suppressed the crystallization, resulting in optically clear materials.

Table 2: Summary of isomeric ratios determined by ^{1}H NMR Spectroscopy

Sample	CBDO			CHDM			DHN	
	Trans %	Cis %	mol. %	Cis %	Trans %	mol. %	Cis %	Trans %

Poly(1,4-CHDN)$_{89}$-*co*-Poly(CBDN)$_{11}$	65	35	11	32	68	89	8	92
Poly(1,4-CHDN)$_{69}$-*co*-Poly(CBDN)$_{31}$	66	34	31	27	73	69	9	91
Poly(1,4-CHDN)$_{60}$-*co*-Poly(CBDN)$_{40}$	66	34	40	32	68	60	9	91
Poly(1,4-CHDN)$_{35}$-*co*-Poly(CBDN)$_{65}$	68	32	65	26	74	35	10	90

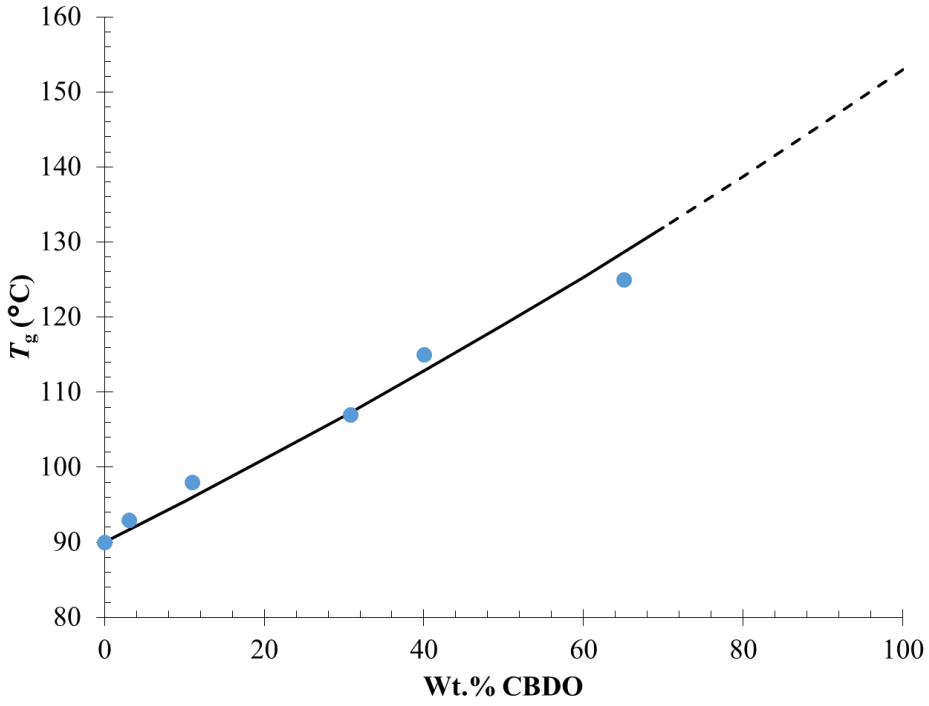

Figure 1: Fox plot identifying predictable T_gs as a function of comonomer. Adherence to theory provides insight into randomness of copolymer sequence.

Dynamic mechanical analysis (DMA) corroborated the trends observed in DSC. The α-relaxation increased systematically with CBDO incorporation, and agreed well with the T_g identified by DSC (Figure 2). Furthermore, several low temperature relaxations highlighted local mobility, and provided an avenue for high-energy absorption. This behavior reinforced previous observations for similar decahydronaphthalene-containing polyesters.[10] A systematic change in CBDO content elucidated the structural origin of the β- and γ-relaxations (Figure 3). As a result, the γ-relaxation was associated with conformational changes of the cyclohexane ring,

while the rigid butane ring did not provide energy absorption in the range probed. The bulkier, fused, cycloaliphatic rings required a longer time scale for conformational change and absorbed energy at a higher temperature, resulting in the β-relaxation. In comparison to a commercial BPA-polycarbonate, the intensities of these low-temperature relaxations in the copolyesters were significantly larger, and suggested a comparable ability to absorb energy in the glassy state.[24, 25] Furthermore, the similar temperature range of the β- and γ-relaxations in these copolyesters highlighted a comparable frequency range of energy absorption relative to BPA-polycarbonate.

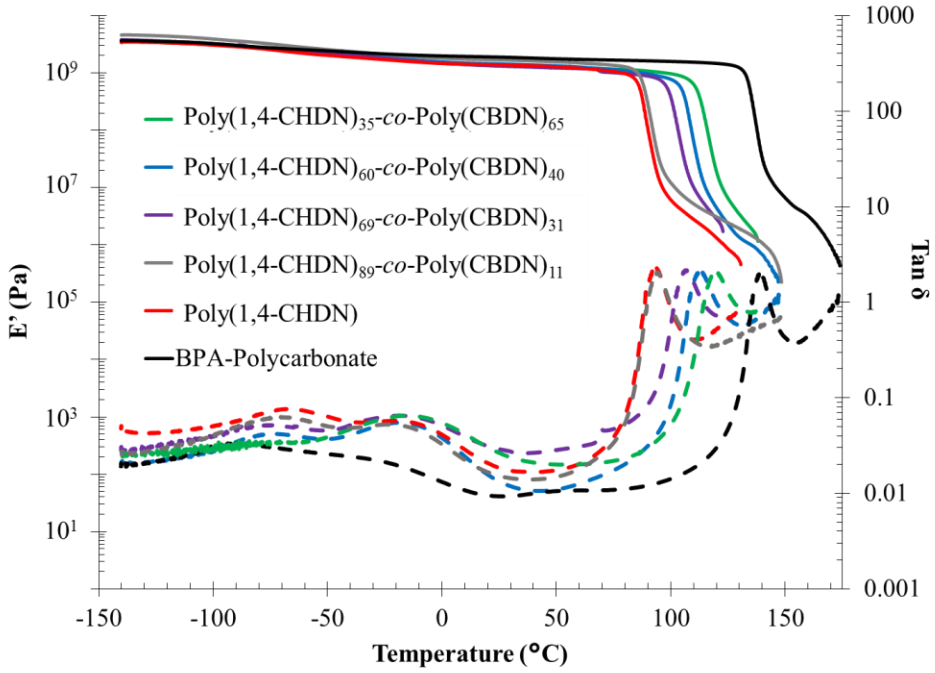

Figure 2: Dynamic mechanical analysis illustrating thermomechanical properties of copolyesters in comparison to a commercial BPA-polycarbonate (black).

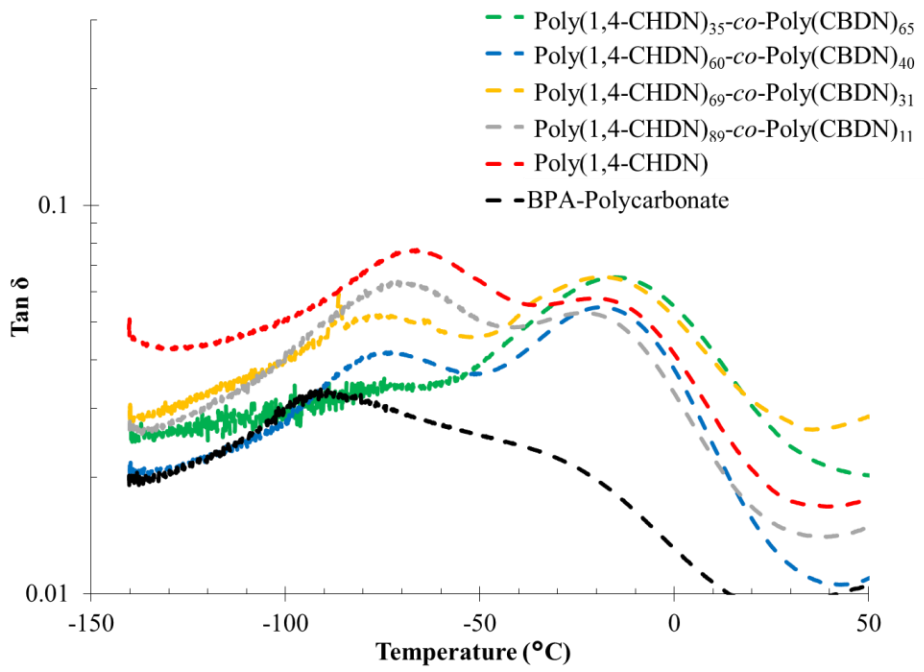

Figure 3: Low temperature range of DMA highlighting β- and γ-relaxations of copolyesters.

Shifting of frequency sweeps following the time-temperature superposition (TTS) principle generated master curves and identified the rheological simplicity of these copolyesters across a wide range of temperatures and timescales. Figure 4 portrays representative storage and loss moduli curves for the two compositional extremes. Using a common reference temperature (T_r) of 160 °C, the impact of the rigid cyclobutane ring was realized. In particular, these master curves illustrated a systematic change in the characteristic relaxation times of various polymer chain segments, as identified by crossover points in the relaxation curves. Figure 5 more clearly compares the various characteristic relaxation times across CBDO incorporation. The rigid CBDO segment increased the timescale for relaxation of the polymer chain across all length scales, from cooperative segmental relaxation (τ_0) to reptation of the entangled chains (τ_{rep}).

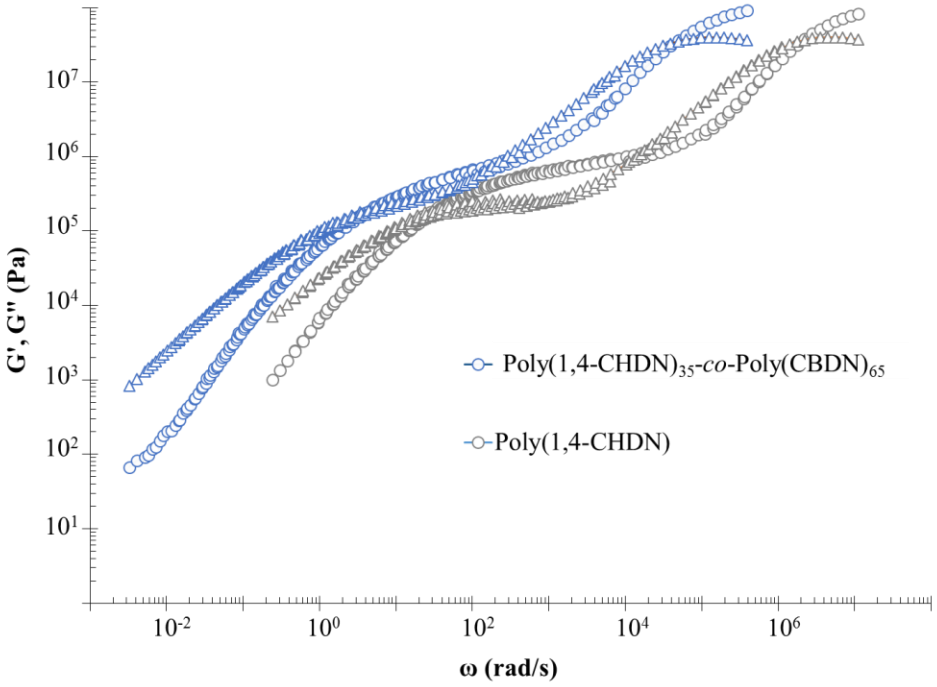

Figure 4: Representative storage and loss moduli master curves of copolyesters, T_r = 160 °C.

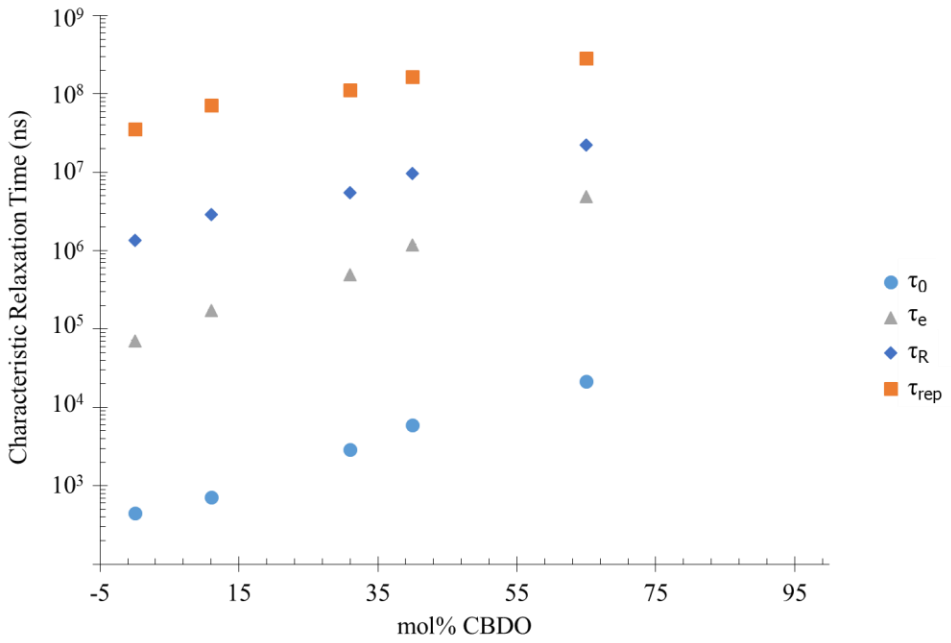

Figure 5: Characteristic relaxation times of copolyesters as determined by TTS at 160 °C, where τ_0, τ_e, τ_R, and τ_{rep} are the segmental, entanglement, Rouse, and reptation relaxation times, respectively.

Importantly, these master curves corroborated previous literature understanding of viscoelastic properties in the melt.[10, 26, 27] At frequencies higher than τ_0, the chain behaved as rigid units and resulted in a characteristic glassy state. Lower frequencies resulted in a rubbery behavior. The plateau modulus of this regime (G_N^0) depended on the entanglement molecular weight (M_e) for non-interacting, linear polymer melts (Equation 1).[26, 27] As a result of the rheological simplicity of the polyesters, G_N^0 was readily obtained from the master curve at the point of intersection noted as $1/\tau_e$. Table 1 reports M_e as determined using Equation 1. Furthermore, interrelationships between the characteristic relaxation times (Equation 2) corroborated the reduction in entanglements per chain (N/N_e, Figure 6).[28] In agreement with the reduction in chain relaxation, increasing the rigid CBDO incorporation decreased the propensity

for entanglement. Therefore, the M_e increased systematically with CBDO incorporation (Figure 6), which resulted in the loss in mechanical strength at similar molecular weights.

$$M_e = {nRT}/{G_N^0} \qquad (Eq.1)$$

$$\tau_{rep} = 6\tau_0 \frac{N^3}{N_e} = 6\tau_e \left(\frac{N}{N_e}\right)^3 = 6\tau_R \frac{N}{N_e} \qquad (Eq.2)$$

$$C_1^g = \frac{C_1 C_2}{C_2 + (T_g - T_r)} \qquad (Eq.3)$$

$$C_2^g = C_2 + (T_g - T_r) \qquad (Eq.4)$$

$$f_g = \frac{B}{2.303 C_1^g} \qquad (Eq.5)$$

$$\alpha_f = \frac{B}{2.303 C_1^g C_2^g} \qquad (Eq.6)$$

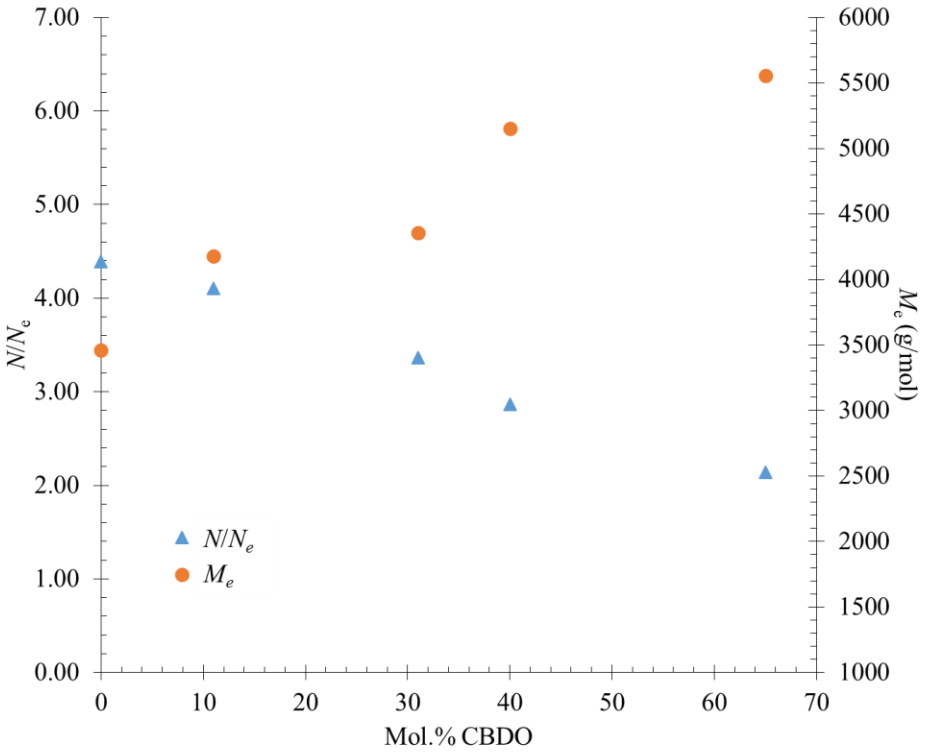

Figure 6: Number of entanglements per chain (N/N_e) determined through characteristic relaxation times and critical entanglement molecular weight (M_e) determined using Equation 1.

TTS also provided the fractional free volume. By examining the TTS shift factors, a_T, the WLF relationship elucidated the fractional free volume at the T_g (f_g, Equation 5) and also its thermal expansion coefficient (α_f, Equation 6).[27] The f_g decreased with increasing CBDO incorporation (Figure 7). Again, the rigid cyclobutane ring reduced the local conformational perturbations, which allowed the chains to densify in the melt. Interestingly, comparing the f_g with average hole volumes determined by positron annihilation lifetime spectroscopy (PALS) highlighted the importance of using different techniques to measure free volume (Figure 7). PALS performed on films at room temperature revealed an increasing hole size with increasing CBDO content in accord with earlier established correlations between the

average hole volume and the T_g.[29] Although further analysis is required to assess the hole size, shape distribution, and number density to directly compare the observations from WLF and PALS,[30-33] the increase in average hole size provided insight into the gas transport properties.

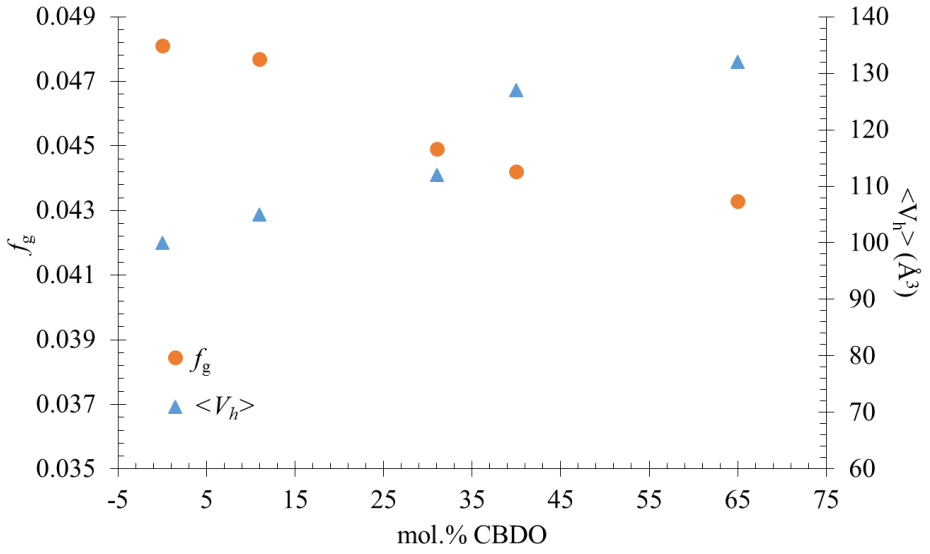

Figure 7: Free volume determined by rheology and PALS. The WLF relationship determined free volume at the T_g (f_g), while PALS explored average hole volume at room temperature ($<V_h>$).

Table 3 illustrates the oxygen permeability in comparison to a commercial CBDO-containing polyester, Tritan®. Introduction of the rigid cyclobutane diol increased the permeability of oxygen through the amorphous film. The larger average hole size, determined by PALS, correlated well with an increased permeability of oxygen through the films and complements previous literature.[34, 35] Furthermore, the oxygen permeability of Poly(1,4-CHDN)$_{89}$-*co*-Poly(CBDN)$_{11}$ approached the permeability observed in Tritan®, which contains a similar CBDO content. Embrittlement at higher CBDO incorporation prevented further studies.

Table 3: Summary of oxygen permeability of CBDO-containing copolyesters

Sample	Permeability	Permeability

	(cc·cm/m^2/atm/day)	Relative to Tritan®
Poly(CHDN)	1.816 ± 0.067	0.24
Poly(1,4-CHDN)$_{89}$-*co*-Poly(CBDN)$_{11}$	4.774 ± 0.050	0.97
Tritan®	4.920 ± 0.150	1.00

6.5 Conclusion

A two-step, melt transesterification polymerization of dimethyl decahydronaphthalate-2,6-dicarboxylate with CBDO and CHDM afforded optically clear, high molecular weight copolyesters. Introduction of the rigid CBDO monomer systematically increased the T_g, according to the Fox equation for randomly sequenced copolymers. Thermomechanical analysis confirmed the trends in T_g, and identified low-temperature relaxations associated with high-energy absorption in the glassy regime. The systematic change in copolymer composition elucidated the origin of each relaxation to the cycloaliphatic rings of CHDM and DHN. The rheological simplicity of these non-interacting copolymers enabled TTS analysis across a wide range of frequencies, which provided insight into chain dynamics. PALS probed hole size in the solid state, and indicated an increase in hole size with increasing CBDO incorporation. This increase correlated well with the oxygen permeability of the polyesters, and complements previous literature on the importance of hole size on gas transport in polymer materials.

6.6 References

1. Nelson, A. M.; Long, T. E. A perspective on emerging polymer technologies for bisphenol-A replacement, *Polym. Int.* **2012,** 61, (10), 1485-1491.
2. Crawford, E. D.; Pecorini, T. J.; McWilliams, D. S.; Porter, D. S.; Connell, G. W.; Germroth, T. C.; Barton, B. F.; Shackelford, D. B. Polyester Compositions Containing

Cyclobuntanediol Having a Certain Combination of Inherent Viscosity and Moderate Glass Transition Temperature and Articles Made Therefrom. US2006042292, 2007.

3. Crawford, E. D.; Porter, D. S.; Connel, G. W. Polyester compositions which comprise cyclobutanediol having certain cis/trans ratios. EP20090012051, 2011.
4. Scott, C. E.; Morris, J. C.; Bradley, J. R. Clear polycarbonate and polyester blends. US6043322 A, 1997.
5. Scott, C. E.; Morris, J. C.; Bradley, J. R. Clear blends of polycarbonates and polyesters. US6037424 A, 1997.
6. Kelsey, D. R.; Scardino, B. M.; Grebowicz, J. S.; Chuah, H. H. High Impact, Amorphous Terephthalate Copolyesters of Rigid 2,2,4,4-Tetramethyl-1,3-cyclobutanediol with Flexible Diols, *Macromolecules* **2000,** 33, (16), 5810-5818.
7. Barton, B. F.; Shackelford, D. B. Process for the Preparation of Copolyesters Based on 2,2,4,4-Tetramethyl-1,3-Cylclobutanediol and 1,4-Cyclohexanedimethanol US2008005799, 2007.
8. Beall, G. W.; Powell, C. E.; Hancock, J.; Kindinger, M.; McKenzie, H. R.; Bray, A. V.; Booth, C. J. Physical properties of CBDO based co-polyterephthalate nanocomposites, *Appl. Clay Sci.* **2007,** 37, (3–4), 295-306.
9. Booth, C. J.; Kindinger, M.; McKenzie, H. R.; Handcock, J.; Bray, A. V.; Beall, G. W. Copolyterephthalates containing tetramethylcyclobutane with impact and ballistic properties greater than bisphenol A polycarbonate, *Polymer* **2006,** 47, (18), 6398-6405.
10. Dennis, J. M.; Enokida, J. S.; Long, T. E. Synthesis and Characterization of Decahydronaphthalene-Containing Polyesters, *Macromolecules* **2015,** 48, (24), 8733-8737.

11. Wyzgoski, M.; Yeh, G. Origin of Impact Strength in Polycarbonate: II. Effect of Thermal Treatments, *Int. J. Polym. Mater.* **1974,** 3, (2), 149-163.
12. Wyzgoski, M.; Yeh, G. Origin of Impact Strength in Polycarbonate: I. Effect of Crystallization and Residual Solvent, *Int. J. Polym. Mater.* **1974,** 3, (2), 133-148.
13. Heijboer, J. Modulus and damping of polymers in relation to their structure, *Brit. Polym. J.* **1969,** 1, (1), 3-14.
14. Heijboer, J. Molecular Origin of Relaxations in Polymers, *Ann. NY Acad. Sci.* **1976,** 279, (1), 104-116.
15. Heijboer, J. Secondary loss peaks in glassy amorphous polymers, *Int. J. Polym. Mater.* **1977,** 6, (1-2), 11-37.
16. Heijboer, J.; Baas, J. M. A.; van de Graaf, B.; Hoefnagel, M. A. A molecular mechanics study on rotational motions of side groups in poly(methyl methacrylate), *Polymer* **1987,** 28, (3), 509-513.
17. Parham, F. M. Decahydro-bis (hydroxymethyl) naphthalenes. US19620170523, 1966.
18. Storms, P. W.; Farrar, G. L. Hydrogenation of naphthalene esters to tetralin esters, *J. Chem. Eng. Data* **1969,** 14, (4), 489-490.
19. Pethrick, R. A. Positron annihilation—A probe for nanoscale voids and free volume?, *Prog. Polym. Sci.* **1997,** 22, (1), 1-47.
20. Jamieson, A. M.; Olson, B. G.; Nazarenko, S., Positron Annihilation Lifetime Studies of Free Volume in Heterogeneous Polymer Systems. In *Polymer Physics*, John Wiley & Sons, Inc.: 2010; pp 473-522.

21. Kirkegaard, P.; Eldrup, M.; Mogensen, O. E.; Pedersen, N. J. Program system for analysing positron lifetime spectra and angular correlation curves, *Computer Physics Communications* **1981,** 23, (3), 307-335.
22. Eldrup, M.; Lightbody, D.; Sherwood, J. N. The temperature dependence of positron lifetimes in solid pivalic acid, *Chemical Physics* **1981,** 63, (1), 51-58.
23. Zhang, M.; Moore, R. B.; Long, T. E. Melt transesterification and characterization of segmented block copolyesters containing 2,2,4,4-tetramethyl-1,3-cyclobutanediol, *J. Polym. Sci., Part A: Polym. Chem.* **2012,** 50, (18), 3710-3718.
24. Illers, V. K.-H. Der einfluß von wasser auf die molekularen beweglichkeiten von polyamiden, *Makromolekul. Chem.* **1960,** 38, (1), 168-188.
25. Wada, Y.; Kasahara, T. Relation between impact strength and dynamic mechanical properties of plastics, *J. Appl. Polym. Sci.* **1967,** 11, (9), 1661-1665.
26. Herrmann-Schönherr, O.; Schneller, A.; Seifert, A. M.; Soliman, M.; Wendorff, J. H. Chain dimensions, entanglement molecular weights and molecular weight distributions of poly(aryl ethers). A combined rheological and MNDO analysis, *Makromolekul. Chem.* **1992,** 193, (8), 1955-1974.
27. Ferry, J. D., *Viscoelastic properties of polymers*. John Wiley & Sons: 1980.
28. Watanabe, H. Viscoelasticity and dynamics of entangled polymers, *Prog. Polym. Sci.* **1999,** 24, (9), 1253-1403.
29. Yampol'skii, Y. P.; Volkov, V. V. Studies in gas permeability and membrane gas separation in the Soviet Union, *Journal of Membrane Science* **1991,** 64, (3), 191-228.
30. Dlubek, G.; Kilburn, D.; Bondarenko, V.; Pionteck, J.; Krause-Rehberg, R.; Alam, M. Characterisation of Free Volume in Amorphous Materials by PALS in Relation to Relaxation

Phenomena, *24th Arbeitskreistagung 'Nichtkristalline Structuren' of DGK, Jena, Germany, Sept* **2003**.

31. Fujita, H. Notes on Free Volume Theories, *Polym J* **1991,** 23, (12), 1499-1506.
32. Steller, R. Free volume effect on behavior of polymer liquids in shear flows, *Polimery* **2012,** 57, (7-8), 562-570.
33. Jean, Y. C. Positron annihilation spectroscopy for chemical analysis: A novel probe for microstructural analysis of polymers, *Microchemical Journal* **1990,** 42, (1), 72-102.
34. Pazmiño Betancourt, B. A.; Hanakata, P. Z.; Starr, F. W.; Douglas, J. F. Quantitative relations between cooperative motion, emergent elasticity, and free volume in model glass-forming polymer materials, *Proceedings of the National Academy of Sciences* **2015,** 112, (10), 2966-2971.
35. Robeson, L. M.; Smith, C. D.; Langsam, M. A group contribution approach to predict permeability and permselectivity of aromatic polymers, *Journal of Membrane Science* **1997,** 132, (1), 33-54.

6.7 Supporting Information

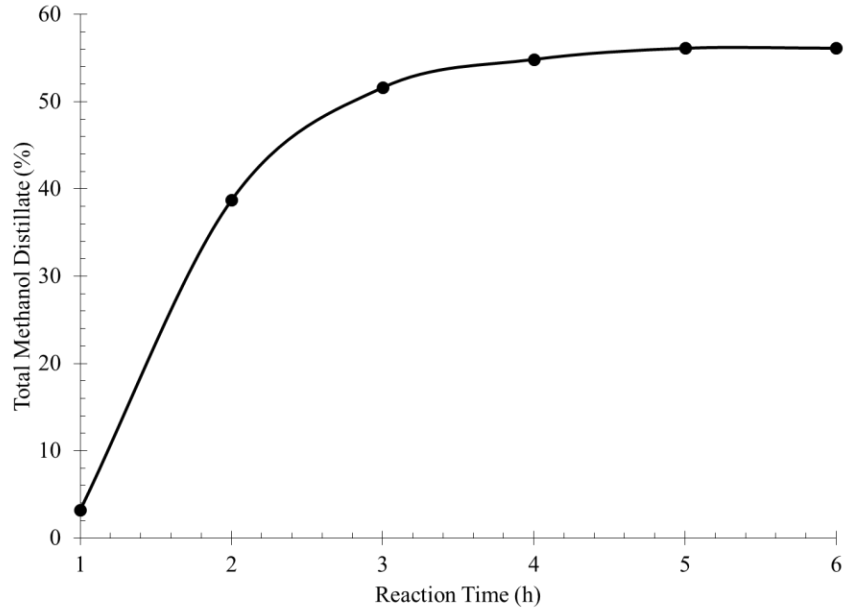

Figure S1: Methanol recovery of 1,1,3,3-tetramethylcyclobutane-2,4-diol transesterification with Dimethyl decahydronaphthalate-2,6-dicarboxylate at 240 °C.

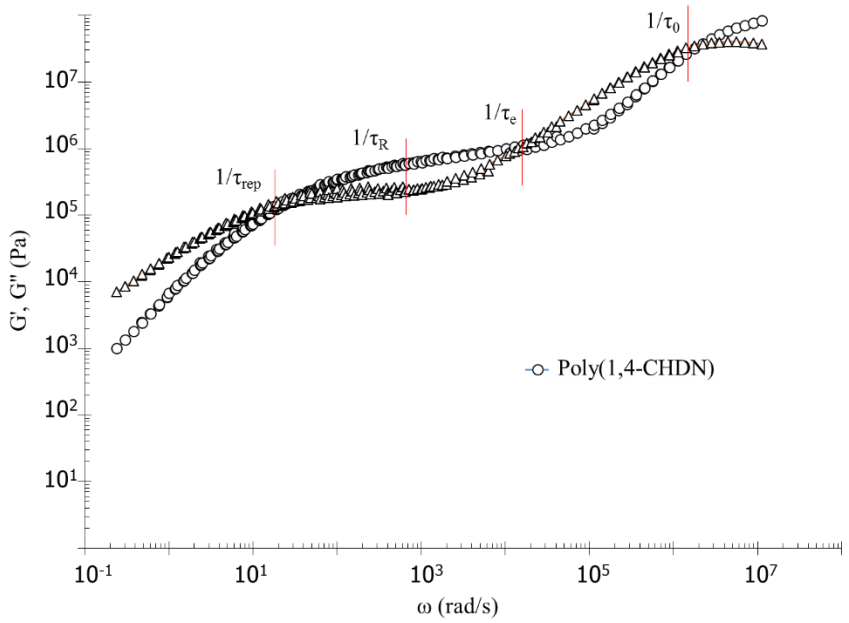

Figure S2: Storage and loss moduli master curve for Poly(1,4-CHDN) with characteristic relaxation times highlighted.

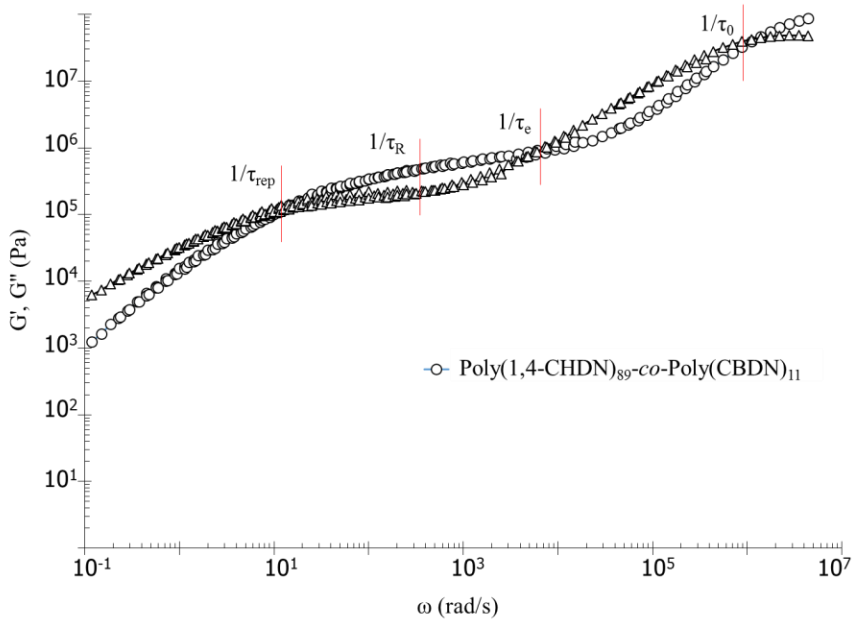

Figure S3: Storage and loss moduli master curve for Poly(1,4-CHDN)$_{89}$-co-Poly(CBDN)$_{11}$ with characteristic relaxation times highlighted.

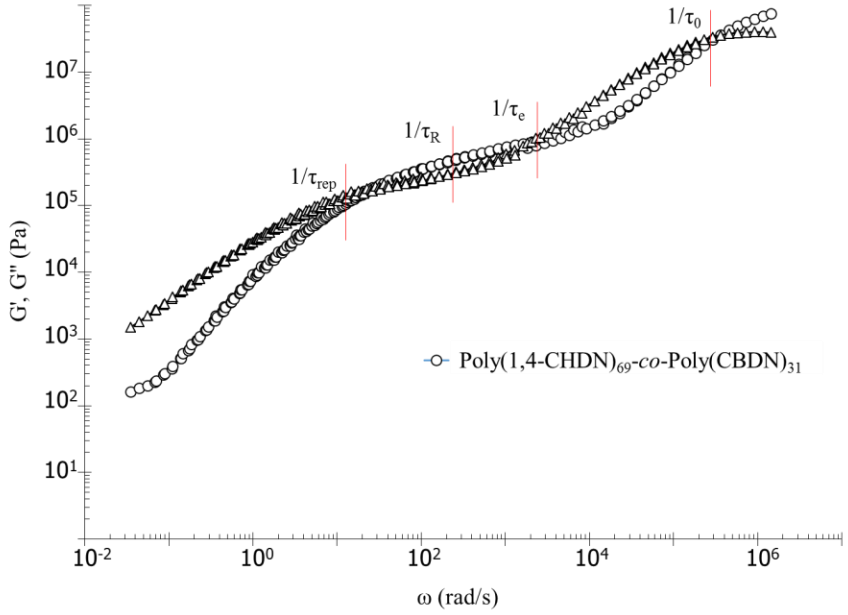

Figure S4: Storage and loss moduli master curve for Poly(1,4-CHDN)$_{69}$-co-Poly(CBDN)$_{31}$ with characteristic relaxation times highlighted.

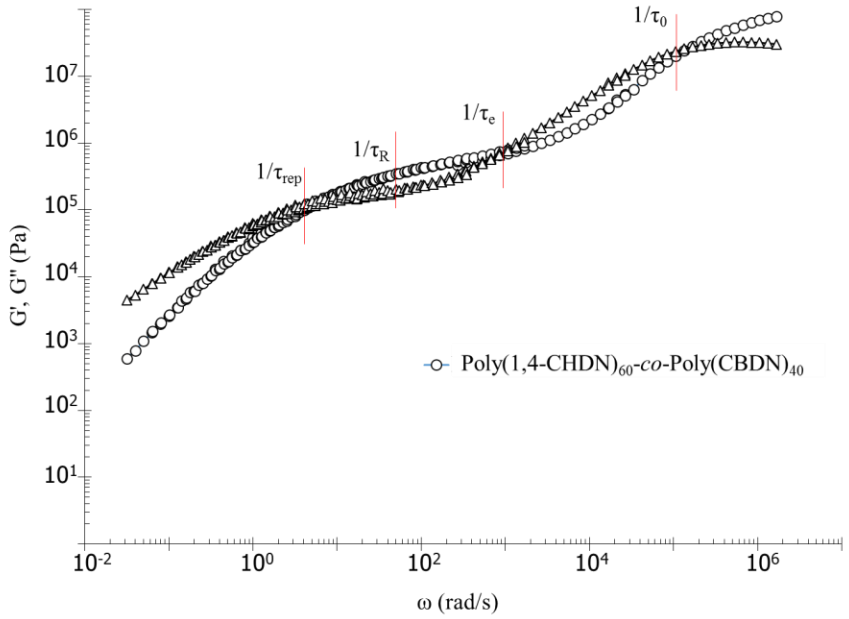

Figure S5: Storage and loss moduli master curve for Poly(1,4-CHDN)$_{60}$-co-Poly(CBDN)$_{40}$ with characteristic relaxation times highlighted.

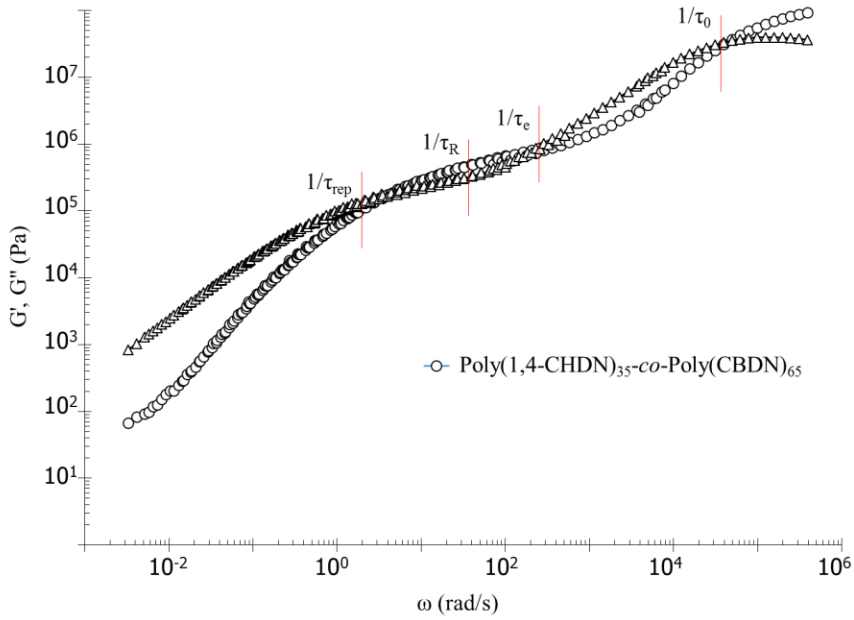

Figure S6: Storage and loss moduli master curve for Poly(1,4-CHDN)$_{35}$-co-Poly(CBDN)$_{65}$ with characteristic relaxation times highlighted.

Table S1: WLF Parameters, Fractional Free Volume (f_g), Flow Activation Energy (E_a), and Thermal Expansion Coefficient (α_f)of decahydronaphthalene-containing copolyesters

Sample	C_1	C_2 (K)	C_1^g	C_2^g (K)	f_g	a_f (x10^{-4} K^{-1})	E_a (kJ/mol)
Poly(1,4-CHDN)	2.75	101	9.03	30.6	0.0481	15.7	119
Poly(1,4-CHDN)$_{89}$-co-Poly(CBDN)$_{11}$	2.74	88.6	9.10	26.6	0.0477	17.9	120
Poly(1,4-CHDN)$_{69}$-*co*-Poly(CBDN)$_{31}$	3.42	82.1	9.66	29.1	0.0449	15.4	147
Poly(1,4-CHDN)$_{60}$-*co*-Poly(CBDN)$_{40}$	4.22	80.5	9.83	34.5	0.0442	12.8	151
Poly(1,4-CHDN)$_{35}$-*co*-Poly(CBDN)$_{65}$	5.26	75.6	10.0	39.6	0.0433	10.9	176

Chapter 7: Synthesis and Characterization of Long-chain Branched Poly(ether imide)s

(In preparation for submission, patent in progress)

Joseph M. Dennis[*], Ryan J. Mondschein[*], Maruti Hegde[*], Roy Odle[#], and Timothy E. Long[*]

[*]*Department of Chemistry, Macromolecules Innovation Institute*

Virginia Tech, Blacksburg, VA 24061

[#]*SABIC Innovative Plastics, Mt Vernon, IN 47620*

7.1 Abstract

Synthesis of a novel trisamine enabled the generation of long-chain branched poly(ether imide)s (LCB-PEIs). Nucleophilic aromatic substitution of 1-chloro-4-nitrobenzene with 1,1,1-tris(4-hydroxyphenyl) ethane resulted in tris((*p*-nitrophenoxy)phenyl) ethane and subsequent reduction afforded tris((*p*-aminophenoxy)phenyl) ethane (TAPE) in good yields (> 90%). Introducing TAPE at low percentages with *m*-phenylene diamine and bisphenol-A dianhydride enabled synthesis of high molecular weight, branched poly(ether imide)s with varied branch lengths. Stoichiometric imbalance and phthalic anhydride controlled molecular weights and achieved phthalimide-endcapped polymers. The compilation of ^{1}H NMR spectroscopy and size exclusion chromatography identified average branch length as a function of TAPE incorporation, and provided overall molecular weights and distributions. Melt viscosity and thermal stability at elevated temperatures (*circa* 340 °C) probed the processing ability of LCB-PEIs in comparison to linear analogs. Below 1.5 mol.% TAPE melt viscosities increased at low shear rates. However, increasing TAPE above 1.5 mol.% decreased melt viscosities at low shear rates, suggesting a correlation of branch length and polydispersity with melt viscosity. Finally,

mechanical testing of injection-molded samples demonstrated minimal changes in tensile and impact properties with branching.

7.2 Introduction

Long-chain branching (LCB) has major implications in the melt strength of polymers.[1-6] The introduction of LCB reduces melt viscosity of high molecular weight polymers at a given processing temperature.[1, 4, 5] Furthermore, LCBs improve shear-thinning and extensional flow processing over linear analogues.[1, 4, 7] Much of the current literature studies the impact of long-chain branches in polyolefins, where branch molecular weights (M_b) are orders of magnitude larger than the molecular weight of entanglement (M_e).[2, 4, 7] With such long-chains, melt viscosity and processability are greatly influenced with minimal branching. The low concentration of branching points in LCB polyolefins causes difficulties in the characterization of critical parameters (e.g. M_b) of the branched polymers.[8-10] Even so, many correlations between rheological properties and degree of branching exist.[7, 11-13] Generally the presence of LCBs decrease viscosity at low shear rates (typically within the Newtonian plateau) as a result of the reduction in radius of gyration (R_g) and entanglements.[11, 12] However, many also report an increase in viscosity with low incorporation of LCBs. It is suspected that at low branching density, the increase in entanglements per chain dominates the flow behavior over the reduction in size.[13]

Other investigations include introducing long-chain branches into polyesters (e.g. poly(ethylene terephthalate)) to improve strength and reduce the rate of crystallization.[14-16] In this instance, very low incorporations of a trifunctional monomer (less than 1 mol.%) resulted in long-chain branched polyesters without gelation.[14-16] In general, increasing the branching density reduced and broadened the melting transition.[17, 18] It is hypothesized that the asymmetry

introduced through the trifunctional monomer and branches frustrated chain alignment, preventing crystallization to occur to the same extent as a linear analogue.[18, 19] However, the difficulties in molecular weight determination and branch length characterization prevented a direct correlation of branching on thermal properties.

Previously, tri-functional aryl-amines were synthesized to promote crosslinking in polyimides.[20] However, the high incorporation of the multifunctional monomers provides an intractable material, and is not conducive for further processing. Recently, many reports identified advantageous separation capabilities of hyperbranched polyimides in gas separation membranes.[21-23] The high mechanical strength, thermal stability, and high modulus encourage the use of polyimides in gas separation membranes. Furthermore, hyperbranched materials with rigid structures provide more porosity between chains because of sterically restricted branched networks.[21-23] Utilizing various pathways to synthesize mechanically robust, hyperbranched polyimide films, analysis of gas permeability and selectivity indicated a strong variability in the preparation method and polymer structure.[21-23] In general, selectivity of hyperbranched polyimides improved, however no strong correlation is drawn on permeability for these materials.

Currently, there lacks a melt-processable, long-chain branched poly(ether imide). Here the synthesis of a tri-functional aryl amine is described and subsequent polymerization with bisphenol-A dianhydride and *meta*-phenylene diamine results in long-chain branched poly(ether imide)s (Schemes 1-3). Careful consideration of reaction conditions and molar ratios permits high percentages of the trisamine without forming an insoluble network. In contrast to the polyester literature, little change in the melt viscosity and processability for the PEIs resulted at low incorporations (*circa 0.5 mol.%*) of the trisamine. However, at high incorporations (*circa* 2

mol.%) the melt viscosity was dramatically reduced. Identified by size exclusion chromatography (SEC), the chain dispersity broadens at the higher incorporation of trisamine. The broader chain distribution includes higher concentrations of high and low molecular weight species. As a result, the low molecular weight chains plasticize the melt reducing the overall viscosity, while the high molecular weight species maintain thermal and mechanical properties.

7.3 Experimental

Materials. Bisphenol-A dianhydride (BPA-DA), and *m*-phenylene diamine (MPD) were kindly provided by SABIC in high purity. Sublimation of MPD under reduced pressure afforded a white solid, which was stored under vacuum. BPA-DA was dried with heating under a nitrogen blanket and stored under vacuum. 1,1,1-Tris(4-hydroxyphenyl)ethane (99%), 1-chloro-4-nitrobenzene (99%), dimethylacetamide, and *o*-dichlorobenzene were purchased from Sigma Aldrich and used as received. Potassium carbonate was purchased from Sigma Aldrich and dried at 120 °C prior to use. All deuterated solvents were purchased from Cambridge Isotope Laboratories, Inc. All other solvents were purchased from Spectrum Chemical and used as received.

Analytical Methods. ^{1}H and ^{13}C NMR spectroscopy utilized a Varian Unity 400 spectrometer operating at 399.87 MHz and 23 °C (*circa* 8 mg/mL). A 1101D Mel-Temp digital melting point apparatus operating at 1 °C/min provided melting points for small molecule compounds. A TA Instruments TGA Q500 with a heating rate of 10 °C/min from room temperature to 600 °C under constant N_2 purge enabled thermogravimetric analysis (TGA). Differential scanning calorimetry (DSC) utilized a TA Instruments DSC Q2000 under a N_2 atmosphere with heat/cool/heat cycles of 10 °C/min, 100 °C/min, and 10 °C/min, respectively. Compression molding between Kapton® sheets at 315 °C using a PHI hydraulic press generated freestanding films.

Melt rheological experiments employed a TA Instruments AR-G2 rheometer with a disposable, parallel-plate geometry. Initial strain-sweep experiments identified 1.0 % oscillatory strain to be within the linear viscoelastic region. Operating at 1.0 % oscillatory strain under air, isothermal, time-sweep experiments elucidated thermal stability at relevant processing conditions. Temperature-step, frequency-sweep experiments performed at 10 °C increments and a range of 1 to 100 rad/s determined the viscoelastic response. Curve shifting using the TA Instruments TRIOS software generated master curves over a wide range of frequency. Fitting of the shift factors using Williams-Landel-Ferry (WLF) and Arrhenius equations using the TA Instruments TRIOS software further evaluated melt flow properties.

Synthesis of tris((*p*-nitrophenoxy)phenyl) ethane (TNPE). 1,1,1-tris(4-hydroxyphenyl) ethane (20 g, 65.3 mmol), potassium carbonate (45.1 g), dimethylacetamide (115 mL), and toluene (58 mL) were charged to a three-necked, 500-mL, round-bottomed flask. A dean-stark trap with condenser, glass stir rod with Teflon blade and glass bearing, and rubber septa was attached to the three necks, respectively. Purging the whole setup with nitrogen for 20 min provided an inert atmosphere. Next, the round-bottomed flask was lowered into a 180 °C preheated oil bath resulting in a reflux of toluene to the Dean-Stark trap. Deprotonation of the phenol proceeded at 180 °C, monitored through collection of water in the Dean-Stark trap. Once water removal ceased, toluene removal proceeded by distillation through the Dean-Stark trap. A solution of 1-chloro-4-nitrobenzene (33.9 g, 215.5 mmol) in dimethylacetamide (115 mL) was charged drop-wise to the reaction. After addition of the 1-chloro-4-nitrobenzene, the resulting solution color changed from pale pink to dark brown. The reaction proceeded at 180 °C overnight to afford a heterogeneous dark brown solution.

Filtration of the heterogeneous solution through a fritted funnel equipped with a Celite cake (2.5 cm x 15 cm) resulted in a brown, transparent solution. Precipitation into 1.0 M NH_4OH aqueous solution afforded a fine, yellow precipitate. The yellow precipitate was filtered and washed until a filtrate pH of 7 was obtained, and then dried *in-vacuo* at 120 °C overnight. Recrystallization from ethyl acetate isolated the target compound in >90% overall yield. ^{1}H NMR: (Figure S-1) ^{13}C NMR: (Figure S-2)

Synthesis of tris((*p*-aminophenoxy)phenyl) ethane (TAPE). Tris((*p*-nitrophenoxy)phenyl) ethane (60 g, 89.6 mmol) and tetrahydrofuran (270 mL) were charged to a 3 L Parr reactor, and subsequently purged with nitrogen for 20 minutes. Next, 10 wt.% palladium over carbon (10 g) was added and the reactor sealed and purged with nitrogen for 20 minutes. Three successive cycles of pressurizing the reactor to 100 psi with hydrogen ensured saturation of the solution with hydrogen, and the reaction proceeded under 100 psi of hydrogen pressure. After 24 hours, the pressure was released and the black, heterogeneous solution recovered. Filtration of the heterogeneous solution through a fritted funnel equipped with a Celite cake (2.5 cm x 15 cm) resulted in a brown, transparent solution. Evaporation of the solvent afforded the target compound as a light brown powder. (98% yield) ^{1}H NMR: (Figure S-3) ^{13}C NMR: (Figure S-4)

Synthesis of long-chain branched poly(ether imide)s (LCB-PEI). The synthesis of a 45 kg/mol poly(ether imide) branched with 1 mol.% of TAPE follows as an example. TAPE (0.12 g, 0.34 mmol), *m*-phenylene diamine (5.52 g, 51.0 mmol), and *o*-dichlorobenzene (75 mL) were charged to a three-necked, 500-mL, round-bottomed flask. The flask was then equipped with a rubber septum, glass stir rod with Teflon blade, and Dean-Stark trap. A condenser completed the set up on the Dean-Stark trap, and the contents purged with nitrogen for 20 minutes. The round-bottomed flask was then heated to 100 °C to generate a homogeneous solution. Next, BPA-DA

(26.3 g, 50.6 mmol), phthalic anhydride (0.691 g, 4.6 mmol) and *o*-dichlorobenzene (25 mL) were added. The flask was then heated to 180 °C, where the reaction proceeded for 18 hours. Devolatilization of the solvent and thermal imidization was completed utilizing a melt kneader operating at 380 °C, resulting in an orange, transparent product.

7.4 Results and Discussion

The synthesis of a trisamine 1,1,1-tris((*p*-aminophenoxy)phenyl) ethane (TAPE) involved a two-step sequence. The first step utilized a nucleophilic aromatic substitution of 1-chloro-4-nitrobenzene with 1,1,1-tris(4-hydroxyphenyl) ethane. Potassium carbonate deprotonates the phenol to afford a phenoxide *in-situ* providing a sufficiently nucleophilic oxygen to displace the activated chloride. A polar aprotic solvent (e.g. dimethylacetamide) promotes the substitution, while an azeotroping agent (e.g. toluene) enables quantitative removal of water. Isolation of 1,1,1-tris((*p*-nitrophenoxy)phenyl) ethane (TNPE) required filtration through a Celite cake to remove insoluble salts formed during the reaction. Adjusting the pH to 10 with ammonium hydroxide reduces the solubility of the TNPE in water and enables direct precipitation into water to form a fluffy yellow product in quantitative yields. The monomer is further purified by recrystallization from ethyl acetate to afford the target compound in >90% yield. ^{1}H, ^{13}C nuclear magnetic resonance spectroscopy and mass spectroscopy confirmed the structure and purity.

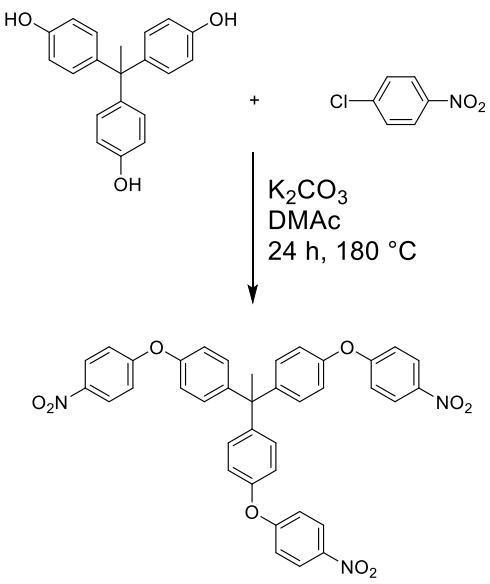

Scheme 1: Synthesis of tris((p-nitrophenoxy)phenyl) ethane (TNPE).

Reduction of TNPE to TAPE follows a typical high-pressure reduction using palladium as a catalyst. Palladium supported on carbon at 10 wt.% loading provided sufficient catalytic activity at 1 wt.% relative to TNPE. TNPE was dissolved in tetrahydrofuran at 20 wt.% solids and charged to a pressure-reactor. After purging with nitrogen, an appropriate amount of Pd/C was added to the pressure-reactor and pressurized to 100 psi with hydrogen. The reaction proceeded at room temperature for 24 h. After releasing the pressure, the reactor was purged with nitrogen and a black heterogeneous solution recovered. Filtration through a one-inch Celite cake removed the insoluble carbon and resulted in a pale yellow filtrate. Vacuum removal of the THF solvent resulted in TAPE as a light brown powder in quantitative yields. Again, ^{1}H, ^{13}C nuclear magnetic resonance spectroscopy and mass spectroscopy confirmed the structure and purity.

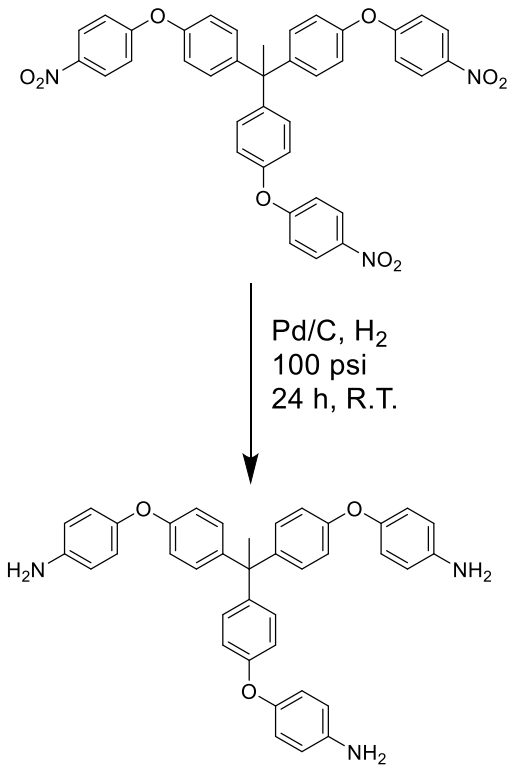

Scheme 2: Reduction of TNPE to tris((p-aminophenoxy)phenyl) ethane (TAPE).

Long-chain branched poly(ether imide)s (LCB-PEIs) followed similar protocol to commercial-scale poly(ether imide) synthesis. (Scheme 3) However, the solubility of TAPE in *o*-dichlorobenzene (*o*-DCB) is limited at room temperature. To circumvent concentration gradients in solution surrounding the dissolving TAPE particle, *m*-phenylene diamine and TAPE were dissolved in *o*-DCB at 100 °C to form a homogeneous solution. Addition of bisphenol-A dianhydride (BPA-DA) and phthalic anhydride followed dissolution of the amines. Immediately, the amic-acid intermediate formed indicated by a two-phase solution and a dramatic increase in viscosity. When the temperature reached 180 °C the viscosity decreased and the solution became homogeneous. After 18 h, the viscous solution was poured from the round-bottomed flask into aluminum trays. Removal of *o*-DCB and completion of imidization proceeded through devolatization at 380 °C under nitrogen.

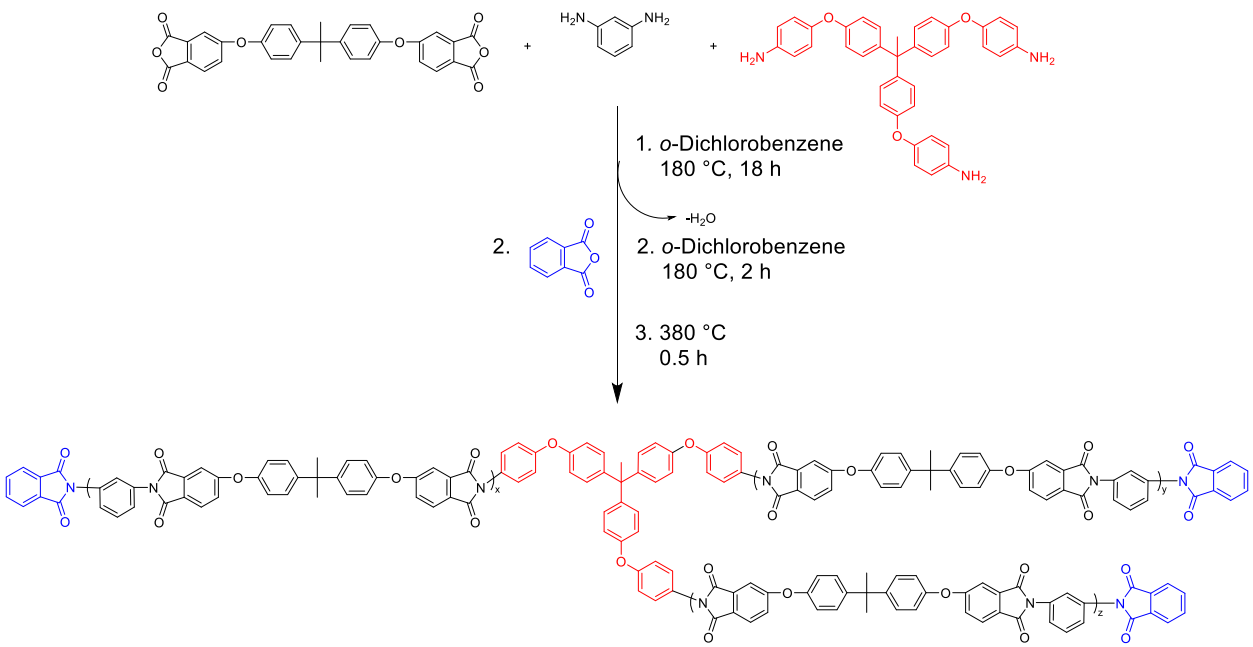

Scheme 3: Synthesis of long-chain branched poly(ether imide)s (LCB-PEIs) using thermal imidization.

Tables 1 and 2 identify the molecular weight and dispersity of a series of synthesized long-chain branched poly(ether imide)s (LCB-PEIs). Minimal changes in polydispersity is observed at incorporations below 1.0 mol%, but at relatively high incorporations of the trisamine the dispersity dramatically increases. Targeting weight-average molecular weights (M_w) enabled the direct correlation between TAPE concentration and dispersity. To help visualize, Figure 1 overlays the resulting molecular weight and distributions determined using a polystyrene calibration curve. With similar weight average molecular weights (M_w), increasing TAPE incorporation lends to a broadening of the distribution suggesting an increased concentration of higher and lower molecular weight chains.

Table 1: Weight-average molecular weight determined by SEC-MALLS in chloroform with dn/dc=0.271.

	TAPE (mol.%)	0	0.11	0.26	0.56	0.92	1.1	1.3	1.5	2	2.5	3
M_w (kg/mol)	M_w (kg/mol)[a]											
45		40.2	42.4	39.9	39.7	33.5	40.7	40.7	44.2	36.4	35.7	39.1
40		30.3	36.8	29.8	36.1	56.2	36.2	38.6	35.4	31.2	40.0	41.3
35		31.6	36.0	39.0	33.6	34.4	37.6	28.7	32.7	N/A	N/A	N/A
30		37.2	N/A	N/A	30.0	28.4	27.7	29.1	26.8	N/A	N/A	N/A

[a]Std. dev. = 5%

Table 2: Dispersity determined by SEC-MALLS in chloroform using dn/dc=0.271.

	TAPE (mol.%)	0	0.11	0.26	0.56	0.92	1.1	1.3	1.5	2	2.5	3
M_w (kg/mol)	Đ[a]											
45		2.41	1.55	1.89	1.99	1.64	2.10	2.04	1.97	4.50	2.50	2.88
40		1.67	2.11	1.76	1.82	2.01	1.82	1.96	2.19	3.72	2.95	2.61
35		2.26	1.54	2.53	2.00	1.75	1.95	1.62	1.93	N/A	N/A	N/A
30		2.06	N/A	N/A	1.79	2.10	2.33	2.67	2.27	N/A	N/A	N/A

[a]Std. dev. = 15%

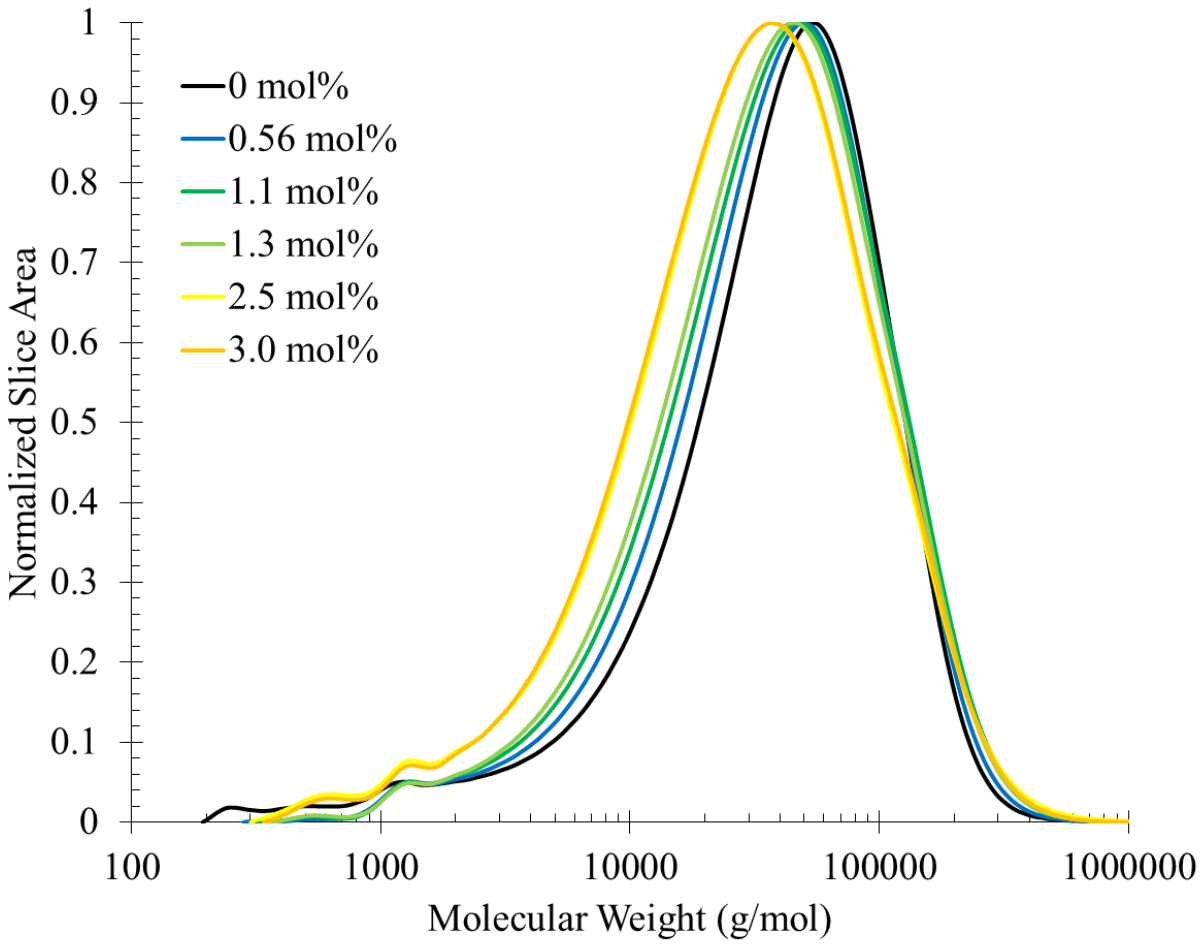

Figure 1. Representative molecular weight and distributions of similar M_w LCB-PEIs with increasing TAPE concentrations. Reference to a polystyrene-based calibration.

Coupling SEC molecular weight information with ^{1}H NMR spectroscopy enabled determination of average molecular weight of the branches (M_b, Figure 2). Comparing experimental result to theoretical predictions provides insight into the reactivity of the ideal case. At high incorporations of trisamine, large deviations between experimental data and theoretical predictions occur presumably a result of increased cyclization. Furthermore, the M_b in all cases remains greater than the molecular weight of entanglements (M_e) indicating that these long-chain branches are of significant length to entangle.

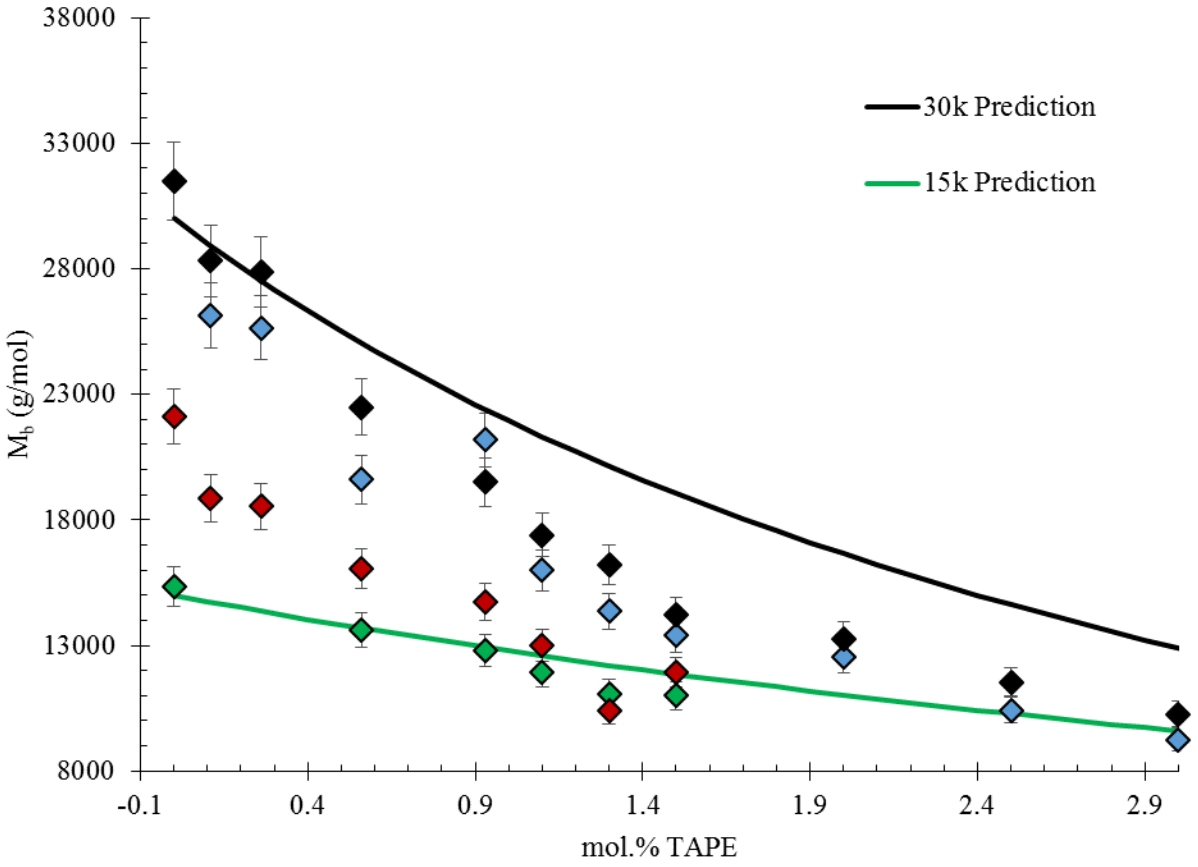

Figure 2: Average branch molecular weight (M_b) as a function of TAPE. Determined through SEC and ^{1}H NMR spectroscopy.

Differential scanning calorimetry (DSC) identified the thermal transitions of the LCB-PEIs. The observation of a glass transition temperature (T_g) near 215 °C correlates well linear PEI controls (Table 3). Increasing the amount of branching agent does not significantly affect the onset of segmental motion. The relatively low concentration of long-chain branches (M_b >> M_e) does not significantly promote or retard the onset of segmental motion, and allows for utility of these branched materials in typical PEI applications. However, introduction of the long-chain branches greatly affect the rheological properties.

Table 3: Glass transition temperatures (T_g) determined from DSC.

	TAPE (mol.%)	0	0.11	0.26	0.56	0.92	1.1	1.3	1.5	2	2.5	3
M_w (kg/mol)	T_g (°C)											
45		214	215	213	214	214	213	210	216	209	209	207
40		212	214	212	220	214	210	212	210	212	207	213
35		212	212	211	214	212	210	210	210	N/A	N/A	N/A
30		212	N/A	N/A	212	212	210	208	208	N/A	N/A	N/A

Measurement of the viscosity as a function of angular frequency provides insight into the processability of the LCB-PEIs as compared to the linear analogue. Importantly, comparing samples with molecular weights within SEC-instrumental error helps to isolate long-chain branching effects from molecular weight effects. Figure 3 highlights the viscosity profiles of LCB-PEIs with various branching densities. Across the relevant processing window of 0.1 to 100 rad/s, the PEIs with high incorporation percentages of branching agent (≥2.0 mol.%) provide significant reductions in the melt viscosity. It is suspected that the length and the dispersity of polymer chains and branches play an instrumental role in this observation. As noted above, the dispersity of the polymer increases dramatically at the higher incorporations of TAPE. As a result, the lower molecular weight chains and branches help to plasticize the melt and reduce the overall viscosity. In contrast, the lower incorporations of TAPE increase the melt viscosity over the linear analogue. The M_b at these incorporations are relatively long and their distribution do not involve molecular weights that plasticize the melt.

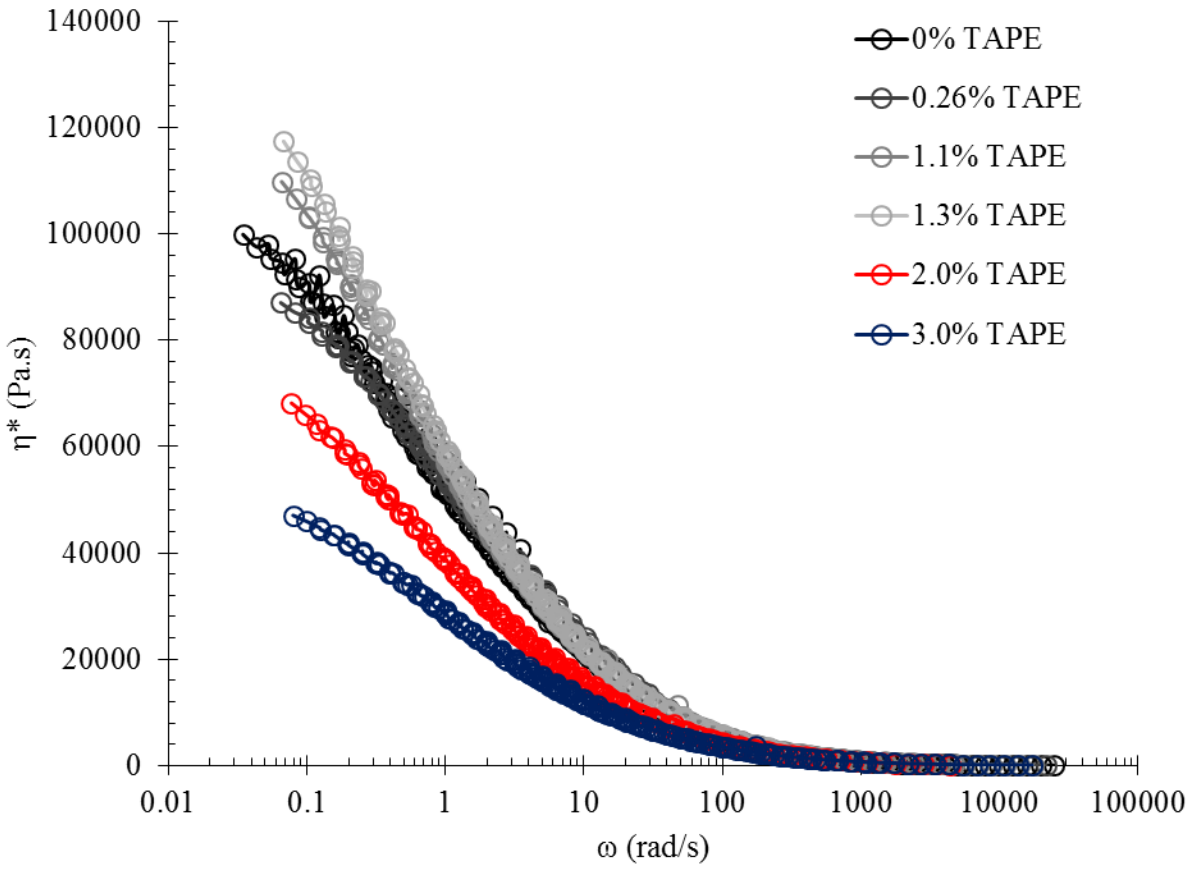

Figure 3: Correlation between viscosity and shear rate at various incorporations of TAPE. M_w = 40,000 ± 1000 g/mol. T_r = 300 °C.

Figure 4 provides flow activation energy (E_a) as a function of TAPE incorporation. Following a similar trend as observed in the viscosity, more energy is required for flow upon incorporation of TAPE. Introducing more TAPE reduces M_b and the energy required for flow decreases. At 3.0 mol.% TAPE, E_a approaches a linear analogue of similar molecular weight. Assuming a constant molecular weight of entanglement (M_e = 3500 g/mol) for LCB-PEIs, the number of entanglements per branch dramatically decrease with TAPE incorporation leading to a less frustrated chain reptation. As a result, reductions in the melt viscosity of these PEIs requires relatively high incorporation of TAPE, and is much higher than polymers that are more flexible.

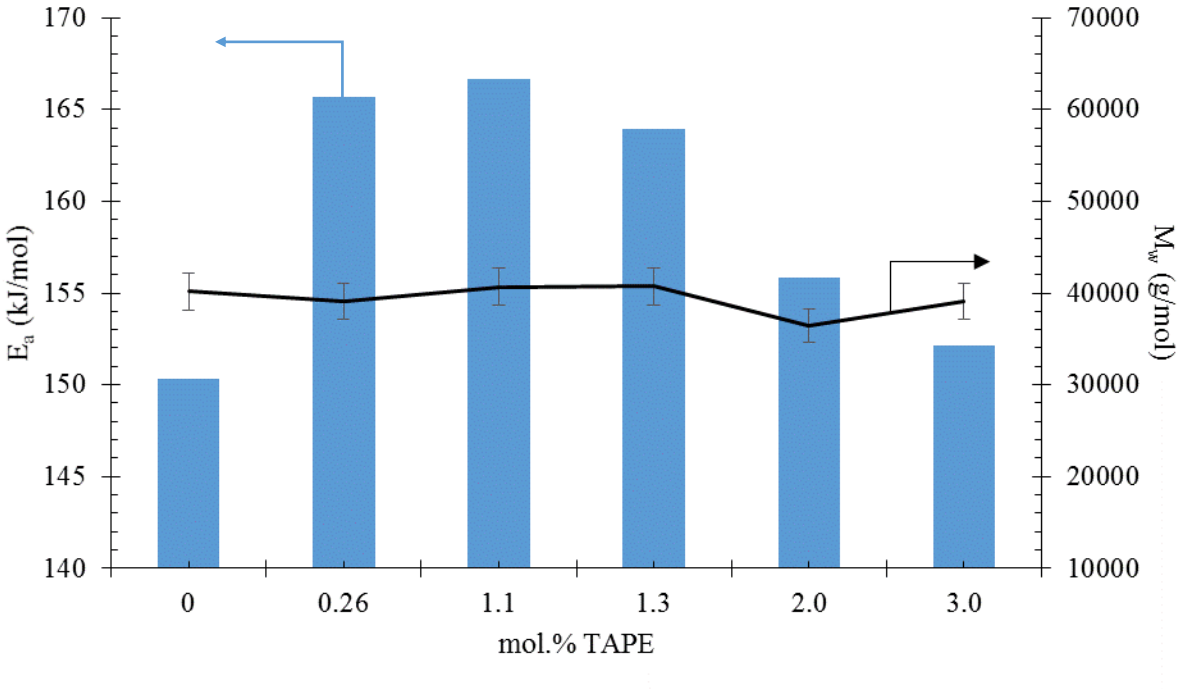

Figure 4: Effect of TAPE incorporation on flow activation energy (E_a) at similar molecular weights.

Mechanical testing following ASTM standard D638 methods provided tensile properties for the LCB-PEIs. As a result of the large quantities of material required to injection mold dog bone specimens, selected compositions with 0.3 and 1.5 mol.% TAPE were targeted with a molecular weight of 33,000 g/mol. Importantly, the robust synthesis of TAPE described here enabled direct scale up to 0.5 kg of trifunctional monomer for pilot-scale, batch reactions of LCB-PEIs. Producing several kilograms of LCB-PEIs, duplicate runs of each composition demonstrated reproducibility in mechanical properties and reaction conditions. Table S1 summarizes the resulting tensile properties of the injection molded dog bone specimens. Minimal changes in Young's moduli and yield strength suggest little influence of branching on tensile properties.

7.5 Conclusion

The synthesis of a novel aromatic trisamine (TAPE) utilized a nucleophilic aromatic substitution and subsequent nitro reduction to achieve quantitative yields in high purity. Incorporation of TAPE into poly(ether imide)s in low concentrations under commercially viable polymerization conditions generated high molecular weight, long-chain branched PEIs. Combination of ^{1}H NMR spectroscopy and SEC enabled the determination of average branch length (M_b) as a function of TAPE incorporation. Furthermore, SEC confirmed targeted molecular weights with increasing dispersity with increased branching. Although DSC highlighted minimal changes in the T_g, rheological analysis elucidated a critical influence of branch length on melt viscosity. Increasing TAPE incorporation reduced the average branch length and the number of entanglements per branch, and resulted in a reduction in the melt viscosity. Finally, minimal changes in the tensile properties of injection-molded specimens highlight the utility of long-chain branching in PEIs to improve melt flow properties while maintaining desired mechanical strength.

7.6 References

1. Mannion, A. M.; Bates, F. S.; Macosko, C. W. Synthesis and Rheology of Branched Multiblock Polymers Based on Polylactide, *Macromolecules* **2016,** 49, (12), 4587-4598.
2. Meissner, J. Basic parameters, melt rheology, processing and end-use properties of three similar low density polyethylene samples, *Pure and Applied Chemistry* **1975,** 42, (4), 551.
3. Hadjichristidis, N.; Xenidou, M.; Iatrou, H.; Pitsikalis, M.; Poulos, Y.; Avgeropoulos, A.; Sioula, S.; Paraskeva, S.; Velis, G.; Lohse, D. J.; Schulz, D. N.; Fetters, L. J.; Wright, P. J.; Mendelson, R. A.; García-Franco, C. A.; Sun, T.; Ruff, C. J. Well-Defined, Model Long

Chain Branched Polyethylene. 1. Synthesis and Characterization, *Macromolecules* **2000,** 33, (7), 2424-2436.

4. Lohse, D. J.; Milner, S. T.; Fetters, L. J.; Xenidou, M.; Hadjichristidis, N.; Mendelson, R. A.; García-Franco, C. A.; Lyon, M. K. Well-Defined, Model Long Chain Branched Polyethylene. 2. Melt Rheological Behavior, *Macromolecules* **2002,** 35, (8), 3066-3075.
5. Kaspar, H.; Hintzer, K. The extensional viscosity properties of long-chain branched fluorothermoplastics and correlations to molecular structure, *Rheologica Acta* **2011,** 50, (5), 577.
6. Jeong, S. H.; Kim, J. M.; Yoon, J.; Tzoumanekas, C.; Kroger, M.; Baig, C. Influence of molecular architecture on the entanglement network: topological analysis of linear, long- and short-chain branched polyethylene melts via Monte Carlo simulations, *Soft Matter* **2016,** 12, (16), 3770-3786.
7. Santamaria, A. Influence of long chain branching in melt rheology and processing of low density polyethylene, *Materials Chemistry and Physics* **1985,** 12, (1), 1-28.
8. Billmeyer, F. W. The Molecular Structure of Polyethylene. III. Determination of Long Chain Branching1, *J. Amer. Chem. Soc.* **1953,** 75, (24), 6118-6122.
9. Otocka, E. P.; Roe, R. J.; Hellman, M. Y.; Muglia, P. M. Distribution of Long and Short Branches in Low-Density Polyethylenes, *Macromolecules* **1971,** 4, (4), 507-512.
10. Bovey, F. A.; Schilling, F. C.; McCrackin, F. L.; Wagner, H. L. Short-Chain and Long-Chain Branching in Low-Density Polyethylene, *Macromolecules* **1976,** 9, (1), 76-80.
11. Bueche, F. Viscosity of Molten Branched Polymers and Their Concentrated Solutions, *The Journal of Chemical Physics* **1964,** 40, (2), 484-487.

12. Chartoff, R. P.; Maxwell, B. Viscoelastic properties of branched polyethylene melts, *Journal of Polymer Science Part A-2: Polymer Physics* **1970,** 8, (3), 455-465.
13. Wild, L.; Ranganath, R.; Knobeloch, D. C. Influence of long-chain branching on the viscoelastic properties of low-density polyethylenes, *Polym. Eng. Sci.* **1976,** 16, (12), 811-816.
14. McKee, M. G.; Unal, S.; Wilkes, G. L.; Long, T. E. Branched polyesters: recent advances in synthesis and performance, *Prog. Polym. Sci.* **2005,** 30, (5), 507-539.
15. Munari, A.; Pezzin, G.; Pilati, F.; Manaresi, P. Rheological characterization of highly branched poly(ethyleneterephthalate), *Rheologica Acta* **1989,** 28, (1), 25-29.
16. Manaresi, P.; Munari, A.; Pilati, F.; Alfonso, G. C.; Russo, S.; Sartirana, M. L. Synthesis and characterization of highly-branched poly(ethylene terephthalate), *Polymer* **1986,** 27, (6), 955-960.
17. Jayakannan, M.; Ramakrishnan, S. Effect of branching on the crystallization kinetics of poly(ethylene terephthalate), *J. Appl. Polym. Sci.* **1999,** 74, (1), 59-66.
18. Rosu, R. F.; Shanks, R. A.; Bhattacharya, S. N. Synthesis and Characterisation of Branched Poly(ethylene terephthalate), *Polym. Int.* **1997,** 42, (3), 267-275.
19. Jabarin, S. A. Crystallization kinetics of polyethylene terephthalate. II. Dynamic crystallization of PET, *J. Appl. Polym. Sci.* **1987,** 34, (1), 97-102.
20. Tan, L. S.; Wang, D. H. Multifunctional crosslinkers for shape-memory polyimides, polyamides and poly(amide-imides) and methods of making the same. 2013.
21. Chen, Y.; Zhang, Q.; Sun, W.; Lei, X.; Yao, P. Synthesis and gas permeation properties of hyperbranched polyimides membranes from a novel (A2+B2B′+B2)-type method, *Journal of Membrane Science* **2014,** 450, 138-146.

22. Fang, J.; Kita, H.; Okamoto, K.-i. Gas permeation properties of hyperbranched polyimide membranes, *Journal of Membrane Science* **2001,** 182, (1–2), 245-256.
23. Fang, J.; Kita, H.; Okamoto, K.-i. Hyperbranched Polyimides for Gas Separation Applications. 1. Synthesis and Characterization, *Macromolecules* **2000,** 33, (13), 4639-4646.
24. Herrmann-Schönherr, O.; Schneller, A.; Seifert, A. M.; Soliman, M.; Wendorff, J. H. Chain dimensions, entanglement molecular weights and molecular weight distributions of poly(aryl ethers). A combined rheological and MNDO analysis, *Makromolekul. Chem.* **1992,** 193, (8), 1955-1974.

7.7 Supporting Information

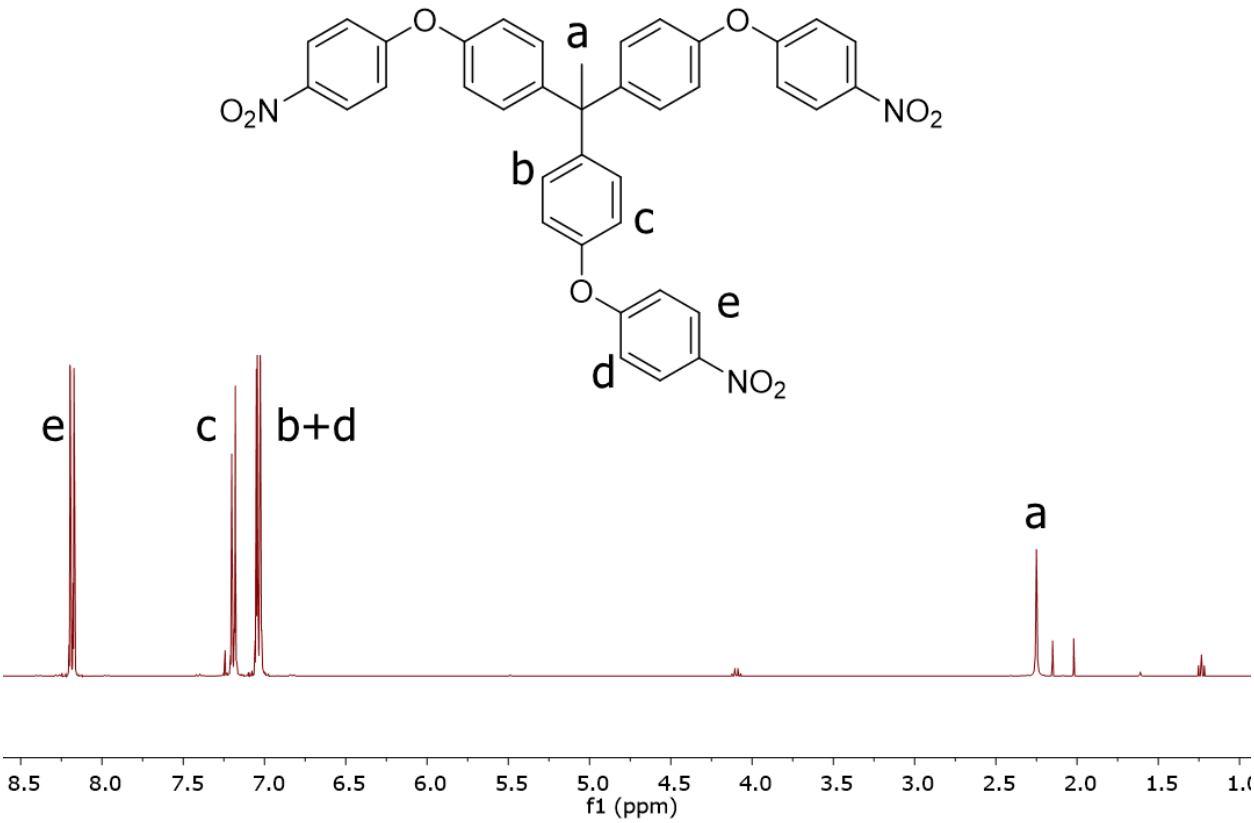

Figure S1: ^{1}H NMR spectroscopy of tris((p-nitrophenoxy)phenyl) ethane.

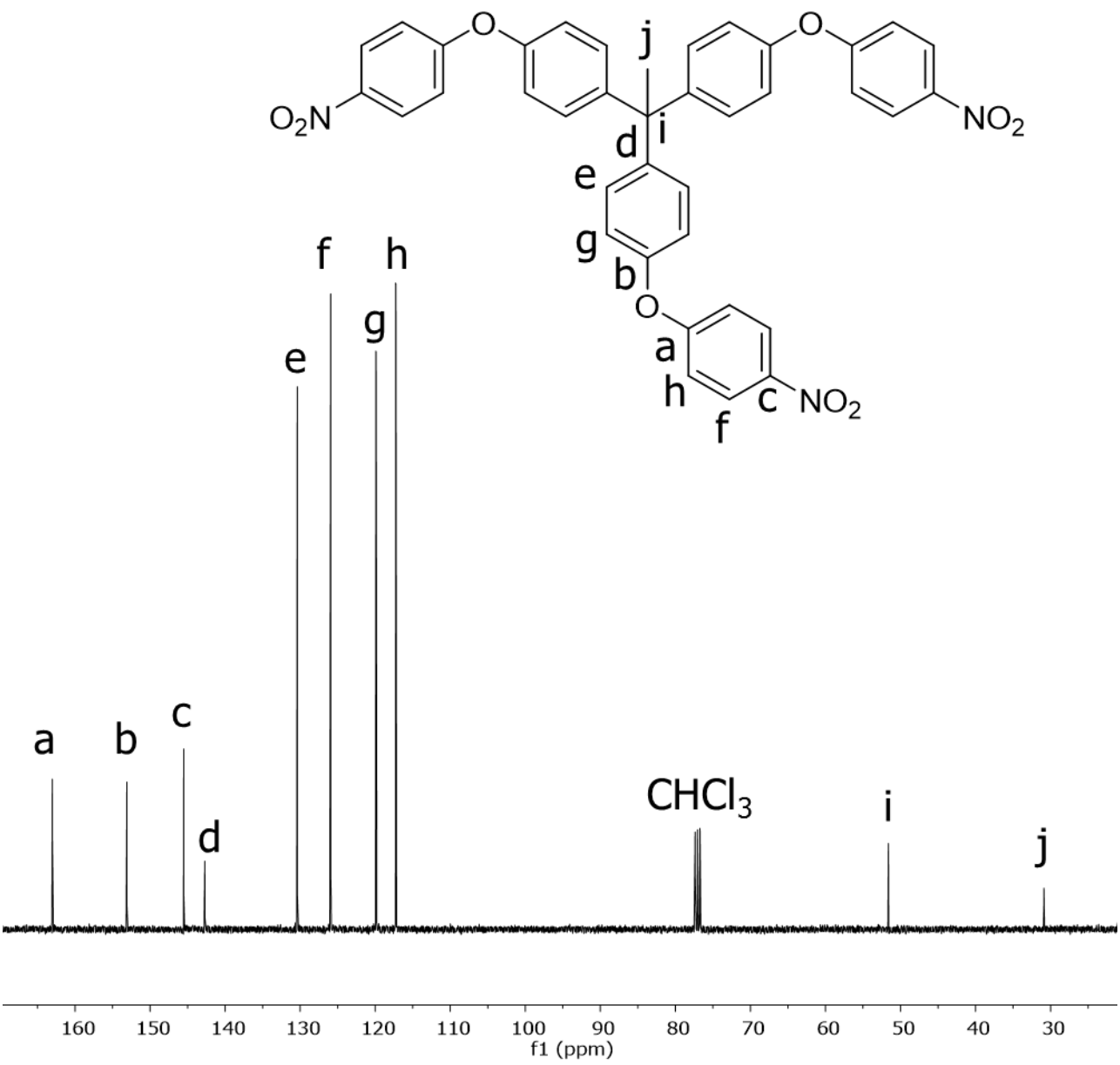

Figure S2: ^{13}C NMR spectroscopy of tris((p-nitrophenoxy)phenyl) ethane.

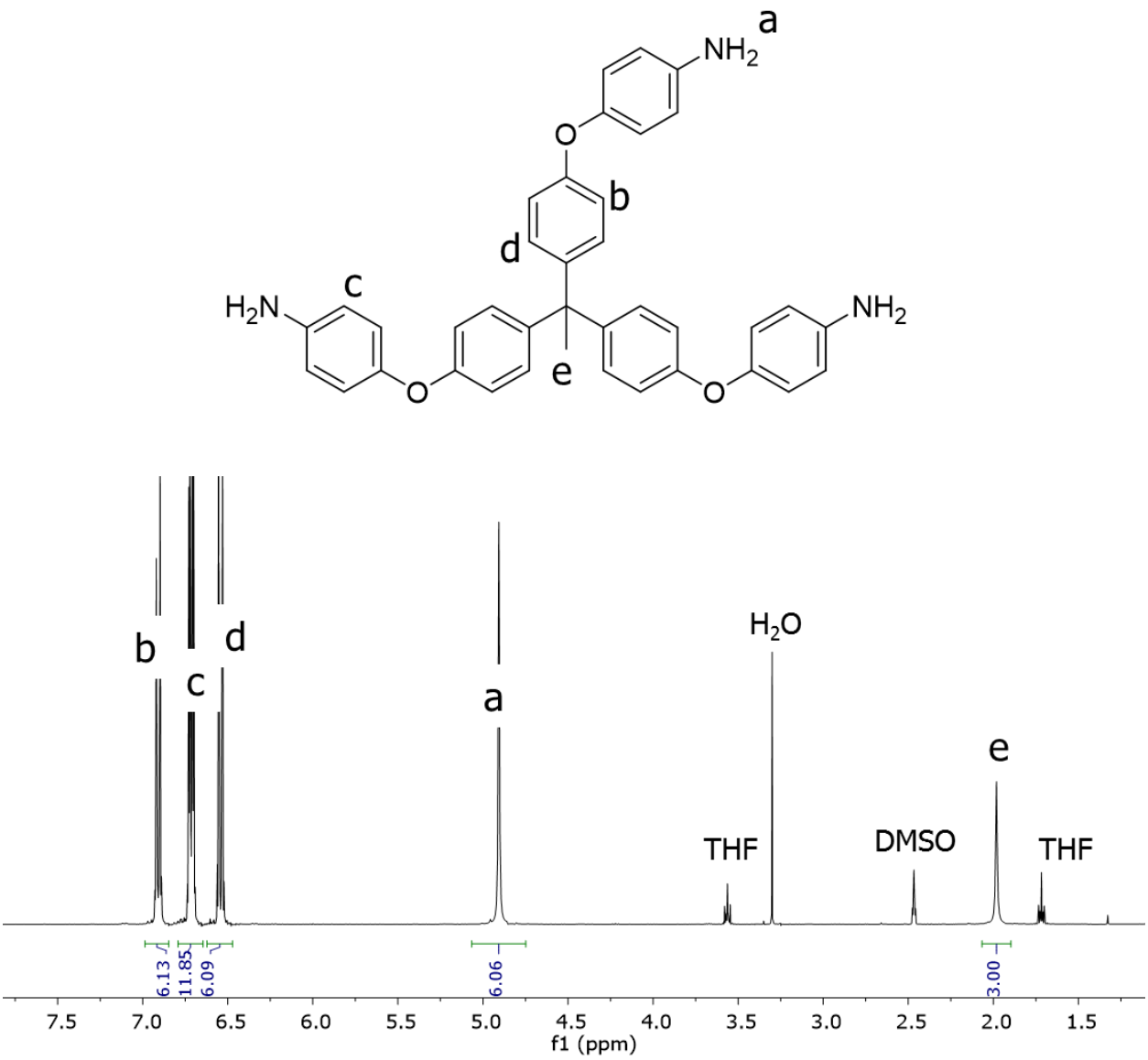

Figure S3: ^{1}H NMR spectroscopy of tris((p-aminophenoxy)phenyl) ethane (TAPE).

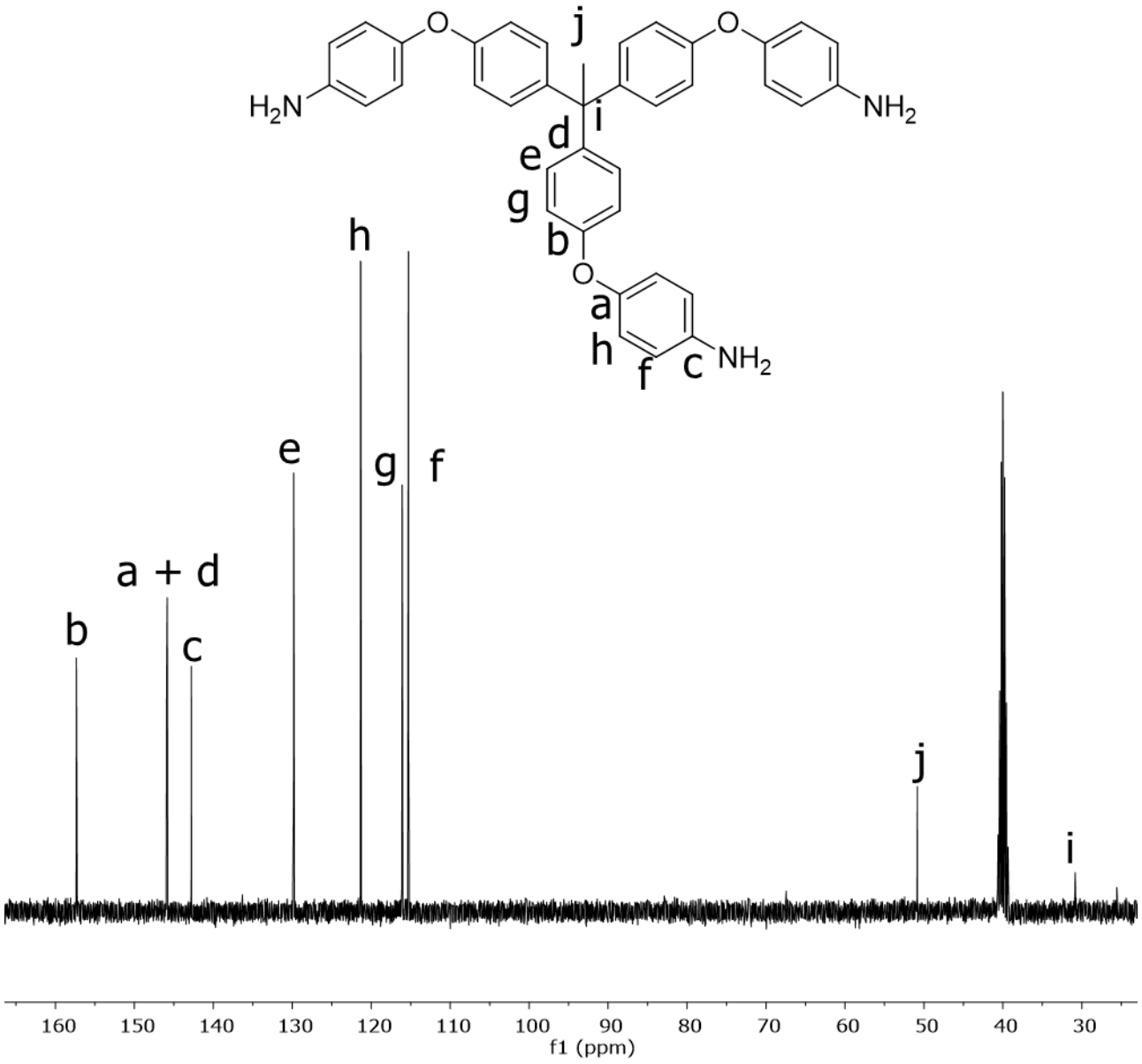

Figure S4: ^{13}C NMR spectroscopy of tris((p-aminophenoxy)phenyl) ethane.

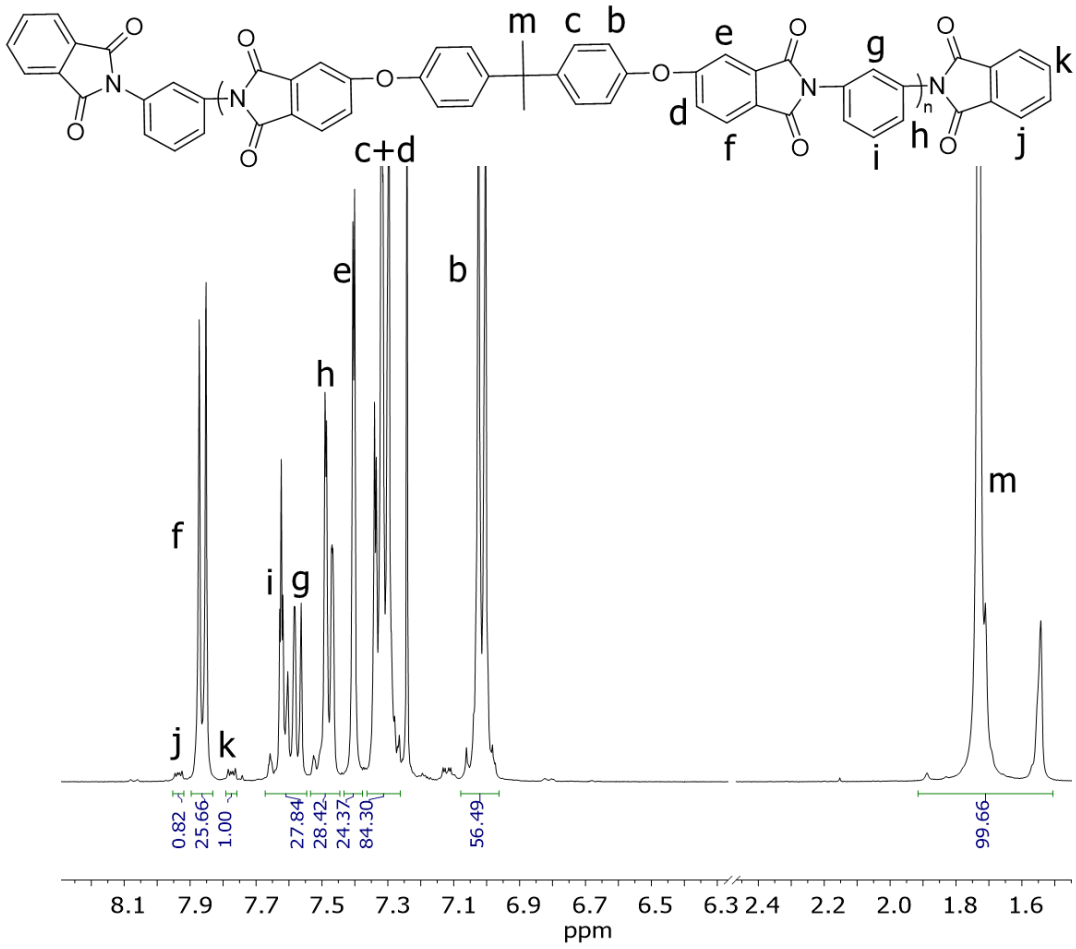

Figure S5: ^{1}H NMR spectroscopy of linear poly(ether imide) with endgroup protons indicated.

Table S6: Summary of tensile properties of LCB-PEIs following ASTM D638.

		33k PEI Linear	38k PEI Linear	33K PEI 0.3 mol.% TAPE		33K PEI 1.5 mol.% TAPE	
TENSILE ASTM				Run 1	Run 2	Run 1	Run 2
Modulus of Elasticity-Avg	MPa	3380	3382	3366	3390	3364	3396
Tensile Strength at Yield-Avg	MPa	116	117	117	117	117	117
Tensile Strength at Break-Avg	MPa	90	88	95	96	92	106
%Elongation at Yield-Avg	%	7.20	7.08	7.02	7.00	7.00	7.04
%Elongation at Break-Avg	%	95	72	11	12	12	9
Nominal Strain at Break-Avg	%	48	37	8	8	8	7
Modulus of Elasticity-Std	MPa	16	33	23	19	27	9
Tensile Strength at Yield-Std	MPa	0.5	0.0	0.0	0.0	0.0	0.0
Tensile Strength at Break-Std	MPa	1	2	10	10	10	7
%Elongation at Yield-Std	%	0.01	0.03	0.01	0.02	0.01	0.02
%Elongation at Break-Std	%	12	30	5	2	2	3
Nominal Strain at Break-Std	%	7	15	2	1	1	2

Chapter 8: Synthesis and Characterization of Isocyanate-free Polyureas

(In preparation, targeting *Green Chemistry*)

Joseph M. Dennis[1], Limor I. Steinberg[1], Allison M. Pekkanen[1], Jon Maiz[2], Maruti Hegde[1], Alejandro J. Muller[2] and Timothy E. Long[1*]

[1]*Virginia Tech, Department of Chemistry, Macromolecules Innovation Institute (MII)*

Blacksburg, Virginia 24061 USA

[2]*Polymat and Polymer Science and Technology Department, University of the Basque Country*

UPV/EHU, Paseo Manuel de Lardizábal 3, 20018 Donostia-San Sebastián, Spain

8.1 Abstract

With increased health and safety concerns surrounding isocyanates, alternative synthetic routes to obtain urea-containing polymers is gaining much attention. Melt polycondensation of urea with diamines achieved polyureas without catalyst or solvents. ^{1}H NMR spectroscopy and thermal gravimetric analysis confirmed targeted compositions and thermal degradation, respectively. Differential scanning calorimetry and dynamic mechanical analysis provided insight into the copolymers thermal behavior. A steady increase in the melting temperature across the range of compositions suggested a co-crystallization of the different repeating units, which contrasted behavior of non-hydrogen bonded copolymers. Furthermore, the wide range of T_ms and mechanical performance illustrated the applicability of these copolymers in high performance applications. Finally, initial biodegradation studies using a naturally occurring, soil enzyme (urease) demonstrated steady degradation over 4 weeks, during which the release of ammonia provided a nitrogen source for potential plant uptake.

8.2 Introduction

Polyureas are a unique class of polymers that have found utility in a wide array of applications from protective coatings[1, 2] to foams and biomedical implants[3, 4]. The high propensity for hydrogen bonding and semicrystallinity provides advantageous solvent resistance, while their relatively high melting points (T_ms) garner attention as thermally resilient thermoplastics.[1-7] Furthermore, the myriad of synthetic avenues developed to generate the urea motif from urea[3, 4, 8], isocyanates[9, 10], phosgene[11], and carbon dioxide[2] highlights a small portion of the historical precedence of these materials.

The typical synthesis of polyurea utilizes the quantitative reaction between a diamine and a diisocyanate.[9, 10, 12] The combination of small and low-T_g, oligomeric diamines with diisocyanates results in thermoplastic elastomers with high extensibility and low hysteresis.[9, 10, 12] However, the use of toxic and highly reactive isocyanates poses many health and environmental concerns.[13] Recently, advances in the sequestering of carbon dioxide provides an exciting avenue for biorenewable feedstocks. Direct incorporation of CO_2 into polyureas with diamines illustrates a promising route to generate polyureas from inexpensive raw materials.[2] However, the low polymer yields, high pressures, and exotic solvent requirements hinders wide application, and limits favorable environmental impact. Another technique to synthesize polyureas includes microwave irradiation.[5, 14, 15] However, the necessity of high boiling point solvents (e.g. dimethylacetamide or *o*-dichlorobenzene) raises health and environmental concerns.[5, 14]

In addition to greener feedstocks and synthetic avenues, investigation into the biodegradation of polymeric materials continues to grow rapidly.[16, 17] As a result of the established biodegradability of urea[18, 19] and ester[20] moieties, many poly(urea ester)s provide

advantageous mechanical durability while maintaining biodegradability.[3, 4] Although the bulk polycondensation of urea-containing diols with aliphatic diacids generates the polymer, the synthesis of urea-containing diols requires several steps.[3, 4] Interestingly, the bulk polycondensation of diamines with urea has received minimal attention.[6-8, 21-23] Leibler *et al.* utilized the reaction of highly branched, oligoamines with urea to afford self-healing rubber networks.[8] The remaining literature resides in patents.[6, 7, 21-23]

Herein we report the direct polycondensation of two diamines with urea to afford high molecular weight, linear polyureas. Use of an inexpensive, biological feedstock and solvent free conditions provides an industrially relevant and environmentally benign synthesis for a novel family of polyureas. Furthermore, the elimination of solvents, isocyanates and inherent biodegradability enables a robust platform to generate a library of materials with tailored properties and degradation.

8.3 Experimental

Materials. Urea (BioReagent), and 2,2-(ethylenedioxy)bis(ethylamine) (98%) were purchased from Sigma Aldrich and used as received. 1,8-diaminooctane (98%) was purchased from Sigma Aldrich and distilled under vacuum at 140 °C. Urease from Canavalia ensiformis (Jack Bean) Type III (15,000-30,000 U/g) was purchased from Sigma Aldrich. Phosphate buffered saline (PBS) was purchased from Life Technologies. An ammonia assay kit was purchased from Sigma Aldrich. The urease activity kit was purchased from Sigma Aldrich. All deuterated solvents were purchased from Cambridge Isotope Laboratories, Inc.

Analytical Methods. ^{1}H NMR spectroscopy utilized a Varian Unity 400 spectrometer operating at 399.87 MHz and 23 °C with a 0.1 M LiBr salt solution in DMSO-d_6 at approximately 8 mg/mL. Utilizing a TA Instruments TGA Q500 from room temperature to 600 °C at a heating

rate of 10 °C/min under constant N_2 purge provided thermogravimetric analysis (TGA). Differential scanning calorimetry (DSC) probed thermal transitions with a TA Instruments DSC Q2000 operating under a N_2 atmosphere and heat/cool/heat cycles of 10 °C/min, 100 °C/min, and 10 °C/min, respectively. Dynamic mechanical analysis (DMA) revealed thermomechanical behavior using a TA Instruments DMA Q800 in oscillatory tension mode at 1 Hz and 3 °C/min. Polyureas were dried at 120 °C under vacuum prior to melt processing. Compression molding between Kapton® sheets at 270 °C with a PHI hydraulic press generated free-standing films, which were cooled in air over 1 hour.

Synthesis of Poly(octamethylene urea)-*co*-Poly(di(ethylene oxide) ethylene urea)s [Poly(OMU)-*co*-Poly(DEOEU)s]. The synthesis of biosourced, isocyanate-free polyureas utilized a facile melt transamidification process, and the synthesis of poly(OMU)$_{50}$-*co*-poly(DEOEU)$_{50}$ follows as an example. Urea (4.805 g, 0.08 mol), 1,8-diaminooctane (8.656 g, 0.06 mol), and 2,2-(ethylenedioxy)bis(ethylamine) (8.892 g, 0.06 mol) were charged to a 100-mL, single-necked, round-bottomed flask. The flask was equipped with a nitrogen inlet, overhead metal stir rod, and condensing tube with collection flask. Subsequent vacuum and N_2 purge cycles (3x) ensured removal of oxygen to provide an inert atmosphere for polymerization. Under a constant N_2 flow (*circa* 10 mL/min), the contents were heated to 170 °C and held for 1 h. Immediately, ammonia gas was observed during the first 30 min, and condensation of ammonia in a dry ice cooled flask provided insight into reaction progress. After 1 h, the temperature was increased step-wise from 200 °C to 250 °C over 1.5 h. Application of vacuum at 250 °C removed any residual ammonia and enabled the distillation of excess diamines generated through transamidification. The reaction continued for 2 h at 250 °C under vacuum

with dramatic increases in melt viscosity observed for all compositions. The polymer was isolated directly and used without further purification.

Ammonia Release Assay. A 500 U/mL solution of urease in phosphate buffered saline was prepared for all ammonia release experiments. Sections of polymer film were placed in the bottom of a 2-dram vial, onto which urease solution or phosphate buffered saline were placed. 20 U of urease per mg of sample were added, and additional phosphate buffered saline was added to maintain similar hydrostatic pressure (2 mL) between all samples. Ammonia release was analyzed each week at 25 °C over a four week period according to manufacturer's protocol. Briefly, 100 μL of sample was placed into 1 mL ammonia assay reagent in a disposable, small volume cuvette. The absorbance at 340 nm was analyzed on a SpectraMax M2 plate reader in absorbance mode. A blank of 100 μL of water in ammonia assay reagent was read for a control sample. L-Glutamate dehydrogenase was added to each cuvette and allowed to react for 5 min. Finally, the solution was mixed and absorbance at 340 nm analyzed. Calculations to determine ammonia concentration were conducted according to manufacturer's protocol. Following the assay each week, fresh solutions containing urease and phosphate buffered saline were added to each film.

Statistical Analysis. A multiple linear regression fit was performed on ammonia release as a function of composition and time through analysis of variance (ANOVA) in JMP software. Following ANOVA, a Tukey's HSD test determined statistical differences between groups. For percent remaining polymer and total released ammonia, an ANOVA test followed by a Tukey's HSD determined statistical significance between groups.

8.4 Results and Discussion

Previous reports for polyurea synthesis utilized diamines with diisocyanates to generate the urea linkage.[9, 10] Although quantitative and well established, the high reactivity of the diisocyanates introduces many hazards.[13] Furthermore, the hydrogen-bonding motif of the symmetric urea lends to poor solubility in many common organic solvents restricting the length of the urea segment in segmented block copolymers.[12] To circumvent these concerns, melt polycondensation provided a facile approach to the synthesis of polyureas using a biosourced monomer and solvent-free conditions (Scheme 1).

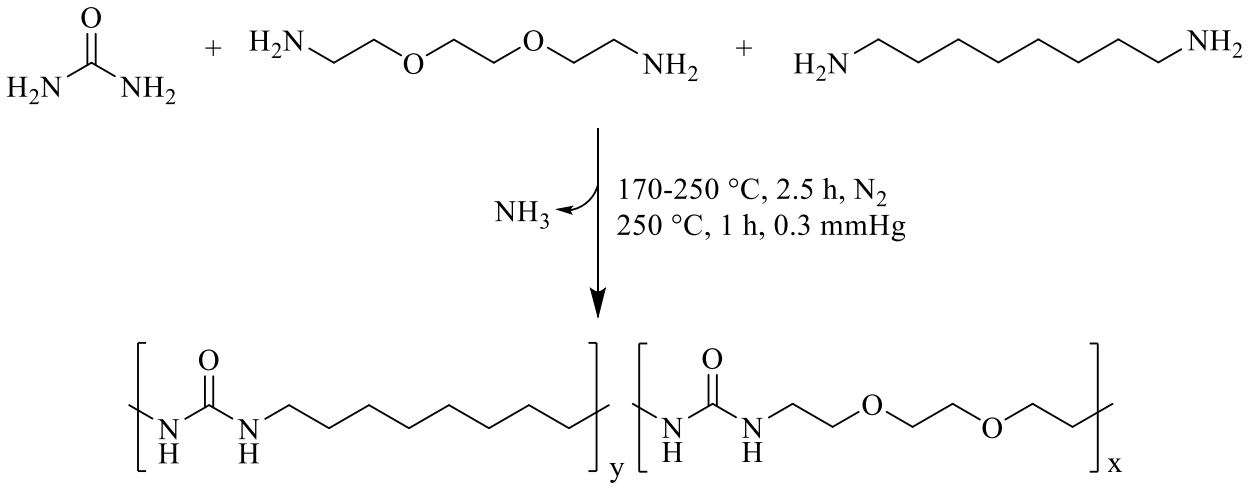

Scheme 1. Synthesis of biosourced, isocyanate-free poly(octamethylene urea)-co-poly(di(ethylene oxide) ethylene urea) [poly(OMU)-co-poly(DEOEU)] utilizing melt polycondensation.

Similar to a poly(ethylene terephthalate) polymerization, heating the small-molecule diamines with urea to 170 °C afforded a homogeneous melt. Ammonia gas evolution from the reaction flask provided a visual aid to the reaction progress, and determined reaction temperatures and times. After 1 h, the rate of ammonia generation slowed and the melt viscosity increased significantly. Increasing the reaction temperature to 250 °C reduced the melt viscosity

and ensured higher conversions before reducing the pressure. In the final stage of the reaction, vacuum at elevated temperatures enabled the distillation of the excess diamines, and drove the reaction to high conversions and high molecular weights. The reaction proceeded until the melt viscosity remained stable. At this point, the high melt viscosity prevented stirring, and indicated high molecular weight formation. Aggregation, determined through dynamic light scattering, in most organic solvents prevented molecular weight determination using size exclusion chromatography.

Detailed evaluations of the reaction mechanism for alkyl substitutions on urea using amines are well understood.[8, 24, 25] In summary, the reaction proceeds through an initial decomposition of urea into ammonia and isocyanic acid which react with an amine to produce a monosubstituted alkyl urea. Further elimination of ammonia from the alkyl urea and subsequent reactions with another amine provides the disubstituted alkyl urea. Although several side reactions are possible, at elevated temperatures (>170 °C) the primary substitution results in the 1,1-dialkyl urea and produces linear polyureas.[24]

^{1}H NMR spectroscopy in a 0.1 M LiBr DMSO-d_6 solution probed polymer compositions for the copolymers (Table 1). Unique chemical shifts for the methyl protons adjacent to the urea illustrated a retention of targeted compositions, and the compositional variation permitted the derivation of structure-property relationships for these novel polyureas. Thermal gravimetric analysis (TGA) demonstrated high thermal decomposition temperatures (*circa* 320 °C) with a minimal weight loss of < 1% near 100 °C attributed to absorbed water loss. To further probe the water absorption rate, thermal gravimetric analysis coupled with sorption analysis (TGA-SA) identified a similar water sorption profile for representative compositions (Figure S1). As a

result, melt processing required a drying procedure to minimize bubbles in the compression-molded films.

Table 1. Summary of composition, $T_{d,5\%}$ and thermal transitions from ^{1}H NMR spectroscopy, TGA, DSC and DMA, respectively.

	^{1}H NMR		TGA	DSC[a]				DMA[e]	
	EBA (mol %)	DAO (mol %)	$T_{d,5\%}$ (°C)	T_g[b] (°C)	T_c[c] (°C)	T_m[c] (°C)	ΔH_m[d] (J/mol)	T_g[f] (°C)	T_f[g] (°C)
Poly(DEOEU)	100	0	325	23	107	132	4.7	-1.9	125
Poly(OMU)$_{22}$-*co*-Poly(DEOEU)$_{78}$	78	22	314	26	74	147	16	16.9	133
Poly(OMU)$_{43}$-*co*-Poly(DEOEU)$_{57}$	57	43	306	39	N/A	190	36	25.2	170
Poly(OMU)$_{51}$-*co*-Poly(DEOEU)$_{49}$	51	49	319	38	N/A	210	48	26.4	199
Poly(OMU)$_{57}$-*co*-Poly(DEOEU)$_{43}$	43	57	326	48	N/A	224	61	37.9	210
Poly(OMU)$_{78}$-*co*-Poly(DEOEU)$_{22}$	22	78	325	39	N/A	242	76	51.3	230
Poly(OMU)	0	100	326	N/A	N/A	250	56	N/A	N/A

[a]Heat/cool/heat thermal cycles of 10, 100, 10 °C/min, values determined from second heat.
[b]T_g reported as the inflection point.
[c]T_c and T_m are measured as the peak temperature in the exotherm and endotherm, respectively.
[d] ΔH_m determined as area under the endothermic event.
[e]Heat rate of 3 °C/min, 1 Hz
[f] T_g reported as peak temperature from tan δ
[d]T_f reported as highest temperature before failure

Differential scanning calorimetry (DSC) provided insight into the thermal transitions of the polyurea copolymers (Figure 1). Interestingly, all compositions exhibited a melting transition, with a systematic increase in melt temperature (T_m) and melt enthalpy (ΔH_m) with 1,8-diaminooctane incorporation. This is in contrast to non-hydrogen bonded, semicrystalline copolymers in which the T_m decreased with comonomer incorporation.[26, 27] Incorporation of up to 43 mol.% OMU caused an increase and broadening in T_g. Further increasing OMU content suppressed the T_g's endothermic event suggesting the existence of a rigid amorphous phase.[28, 29]

Furthermore, the hysteresis (or enthalpic relaxation) in the T_g at 0 and 22 mol.% OMU suggested a lack of a thermodynamic equilibrium within the polymer chains, presumably from the electronegative oxygen atoms in the DEOEU segment influencing polymer chain packing.[30, 31] The hysteresis peak, low T_g and minimal ΔH_m obtained for the high DEOEU containing polyureas strongly suggested that an 'equilibrium conformational state' is not achieved as a result of participation of the oxygen in hydrogen bonding through short-range dipolar interactions. Reducing the oxygen content in the polymer backbone by incorporating the homoatomic 1,8-diaminooctaneresulted in an increase in T_g, T_m and enthalpy (crystallinity). Moreover, T_m peak broadening suggested imperfect crystallites. Further studies are underway to understand the crystallization dynamics and the crystallite type formed in these copolymers. In summary, these results demonstrated the significance of oxygen in modulating polyurea thermal properties and obtaining a melt processable material.

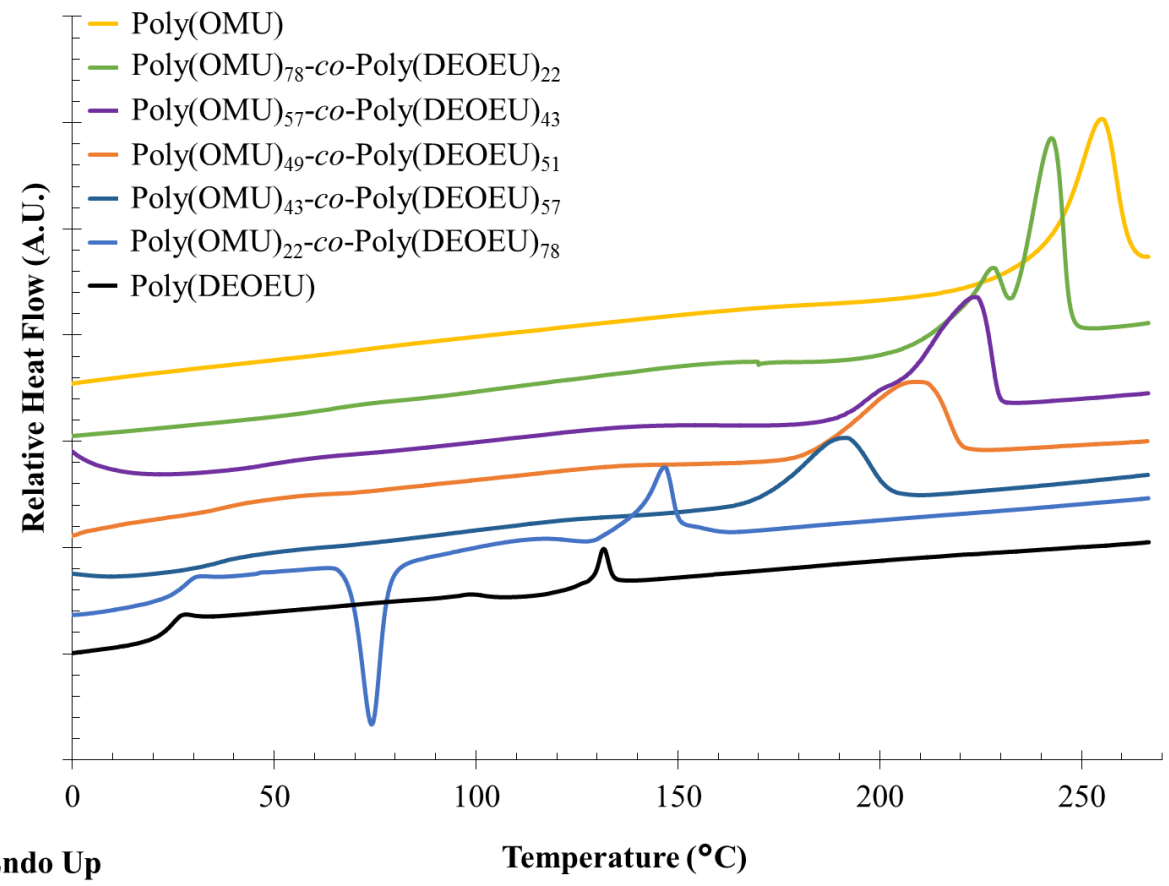

Figure 1. DSC thermograms of Poly(OMU)-co-Poly(DEOEU) copolymers, 2nd heat reported. Vertical shifts applied for clarity.

Dynamic mechanical analysis (DMA) using melt pressed films evaluated storage modulus as a function of temperature and confirmed the thermal transitions observed in DSC (Table 1, Figure 2). The complementary analytical technique also provided more distinct transitions for the T_gs as a result of the high sensitivity of dynamic mechanical properties to temperature. Above the T_g, all copolymers observed a plateau region associated with the physical crosslinks introduced by the crystalline domains. In conjunction with an increase in ΔH_m, the plateau modulus systematically increased with 1,8-diaminooctane incorporation, and further suggested an increase in rigid amorphous phase and crystal content. Finally, the absence of a plateau above T_m suggested that the thermally labile, hydrogen-bonding network is highly

disassociated at the temperatures required to melt the crystal network. This correlated well with previous reports on hydrogen-bond disassociation temperatures.[10, 12, 32]

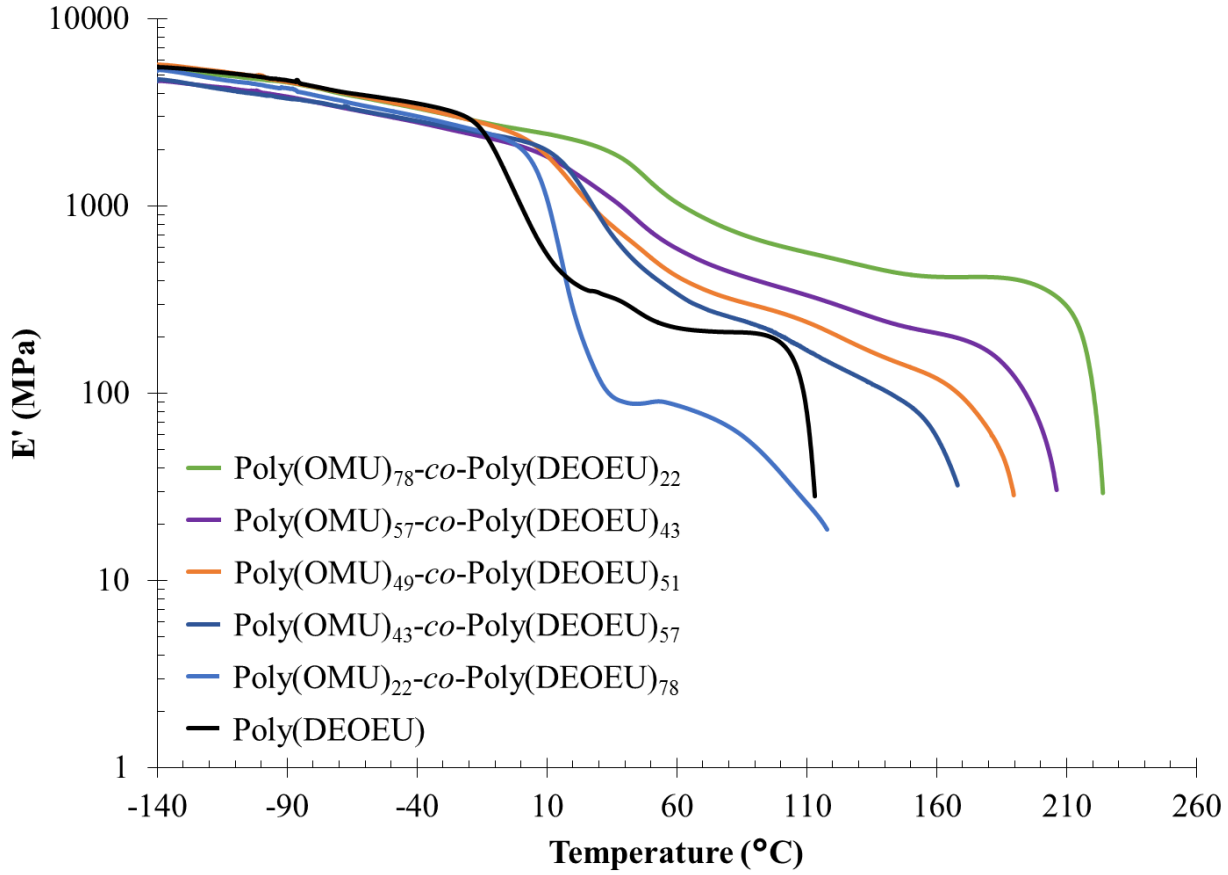

Figure 2. Thermomechanical analysis of poly(OMU)-co-poly(DEOEU) copolymers.

Mechanical analysis of this novel family of polyureas demonstrated the range of properties obtainable (Table 2). Even though the T_gs for Poly(DEOEU) and Poly(OMU)$_{22}$-*co*-Poly(DEOEU)$_{78}$ were sub ambient, the combination of hydrogen-bonding and crystallinity enabled film formation and tensile analysis. Increasing the diaminooctane content resulted in less ductility in conjunction with an increase in the T_g, T_m, and ΔH_m thermal properties. For Poly(DEOEU) and Poly(OMU)$_{22}$-*co*-Poly(DEOEU)$_{78}$ a strain-induced hardening occurred above 100 % strain. Furthermore, the systematic increase in Young's moduli with diaminooctane illustrated an increase in material stiffness with diaminooctane incorporation. However, the

compositionally independent yield stress suggested similar mechanisms for chain-chain slippage during deformation.

Table 2. Summary of tensile results. Averaged five runs with a 12 mm/min grip separation rate at ambient temperature.

		Tensile stress at Break (MPa)	Tensile strain at Break (%)	Tensile stress at Yield (MPa)	Young's Modulus (MPa)
Poly(OMU)$_{78}$-co-Poly(DEOEU)$_{22}$	Mean	38	10	47	1831
	SD	14	2	15	204
Poly(OMU)$_{57}$-co-Poly(DEOEU)$_{43}$	Mean	22	11	35	1501
	SD	8	4	7	169
Poly(OMU)$_{49}$-co-Poly(DEOEU)$_{51}$	Mean	31	6	17	1550
	SD	8	1	4	134
Poly(OMU)$_{43}$-co-Poly(DEOEU)$_{57}$	Mean	42	146	49	1837
	SD	21	60	4	272
Poly(OMU)$_{22}$-co-Poly(DEOEU)$_{78}$	Mean	31	176	30	889
	SD	14	90	1	22
Poly(DEOEU)	Mean	31	252	27	494
	SD	15	98	12	90

Advantages of utilizing a polyureas over other polymers resides in the biodegradability from natural soil enzymes (e.g. Urease). The action of urease requires the cooperative action of a hinged group to sequester urea into the enzyme for subsequent degradation.[18, 33] Previous studies highlight the wide range of ammonia release profiles obtained in polymeric substrates and microenvironments[34, 35], and necessitated additional studies to confirm biodegradability of

polyureas. In Figure 3, released ammonia as a function of time and composition achieved significant levels of ammonia within 4 weeks. Furthermore, acceleration of ammonia release for all compositions in weeks 3 and 4 suggested a significant increase in urea availability (Table S1). Despite ammonia release at short times, over 99 % of the polyureas remained after four weeks (Figure S3). The compositionally independent biodegradation suggested similar urea accessibility, permitting material selection based solely on processing condition requirements. Further investigation into the influence of hydrophilicity is underway.

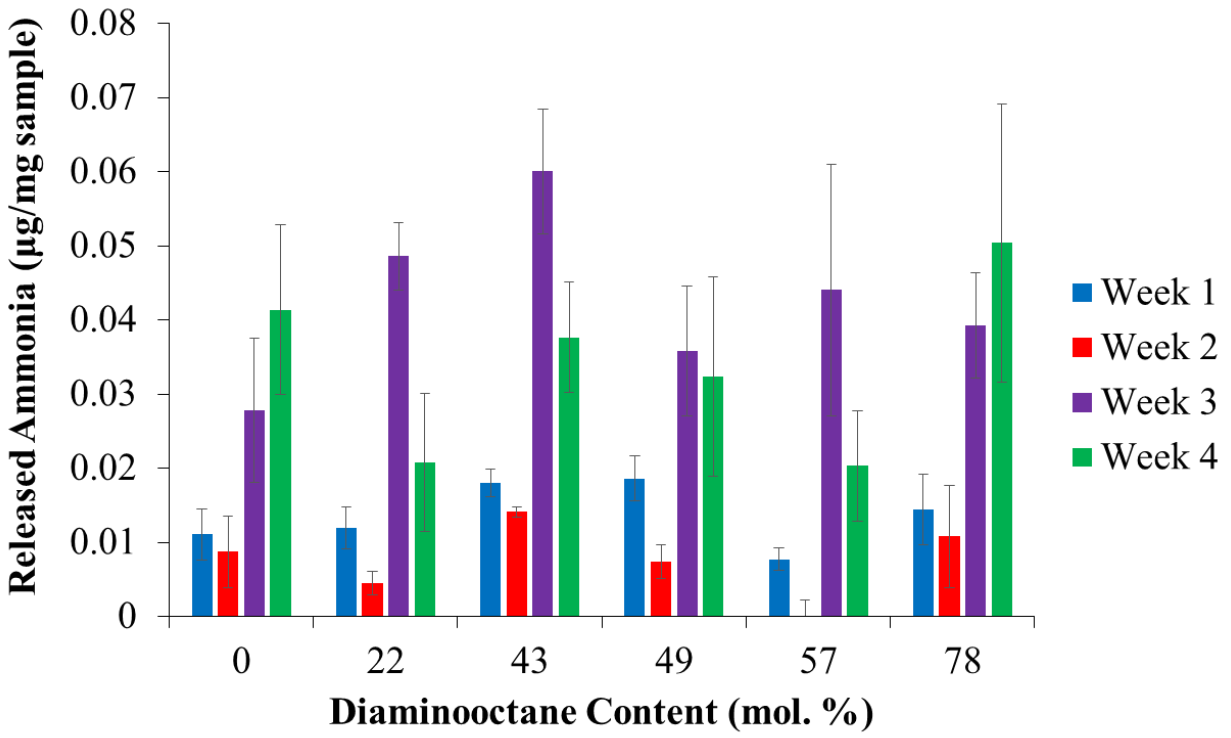

Figure 3. Concentration of ammonia released over each week as a function of composition. Released ammonia increases with increasing time but does not change with composition. Data is presented as average ± standard deviation.

8.5 Conclusions

Urea, a biosourced monomer, provided an inexpensive and biorenewable feedstock to generate polyureas under melt polycondensation conditions. Copolymerization with commercially available diamines generated a family of copolymers and illustrated the versatility of this method. A compilation of analytical techniques evaluated the thermal and mechanical properties. The steady increase in T_m with 1,8-diaminooctane incorporation suggested co-crystallization of the two repeat units. Collaborative efforts are underway to further understand the crystallization behavior of these copolyureas, including variable temperature WAXS and isothermal crystallization studies. DMA further confirmed the trends observed in DSC, while tensile testing highlighted a range of mechanical properties for these copolymers. Finally, exploration into environmental stability suggested a slow degradation pathway catalyzed by natural soil enzymes that liberated ammonia for plant uptake.

8.6 References

1. Li, Q.; Wang, P.; Liu, S.; Fei, Y.; Deng, Y. Catalytic degradation of polyurea: synthesis of N-substituted carbamates with CuO-ZnO as the catalyst, *Green Chemistry* **2016,** 18, (22), 6091-6098.
2. Wang, P.; Ma, X.; Li, Q.; Yang, B.; Shang, J.; Deng, Y. Green synthesis of polyureas from CO2 and diamines with a functional ionic liquid as the catalyst, *RSC Advances* **2016,** 6, (59), 54013-54019.
3. Yu, J.; Lin, F.; Lin, P.; Gao, Y.; Becker, M. L. Phenylalanine-Based Poly(ester urea): Synthesis, Characterization, and in vitro Degradation, *Macromolecules* **2014,** 47, (1), 121-129.

4. Tang, D.; Chen, Z.; Correa-Netto, F.; Macosko, C. W.; Hillmyer, M. A.; Zhang, G. Poly(urea ester): A family of biodegradable polymers with high melting temperatures, *J. Polym. Sci., Part A: Polym. Chem.* **2016**, n/a-n/a.
5. Banihashemi, A.; Hazarkhani, H.; Abdolmaleki, A. Efficient and rapid synthesis of polyureas and polythioureas from the reaction of urea and thiourea with diamines under microwave irradiation, *J. Polym. Sci., Part A: Polym. Chem.* **2004,** 42, (9), 2106-2111.
6. Bouboulis, C. J.; Isidor, K. Polyureas. US3412072, 1968-11-19, 1968.
7. Bouboulis, C. J.; Isidor, K.; White, C. M. Flexible polyureas. US3390137, 1968.
8. Montarnal, D.; Cordier, P.; Soulié-Ziakovic, C.; Tournilhac, F.; Leibler, L. Synthesis of self-healing supramolecular rubbers from fatty acid derivatives, diethylene triamine, and urea, *J. Polym. Sci., Part A: Polym. Chem.* **2008,** 46, (24), 7925-7936.
9. Buckwalter, D. J.; Hudson, A. G.; Moore, R. B.; Long, T. E. Synthesis and characterization of poly(propylene glycol) polytrioxamide and poly(urea oxamide) segmented copolymers, *Polym. Int.* **2014,** 63, (7), 1184-1191.
10. Buckwalter, D. J.; Zhang, M.; Inglefield Jr, D. L.; Moore, R. B.; Long, T. E. Synthesis and characterization of siloxane-containing poly(urea oxamide) segmented copolymers, *Polymer* **2013,** 54, (18), 4849-4857.
11. Wittbecker, E. L. Process for preparing polyureas utilizing immiscible phases. US2816879, 1957.
12. Buckwalter, D. J.; Dennis, J. M.; Long, T. E. Amide-containing segmented copolymers, *Prog. Polym. Sci.* **2015,** 45, 1-22.
13. Redlich, C. A.; Karol, M. H. Diisocyanate asthma: clinical aspects and immunopathogenesis, *International Immunopharmacology* **2002,** 2, (2–3), 213-224.

14. Wu, S.; Li, W.; Lin, M.; Burlingame, Q.; Chen, Q.; Payzant, A.; Xiao, K.; Zhang, Q. M. Aromatic Polythiourea Dielectrics with Ultrahigh Breakdown Field Strength, Low Dielectric Loss, and High Electric Energy Density, *Advanced Materials* **2013,** 25, (12), 1734-1738.
15. Hoogenboom, R.; Schubert, U. S. Microwave-Assisted Polymer Synthesis: Recent Developments in a Rapidly Expanding Field of Research, *Macromolecular Rapid Communications* **2007,** 28, (4), 368-386.
16. Briassoulis, D.; Dejean, C. Critical Review of Norms and Standards for Biodegradable Agricultural Plastics Part I. Biodegradation in Soil, *Journal of Polymers and the Environment* **2010,** 18, (3), 384-400.
17. Kasirajan, S.; Ngouajio, M. Polyethylene and biodegradable mulches for agricultural applications: a review, *Agronomy for Sustainable Development* **2012,** 32, (2), 501-529.
18. Pratt, C. W.; Cornely, K., *Essential biochemistry*. Third edition. ed.; Wiley ;: Hoboken, N.J. :, 2014.
19. Krajewska, B. Ureases I. Functional, catalytic and kinetic properties: A review, *Journal of Molecular Catalysis B: Enzymatic* **2009,** 59, (1–3), 9-21.
20. Tokiwa, Y.; Suzuki, T. Hydrolysis of polyesters by lipases, *Nature* **1977,** 270, (5632), 76-78.
21. Peter, B.; Wolfgang, I. Thermoplastic polyureas prepared from araliphatic diamines. US3388103, 1968.
22. Helmut, M.; Rudolf, G. Preparation of linear polyurea polymers from urea and an alicyclic diamine. US3223682, 1965.
23. Mathis, R. Polyurea fibers based on poly(4,4-methylenedicyclohexylene)urea. US3857819, 1974-12-31, 1974.

24. Erickson, J. G. Reactions of Long-chain Amines. II. Reactions with Urea1, *J. Amer. Chem. Soc.* **1954,** 76, (15), 3977-3978.
25. Harold, W. A. Process of making aliphatic polyureas. US2145242, 1939-01-31, 1939.
26. Schiraldi, D. A.; Occelli, M. L.; Gould, S. A. C. Atomic force microscopy (AFM) study of poly(ethylene terephthalate-co-4,4′-bibenzoate): A polymer of intermediate structure, *J. Appl. Polym. Sci.* **2001,** 82, (11), 2616-2623.
27. Biswas, A.; Blackwell, J. Three-dimensional structure of main-chain liquid-crystalline copolymers. 1. Cylindrically averaged intensity transforms of single chains, *Macromolecules* **1988,** 21, (11), 3146-3152.
28. Menczel, J.; Wunderlich, B. Heat capacity hysteresis of semicrystalline macromolecular glasses, *Journal of Polymer Science: Polymer Letters Edition* **1981,** 19, (5), 261-264.
29. Huo, P.; Cebe, P. Effects of thermal history on the rigid amorphous phase in poly(phenylene sulfide), *Colloid and Polymer Science* **1992,** 270, (9), 840-852.
30. Wunderlich, B. Reversible crystallization and the rigid–amorphous phase in semicrystalline macromolecules, *Prog. Polym. Sci.* **2003,** 28, (3), 383-450.
31. Ruokolainen, J.; ten Brinke, G.; Ikkala, O.; Torkkeli, M.; Serimaa, R. Mesomorphic Structures in Flexible Polymer−Surfactant Systems Due to Hydrogen Bonding: Poly(4-vinylpyridine)−Pentadecylphenol, *Macromolecules* **1996,** 29, (10), 3409-3415.
32. Zhang, K.; Fahs, G. B.; Aiba, M.; Moore, R. B.; Long, T. E. Nucleobase-functionalized ABC triblock copolymers: self-assembly of supramolecular architectures, *Chemical Communications* **2014,** 50, (65), 9145-9148.
33. Follmer, C. Insights into the role and structure of plant ureases, *Phytochemistry* **2008,** 69, (1), 18-28.

34. Metelitsa, D. I.; Tarun, E. I.; Puchkaev, A. V.; Losev, Y. P. Urease Inhibition by Polymeric Substrate Analogues and Thiophosphamides, *Applied Biochemistry and Microbiology* **2001,** 37, (2), 168-173.

35. Sundaram, P. V. The kinetic properties of microencapsulated urease, *Biochimica et Biophysica Acta (BBA) - Enzymology* **1973,** 321, (1), 319-328.

8.7 Supporting Information

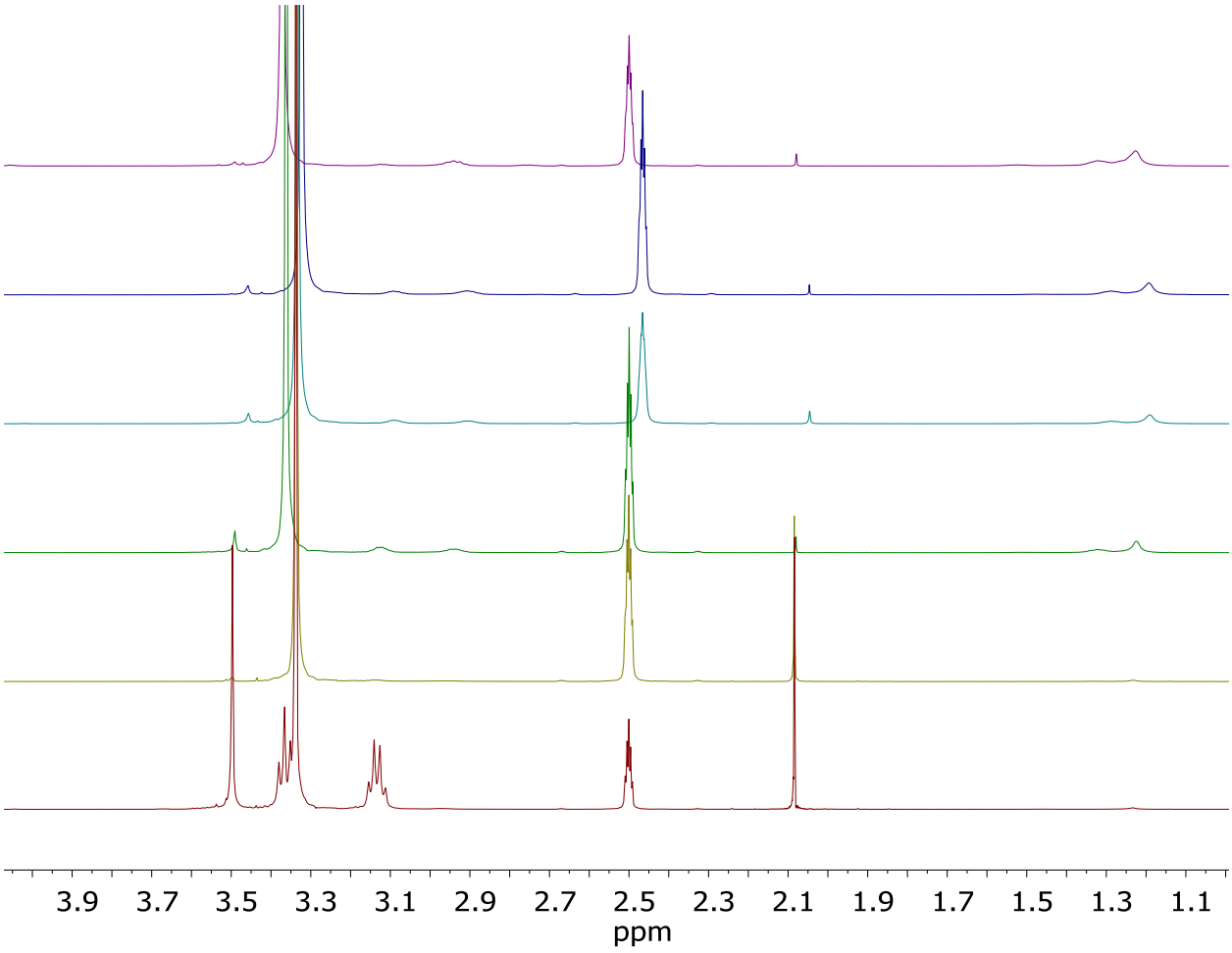

Figure S1: ^{1}H NMR spectroscopy of copolyureas in DMSO-d_6 with 0.1 M LiBr.

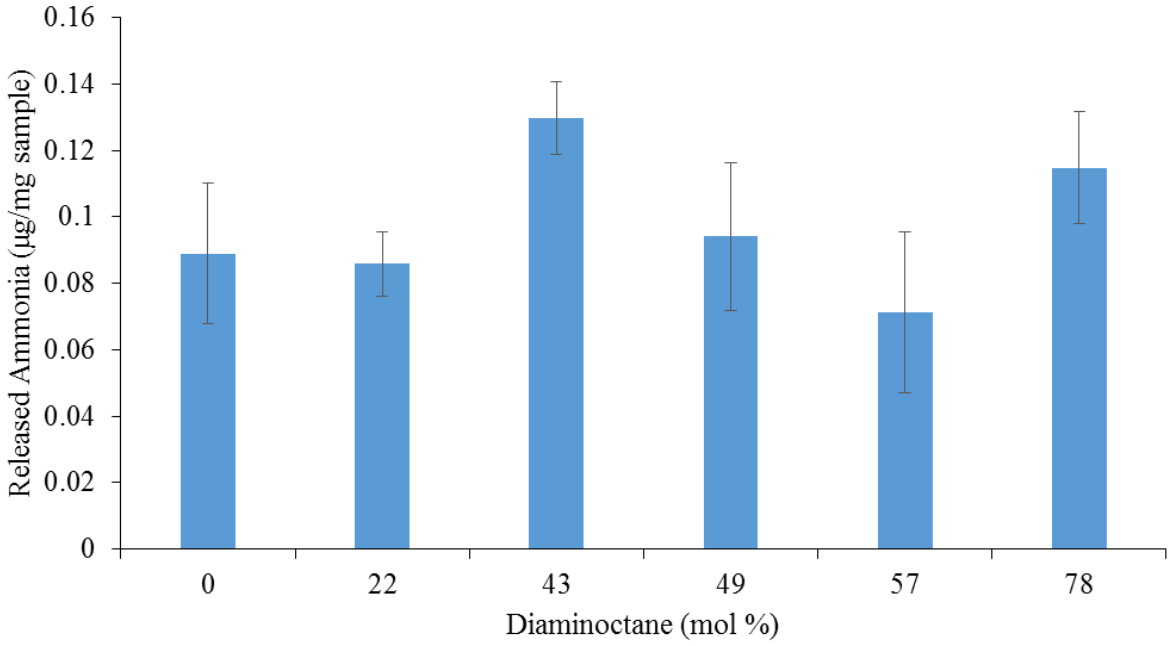

Figure S2: Total ammonia release after 4 weeks, identifying a compositional independence of Urease-derived degradation.

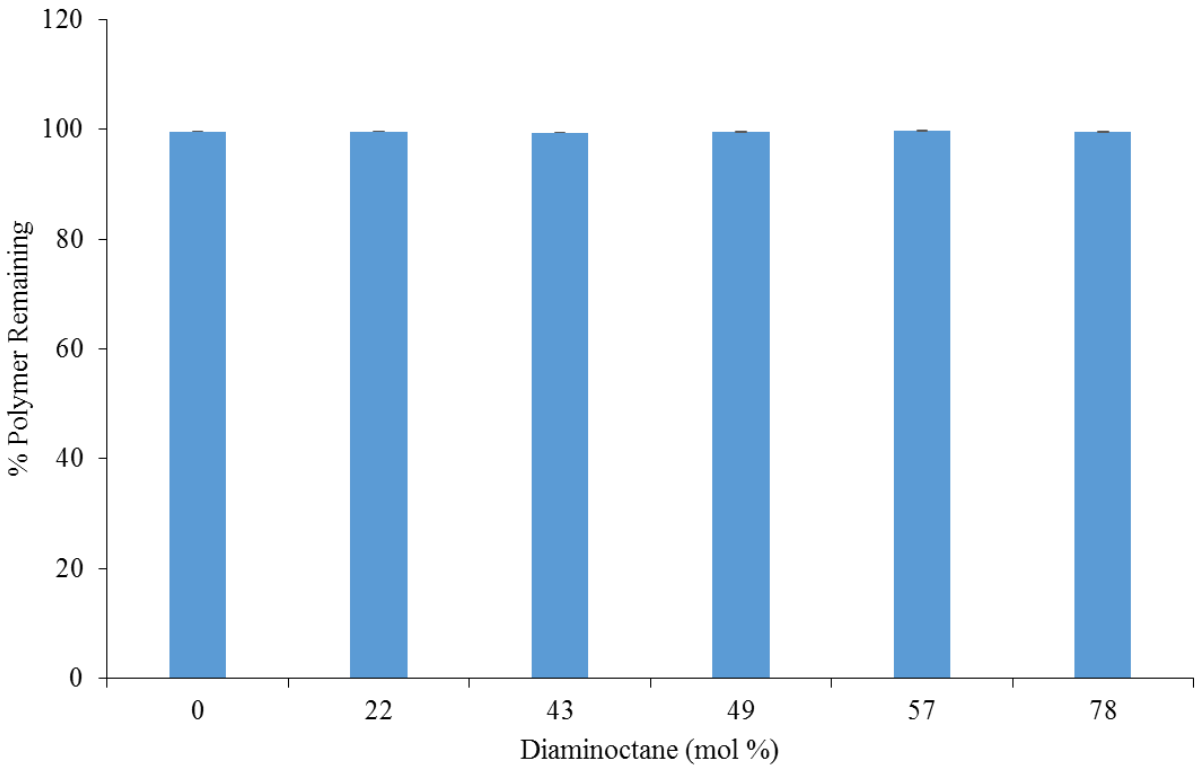

Figure S3: Polyurea percent remaining after 4-week exposure to Urease.

Table S1: Results of Tukey's HSD for the 4-week profile of ammonia release . Groups not connected by the same letter are significantly different (i.e. Weeks 3 and 4 are statistically different from weeks 1 and 2)

WEEK			LEAST SQ MEAN
3	**A**		**0.042585**
4	**A**		**0.033789**
1		**B**	**0.013634**
2		**B**	**0.007455**

Table S2: Results of Tukey's HSD for the total ammonia release after 4 weeks. All copolymers are statistically similar.

LEVEL		LEAST SQ MEAN
43	A	0.129745
78	A	0.114784
49	A	0.094098
0	A	0.088957
22	A	0.085867
57	A	0.071329

Table S3: Results of Tukey's HSD for the percent polymer remaining after 4 weeks indicating similar degradation percentages across the composition range.

LEVEL			LEAST SQ MEAN
57	A		99.66497
22	A	B	99.59313
0	A	B	99.58475
49	A	B	99.55715
78	A	B	99.46368
43		B	99.38846

Chapter 9: Sulfonate-endcapped Long-chain Branched Poly(ether imide)s

(Submitted to VTIP, Invention Disclosure)

Joseph M. Dennis[*], Ryan J. Mondschein[*], Maruti Hegde[*], Roy Odle[#], and Timothy E. Long[*]

[*]*Department of Chemistry, Macromolecules Innovation Institute*

Virginia Tech, Blacksburg, VA 24061

[#]*SABIC Innovative Plastics, Mt Vernon, IN 47620*

9.1 Introduction

Long-chain branching (LCB) has major implications in the melt strength of polymers.[1-4] The introduction of LCB reduces melt viscosity of high molecular weight polymers at a given processing temperature.[1,4] Furthermore, LCBs improve shear-thinning and extensional flow processing over linear analogues.[1,4] Much of the current literature studies the impact of long-chain branches in polyolefins, where branch molecular weights (M_b) are orders of magnitude larger than the molecular weight of entanglements (M_e).[2,4] With such long-chains, melt viscosity and processability are greatly influenced with minimal branching. Other investigations include introducing long-chain branches into polyesters (e.g. poly(ethylene terephthalate)) to improve strength and reduce the rate of crystallinity.[5] In this instance, very low incorporations of a trifunctional monomer (less than 1 mol.%) resulted in long-chain branched polyesters without gelation.[5] Recently, investigation into long-chain branched poly(ether imide)s highlighted improved melt processability with relatively high amounts of branching agents (*circa* 2 mol.%).(REF previous invention disclosure) Following our previous report, the novel synthesis of long-chain branched PEIs (LCB-PEIs) with sulfonated endgroups provides highly associative

groups that influence thermal, mechanical and rheological behavior. Importantly, introducing these sulfonated salts at the chain ends improves the mechanical integrity of low molecular weight LCB-PEIs over non-sulfonated analogues. The aggregation of the sulfonate moiety forms a non-covalent network, which lends to the increases in mechanical strength, and thermal resilience.

9.2 Results and Discussion

The synthesis of a trisamine 1,1,1-tris((*p*-aminophenoxy)phenyl) ethane (TAPE) involved a two-step sequence, which is described previously.(REF previous disclosure) To summarize, nucleophilic aromatic substitution of 1-chloro-4-nitrobenzene with 1,1,1-tris(4-hydroxyphenyl) ethane generated 1,1,1-tris((*p*-nitrophenoxy)phenyl) ethane (TNPE). Next, reduction of TNPE to TAPE follows a typical high-pressure reduction using palladium as a catalyst. The synthesis of a monofunctional, sulfonated monomer follows a simple neutralization of sulfanilic acid with base. Beginning with a slurry of sulfanilic acid in deionized water, titration of dilute base (*e.g.* calcium carbonate) resulted in dissolution of the sulfanilate salt into water (Scheme 1). The change in optical clarity from a slurry to a transparent solution, and the bubbling of CO_2 during the titration visually identified a successful neutralization. Further confirmation followed with color metric titration in a phenolphthalein-containing solution. The immediate color change from clear to pink with a single drop of 1 N sodium hydroxide solution strongly suggested a successful neutralization without over titration. Isolation of the sulfanilate salt followed with evaporation of water resulting in a white powder.

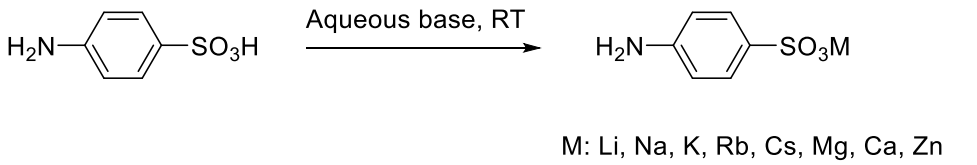

Scheme 3: Synthesis of sulfanilate salts.

Sulfonate-endcapped, long-chain branched poly(ether imide)s (SLCB-PEIs) followed similar protocol to commercial-scale poly(ether imide) synthesis. (Scheme 2) Although *o*-dichlorobenzene is preferred, the poor solubility of TAPE and the sulfanilate salt in *o*-dichlorobenzene required utility of *N*-methylpyrrolidinone (NMP) to achieve a homogeneous solution at elevated temperatures. Furthermore, dissolution of TAPE and m-phenylene diamine in NMP at room temperature prior to addition of bisphenol-A dianhydride (BPA-DA) circumvented concentration gradients surrounding the dissolving TAPE particle, which led to gelled particulates. Addition of bisphenol-A dianhydride (BPA-DA) followed dissolution of the amines. Immediately, the amic-acid intermediate formed, indicated by a two-phase solution and a dramatic increase in viscosity. When the temperature reached 180 °C, the viscosity decreased and the solution became homogeneous. Control over the stoichiometry of the reaction enabled an anhydride-endcapped telechelic intermediate *in-situ*, with a targeted molecular weight. After 18 h at 180 °C, addition of the sulfanilate salt to the viscous solution generated the targeted SLCB-PEIs with controlled molecular weights. Finally, removal of NMP and complete imidization proceeded through devolatization at 380 °C under nitrogen.

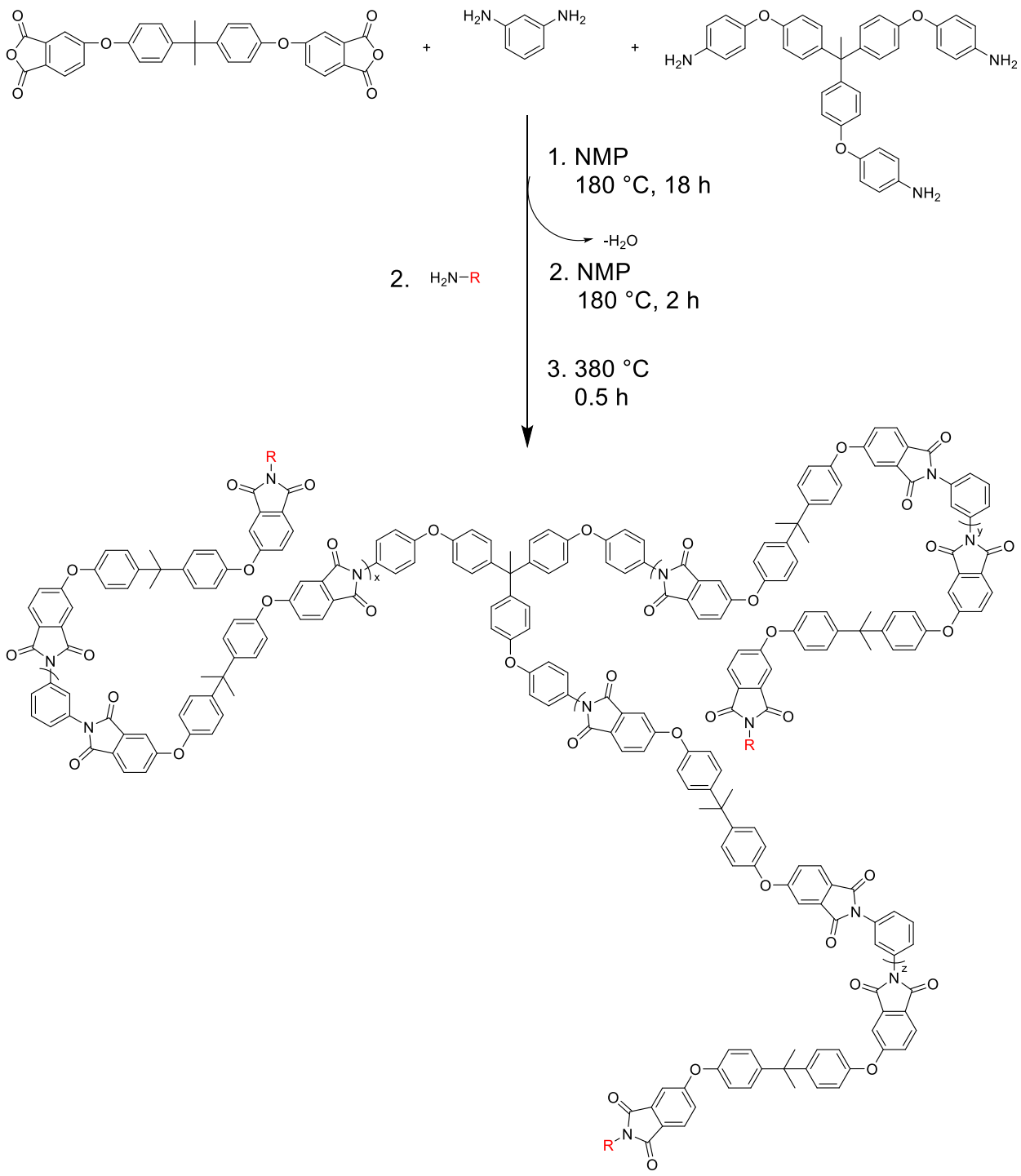

Scheme 4: Synthesis of sulfonate-endcapped poly(ether imide)s

Thermal gravimetric analysis (TGA) performed on a TA Instruments Q500 with constant nitrogen purge provided weight loss as a function of temperature (Figure 1). All PEIs exhibited significant weight loss above 500 °C, indicating a minimal influence of thermal weight loss with

ionic incorporation. Probing the thermal stability further, oscillatory shear experiments on polymer melts, using a TA Instruments AR-G2 rheometer, highlighted similar time-dependent viscosity profiles for ionic and non-ionic PEIs (Figure 2). Operating at 340 °C under air, the viscosity of sulfonated and non-sulfonated PEIs are stable up to approximately 2 min. After which, the viscosity increased exponentially with time. The similar degradation profiles in TGA and rheology suggested the degradation pathway is independent of the sulfonated endgroup. Furthermore, these studies provided evidence of comparable thermal stability of non-sulfonated and sulfonated PEIs, and illustrated the compatibility for processing temperatures and times to current protocol.

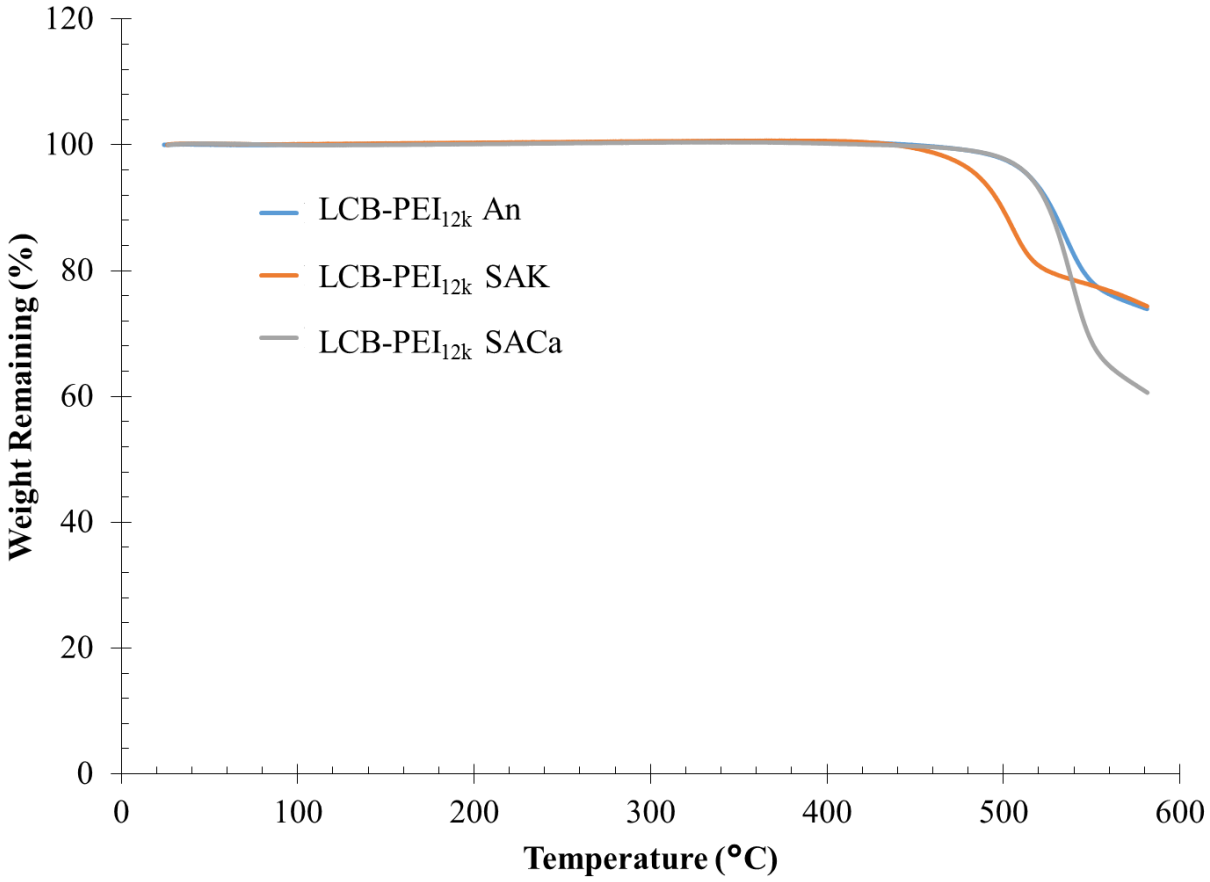

Figure 10: Thermal gravimetric analysis of LCB-PEIs with sulfonated and non-sulfonated endgroups.

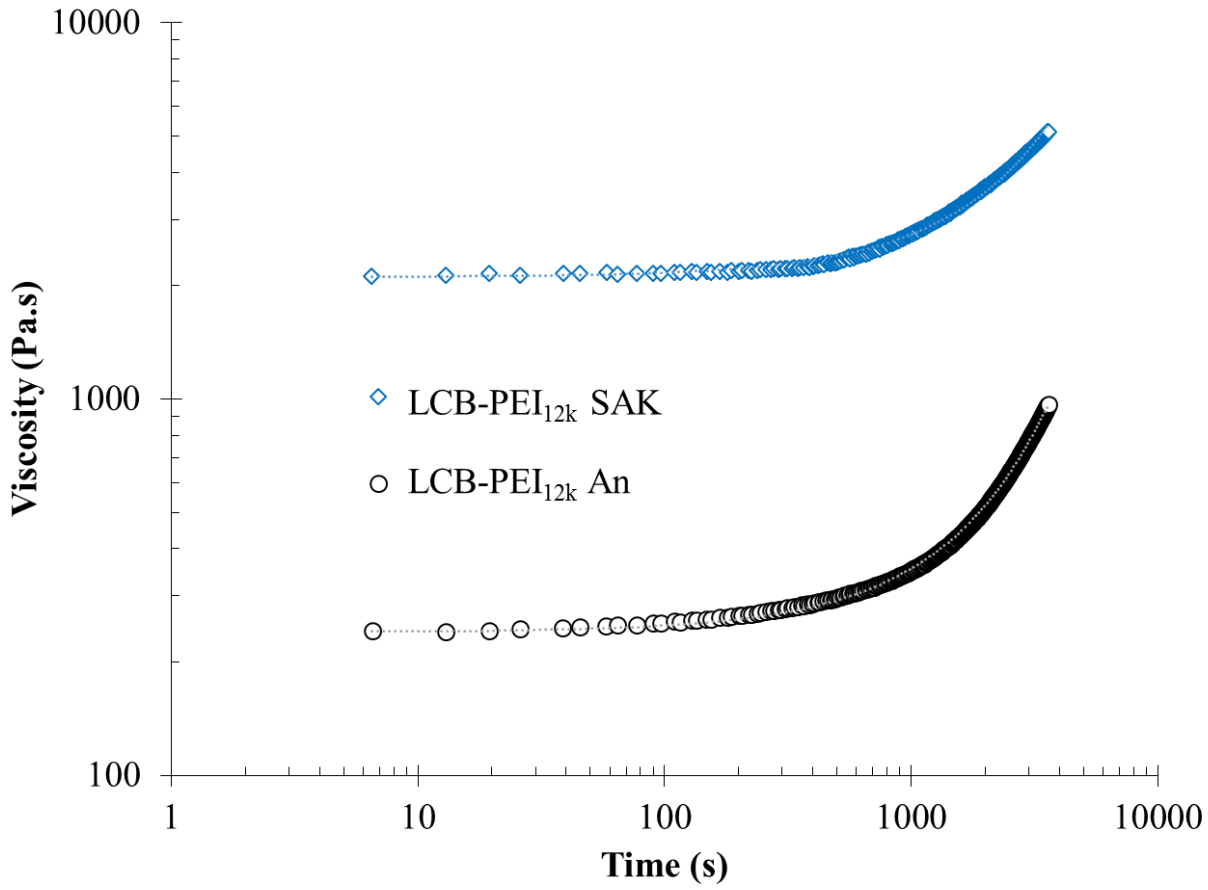

Figure 11: Viscosity-time stability at 340 °C for non-ionic and sulfonate-endcapped LCB PEIs.

Differential scanning calorimetry (DSC), executed on a TA Instruments Q2000 with a heat/cool/heat cycle of 10 °C/100 °C/10 °C, respectively, under constant nitrogen purge probed the thermal transitions in the PEIs (Figure 3). The amorphous PEIs exhibited a single glass transition temperature (T_g) above 200 °C. Importantly, introducing the ionic endgroups increased the T_g from 205 °C to 211 °C, which suggested a restriction in endgroup mobility with aggregation of the sulfonated endgroups. Furthermore, the restriction of the endgroups through sulfonate aggregation increased the T_g to within a few degrees of the linear commercial sample, which is a critical metric for these high temperature thermoplastics.

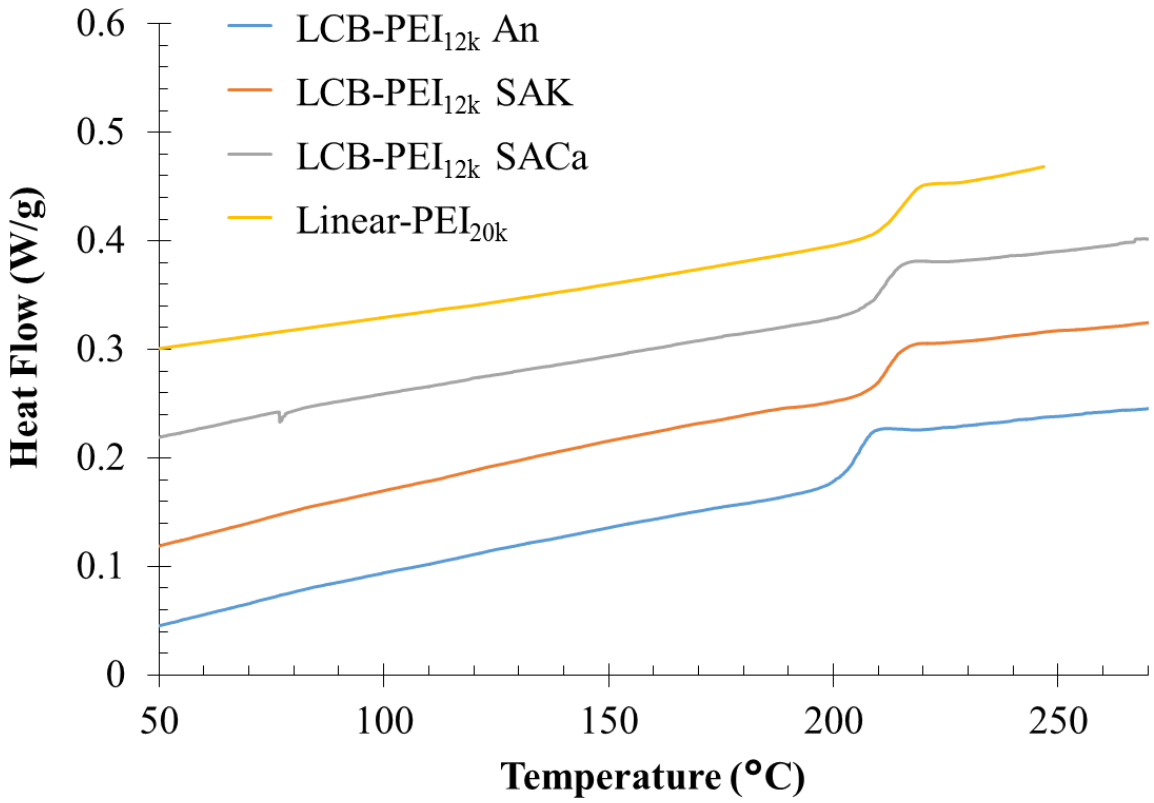

Figure 12: Differential scanning calorimetry of linear and sulfonate-endcapped LCB PEIs. Endothermic events are positive heat flows. Curves shifted vertically for clarity.

Dynamic mechanical analysis (DMA), evaluated using a TA Instruments Q800 in tension mode and operating at 1 Hz, provided thermomechanical performance in the sulfonate-endcapped LCB-PEIs across a wide range of operating temperatures (Figure 4). Below the α-relaxation, all PEI samples exhibited a temperature-independent modulus >1 GPa, typical for polymer glasses. However, the brittleness of the non-sulfonated, low-molecular weight PEI prevented observation of an α-relaxation. Several attempts were made, but each sample broke before reaching a flow temperature. In contrast, the sulfonate-endcapped PEIs provided mechanically robust films at the same molecular weight, and observed similar thermomechanical behavior as the linear, high molecular weight sample. In conclusion, the results from DSC and

DMA illustrated an improvement of thermal and mechanical properties by introducing sulfonated endgroups to long-chain branched PEIs.

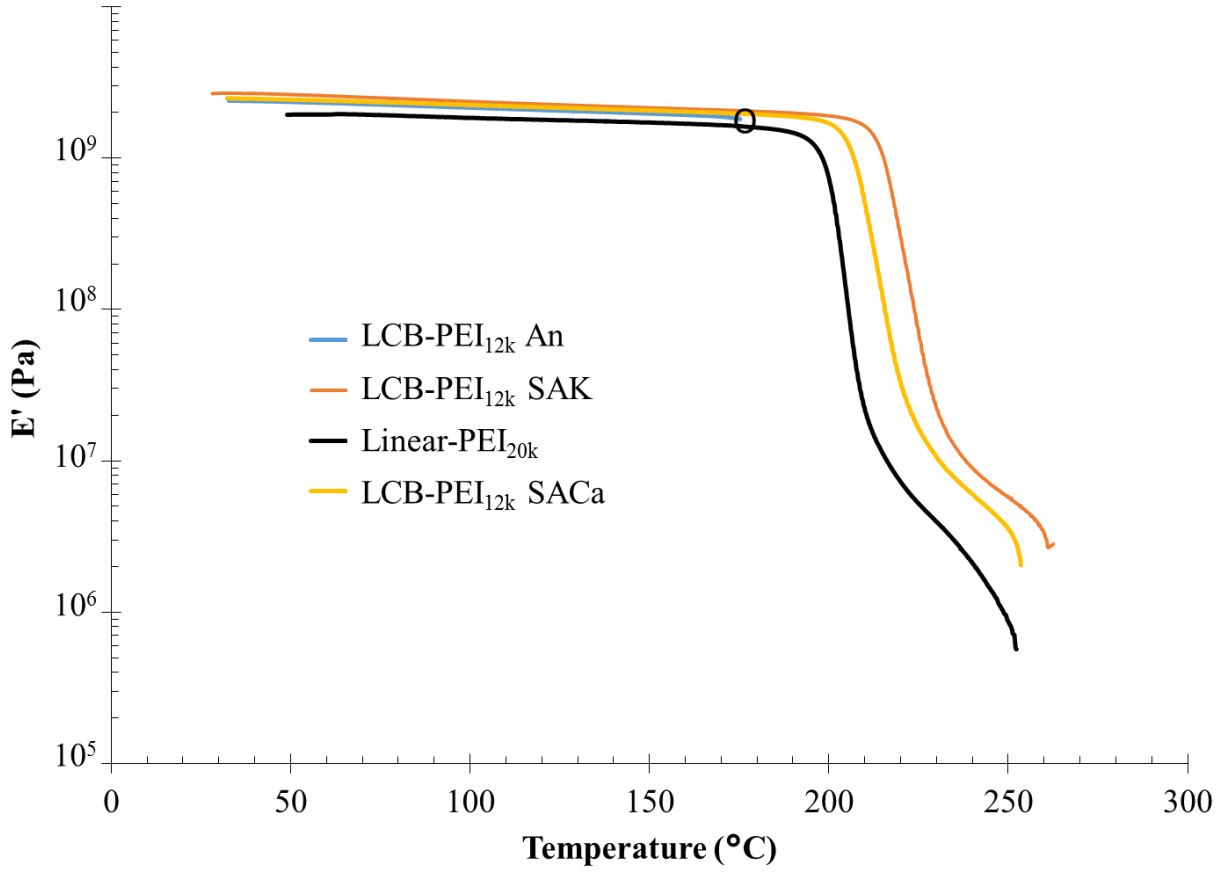

Figure 13: Thermomechanical response of linear and sulfonate-endcapped LCB PEIs. Open circle illustrates break point of sample.

Other critical attributes for thermoplastics is the melt processing ability, and flow behavior at elevated temperatures. Employing a TA Instruments AR-G2 rheometer equipped with 8 mm parallel plates evaluated the temperature dependence of viscosity and modulus above the T_g (Figures 5 and 6). Interestingly, the viscosity of the calcium-neutralized, sulfonate-endcapped PEIs exhibited similar viscosities across the temperature range as the high molecular weight control. A combination of the sulfonate aggregation and calcium charge provided substantial physical crosslinking above 250 °C, restricting flow of the polymer chains. Above 290 °C, there

is a crossover between the viscosity of the high molecular weight PEI control and the calcium sulfonate-endcapped PEI sample. Furthermore, the absence of a significant step change suggests that the calcium-sulfonate complex remains stable well above 300 °C.

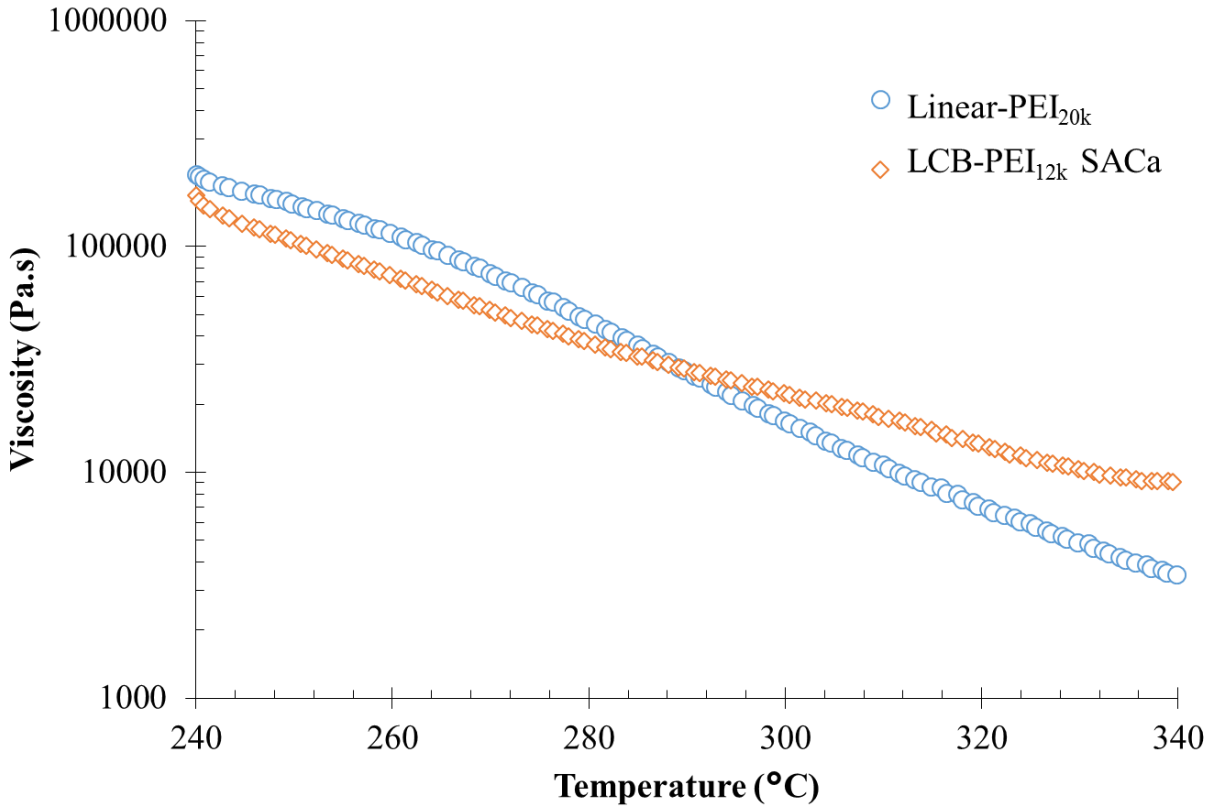

Figure 14: Temperature influence on viscosity of linear and calcium sulfonate-endcapped PEIs.

Monitoring the storage and loss moduli as a function of temperature (Figure 6) further highlights the influence of sulfonated endgroups on melt behavior in PEIs. In concert with viscosity, the high molecular weight sample and calcium sulfonate-endcapped PEI observed similar storage and loss moduli at 240 °C. However, at *circa* 280 °C the non-sulfonated control exhibited a crossover in the storage and loss moduli, indicative of chain reptation. Contrastingly, the calcium sulfonate-endcapped PEI never observed a crossover of storage and loss moduli, indicating a large increase in the chain relaxations associated with chain reptation. This also

indicates that at elevated temperatures, the sulfonate-endcapped PEIs mechanical response is more elastic than analogous linear high molecular weight samples and is suspected to improve flame resistance.

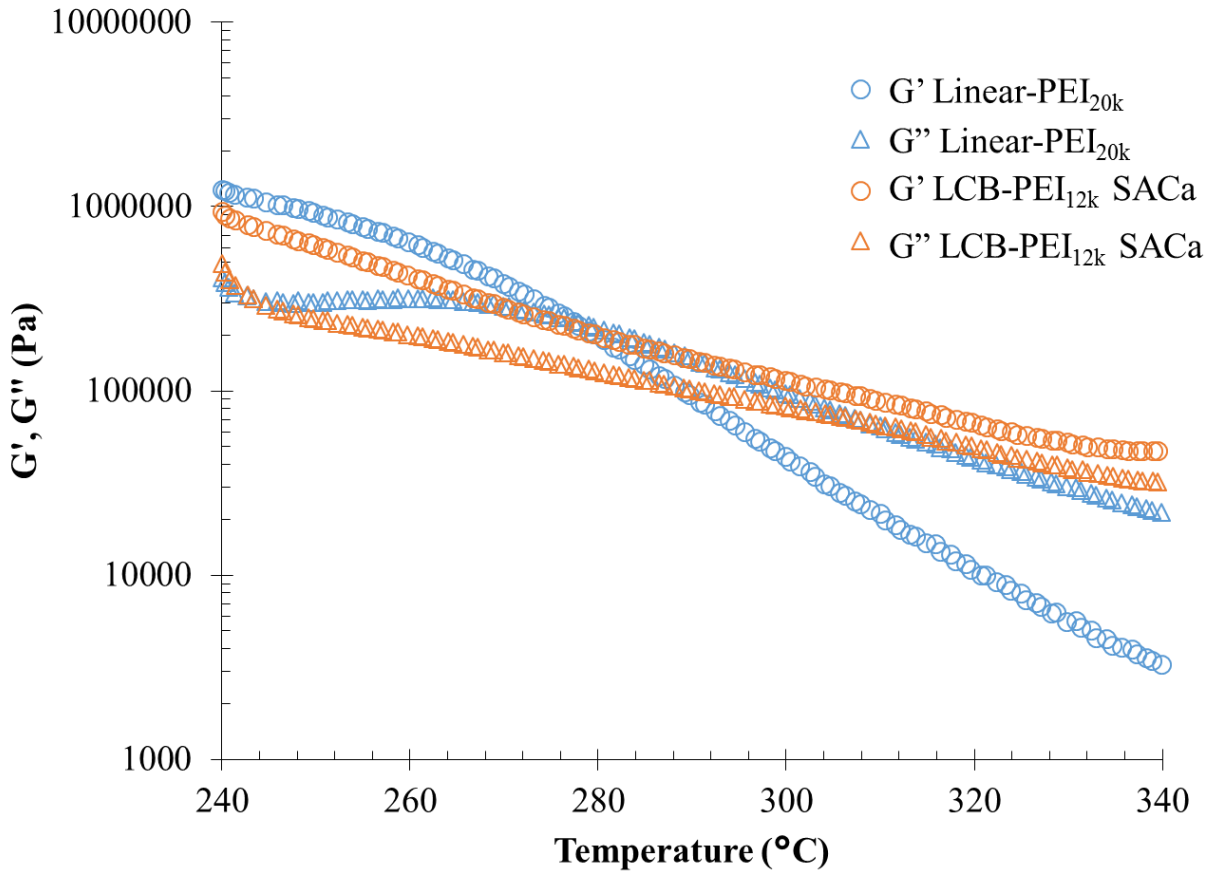

Figure 15: Temperature dependence of storage and loss moduli of linear and calcium sulfonate-endcapped LCB PEIs.

In conclusion, introducing sulfonate salts to the endgroups of long-chain branched PEIs improves thermal and mechanical properties over analogous low molecular weight, neutral controls. Evaluating the thermal stability highlights a similar degradation profile for sulfonate-endcapped PEIs with neutral analogues, permitting direct use in high temperature applications typically associated with PEIs. Finally, the physical interactions of sulfonate aggregation and calcium complexation greatly influenced the PEI melt behavior. The elevated viscosity of the

sulfonate-endcapped PEIs suggested that the physical crosslinks remain stable well above 300 °C. Furthermore, the change in melt elasticity with sulfonated endgroups illustrates potential for improved flame resistance above the neutral, linear analogue.

9.3 Examples

Example 1:

Synthesis of sodium sulfanilate: Sulfanilic acid (10 g, 0.0577 mol) and sodium carbonate (3.06 g, 0.02885 mol) were suspended in 10 mL of deionized water in a 100-mL, round-bottomed flask equipped with a magnetized stirrer. Within a few minutes of stirring at room temperature, the suspension cleared. Titration with base and phenolphthalein indicator confirmed complete conversion. Isolation followed by evaporation of water under vacuum at 35 °C.

Example 2:

Synthesis of potassium sulfanilate followed the procedure for Example 1 except with potassium carbonate. Sulfanilic acid (10 g, 0.0577 mol) and potassium carbonate (3.99 g, 0.02885 mol) were suspended in 10 mL of deionized water in a 100-mL, round-bottomed flask equipped with a magnetized stirrer. Within a few minutes of stirring at room temperature, the suspension cleared. Titration with base and phenolphthalein indicator confirmed complete conversion. Isolation followed by evaporation of water under vacuum at 35 °C.

Example 3:

Synthesis of calcium sulfanilate followed the procedure for Example 1 except with calcium carbonate, and 40 °C. Sulfanilic acid (10 g, 0.0577 mol) and calcium carbonate (2.91 g, 0.02885 mol) were suspended in 10 mL of deionized water in a 100-mL, round-bottomed flask equipped with a magnetized stirrer. Within a few minutes of stirring at 40 °C, the suspension cleared.

Titration with base and phenolphthalein indicator confirmed complete conversion. Isolation followed by evaporation of water under vacuum at 35 °C.

Example 4:

Synthesis of long-chain branched poly(ether imide)s follows similar procedures as reported previously. The synthesis of a 12 kg/mol poly(ether imide) branched with 5.2 mol% of TAPE follows as an example. TAPE (1.94 g, 2.898 mmol), *m*-phenylene diamine (8.577 g, 79.3 mmol), and *N*-methylpyrrolidinone (90 mL) were charged to a three-necked, 500-mL, round-bottomed flask. The flask was then equipped with a rubber septum, glass stir rod with Teflon blade, and Dean-Stark trap. A condenser completed the set up on the Dean-Stark trap, and the contents purged with nitrogen for 20 minutes. Next, BPA-DA (46.19 g, 87.3 mmol) was dissolved in *N*-methylpyrrolidinone (90 mL) and then added to the flask. The flask was then heated to 180 °C, where the reaction proceeded for 18 hours. After cooling to room temperature, the reaction was split evenly into four parts and the endcapper added. This ensured the molecular weights and distributions are equivalent between samples from one batch. Aniline (0.2699 g, 2.8977 mmol), sodium sulfaniliate (0.5655 g, 2.8977 mmol), potassium sulfanilate (0.6122 g, 2.8977 mmol), or calcium sulfanilate (0.5570 g, 1.4488 mmol) were added one to each of the four fractions. Devolatilization of the solvent and thermal imidization was completed utilizing a metal bath operating at 380 °C, resulting in an orange, transparent product.

9.4 References

1. Mannion, A. M.; Bates, F. S.; Macosko, C. W. Synthesis and Rheology of Branched Multiblock Polymers Based on Polylactide, *Macromolecules* **2016,** 49, (12), 4587-4598.
2. Meissner, J. Basic parameters, melt rheology, processing and end-use properties of three similar low density polyethylene samples, *Pure and Applied Chemistry* **1975,** 42, (4), 551.

3. Hadjichristidis, N.; Xenidou, M.; Iatrou, H.; Pitsikalis, M.; Poulos, Y.; Avgeropoulos, A.; Sioula, S.; Paraskeva, S.; Velis, G.; Lohse, D. J.; Schulz, D. N.; Fetters, L. J.; Wright, P. J.; Mendelson, R. A.; García-Franco, C. A.; Sun, T.; Ruff, C. J. Well-Defined, Model Long Chain Branched Polyethylene. 1. Synthesis and Characterization, *Macromolecules* **2000,** 33, (7), 2424-2436.
4. Lohse, D. J.; Milner, S. T.; Fetters, L. J.; Xenidou, M.; Hadjichristidis, N.; Mendelson, R. A.; García-Franco, C. A.; Lyon, M. K. Well-Defined, Model Long Chain Branched Polyethylene. 2. Melt Rheological Behavior, *Macromolecules* **2002,** 35, (8), 3066-3075.
5. McKee, M. G.; Unal, S.; Wilkes, G. L.; Long, T. E. Branched polyesters: recent advances in synthesis and performance, *Prog. Polym. Sci.* **2005,** 30, (5), 507-539.

Chapter 10: Conclusions and Future Work

The facile synthetic approach to segmented polysulfone-containing polyesters afforded a versatile family of high temperature thermoplastics with tunable thermomechanical properties. Generating a hydroxyethyl telechelic oligomer enabled utility in melt transesterification polymerizations with dimethyl terephthalate and 1,4-butanediol to yield high molecular weight segmented block copolymers with alternating polysulfone and poly(butylene terephthalate) (PBT) sequences. Systematic variation in polysulfone and PBT segment lengths isolated their influence on thermal and mechanical properties. Importantly, strong interrelationships developed through a myriad of analytical techniques between segment length and the crystallization behavior and thermal properties provided critical structural characteristics for future studies. Thus far, the copolymers developed incorporate an amorphous, high-T_g segment (e.g. polysulfones) with a semicrystalline polyester (e.g. PBT). However, the synthetic method developed here permits exploration into other engineering thermoplastics. For instance, Scheme 1 illustrates another permutation of these segmented block copolymers. The semicrystalline poly(ether ether ketone) (PEEK) provides a second crystallizable segment in conjunction with PBT. The added complexity of the second crystallizable segment provides a unique prospect for co-crystallization and/or thermal behavior.

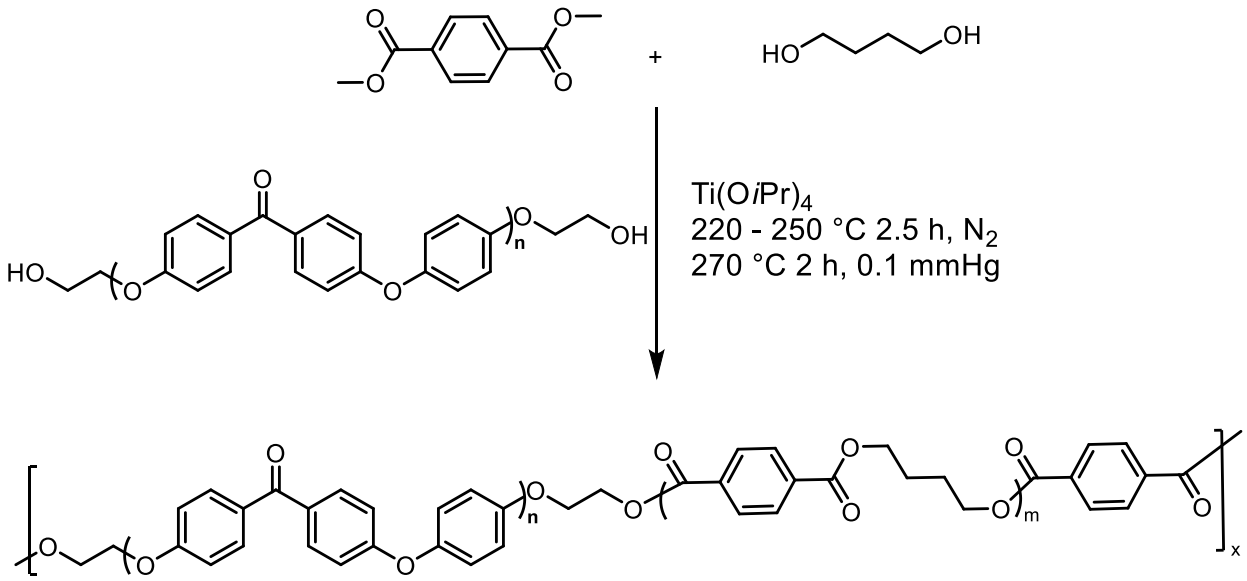

Scheme 1: Proposed synthesis of PEEK-containing PBT segmented block copolymers.

As described in Chapter 4, the melt solubility of each component is critical to couple the segments, and achieve high molecular weights. Utilizing van Krevlen's group contribution theory, tailoring the structure of the PEEK segment to provide a similar solubility profile as PBT will help eliminate possible issues. To further probe the solubility experimentally, melt polymerization of a series of functional PEEK oligomer molecular weights (e.g. 3, 6, 10 and 15 kg/mol) with PBT will help correlate the expected solubility results as described by the group contribution theory. Following the observations provided in Chapters 3 and 4, at high wt.% of PEEK the copolymers will observe a transition from phase mixing to phase separated. Studying this phase behavior in comparison to the segment length of both PEEK and PBT will continue to evaluate the conclusions developed with the PESu-PBT copolymers.

Melt polycondensation of decahydronaphthalate dimethylester with various diols enabled the synthesis of novel, high molecular weight polyesters containing hydrogenated naphthalene rings. By understanding the segmental mobility through oscillatory experiments, characteristic properties (e.g. chain entanglement molecular weights, and monomer rigidity) correlated well

with thermal and mechanical properties. Although introduction of a rigid cyclobutane monomer increased the glass transition temperature, the reduction in entanglements per chain resulted in a loss of ductility in the copolyesters. Using the concepts generated in the long-chain branched PEIs, Scheme 2 proposes a synthetic route to improve mechanical ductility through branching. In this instance, incorporating 2-(hydroxymethyl)-2-methylpropane-1,3-diol provides a commercially available multifunctional diol to branch the copolyesters. The expected broadening of the molecular weight distribution increases the concentration of higher molecular weight species, potentially increasing the average number of chain entanglements per chain and improving the extensibility of these copolyesters.

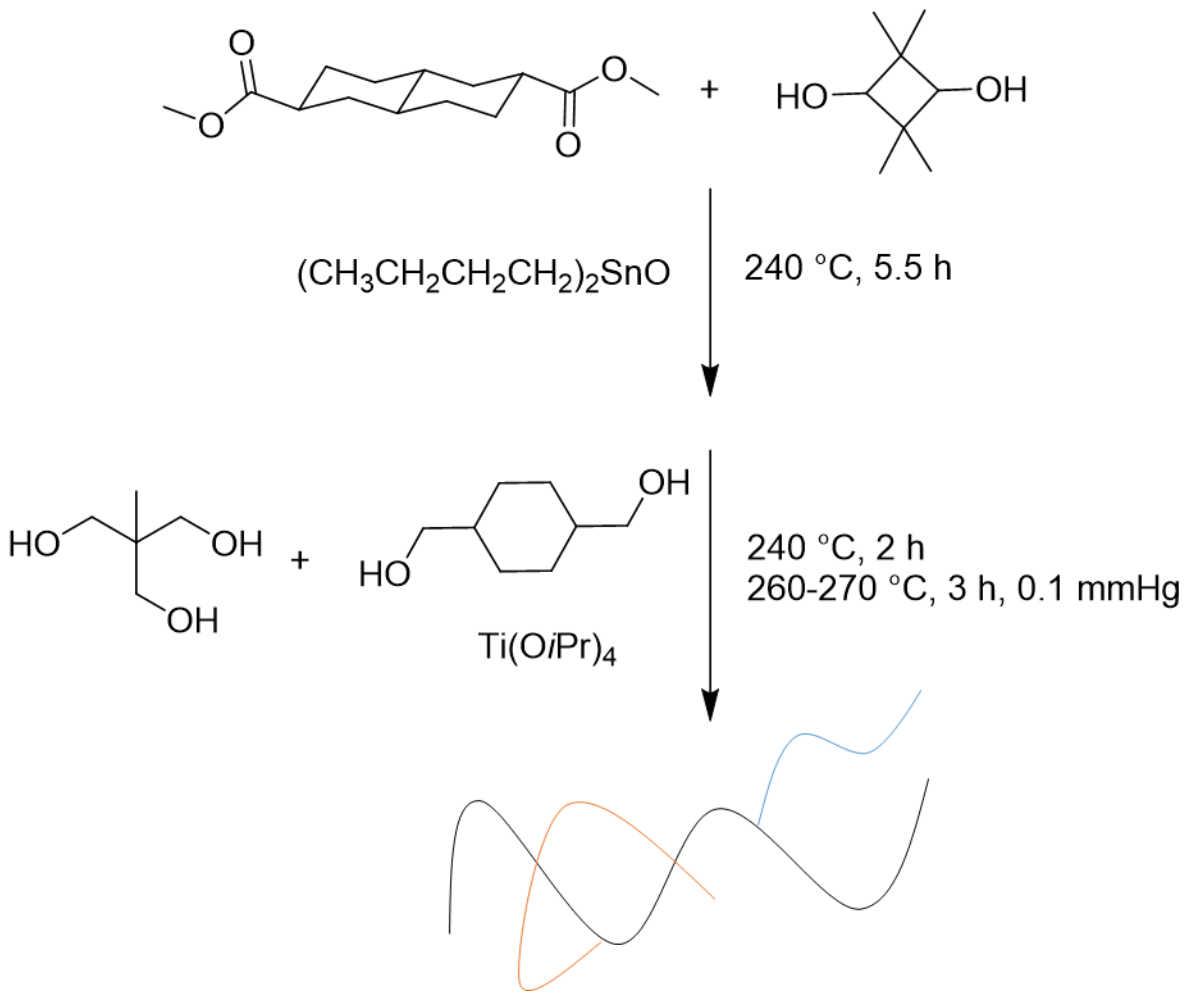

Scheme 2: Proposed method to generate branched copolyesters.

Following Chapters 5 and 6, monitoring thermomechanical relaxations with long-chain branching through dynamic mechanical analysis will highlight the influence of chain topology on chain dynamics in the glassy regime (e.g. β-relaxations). Furthermore, comparing the rheological behavior of these branched copolyesters with the linear analogues will complement the studies described in Chapter 7. Finally, investigation into the impact of long-chain branching on tensile properties for these copolyesters provides the necessary conclusion to targeting BPA-polycarbonate replacements. It is expected that without molecular weight targeting, the introduction of the trifunctional monomer will enable access to higher molecular weight fractions otherwise not realized in the linear analogs. As a result of the increased concentration of high

molecular weight fractions, the average number of entanglements should increase and improve the mechanical properties of the currently brittle copolymers.

The synthesis and subsequent incorporation of a novel aromatic trisamine (TAPE) generated high molecular weight, long-chain branched PEIs. Combination of ^{1}H NMR spectroscopy and SEC enabled the determination of average branch length (M_b) as a function of TAPE incorporation. Furthermore, SEC confirmed targeted molecular weights with increasing dispersity with increased branching. Although DSC highlighted minimal changes in the T_g, rheological analysis elucidated a critical influence of branch length on melt viscosity. The reduction in melt viscosity with long-chain branching illustrates a critical advantage for processing high molecular weight thermoplastics. Leveraging the fundamental understanding of TAPE on branching length and density, Scheme 3 describes a future step for long-chain branched PEIs.

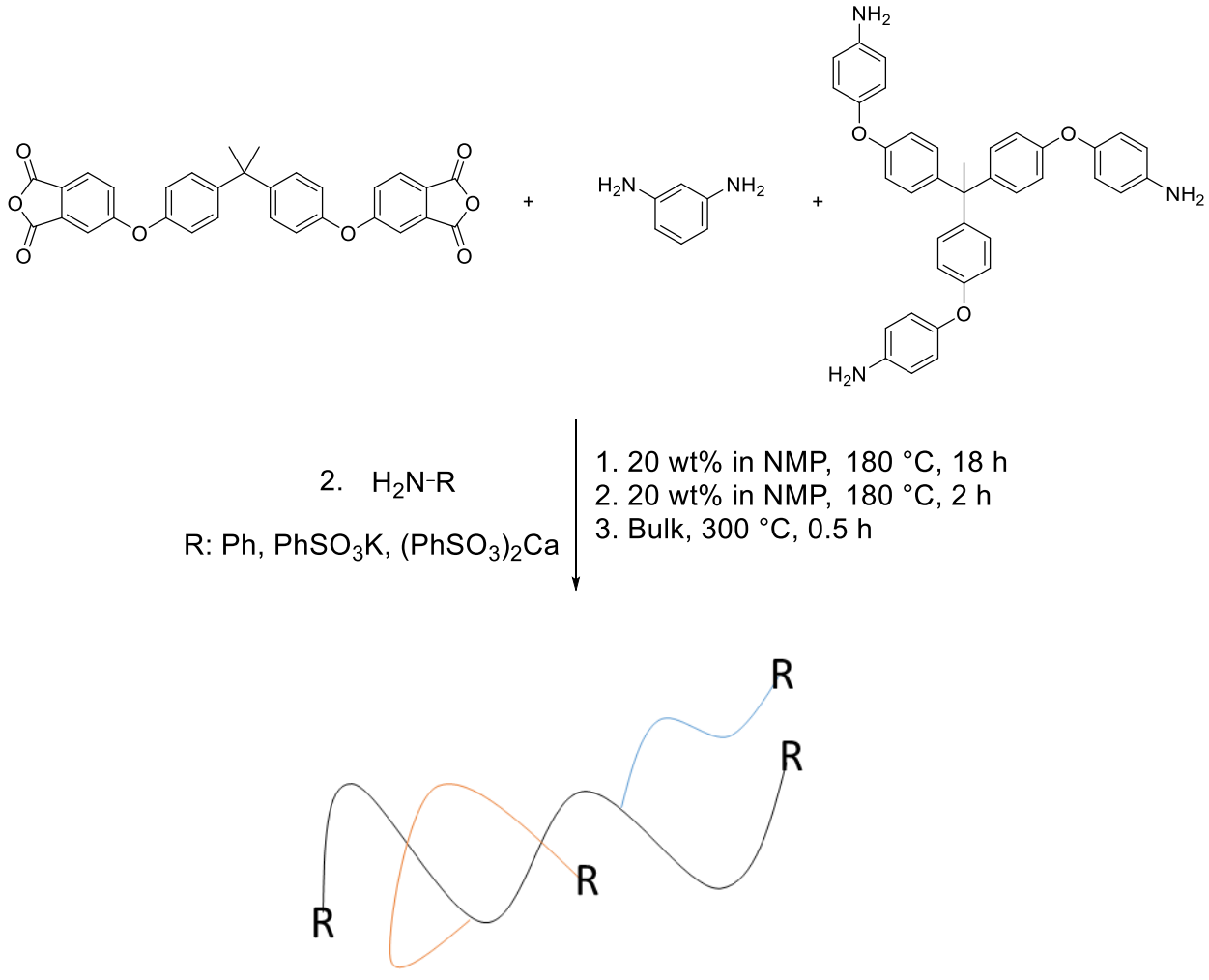

Scheme 3: Proposed synthesis of sulfonate-endcapped, long-chain branched PEIs

Incorporating interactive end-groups provides functionality and unique physical attributes otherwise not observed in PEIs. The advantageous thermal stability of sulfonated salts enables direct incorporation into PEIs with minimal impact on the thermal degradation. Furthermore, the increased concentration of end groups in the LCB-PEIs with respect to linear PEIs permits higher concentrations of ionic groups at high molecular weights. The high thermal stability of PEIs provides a unique opportunity to explore the disassociation temperatures for various sulfonate metal salt complexes, and the impact on the resulting thermal and rheological properties. The strong associating sulfonates entertain the possibility of improving low molecular weight

mechanical properties by increasing apparent molecular weights below the dissociation temperatures. Above the dissociation temperature, these low molecular weight oligomers have the potential for low viscosities because of minimal entanglements per chain. Although Scheme 3 identifies metal counterions as the initial study, investigation into organic counterions may elucidate important ion-ion interactions on physical properties.

In conjunction with introducing interactive groups to the ends of PEIs, further investigation into the influence of pendant group rigidity is realized in Scheme 4. Synthesis of the novel monomers illustrated, provides a synthetic handle to finitely control the pendant group structure and probe the impact on thermal and mechanical properties. Considering PEIs applications and advantageous thermal resilience, the phenyl ether linkage provides a critical thermal stability over other functionalities. Furthermore, the synthetic ease in monomer preparation enables a wide range of pendant group length and rigidity, and provides a complementary relationship to branched PEIs.

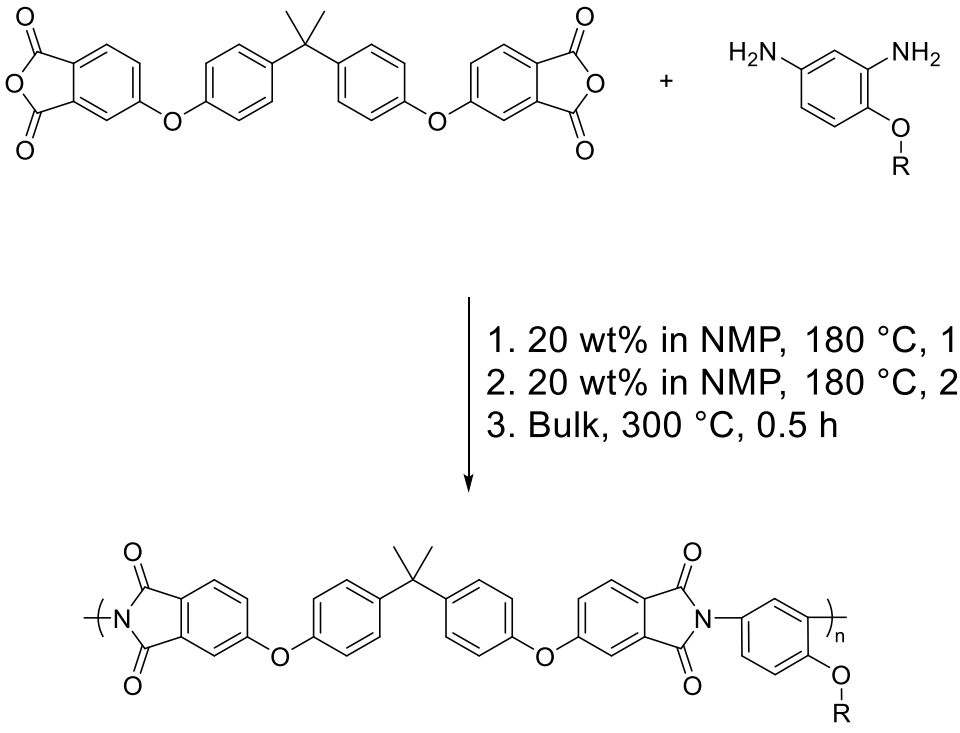

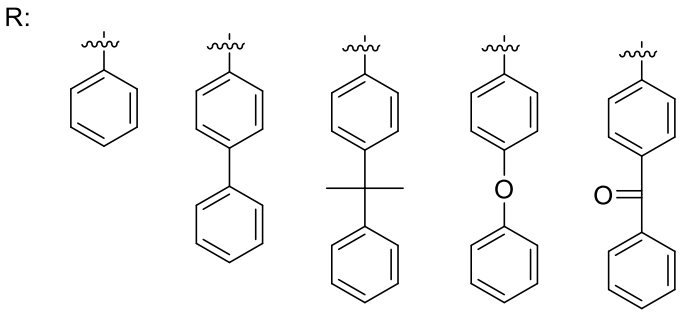

Scheme 4: Proposed research probing the influence pendant group length and rigidity on PEIs.

The preliminary results demonstrated in Chapter 8, identifying a novel method to synthesize polyureas, does not fully establish the breadth of impact capable. One particular instance is the introduction of low-T_g, oligomer segments into the polyurea backbone to provide extensibility and mimic current thermoplastic elastomers developed through isocyanate chemistry. Scheme 5 proposes a synthetic route to obtain the generic thermoplastic elastomer structure described in detail in Chapter 2. Building on the experience developed while studying bulk polymerization strategies of segmented block copolymers, a foreseeable hurdle will entail solubility constraints of the oligomer and small molecules. However, leveraging theoretical calculations to predict solubility parameters and isolate possible synthetic combinations provides an exciting route to reduce experimental trials and further develop the hypothesis proposed in Chapter 4. Unlocking this potential family of urea-containing segmented block copolymers highlights the possibility for dramatic impact on industrial production of thermoplastic elastomers by eliminating solvent streams and the dangers surrounding isocyanate chemistry. Advantageously, a wealth of knowledge describes the structure-morphology-property relationships surrounding the current state-of-the-art urea-containing segmented copolymers, and combining these theories with those developed in Chapters 3 and 4 provide a road map to the design of the next generation of green materials.

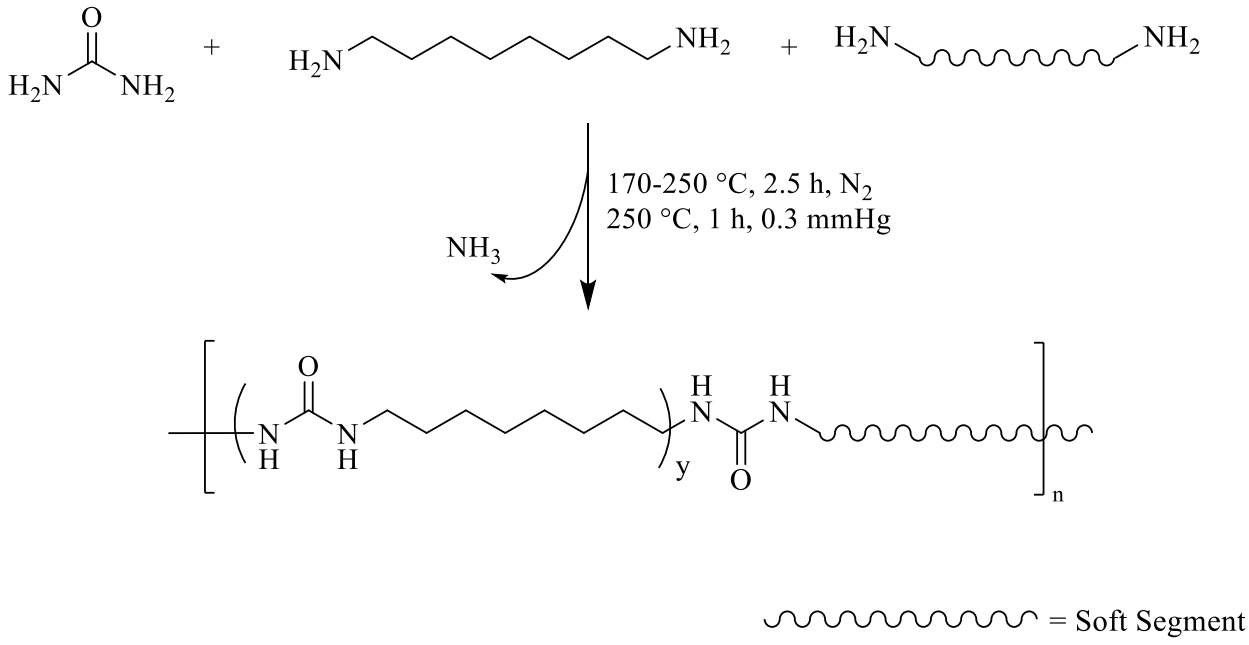

Scheme 5: Proposed synthesis of segmented Polyurea thermoplastic elastomers utilizing a biorenewable feedstock.